(NASA-CR-159790) ADVANCED COOLING TECHNIQUES FOR HIGH-PRESSURE HYDROCARBON-FUELED ENGINES Final Report, Aug. 1978 - Oct. 1979 (Rocketdyne) 230 p HC A11/MF A01

N80-17141

CSCL 21H G3/20

Unclas 47209

NASA CR-159790
RI/RD79-310

NASA

FINAL REPORT

ADVANCED COOLING TECHNIQUES FOR HIGH-PRESSURE HYDROCARBON-FUELED ENGINES

by

R. T. Cook

Rockwell International
Rocketdyne Division

prepared for
NATIONAL AERONAUTICS AND SPACE ADMINISTRATION

October 1979

NASA-Lewis Research Center
Contract NAS3-21381
R. Quentmeyer, Project Manager

FOREWORD

This program was conducted by the Rocketdyne Division of Rockwell International for the NASA-Lewis Research Center under Contract NAS3-21381. The program was directed by Mr. Richard Quentmeyer at NASA, and Messrs. Frank Kirby, Program Manager, and Ronald Cook, Project Engineer, at Rocketdyne.

The thermal design analyses were performed by Dennis Romine, Mike Ladd, Gary Ledbetter, and John Page. Propellant properties were generated by John Weber. Performance analyses were performed by Wally Geniec, Elden Cross, and Vance Jacqua.

CONTENTS

PAGE [illegible] INTENTIONALLY BLANK

ILLUSTRATIONS

TABLES

SUMMARY

A parametric study was conducted defining the regenerative cooling limits (maximum chamber pressure) for O_2/hydrocarbon gas generator and staged combustion cycle rocket engines over a thrust range of 89,000 N (20,000 lbf) to 2,669,000 N (600,000 lbf) for a reusable life of 250 missions. Maximum chamber pressure limits were first determined for the three propellant combinations (O_2/CH_4, O_2/C_3H_8, and O_2/RP-1) without a carbon layer (unenhanced designs). Chamber pressure cooling enhancement limits were then established for seven thermal barriers. The thermal barriers evaluated for these designs were: carbon layer, ceramic coating, graphite liner, film cooling, transpiration cooling, zoned combustion, and a combination of two of the above. All fluid barriers were assessed a 3% performance loss. Sensitivity studies were then conducted to determine the influence of cycle life and RP-1 decomposition temperature on chamber pressure limits. Chamber and nozzle design parameters are presented for the unenhanced and enhanced designs.

The maximum regenerative-cooled chamber pressures are attained with the O_2/CH_4 propellant combination. O_2/RP-1 designs must rely on a carbon layer and liquid-gas injection chamber contours, "short chamber", to be competitive with the other two propellant combinations. This is attributed to the low decomposition temperature of RP-1.

The chamber pressure trend with thrust differs from the normal acceptable trend of higher chamber pressure for the larger thrust level. The reverse trend of this study is attributed to maintaining a constant life criterion instead of a constant wall temperature criterion. The maximum enhancement benefit was attained with the combined thermal barriers. These were carbon layer and ceramic coating for the O_2/RP-1 designs, and film cooling and ceramic coating for the O_2/CH_4 and O_2/C_3H_8 designs.

INTRODUCTION

This program was a 12-month analytical study under NASA-LeRC Contract NAS3-21381 to investigate advanced cooling techniques related to hot-gas heat barriers for high chamber pressure oxygen/hydrocarbon rocket engines. The program provides NASA and vehicle designers with chamber pressure limits for hydrocarbon regeneratively cooled thrust chambers, extended chamber pressure limits when advanced cooling techniques are applied, and identification of technology items that require substantiation before the advanced cooling techniques can be implemented confidently.

This program is subdivided into two technical tasks. Task I is devoted to defining the regenerative cooling limits (maximum chamber pressure) for the three hydrocarbon propellants (RP-1, methane, and propane) without enhancements and generating the cooling circuit design parameters at these limits. Task II defines the cooling enhancement techniques investigated and applied to the designs developed in Task I to determine how far the chamber pressure can be increased beyond the conventional regenerative cooling limit. The status of these cooling enhancement techniques are assessed to identify the technology needs required before the concepts can be confidently incorporated into thrust chamber designs.

As a result of the Task I and Task II analytical efforts, after it was determined that these cases would not provide useful data, some sensitivity analyses were substituted for some planned design analyses. Cyclic life and RP-1 decomposition temperature sensitivity studies were conducted with the approval of the NASA manager.

STUDY GUIDELINES

Task I study guidelines are given in Table 1. Many of these guidelines are the same as those used in past NASA rocket engine design studies. Additional guidelines, which were established in agreement with NASA/LeRC during the Task I study, are presented in Table 2.

The coolant P_{out}/P_c ratio of 1.2 for the gas generator designs (P_{in}/P_c = 1.8) represents a reasonable outlet pressure limit to allow for injector ΔP and parasitic losses (manifold, ducting, etc.). This results in an allowable cooling $\Delta P/P_c$ of 0.6 (1.8 to 1.2), which is typical of combustion chamber designs. This cooling pressure drop limit was used for the staged combustion cycle (P_{in}/P_c = 2.25) and results in the coolant P_{out}/P_c ratio of 1.65. This higher outlet pressure limit is required so that the coolant can do additional work before going to the main injector (such as driving the turbines for the pumps.)

The coolant inlet pressure will be reduced below the P_{inlet}/P_c assigned ratio when the P_c limit is attained for each thrust level. However, at least one series of maximum P_c versus thrust trend will be established for the guideline P_{inlet}/P_c ratio.

The combustion chamber coolant side surface roughness is typical of values measured for milled channels in copper and copper-base alloy chambers. The nozzle coolant side surface roughness is typical of small-diameter tubes. The coolant inlet temperatures for methane and propane are slightly greater than

their respective ambient pressure saturation values. The RP-1 is assumed to be at ambient temperature. The allowable coolant maximum Mach number was less than 0.5 to ensure that choking will not occur in an off-design operating condition.

The Task II basic guidelines are identical to the Task I guidelines with the addition of the thermal barrier guidelines noted in Table 3. The substituted sensitivity studies related to cyclic life and RP-1 decomposition temperature were conducted outside of the specified guidelines.

When the maximum guideline chamber pressure for each thrust level was met, the minimum P_{inlet}/P_c of the coolant established the design for the limiting chamber pressure. This criterion was disregarded for the film-cooling enhanced designs to determine chamber pressure versus thrust trends. Other enhancement techniques were within the P_c guideline limits.

TABLE 1. TASK I STUDY GUIDELINES

PARAMETER	GUIDELINES
PROPELLANTS	• O_2/RP-1 AT MR = 2.8:1 • O_2/CH_4 AT MR = 3.5:1 • O_2/C_3H_8 AT MR = 3.1:1
ENGINE SIZE	• 20 K VACUUM, (ϵ = 400:1), MAX P_c = 4000 • 150 K VACUUM, (ϵ = 400:1), MAX P_c = 5000 • 600 K S.L. (ϵ = 80:1), MAX P_c = 6000 • ϵ_c BETWEEN 1.5:1 AND 4.0:1 • 90% BELL DESIGN NOZZLE
PERFORMANCE	• 98% ERE COMBUSTION EFFICIENCY • CONTRACTOR IN-HOUSE METHODOLOGY (ODE)

COMBUSTION CHAMBER GEOMETRY	• NONTUBULAR (CHANNELS)
	• COOLANT CHANNEL DIMENSION LIMITS
	  • MIN. CW = 0.03"
	  • MIN. WEB = 0.03"
	  • MIN. WALL = 0.025"
	  • MAX. CH/CW = 4:1

COMBUSTION CHAMBER MATERIAL	• COPPER OR COPPER-BASE ALLOY

TABLE 1. (Concluded)

PARAMETER	GUIDELINES
T/C WALL TEMPERATURE LIMITS	• T_{WG} = 1460 R FOR COPPER OR COPPER BASE ALLOY • RP-1 T_{WC} = 1060 R (UNLESS HIGHER VALUE IS JUSTIFIED) • CH_4 T_{WC} = 1760 R • $C_3 H_8$ T_{WC} = T.B.D. BY CONTRACTOR (~1320 R)
HOT-GAS HEAT TRANSFER	• CONTRACTOR IN-HOUSE METHODS AND CORRELATIONS • CARBON DEPOSITION TO BE NEGLECTED
COOLANT HEAT TRANSFER	• P_{IN}/P_C = 1.8 (G.G.) • P_{IN}/P_C = 2.25 (STAGED COMBUSTION) • REGEN COOL TO ϵ = 180:1 FOR 20 K AND 150 K, IGNORE COOLING FOR ϵ = 180:1 TO ϵ = 400:1 • REGEN COOL ENTIRE T/C (ϵ = 80:1) FOR 600 K • CONTRACTOR IN-HOUSE METHODS AND CORRELATIONS • 2-D CONDUCTION EFFECTS INCLUDED • O_2 NOT CONSIDERED AS PRIMARY COOLANT
CYCLE LIFE	• 250 X 4 • $\epsilon_T = K\alpha\Delta T$ • MANSON'S EQUATION WHEN NO DATA AVAILABLE

TABLE 2. ADDITIONAL STUDY GUIDELINES ESTABLISHED DURING TASK I

- YIELD SAFETY FACTOR = 1.1
- ULTIMATE SAFETY FACTOR = 1.5
- TOTAL RUN DURATION = 10 HOURS
- COOLANT P_{OUT}/P_C = 1.2 (GAS GENERATOR CYCLE)
  = 1.65 (STAGED COMBUSTION CYCLE)
- COOLANT SIDE SURFACE ROUGHNESS
  20 MICROINCHES RMS FOR COMBUSTION CHAMBER
  40 MICROINCHES RMS FOR NOZZLE
- COOLANT INLET TEMPERATURES
  RP-1 : 294 K (530 °R)
  C_3H_8 : 233 K (420 °R)
  CH_4 : 117 K (210 °R)
- COOLANT MACH NUMBER < 0.5

TABLE 3. TASK II COOLING ENHANCEMENT THERMAL BARRIER DESIGN GUIDELINES

Physical Barrier	Coating Thickness Constraints	Thermal Conductivity, Kcal/cm-sec- K (Btu/in-sec- R)	Maximum Allowable Temperature
Carbon Layer	Function of Carbon Atom Fraction and Mass Flux	See Fig. 18.	Within Experimental Data Limits
Zirconium Oxide	Minimum: 0.0025 cm (0.001 in) Maximum: 0.0127 cm (0.005 in)	5.28×10^{-6} (2.96×10^{-5}) at 1922 K (3460 R)	1944K (3500 R)
Graphite Liner	0.254 cm (0.10 in) 1.27 cm (0.50 in)	8.698×10^{-5} (0.487×10^{-3}) @ 1367 K 7.805×10^{-5} (0.437×10^{-3}) @ 1922 K 7.394×10^{-5} (0.414×10^{-3}) @ 2478 K	1644K (2960 R)

Fluid Barrier	Performance Loss	Assumed Criteria
Film Cooling	3%	Slot Injection Efficiency = 20%
Transpiration Cooling	3%	Injection Efficiency = 85% Maximum Gas Side Wall Temperature = 589 K (1060 R)
Zoned Combustion	3%	Uniform Injection ρV for Core Flow and Zoned Flow

DESIGN CONSIDERATIONS AND ANALYTICAL TECHNIQUES

DESIGN CONSIDERATIONS

Combustion Chamber

The combustion chamber geometry (liner hot-gas wall contour) affects the weight, performance, heat transfer, and life. Influencing parameters are length, contraction area ratio, and wall contour. The optimum combustion chamber design is one with minimum engine weight, minimum hot-gas wall temperature (maximum life), and maximum performance. In addition, engine constraints are imposed on the chamber design as related to available coolant pressure drop and flowrate requirements established for an engine balance with minimum oxidizer and fuel pump discharge pressure. The optimum coolant passage geometry for maximum life (minimum T_{wg}) normally approaches the minimum wall thickness and minimum channel and land widths.

Nozzle

The thrust chamber nozzle contour primarily affects the performance and weight of an engine. The location of the nozzle attachment to the combustion chamber is of great significance, affecting life and engine weight. The optimum attach point is located as near to the throat as possible and still meet nozzle tube life and coolant ΔP. Care must be taken to ensure the chamber throat coolant is at an efficient bulk temperature. The optimum attachment location normally is between an area ratio of 5:1 and 10:1. The higher the chamber pressure, the larger the attachment area ratio. The minimum tube wall thickness normally provides maximum life for minimum coolant pressure drop.

These design considerations are typical of those employed to attain the maximum cooling and life for the Space Shuttle Main Engine (SSME), Ref. 1.

PERFORMANCE

The performance of a liquid rocket engine system is dependant on how efficiently the propellants can be injected, combusted, and then expanded supersonically through a nozzle. The combustion efficiency (η_{c*}) depends on injector design and combustor contour (length and contraction ratio). Additional thrust is obtained through optimum expansion of these combusted gases as related to the nozzle thrust coefficient efficiency (η_{C_F}). Therefore, certain design criteria must be met to attain realistically high performance. The injector/chamber geometry of this study produces a 98% energy release efficiency (η_{c*}). The nozzles are typically designed for an expansion efficiency (η_{C_F}) of 97.5%. These efficiencies are related to the theoretical optimum efficiencies attainable.

Nozzle Performance

The theoretical one-dimensional gas dynamic thrust coefficients for the propellant combinations considered in this study (O_2/RP-1 at MR = 2.8:1, O_2/C_3H_8 at MR = 3.1:1, and O_2/CH_4 at MR = 3.5:1) are shown in Fig. 1 as a function of

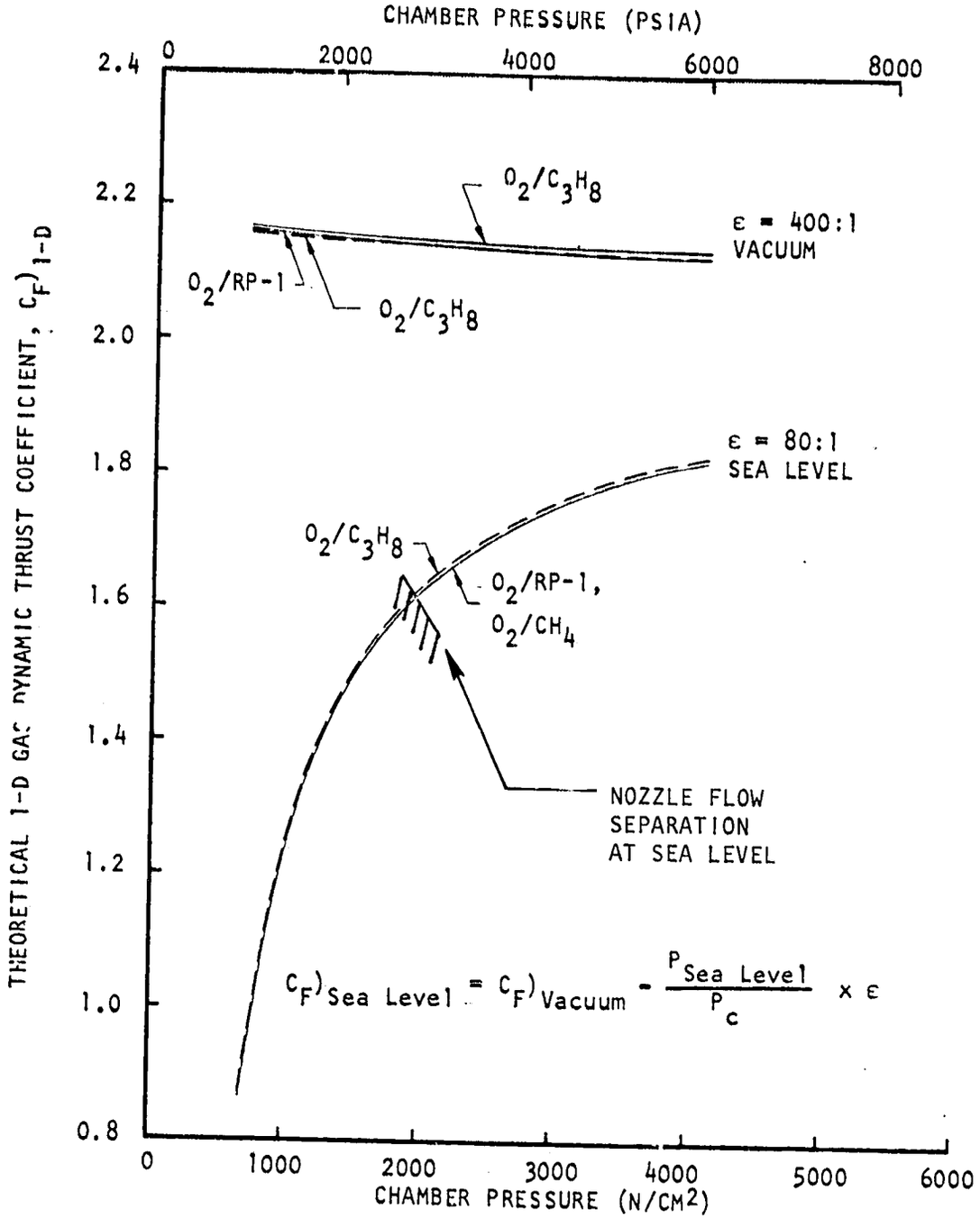

Figure 1. Theoretical Thrust Coefficients

chamber pressure. The vacuum values at an expansion ratio of 80:1 are corrected to sea level using the following equation:

$$C_{F\ \text{Sea Level}} = C_{F\ \text{Vacuum}} - \frac{P_{\text{Sea Level}}}{P_c} \times \varepsilon \qquad (1)$$

This sea level correction produces a large variation in the thrust coefficient because of the high nozzle expansion ratio. A value of 0.975 for the gas dynamic η_{C_F} is used to correct the theoretical thrust coefficients to actual conditions. This is an average value determined from an evaluation of these propellant combinations over the range of thrust levels being considered. This value was attained from the transonic flow analysis and supersonic nozzle contour design analysis for a 90% length bell configuration nozzle.

Once the thrust coefficients are known, the combustion gas flowrate can be determined from the following equation:

$$\dot{w}_g = \frac{F}{c^* C_F} \qquad (2)$$

These flowrates are shown in Fig. 2 for $\eta_{C_F} = 0.975$ and $\eta_{c^*} = 0.980$. Any gas generator flow and its contribution to thrust has not been included in this computation. The large variation in flowrate with chamber pressure at the 2,669,000 N (600,000 lbf) thrust level (ε = 80:1) is due to the large variation in the thrust coefficient (Fig. 1).

Combustion Chamber Performance

The geometric throat radius as a function of chamber pressure and thrust level is shown in Fig. 3. These radius values were evaluated using the following equation:

$$R_t = \left(\frac{F}{C_D \times C_F \times \pi \times P_c} \right)^{1/2} \qquad (3)$$

The discharge coefficient ($C_D = A^*/A_t$) is 0.99 for a throat upstream radius ratio of 1.0. Since the thrust coefficients are nearly the same for each of the three propellant combinations, the throat radius was defined independently of propellant combination by using the average of the three radius values at any set of conditions.

Figure 4 shows the chamber injector-to-throat length as a function of chamber pressure for the three thrust levels being considered. For each thrust level, there is a curve for liquid-liquid (oxidizer-fuel) and liquid-hot-gas propellant injection. Using the radius values from Fig. 3, the normalized injector-to-throat length can be determined as shown in Fig. 5.

The analogous curves for the thrust chamber contraction ratio are shown in Fig. 6. The curves in Fig. 4 and 6 were generated from a computer program that utilizes a curve fit interpolation of data tables that reflect experience and judgement based on numerous engine programs having various propellant combinations. There are two sets of data in this program, one for liquid-liquid injectors and the other for liquid-hot-gas injectors using turbine discharge gases as the fuel.

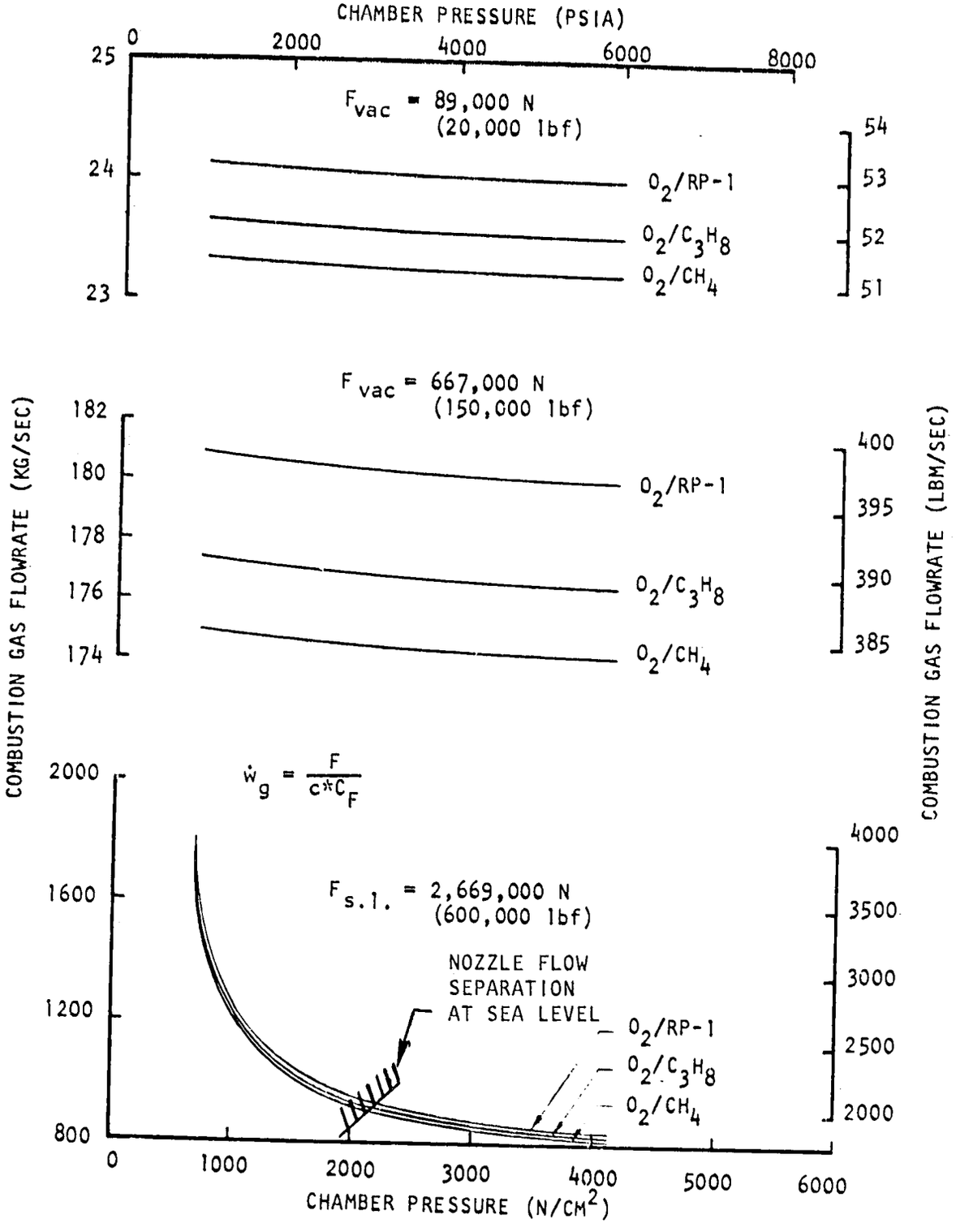

Figure 2. Combustion Gas Flowrate Parametric Data

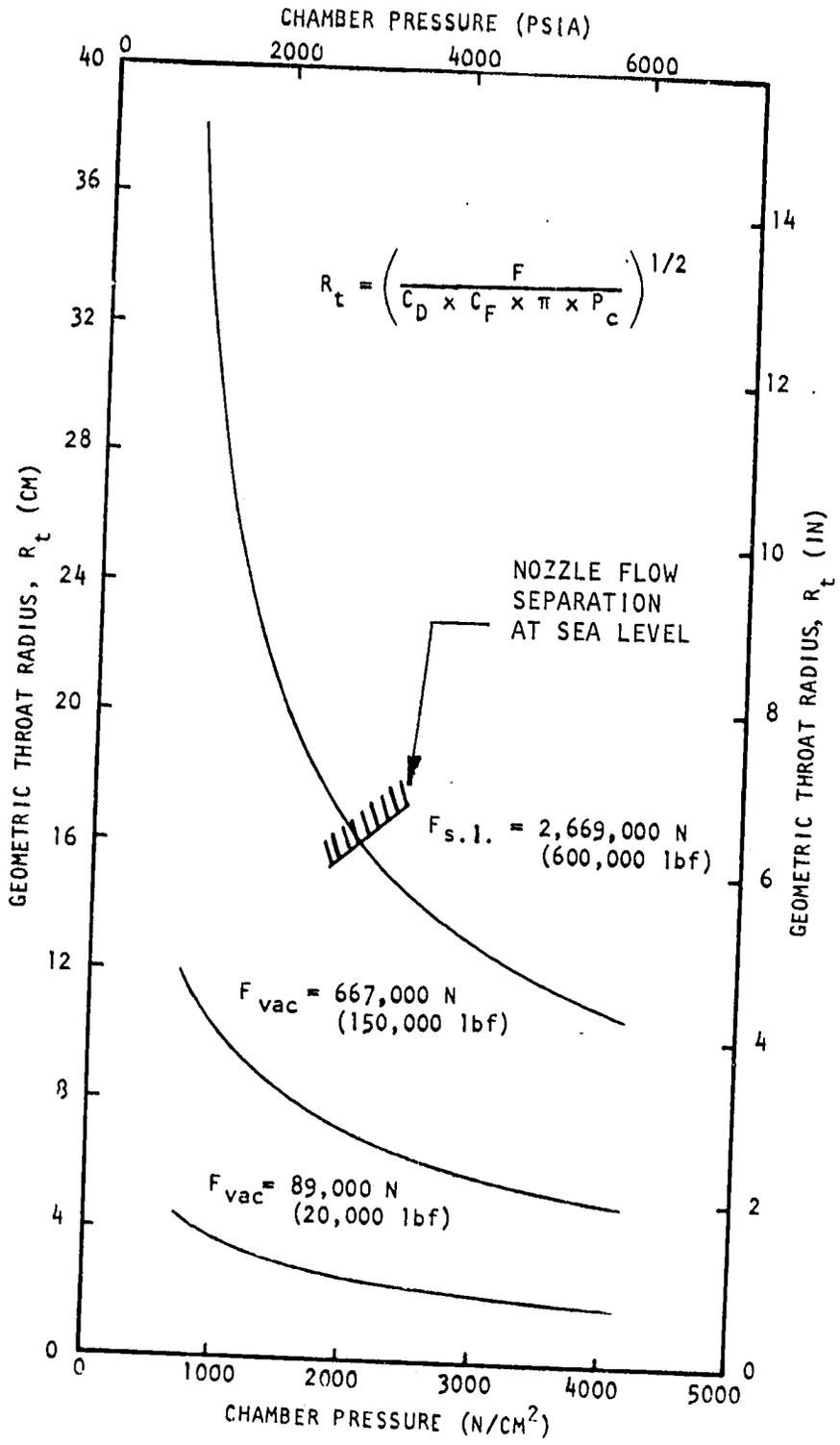

Figure 3. Throat Radii as a Function of Chamber Pressure and Thrust

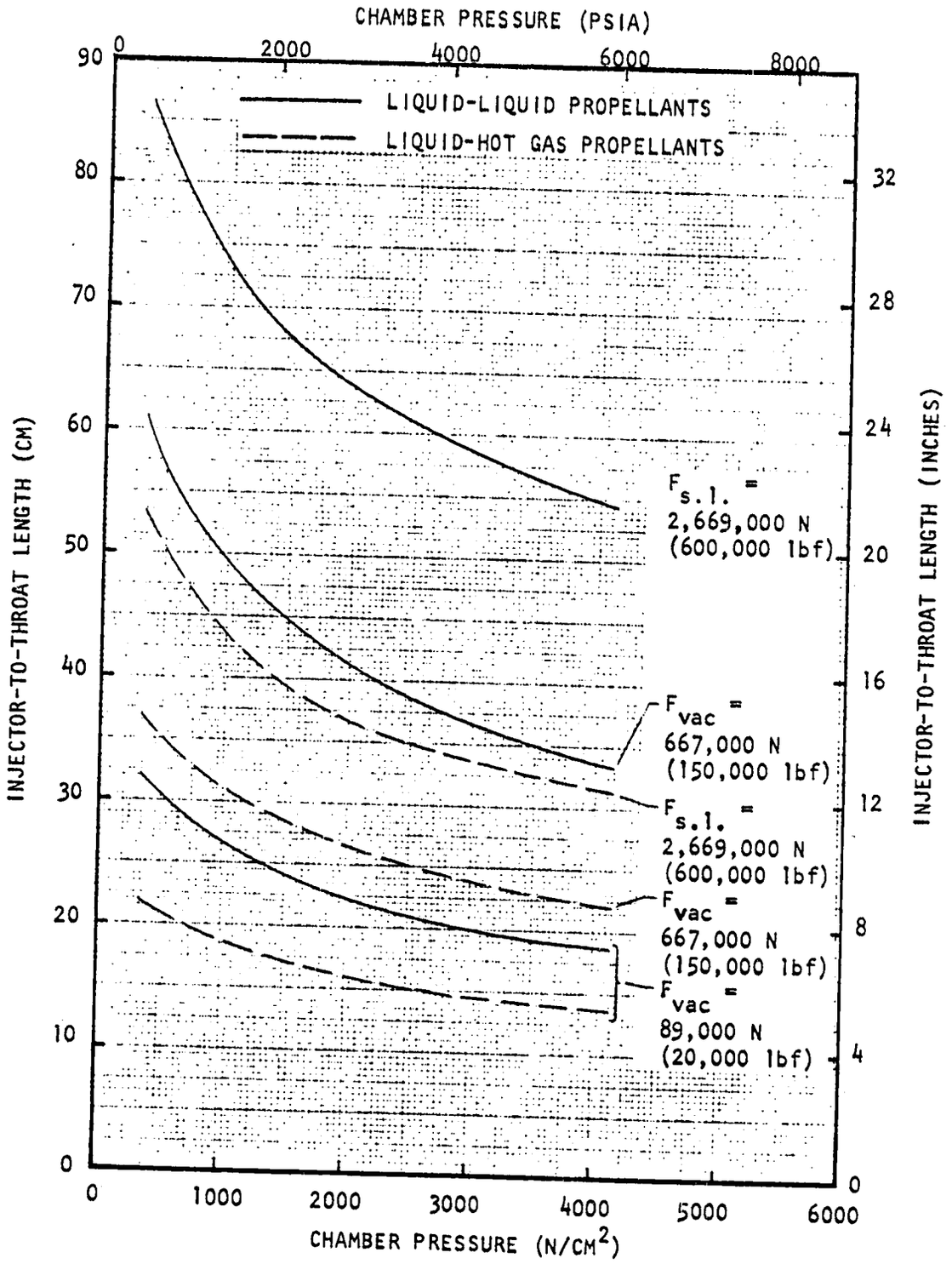

Figure 4. Injector-to-Throat Length Parametric Data

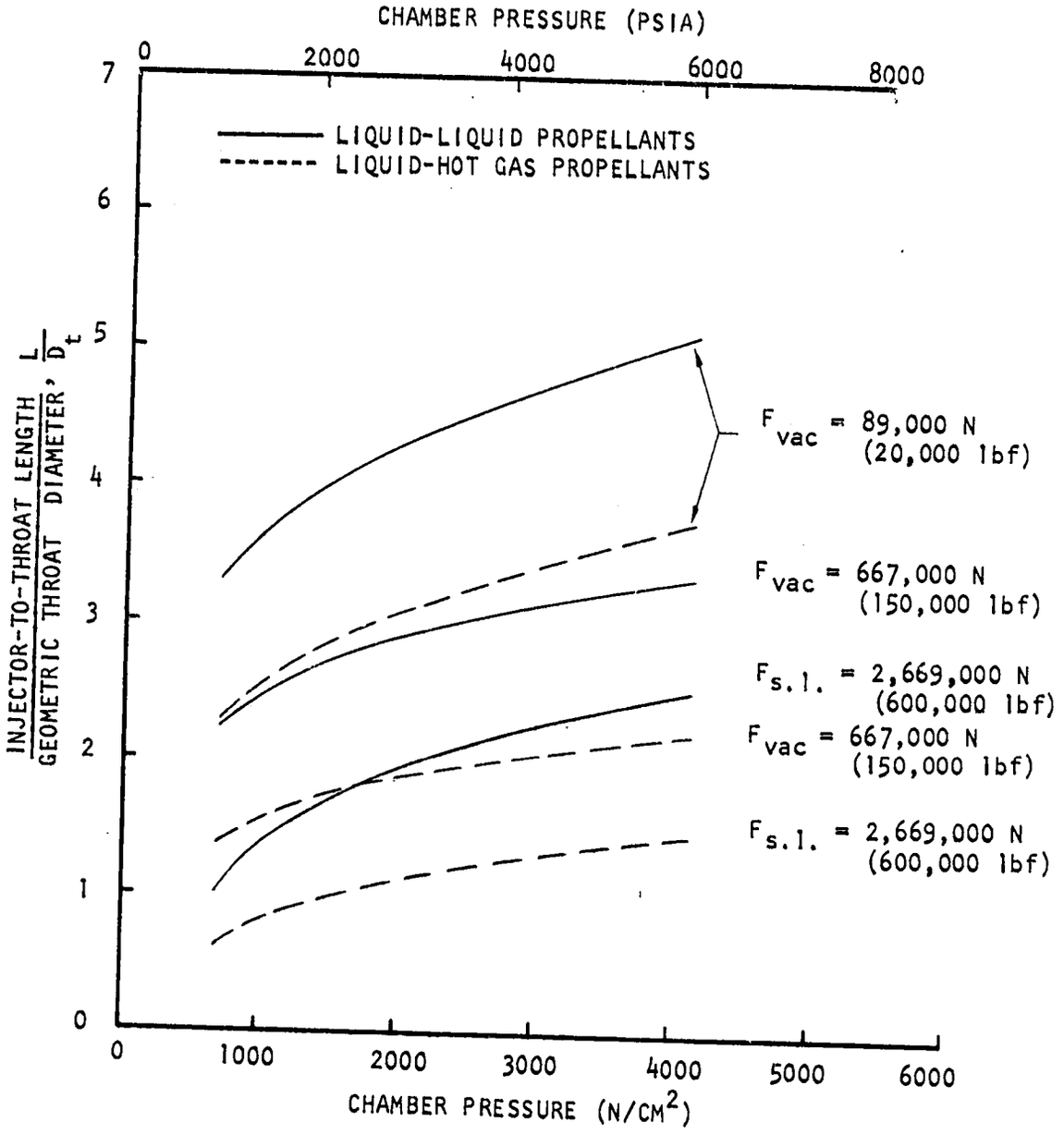

Figure 5. Normalized Injector-to-Throat Length Parametric Data

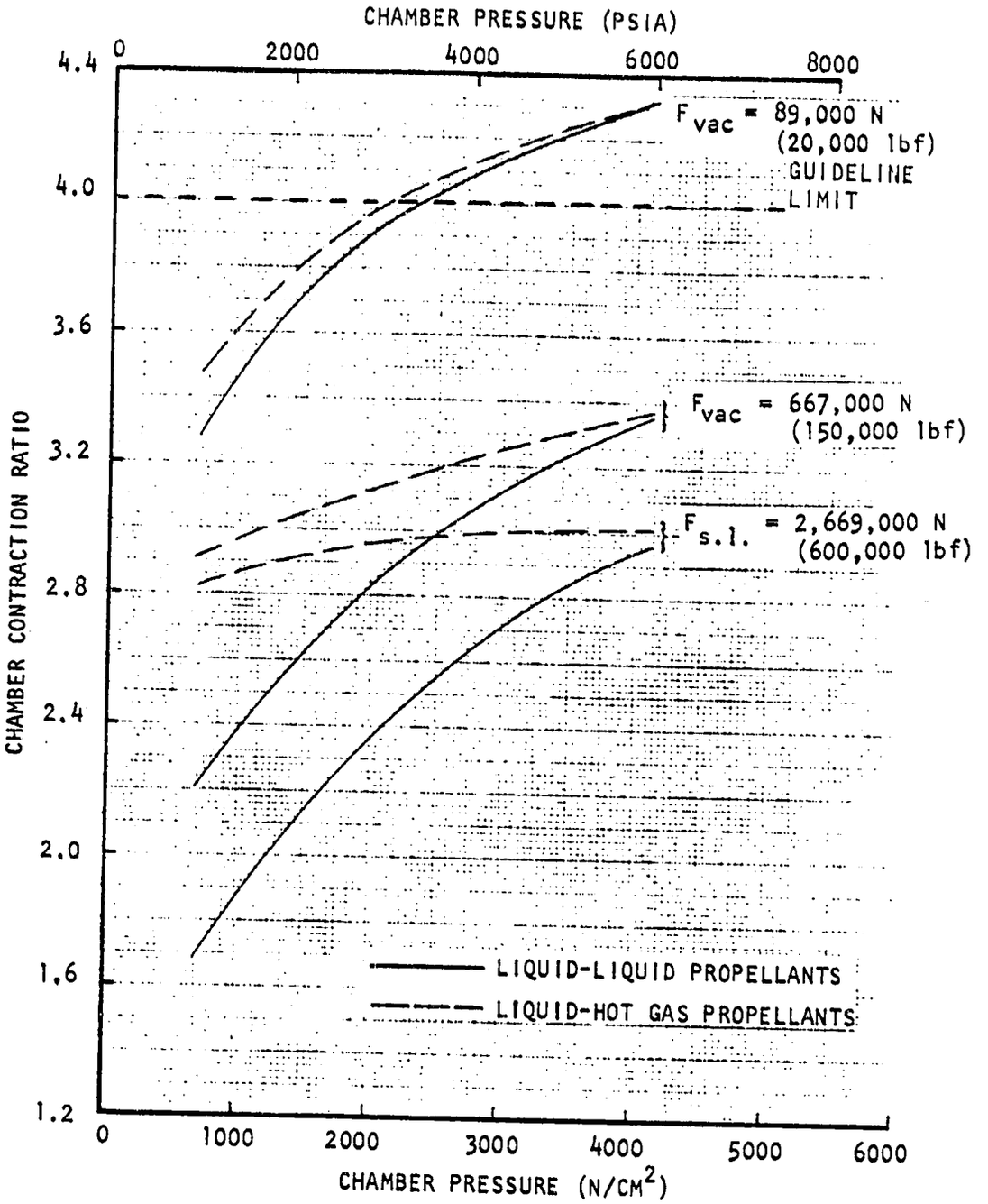

Figure 6 . Chamber Contraction Ratio Parametric Data

The oxidizer (oxygen) is not truly a liquid at the point of injection in that it has a high vapor pressure, low viscosity, and virtually no surface tension. The liquid fuel is the limiting propellant with atomization, vaporization, and mixing being the limiting mechanisms. Liquid-liquid engines require longer residence time (longer length) for complete mixing and combusting of the propellants than do liquid-hot-gas engines as shown in Fig. 4 . The injector-to-throat length is increased as the thrust is increased, primarily because of the coarser injection pattern as the thrust is increased. Where a value of 44.5 N (10 lbf) equivalent thrust per element is practical for a 4450 N (1000 lbf) thrust engine (100 elements), it would not be practical for a 4,450,000 N (1,000,000 lbf) thrust engine where it would result in 100,000 elements. The end result is large injection orifices and large propellant droplets in the high thrust engines where propellant injection rates for each element approach 4450 N (1000 lbf) equivalent thrust. The chamber length can be decreased with increasing chamber pressure because the reaction rates increase with chamber pressure.

Higher chamber pressure operation also leads to larger injection orifices since the mass flowrate per unit injector face area is increased with increasing chamber pressure. Therefore, an increase in contraction ratio is desirable as the chamber pressure increases (Fig. 6). The larger contraction ratio eases the job of manifolding the higher propellant flowrates and provides increased injector face area for more injection orifices. However, as specified in the study guidelines, the maximum contraction ratio was limited to 4.0 to 1. The minimum contraction ratio guideline of 1.5 to 1 will not be encountered.

The chamber sizes in Fig. 4 and 6 are mean recommended values. Any individual actual engine could be sized significantly on either side of these values. Each engine design poses its individual envelope requirements and favors a specific set of compromises. However, these curves define the trends used in the parametric study.

The propane and methane fuels were treated as hot gases for the gas generator cycle because of the large temperature increase each incurs during cooling. The liquid-liquid curves in Fig. 4 and 6 were used for the gas generator cycle design with RP-1 as the fuel using conventional type injectors. However, it is believed that low thrust per element type injectors can be developed to attain an energy release efficiency of 98%. O_2/RP-1 design analyses also were conducted for these prospective gas generator cycle designs for comparison.

Film and Transpiration Cooling Performance Loss

Performance analyses were conducted to determine the amount of fuel available for film or transpiration cooling as a function of specific impulse. The Rocketdyne computer program, FILM, was used to calculate the losses. ODE specific impulse was used at mixture ratios above 1.5, while at lower mixture ratios a nonequilibrium model was used, based on test experience which has shown that much less solid carbon is formed than predicted by equilibrium calculations. A linear mixture ratio profile was assumed, varying from 0.1 at the wall to the core mixture ratio as shown below.

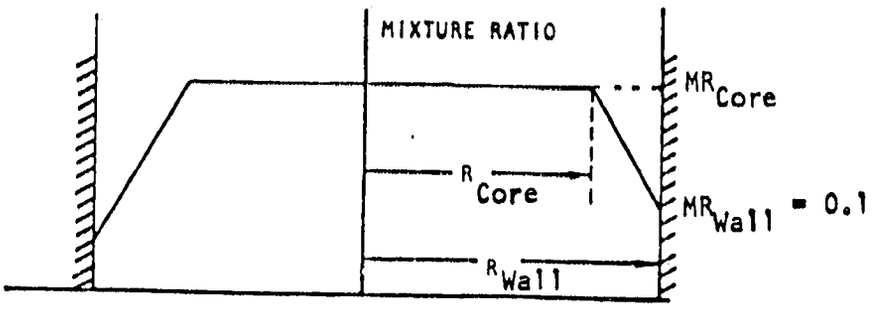

The variable mixture ratio region was divided into zones and the coolant was assumed to react with the main flow at the local mixture ratio. The flow in each zone was then integrated to determine the mixture ratio and specific impulse and a mass-weighted average specific impulse was calculated. This value was then compared to the specific impulse at the same overall thrust chamber mixture ratio to determine the loss due to the coolant flow.

Performance losses were calculated for each propellant combination at chamber pressures of 1379, 2758, and 4137 N/cm^2 (2000, 4000, and 6000 psia). Sea level and vacuum conditions were considered, with area ratios of 80:1 and 400:1, respectively. Since theoretical, rather than delivered, specific impulse was used, the results apply to any thrust level. Similarly, the thrust chamber rather than engine mixture ratio was used, so there is no difference between gas generator and staged combustion cycles. Figures 7 through 9 show the specific impulse loss as a function of coolant flow for each propellant combination. At the 3% performance loss level, the data from Fig. 7 through 9 are plotted in Fig. 10 as a function of chamber pressure. This curve defines the allowable film and transpiration coolant flowrates for the Task II study.

The zoned combustion thermal barrier enhancement performance considerations are presented in the Zoned Combustion section of this report.

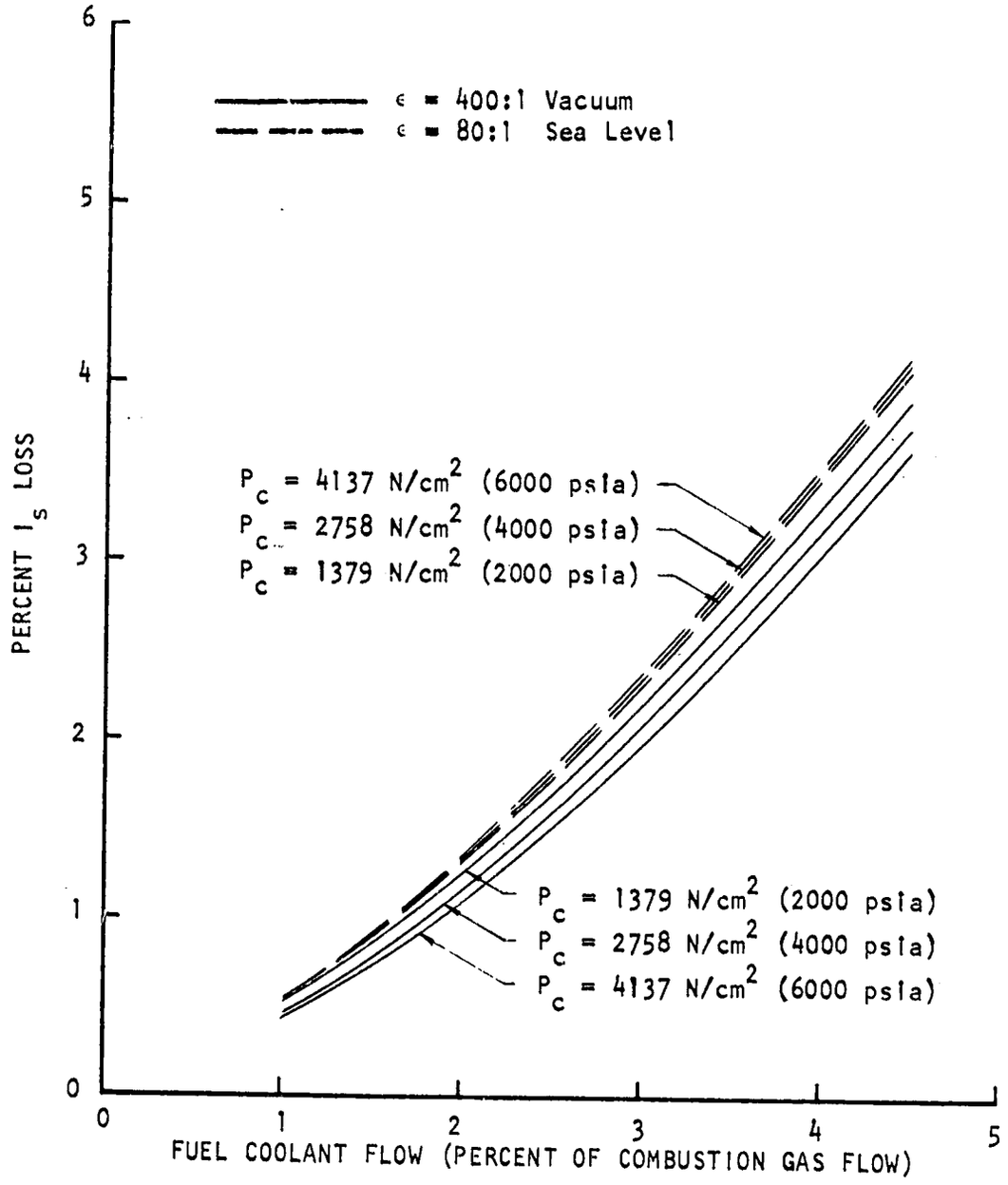

Figure 7. Specific Impulse Loss as a Function of Film/Transpiration Coolant Flow for O_2/RP-1 Propellants at MR = 2.8

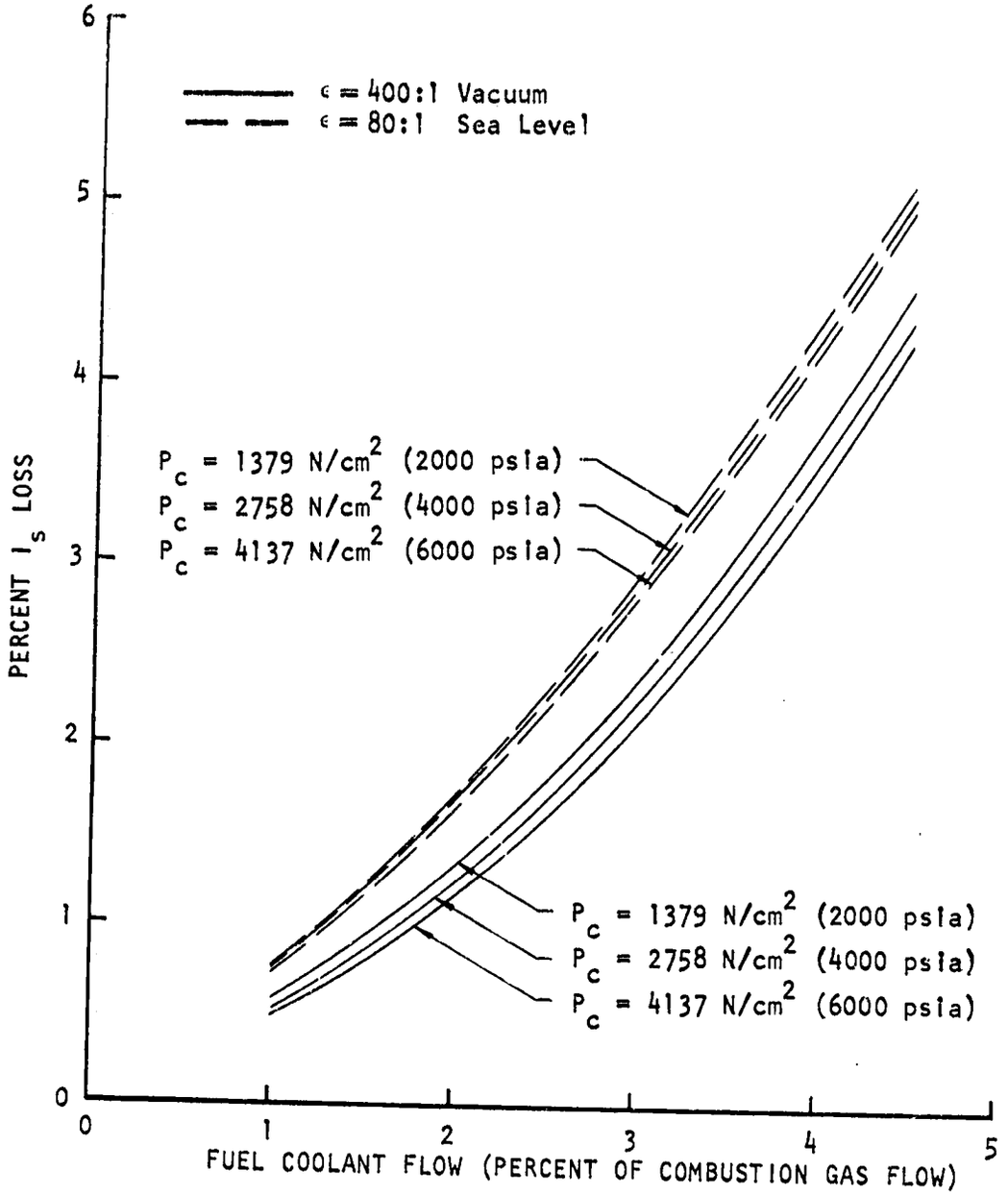

Figure 8. Specific Impulse Loss as a Function of Film/Transpiration Coolant Flow for O_2/C_3H_8 Propellants at MR = 3.1

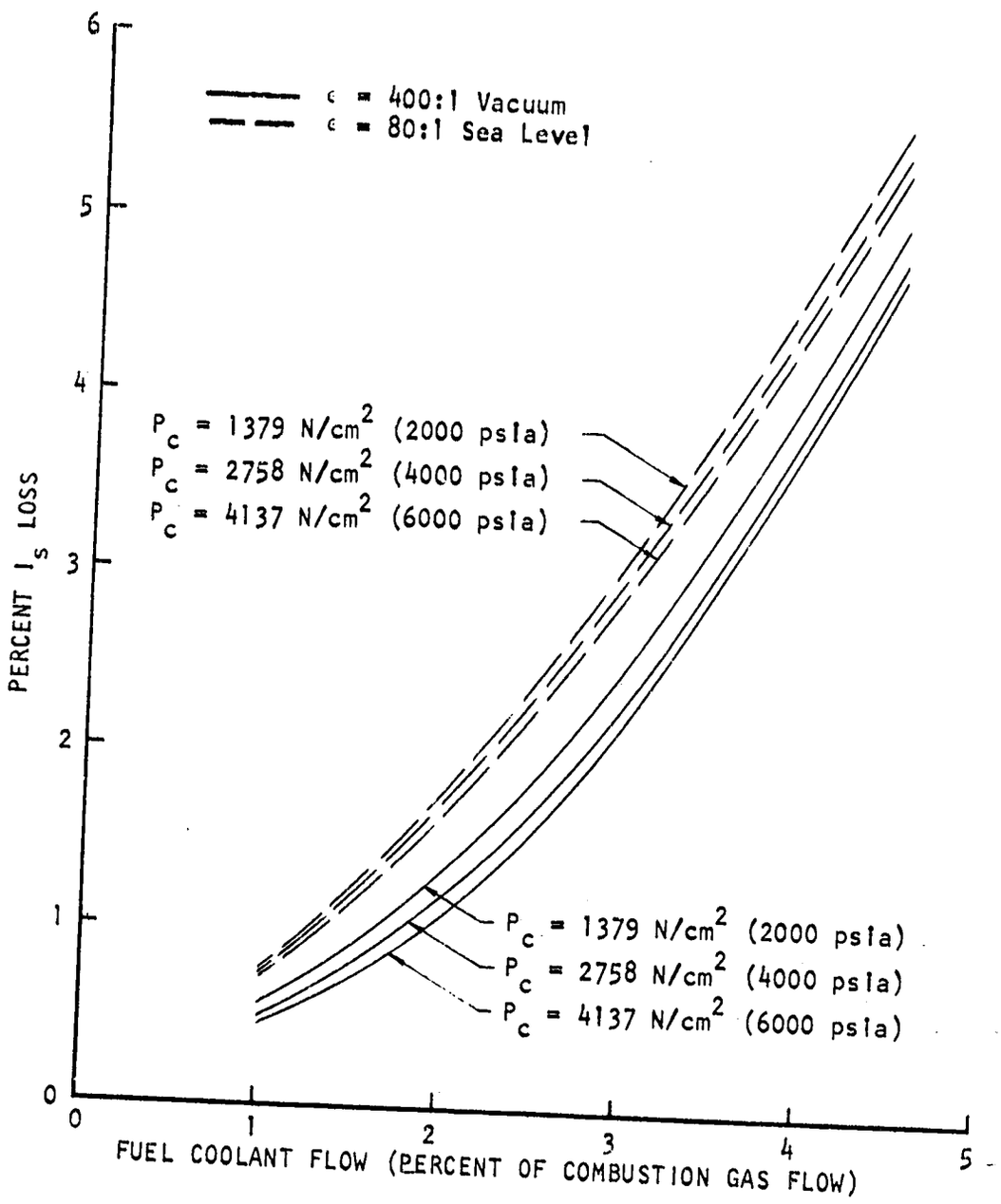

Figure 9. Specific Impulse Loss as a Function of Film/Transpiration Coolant Flow for O_2/CH_4 Propellants at MR = 3.5

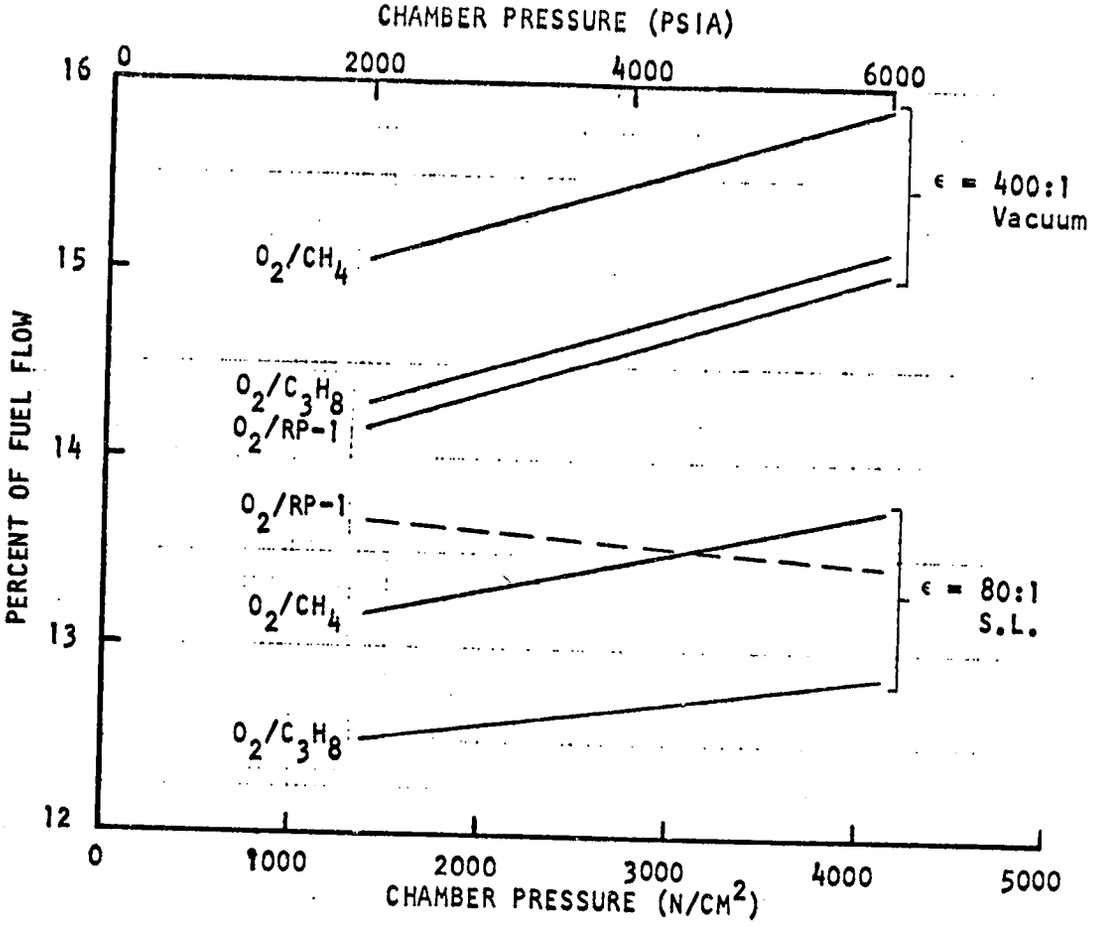

Figure 10. Allowable Film and Transpiration Coolant Flowrates (3% Performance Loss)

CONTOUR DEFINITION

The following parameters were selected for the combustion chamber contour:

- Convergence half-angle
  - 30 degrees for F=2,669,000 N (600,000 lbf) liquid-hot gas propellants
  - 20 degrees for all other designs
- Convergence R/R_t joining cylindrical section with entrance ramp 2.0
- Throat upstream R/R_t 1.0
- Throat downstream R/R_t 0.4

The relatively shallow 20-degree convergence half-angle promotes continuous smooth boundary layer growth. Shallow convergence angles result in a higher average heat flux due to a lower average contraction ratio. However, there is only a small increase in the integrated heat load because the increased average heat flux is nearly offset by the reduced surface area (smaller average diameter and decreased surface length). The shallow convergence angle is incompatible with the short lengths and large contraction ratios of the 2,669,000 N (600,000 lbf) sea level thrust combustors with liquid-hot-gas propellants at low chamber pressures. Therefore, for these configurations, the convergence half-angle has been increased to 30 degrees. Additionally, if necessary, the injector-to-throat length was increased beyond the minimum required for combustion (Fig. 4) so that there is a 5.08 cm (2 in.) cylindrical section for injector-to-chamber compatibility. The 2,669,000 N (600,000 lbf) sea level thrust combustion chamber contours for the liquid-liquid and liquid-hot-gas propellants are compared in Fig. 11. The liquid-hot-gas designs are quite short relative to their contraction ratios. It was decided that it would not be reasonable to consider decreasing their lengths further.

The large upstream convergence R/R_t joining the cylindrical section with the convergence ramp provides a smooth transition to avoid flow separation at the turn, avoid impingement at the initial portion of convergence, and prevent degradation of the coolant film coefficient due to reverse curvature effects. The upstream and downstream throat radius ratios are the same as used for the SSME and ASE combustion chambers.

Nondimensional (R/R_t vs X/R_t) 90% bell nozzle contours for ε = 80:1 and ε = 400:1 were generated for the three propellant combinations. Parabolic nozzle contours are generated that closely approximate a Rao optimum contour. Initial expansion angles of 32 and 37 degrees for the ε = 80:1 and ε = 400:1 contours, respectively, were selected. An exit angle of 6.2 degrees is selected for both expansion ratios. These angles were obtained from curves available from previous optimum contour analyses.

The transonic flow analysis computer program was used to compute the flow properties in the region of flow extending from Mach 0.8 to 1.2. This program calculates iso-Mach lines, streamlines, and characteristic lines for the transonic flow region. One of the iso-Mach lines is used with the contour and

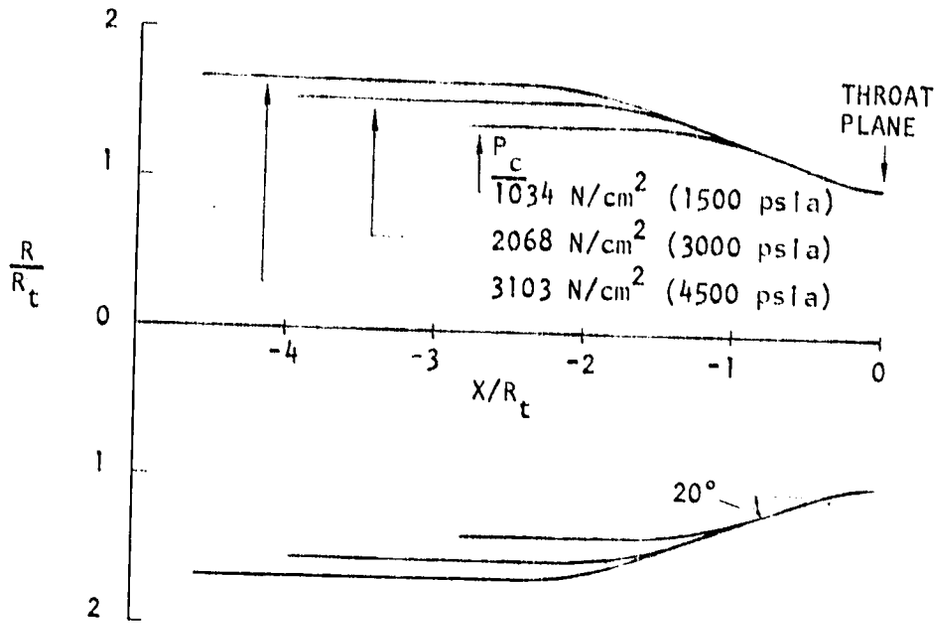

(a) Liquid-Liquid Propellants

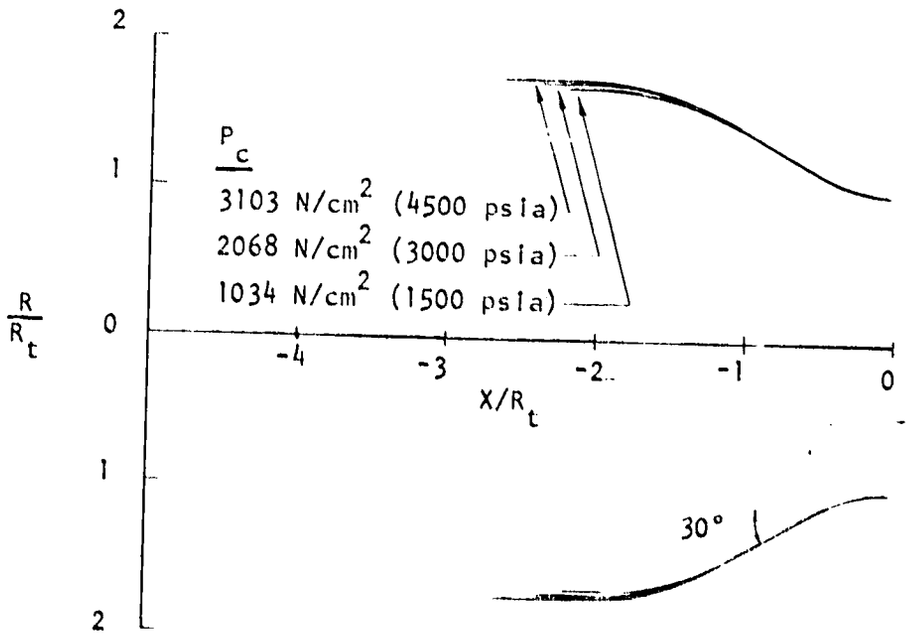

(b) Liquid-Hot Gas Propellants

Figure 11. Comparison of Combustion Chamber Contours for F = 2,669,000 N (600,000 lbf)

the combustion gas properties as input to a computer program that calculates wall properties along the contour. These results are used in the Rocketdyne Boundary Layer Computer Program. This nozzle contour analysis methodology is summarized in Fig. 12. For each propellant combination, the nondimensional nozzle contours need be defined for only one chamber pressure. It is not necessary to generate a nozzle contour for each chamber pressure analyzed because of the small effect of the chamber pressure on the hot-gas properties used to derive the nozzle contour and the fact that the nozzle is not the controlling component in these thermal analyses.

The chamber and nozzle contours are presented for each design case in Appendixes C and D.

CYCLE LIFE AND STRUCTURAL ANALYSIS

Extensive analytical and experimental background in the analysis and prediction of cyclic life and structural integrity of high chamber pressure reusable engines such as the SSME and ASE has led to a realistic yet simplified life cycle analysis technique.

This simplified approach involves the appropriate wall temperature differential, wall material coefficient of thermal expansion, and an empirically derived coefficient. This method has been incorporated into the Regenerative Cooling Design/Analysis Computer Program as part of NASA-LeRC Contract NAS3-16774, and provides a rapid, efficient, low-cost method fully integrated with the coolant passage thermal design. Also, as part of this computer program, a simple structural analysis of the coolant passages can be performed. These features make this computer program an ideal tool for parametric data generation as well as detailed thrust chamber cooling design as required in this study.

Cycle Life

Cycle life consists of assessing the accumulation of damage to a material as cycles of operation occur. The length of time under load as well as repetitions of load are evaluated. The length of time under load is evaluated by using the stress rupture properties of the material while the repetitions of load (cyclic influence) is evaluated by using the fatigue properties of the material.

The fundamental premise used in the life prediction analysis is that failure depends on the accumulation of creep and fatigue damage. A generalized cycle life equation is used to consider the total damage caused by fatigue and creep:

$$4\ (\phi_f + \phi_c) \leq 1.0$$

where 4 is the specified life safety factor and ϕ_f and ϕ_c are the fatigue and creep damage fractions, respectively.

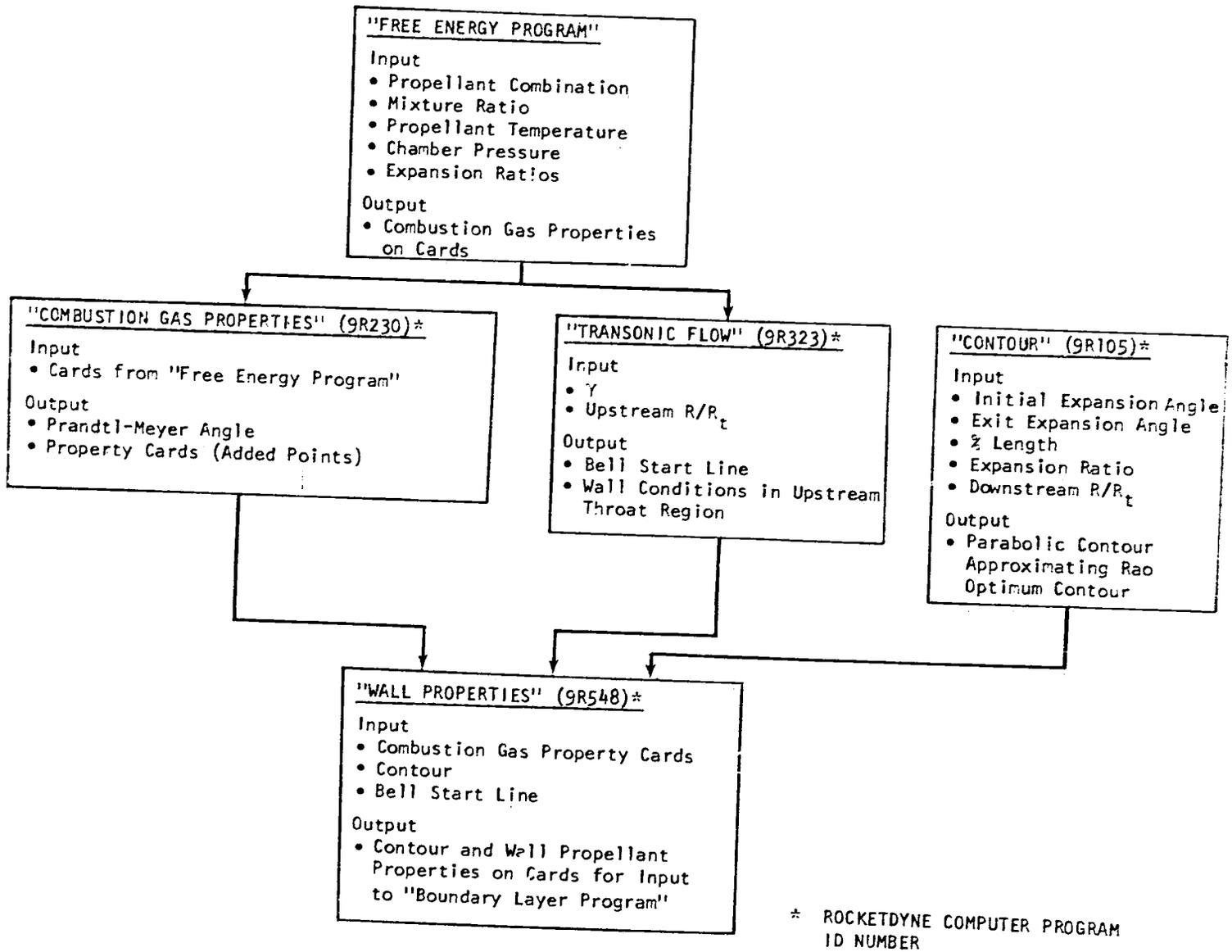

Figure 12. Nozzle Contour Analysis Methodology

Fatigue Damage Fraction

The fatigue damage fraction (ϕ_f) is the ratio of the number of design load cycles (η) to the number of load cycles required to cause failure (N_f):

$$\phi_f = \eta / N_f \tag{4}$$

where N_f is a function of the equivalent uniaxial strain range (ε_e) and the hot-gas surface temperature (T_{wg}). For channels, the equivalent uniaxial strain range is defined as:

$$\varepsilon_e = 2\, \varepsilon_{total}\, \beta \tag{5}$$

where β is a correction factor to correlate results with finite element analyses. From analyses of the ASE and SSME thrust chambers; this factor was determined to be 1.2 for NARloy-Z. The hot-gas surface axial or lateral strain range (ε_{total} is defined as the difference between the steady-state operating hot-gas surface strain (ε_{s-s}) and the initial hot-gas surface axial or lateral strain (ε_i):

$$\varepsilon_{total} = \varepsilon_{s-s} - \varepsilon_i \tag{6}$$

ε_{s-s} and ε_i are based on the hot-gas surface temperature (T_{wg}) and the closeout temperature (T_{bw}):

$$\varepsilon_{s-s} = \left[\alpha \Delta T_{wg} - \alpha \Delta T_{bw}\right]_{s-s} \tag{7}$$

$$\varepsilon_i = \left[\alpha \Delta T_{wg} - \alpha \Delta T_{bw}\right]_{i} \tag{8}$$

The temperature differences (ΔT) are measured from ambient temperature. The initial hot-gas wall and closeout temperatures are assumed to be halfway between the coolant inlet temperature and ambient temperature.

For tubes, the equivalent uniaxial strain range (ε_e) is defined as:

$$\varepsilon_e = 1.155 \left(\varepsilon_{total}^2 + \varepsilon_{total}\, \varepsilon_c + \varepsilon_c^2 \right)^{1/2} \tag{9}$$

where ε_c is one-half of the steady-state strain across the hot-gas wall:

$$\varepsilon_c = \frac{\alpha (T_{wg} - T_{wc})_{s\text{-}s}}{2} \tag{10}$$

Creep Damage Fraction

The creep damage fraction (ϕ_c) is the ratio of the number of design hours the load is applied (T) to the number of hours required to produce rupture (T_R) under the applied stress (σ):

$$\phi_c = T/T_R \tag{11}$$

For channels, the steady-state operating stress (σ) is defined as:

$$\sigma = \frac{(P_{coolant} - P_{hot\ gas})_{s\text{-}s}\ a^2}{2\ (0.9t)^2} \tag{12}$$

where a is the channel width and t is the hot-gas wall thickness.

For tubes, the operating stress is defined as:

$$\sigma = \frac{(P_{coolant} - P_{hot\ gas})_{s\text{-}s}\ r_i\ K}{0.9t} \tag{13}$$

where K is the thick wall tube factor for converting average hoop stress to outer wall stress:

$$K = \frac{2r_i}{r_o + r_i} \tag{14}$$

Structural Analysis

At the high chamber pressures (and high coolant pressures) to be evaluated, the structural integrity of the thrust chamber cooling passages must be analyzed to

ensure a realistic thrust chamber design. The stress analysis is the same for all materials but differs for tubes and channel passages.

For channels, the more critical stress, bending (σ) or shear (τ), is used to define the structural requirements:

$$\sigma = \frac{P_{coolant} a^2}{2(0.9t)^2}, \quad \tau = \frac{3}{2} \frac{P_{coolant} a}{2(0.9t)} \tag{15}$$

For tubes, the average hoop stress is used and is defined as:

$$\sigma = \frac{P_{coolant} r_i}{0.9t} \tag{16}$$

The yield and ultimate safety factors are defined as:

$$\text{Yield safety factor} = \frac{F_{ty}}{\sigma} \text{ or } \frac{0.6 F_{ty}}{\tau} \tag{17}$$

$$\text{Ultimate safety factor} = \frac{F_{tu}}{\sigma} \text{ or } \frac{0.6 F_{tu}}{\tau} \tag{18}$$

The tensile yield strength (F_{ty}) and the tensile ultimate strength (F_{tu}) are based on the average of the hot-gas temperature (T_{wg}) and the coolant side temperature (T_{wc}) of the wall. Yield safety factor of 1.1 and an ultimate safety factor of 1.5 are the requirements.

MATERIALS SELECTION

The materials selected for the combustion chamber and nozzle are discussed below. The properties of these materials are presented in Appendix A.

Combustion Chamber

A high thermal conductivity material is required for minimum wall temperature and minimum thermal strain. Maximum cyclic life demands a high-ductility material. Therefore, material requisites of high thermal conductivity and high ductility necessitates the selection of a compatible copper-base alloy. The strength of the material and heat transfer aspects dictate the coolant channel geometry, which influences the coolant pressure drop, engine weight, life, manufacturing requirements, and cost. It is desirable to have a high-strength material. NARloy-Z, a zirconia-silver- copper alloy, was developed by Rocketdyne for the SSME main combustion chamber liner. It exceeds the life requirements and possesses a relatively higher strength than other commercially available copper base alloys.

Therefore, NARloy-Z was selected as the combustion chamber material. The structural and cyclic life data for the NARloy-Z is shown in Fig. 44 through 47 (Appendix A). The thermal expansion for Inconel 718 (to be considered as the chamber jacket material) is shown in Fig. 48. These data were incorporated into the Regenerative Cooling Design/Analysis Computer Program for the cyclic life evaluation during the chamber cooling analysis.

NARloy-Z thermal conductivity data is shown in Fig. 49. This figure contains a scale showing the NARloy-Z thermal conductivity as a percentage of the thermal conductivity of room temperature OFHC copper. The temperature-dependent curve in Fig. 49 is incorporated into the two-dimensional channel wall temperature distributions that are provided by the Regenerative Cooling Design/Analysis Computer Program.

Nozzle

Wrought A-286 was selected as the nozzle material. This material was also selected for the SSME nozzle. It is a moderate strength, heat-resisting alloy, a high-strength alloyed stainless steel hardenable by solution treating and aging. The alloy is always used in the hardened condition. The material is entirely satisfactory for use at all cryogenic temperatures down to 21 K (37 R) with retention of excellent toughness and ductility properties. At elevated temperatures, the alloy retains moderate strength up to 922 K (1660 R). The alloy is readily formable in the annealed or solution-treated condition. The structural and cyclic life data for A-286 is shown in Fig. 50 through 53. Figure 54 shows the thermal conductivity for A-286. The data in Fig. 50 through 54 have been incorporated as input to the Regenerative Cooling Design/Analysis Computer Program for the structural and cyclic life analyses for the nozzle cooling evaluation.

COMBUSTION GAS HEAT TRANSFER

The Rocketdyne Boundary Layer Computer program is used to calculate the hot-gas heat transfer coefficient profiles for the chamber and nozzle designs. This program utilizes an integral method to solve the momentum and energy equations. Solution of these equations is accomplished using a semiempirical relation between The Stanton number and the energy thickness and between the skin friction coefficient and momentum thickness. The resulting equation for turbulent flow is of the form:

$$N_{ST_\infty} = \frac{0.0122}{(Re_\phi)^{0.25}} \left(\frac{\rho_\infty}{\rho_r}\right)^{1/2} \left(\frac{\mu_r}{\mu_\infty}\right)^{1/4} \frac{1}{N_{Pr}^{2/3}} \qquad (19)$$

The convective film coefficient (h_g) is then found from the relation:

$$h_g = \rho_\infty U_\infty C_p N_{ST_\infty} \qquad (20)$$

The Eckert reference temperature is used to evaluate the film properties.

The injector end heat transfer coefficient for any given case is determined by scaling calorimeter chamber test data from the SSME 40K subscale chamber test program (Ref. 2) using flowrate and property corrections based on the standard Nusselt Number correlation:

$$h_g)_2 = h_g)_1 \frac{k_2}{k_1} \left(\frac{G_2}{G_1} \times \frac{\mu_1}{\mu_2}\right)^{0.8} \left(\frac{Pr_2}{Pr_1}\right)^{0.4} \qquad (21)$$

where subscript 1 = reference conditions (40K subscale test data)
subscript 2 =- O_2/hydrocarbon conditions

This injector end heat transfer coefficient is then blended into the axial profile derived from the boundary layer program. An example of this is shown in Fig. 13.

The combustion hot-gas convective heat transfer coefficient (hg) profile is shown in Appendix C for the unenhanced designs and in Appendix D for the enhanced designs. The combustion gas properties are presented in Appendix B for the chamber pressure and mixture ratio ranges of this study.

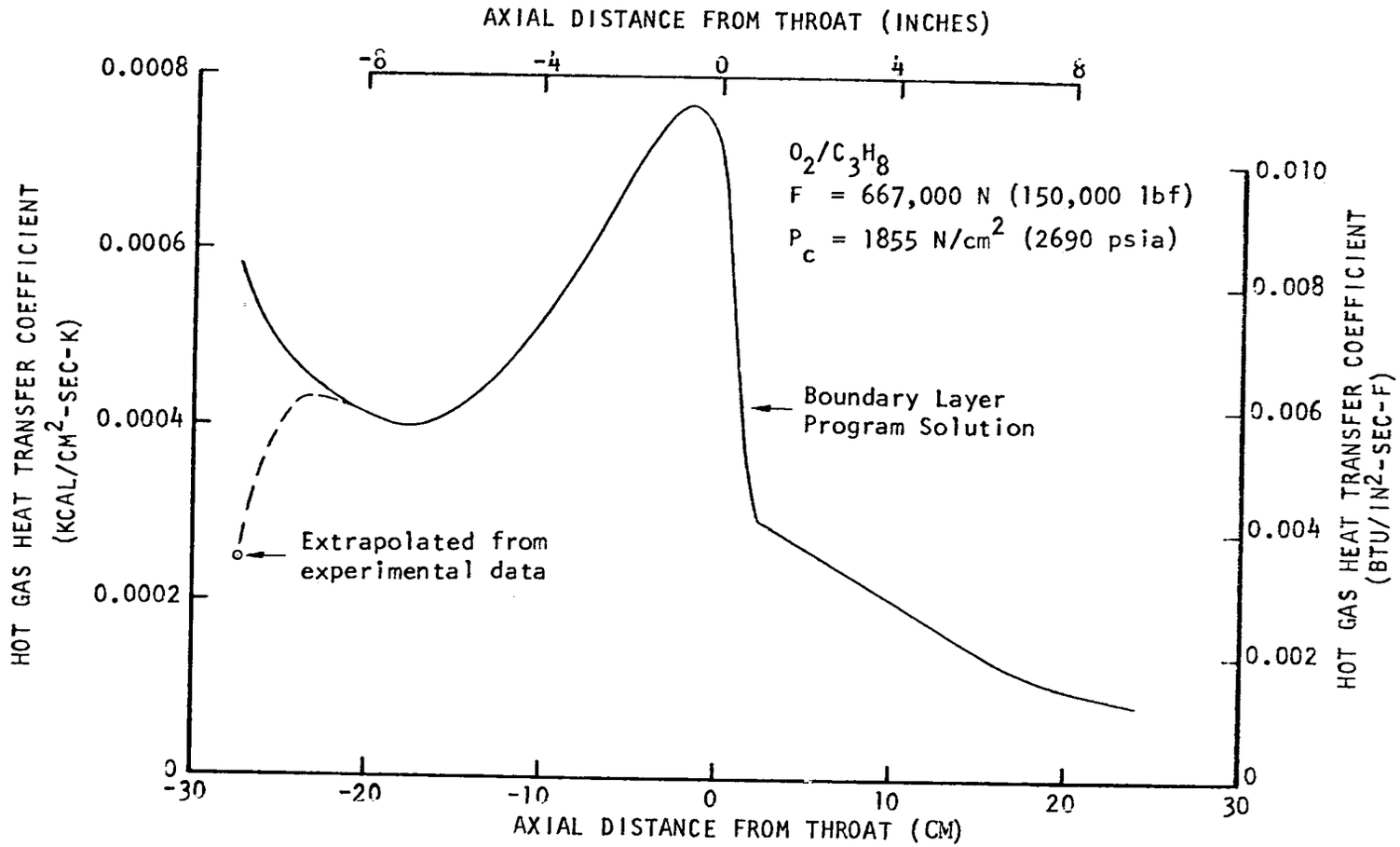

Figure 13. Hot-Gas Heat Transfer Coefficient Profile

COOLING CORRELATIONS

Rocketdyne has considerable experience in RP-1 cooling through its successful rocket engine programs that use RP-1 as a coolant (Atlas, Thor, H-1, F-1, etc.). In support of these programs, Rocketdyne has made analytical studies and done extensive testing to determine the cooling characteristics of RP-1 (Ref. 3, 4, and 5). From this work, the following cooling correlation for RP-1 was developed:

$$h_c = 0.0056\ (k/D_h)\ Re^{0.95}\ Pr^{0.4}\ \phi_R \qquad (22)$$

ϕ_R is the roughness enhancement factor and is determined by taking the ratio of the ε/D_h of the passage to friction factor for an ε/D_h of 0.0001.

The standard Nusselt number correlation with the roughness enhancement factor included is used for methane cooling:

$$h_c = 0.023\ (k/D_h)\ Re^{0.8}\ Pr^{0.4}\ \phi_R \qquad (23)$$

A Rocketdyne company-funded task to evaluate hydrocarbon coolants has resulted in the following cooling correlation for propane:

$$h_c = 0.00696\ (k/D_h)\ Re^{0.88}\ Pr^{1.2}\ (T_c/T_{wc})^{1.0}\ \phi_R \qquad (24)$$

This experimental cooling correlation is compared with the standard Nusselt number correlation in Fig. 14. This figure was generated for a propane pressure of 2760 N/cm^2 (4000 psia) and a Reynolds number of 7 x 10^5 which are representative of the values encountered in this study. The bulk-to-wall temperature correction (T_c/T_{wc}) in the experimental correlation causes the experimental correlation to decrease relative to the standard correlation as the coolant wall temperature (T_{wc}) increases. The 733 K (1320 R) coolant wall temperature curve is the propane decomposition limit used in this study. To compare the equations at Reynolds numbers different than 7 x 10^5, the curves can be ratioed by the factor $(Re/7 \times 10^5)0.08$.

The coolant curvature enhancement factor profile as a function of turning angle is shown in Fig. 15. This is the same profile as is used for the SSME main combustion chamber. The curvature enhancement factor has been limited to a maximum value of 1.4 (same limitation as for the SSME and ASE combustors). For the two-dimensional channel wall temperature distribution analyses, the full curvature enhancement value is used on the coolant side of the hot-gas wall. This value is linearly varied along the side walls (channel height) of the coolant channel to unity at the closeout surface. A value of 1 is used along the closeout surface.

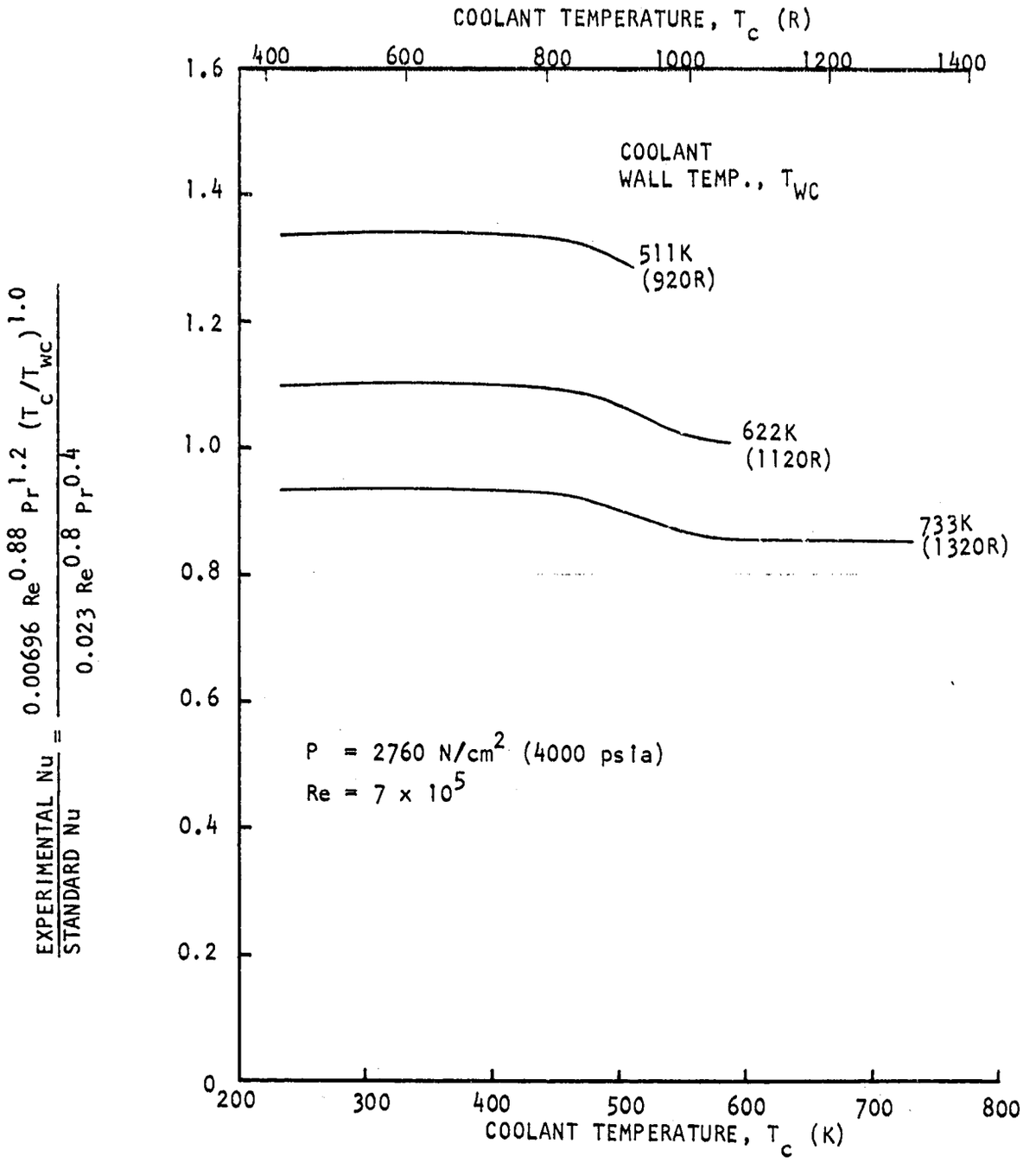

Figure 14. Comparison of Propane Experimental Cooling Correlation With Standard Nusselt Number Correlation

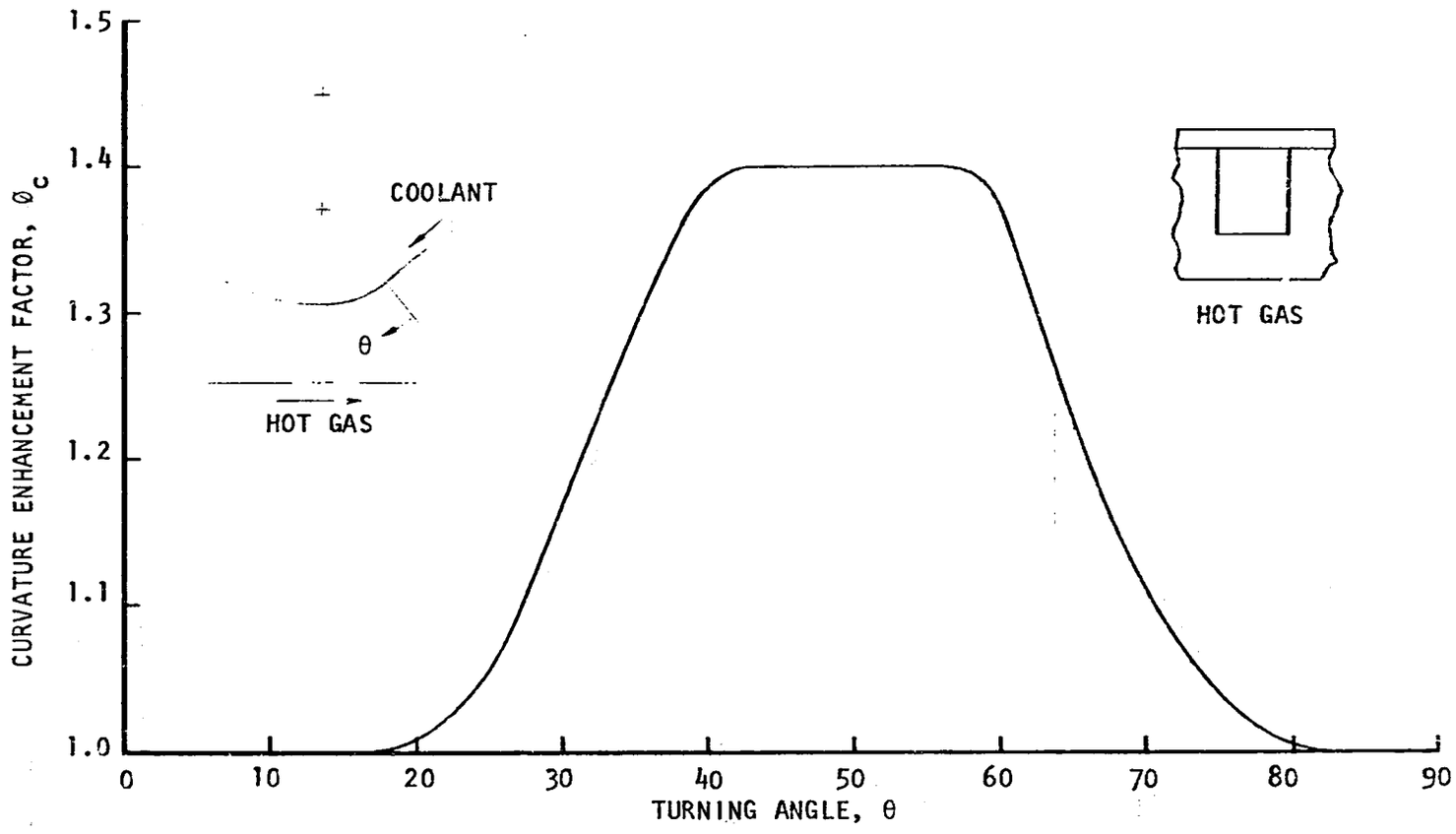

Figure 15. Curvature Enhancement Factor Profile

The curvature enhancement of hot-gas heated channel configured coolant passages were evaluated during the early phases of the SSME program (Ref. 6). The channel geometry was identical to the SSME combustor, which is typical of those used for this study. The results of these experimental studies verified the empirical relationships used for the SSME (Ref. 6). The curvature enhancement experimental data were correlated based on the above-noted two-dimensional distribution criteria used for this study. The curvature enhancement techniques used for the SSME combustor and this study are slightly conservative relative to the experimental results of Ref. 6 .

UNENHANCED DESIGN COOLING ANALYSIS AND RESULTS

INFLUENCE OF THRUST LEVEL

Low Thrust Designs - 89,000N (20,000 lbf)

Because of the small amount of fuel available for cooling relative to the hot-gas surface area, a series circuit using all of the fuel is utilized to minimize the coolant temperature rise in the combustion chamber. The combustion chamber is cooled first in an uppass, then the nozzle is cooled in a downpass. Normally, the most efficient cooling is ensured by using the minimum allowable channel width (CW) of 0.0762 cm (0.03 in.) and the maximum number of channels. The minimum allowable land width (LW) of 0.0762 cm (0.03 in.) is generally used in the throat along with the minimum channel width to obtain the maximum number of channels. The minimum wall thickness value of 0.0635 cm (0.025 in.) typically used throughout the combustion chamber, which does not present a heat transfer problem, is increased to minimize coolant pressure drop.

Because of the low coolant flowrate, small-diameter tubes and a high chamber-to-nozzle attachment area ratio must be used to keep the nozzle coolant velocity high enough relative to the local heat flux to meet the cycle life requirement. The minimum attachment area ratio that meets the above criteria is 10:1. The unformed tube diameter (UTD) and wall thickness at this location are minimal. A variable wall thickness (WT) is required to keep the coolant wall temperature below the decomposition T_{wc} limit. The nozzle is split at an area ratio of 180:1. The nozzle extension goes from ε = 180:1 to ε = 400:1.

Because the total fuel flowrate is small, the nozzle extension section cannot be dump cooled and, hence, also is regeneratively cooled. In calculating the series pressure drop, one velocity head was assumed to be lost at both chamber outlet and the nozzle inlet to account for parasitic losses.

Intermediate Thrust Designs-667,000 N (150,000 lbf)

The intermediate thrust designs are similar to the low thrust designs, As with the low thrust designs, a series coolant circuit (uppass chamber, downpass nozzle) using all of the fuel maximizes the chamber pressure that can be regeneratively cooled. However, the channel size must be slightly greater than the minimum allowable to accommodate the coolant flow. The minimum allowable wall thickness of 0.0635 cm (0.025 in.) is used throughout the combustion chamber length, similar to the low thrust designs.

Cooling of the nozzle is not a significant problem. However, the chamber-to-nozzle attachment area ratio must be selected to maximize the chamber pressure that can be cooled. Because of the series cooling circuit, this involves trading off the increased nozzle pressure drop when decreasing the attachment area ratio (due to higher velocity required for cooling) with the increased chamber pressure drop when increasing the attachment area ratio (due to the increased coolant temperature). The area ratio optimizes at a value of 10:1, the same as for low thrust designs.

High Thrust Designs - 2,669,000 N (600,000 lbf)

At this thrust level, there is so much coolant flow available that only a fraction of the fuel can be used for cooling the chamber while maintaining reasonable channel dimensions. A split flow (uppass chamber, downpass nozzle) cooling circuit is required with approximately 50% of the available coolant going to the chamber and the remaining 50% to the nozzle. The channel width must be optimized by trading off the increased flowrate (decreased coolant temperature and increased average coolant density) with the decreased cooling efficiency as the channel width is increased. A throat region and combustion zone channel width of approximately 0.1397 cm (0.055 in.) was determined to be optimum. To minimize the pressure drop, a channel width of approximately 0.2286 cm (0.09 in.) is used in the low expansion ratio section of the chamber. The channel wall thickness is adjusted to accommodate the increased channel widths.

The chamber-to-nozzle attachment area ratio is decreased to 5:1. Meeting the cycle life in the nozzle becomes increasingly difficult if the attachment area ratio is decreased beyond this value. The nozzle minimum unformed tube diameter at the attachment point is reduced to accommodate the higher heat flux at the lower area ratio, compared to the low thrust and intermediate thrust designs.

INFLUENCE OF ENGINE CYCLE

The staged combustion (SC) cycle operates at a coolant $P_{inlet}/P_c = 2.25$, which the gas generator (GG) cycle uses a coolant $P_{inlet}/P_c = 1.8$. This requires an adjustment to channel and tube wall thickness to accommodate the higher pressure gradient across the wall for staged combustion designs, otherwise, the cooling rationale used for gas generator cycle designs is analogous for SC designs. It will be shown later in the Design Results section that the chamber pressure limits of the two cycles considered are within 3% at all thrust levels.

Both engine cycles used a series flow circuit for the low and intermediate thrust levels. Both cycles used nearly a 50/50% flow split for the high thrust level designs.

INFLUENCE OF PROPELLANT COMBINATION

The unenhanced hot-gas convective heat transfer is similar for all three propellant combinations. Therefore, their chamber pressure limits, and coolant passage geometry are derived from the fuel cooling capabilities. This study resulted in design similarities between all three propellant combinations. However, for the O_2/RP-1 propellant combination, the RP-1 decomposition temperature is very low. Because of this low coking temperature limit, the cooling of O_2/RP-1 designs without a carbon layer enhancement is virtually impossible within the design guidelines. Therefore, a parametric study was conducted to see if either the "short chamber" (gas-liquid injection) or the "long chamber" (liquid-liquid injection) could be realistically cooled without enhancement at an energy release efficiency of 98%. This study showed that only the "short

chamber" design at the high thrust level could be cooled above 6895 N/cm^2 (1000 psia). None of the lower thrust levels could be cooled above 6895 N/cm^2 (1000 psia). The increased heat load and coolant pressure drop of the "long chamber" provided lower cooling limits than the "short chamber".

The use of a short chamber" for the O_2/RP-1 propellant combination would represent the combustor configuration of a staged-combustion cycle. The combustor configuration for a gas generator cycle would be a "long chamber" for typical injector configurations. However, a micro-orifice-type injector could probably be developed for 98% energy release efficiency using a "short chamber" for a gas generator cycle liquid-liquid injector.

DESIGN RESULTS

The results of the unenhanced regeneratively cooled limit designs are presented in Table 4. The maximum chamber pressure as a function of thrust is shown in Fig. 16. Individual chamber and nozzle designs are graphically presented in Appendix C.

Significant results of this study are:

1. O_2/RP-1 design cooling limits are at very low chamber pressures as dictated by a limiting RP-1 coolant decomposition temperature at T_{wc} ≤589 K (1060 R). The O_2/RP-1 cooling limit chamber pressure decreases with a decrease in thrust. These designs are not life-limited.

2. The cooling limit chamber pressure of the O_2/CH_4 and O_2/C_3H_8 designs decreases with an increase in thrust. These designs are life-limited, but are not limited by a decomposition temperature.

3. The chamber pressure limits slightly favor a gas generator cycle for the O_2/CH_4 designs and a staged combustion cycle for the O_2/C_3H_8 designs.

The noted results are discussed below.

The O_2/RP-1 designs limited by the allowed coolant wall temperature (T_{wc}) favor the large thrust level. This is because the propellant flowrate and, therefore, the coolant flowrate to total heat load and surface area ($\dot{W}_c/Q$), is the largest. This is typical of all chamber designs. To maintain a limited T_{wc}, the coolant bulk temperature (T_b) must be approximately 140 K (250 R) lower than the T_{wc} at the chamber injector end and/or 55 K (100 R) lower than the T_{wc} at the nozzle exit. Therefore, the lower thrust level designs are at lower chamber pressure. A split coolant flow circuit for the low thrust designs would be at a lower chamber pressure than for a series circuit. These T_{wc} limited designs are not life-limited.

The life-limited O_2/RP-1, O_2/CH_4, and O_2/C_3H_8 designs result in an increased chamber pressure with a decreased thrust level. This is not typical since the $(\dot{W}_c/Q)$ trend favors the higher thrust level for cooling, as reflected for the T_{wc} limited O_2/RP-1 designs. One basic reason the O_2/CH_4 and O_2/C_3H_8 designs reflect reverse trends is related to a constant low cycle fatigue life criterion. These curves do not reflect a constant coolant wall or hot-gas wall temperature.

TABLE 4. SUMMARY OF HIGH-PRESSURE HYDROCARBON-FUELED ENGINE REGENERATIVE COOLING LIMITS

Metric Units

	Propellant Combination	Thrust (Newtons)	Coolant P_{in}/P_c	Max. P_c (Newton/cm^2)	P_c Limiting Factor	Cooling Circuit	Chamber-to-Nozzle ε	Minimum LW (cm)	Channel Width (cm)	Channel Wall Thickness (cm)	Nozzle Min. UTD (cm)	Nozzle Min. Wall Thk. (cm)
	O_2/C_3H_8	89,000 vac	1.8	2070	T_{wg}, T_{wc}, Life	Series	10:1	0.076	0.102/0.076	0.064	0.152/0.434	0.023
	O_2/C_3H_8	89,000 vac	2.25	2140	T_{wg}, T_{wc}, Life	Series	10:1	0.076	0.102/0.076	0.064	0.152/0.434	0.023
	O_2/C_3H_8	667,000 vac	1.8	1850	Life	Series	10:1	0.076	0.127/0.086/0.127	0.064	0.267/0.434	0.023/0.051
	O_2/C_3H_8	667,000 vac	2.25	1900	Life	Series	10:1	0.076	0.127/0 086/0.127	0.064	0.267/0.434	0.023/0.051
	O_2/C_3H_8	2,669,000 s.l.	1.8	1590	Life	Split	5:1	0.076	0.229/0.140	0.102/0.064	0.203	0.025
	O_2/C_3H_8	2,669,000 s.l.	2.25	1610	Life	Split	5:1	0.076	0.229/0.140	0.102/0.066	0.203	0.025
	O_2/CH_4	89,000 vac	1.74**	2760	Life	Series	12:1	0.076	0.102/0.076	0.064	0.178/0.432	0.020/0.076
	O_2/CH_4	89,000 vac	2.15**	2760	Life	Series	12:1	0.076	0.102/0.076	0.089/0.064	0.178/0.432	0.020/0.076
	O_2/CH_4	667,000 vac	1.8	2620	Life	Series	10:1	0.076	0.127/0.086/0.127	0.089/0.064	0.267/0.434	0.025/0.051
	O_2/CH_4	667,000 vac	2.25	2560	Life	Series	10:1	0.076	0.127/0.086/0.127	0.102/0.064/0.076	0.267/0.434	0.025/0.051
	O_2/CH_4	2,669,000 s.l.	1.8	2140	Life	Split	5:1	0.076	0.229/0.140	0.114/0.064	0.203	0.020
	O_2/CH_4	2,669,000 s.l.	2.25	2070	Life	Split	5:1	0.076	0.229/0.140	0.140/Variable	0.203	0.020
"S"	O_2/RP-1	2,669,000 s.l.	1.8	1586	Life	Split	5:1	0.076	0.229/0.140	0.102/0.069	0.178	0.020
"L"	O_2/RP-1	2,669,000 s.l.	1.8	1180 *	Life, T_{wg}	Split	5:1	0.076	0.229/0.140	0.102/0.064	0.203	0.025
"S"	O_2/RP-1	2,669,000 s.l.	1.8	896	T_{wc}	Split	5:1	0.076	0.229/0.140	0.089/0.069	0.190	0.025

* T_{wc} LIMIT IGNORED

** REDUCED COOLANT P_{in}/P_c

"S" = SHORT CHAMBER
"L" = LONG CHAMBER

TABLE 4. (Concluded)

English Units

	Propellant Combination	Thrust (lbf)	Coolant P_{in}/P_c	Max. P_c (psia)	P_c Limiting Factor	Cooling Circuit	Chamber-to-Nozzle ε	Minimum LW (in)	Channel Width (in)	Channel Wall Thickness (in)	Nozzle Min. UTD (in)	Nozzle Min. Wall Thk. (in)
	O_2/C_3H_8	20,000 vac	1.8	3000	T_{wg}, T_{wc}, Life	Series	10:1	0.03	0.04/0.03	0.025	0.06/0.171	0.009
	O_2/C_3H_8	20,000 vac	2.25	3100	T_{wg}, T_{wc}, Life	Series	10:1	0.03	0.04/0.03	0.025	0.06/0.171	0.009
	O_2/C_3H_8	150,000 vac	1.8	2690	Life	Series	10:1	0.03	0.05/0.034/0.05	0.025	0.105/0.171	0.009/0.02
	O_2/C_3H_8	150,000 vac	2.25	2750	Life	Series	10:1	0.03	0.05/0.034/0.05	0.025	0.105/0.171	0.009/0.02
	O_2/C_3H_8	600,000 s.l.	1.8	2300	Life	Split	5:1	0.03	0.09/0.055	0.04/0.025	0.08	0.01
	O_2/C_3H_8	600,000 s.l.	2.25	2340	Life	Split	5:1	0.03	0.09/0.055	0.044/0.026	0.08	0.01
	O_2/CH_4	20,000 vac	1.74**	4000	Life	Series	12:1	0.03	0.04/0.03	0.025	0.07/0.170	0.008/0.03
	O_2/CH_4	20,000 vac	2.15**	4000	Life	Series	12:1	0.03	0.04/0.03	0.035/0.025	0.07/0.170	0.008/0.03
	O_2/CH_4	150,000 vac	1.8	3800	Life	Series	10:1	0.03	0.05/0.034/0.05	0.035/0.025	0.105/0.171	0.01/0.02
	O_2/CH_4	150,000 vac	2.25	3720	Life	Series	10:1	0.03	0.05/0.034/0.05	0.04/0.025/0.03	0.105/0.171	0.01/0.02
	O_2/CH_4	600,000 s.l.	1.8	3110	Life	Split	5:1	0.03	0.09/0.055	0.045/0.025	0.08	0.008
	O_2/CH_4	600,000 s.l.	2.25	3000	Life	Split	5:1	0.03	0.09/0.055	0.055/Variable	0.08	0.008
"S"	O_2/RP-1	600,000 s.l.	1.8	2300	Life	Split	5:1	0.03	0.09/0.055	0.04/0.027	0.07	0.008
"L"	O_2/RP-1	600,000 s.l.	1.8	1710*	Life, T_{wg}	Split	5:1	0.03	0.09/0.055	0.04/0.025	0.08	--
"S"	O_2/RP-1	600,000 s.l.	1.8	1300	T_{wc}	Split	5:1	0.03	0.09/0.055	0.035/0.027	0.075	0.01

* T_{wc} LIMIT IGNORED

** REDUCED COOLANT P_{in}/P_c

"S" = SHORT CHAMBER

"L" = LONG CHAMBER

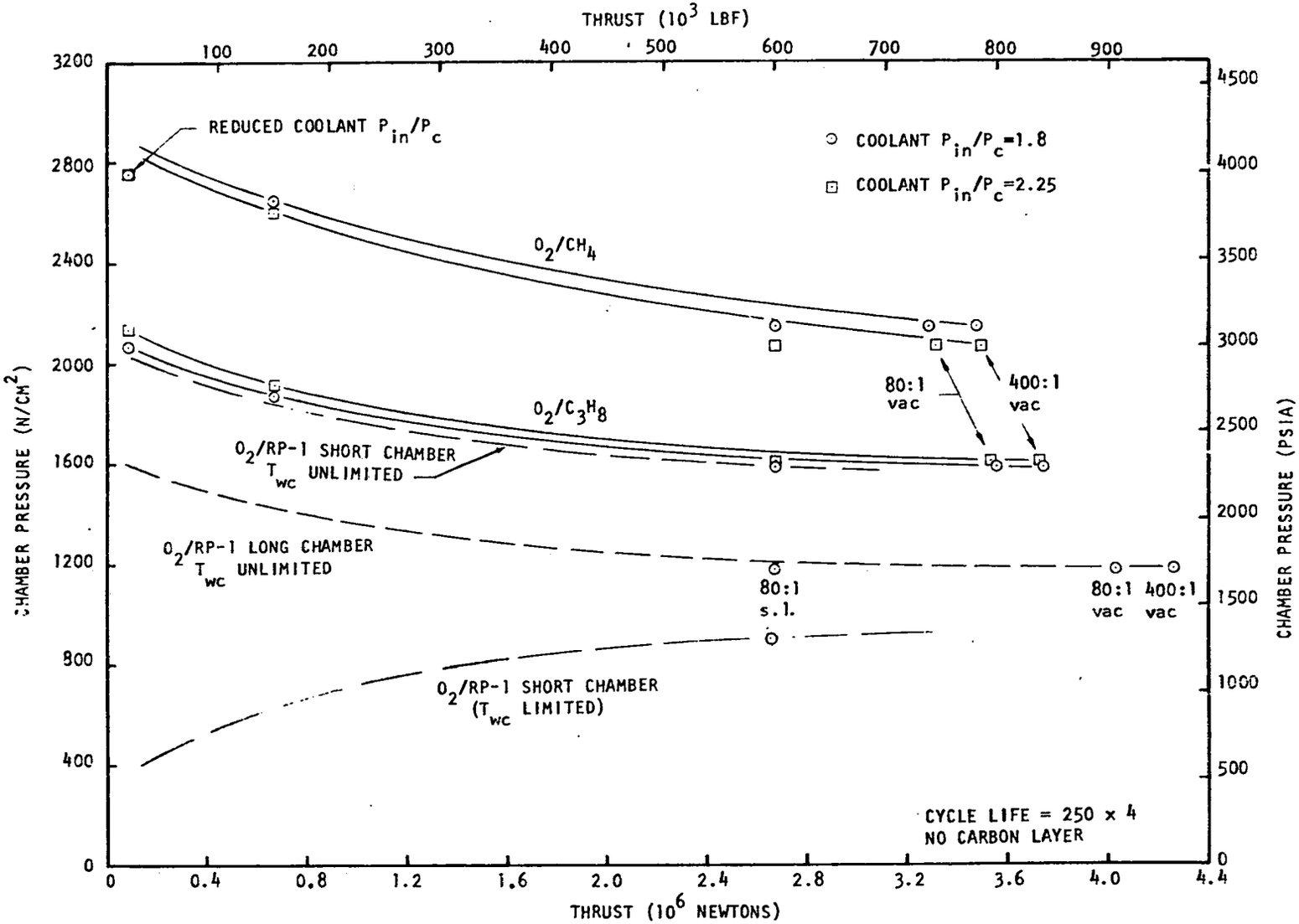

Figure 16. Effect of Thrust on Regenerative Cooling Limit (unenhanced designs)

For a constant life, the low thrust designs operate at higher T_{wg} because of the higher bulk temperature in the high heat flux regions. This higher T_{wg} is acceptable if its within the guideline temperature, which is true. Cyclic life is a function of the temperature gradient between the hot-gas wall (T_{wg}) and the closeout structure backwall temperature (T_{bw}), which is approximately the bulk temperature (T_b). Therefore, cyclic life (4 x 250) is met for all thrust levels but requires lower T_{wg} for the higher thrust designs because of the lower coolant temperature in the throat and convergence region of the chamber. Another contributor for the reversed P_c versus F trend is the combustion chamber length (injector to throat) and contraction area ratio criteria to attain a 98% energy release efficiency. These criteria result in a combustor (injector to throat) average heat flux ($\overline{Q/A}$) decrease for the lower thrust designs.

As shown in Fig. 16, the O_2/CH_4 designs favor a gas generator cycle, while the O_2/C_3H_8 designs favor a staged combustion cycle. This reversal is also a function of the limiting criteria. This condition is forced by the minimum allowable wall thickness. If this were not a limiting criterion, the gas generator cycle would be favored. This is because the lower chamber pressure O_2/C_3H_8 designs could meet the ultimate and yield safety factors with a wall thickness less than the limit criterion of 0.064 cm (0.025 in.).

ENHANCED DESIGN TECHNIQUES, ANALYSIS, AND RESULTS

Three physical thermal barriers and three fluid thermal barriers were evaluated plus one "other." The "other" thermal barrier was a combination of two of the above-noted heat barriers.

The physical barriers considered for cooling enhancement were carbon-layer, ceramic coating (ZrO_2), and ATJ graphite liner. These are applied to the parent material hot-gas-wall surface as thermal resistances. These thermal barriers were not applied to the tubular nozzle, except as required for some O_2/RP-1 nozzles to maintain a $T_{wc} \leq 600$ F. These thermal barriers were utilized for the channel constructed combustion chamber. The reasons for using unenhanced nozzles are as follows:

1. The nozzle coolant ΔP is low compared to the combustion chamber ΔP. Therefore, cooling enhancement techniques applied to the nozzle will not significantly increase the chamber pressure limit.
2. The adherance of a physical barrier to the smooth surface of the combustion chamber is more practical than to a tubular nozzle surface. This can be realized by the fact that the breakdown of physical barriers is typically comprised of flaking of the carbon layer or ceramic coating. This flaking or cracking is caused by large thermal strains across the thermal barrier and stress deformations caused by flexing of the parent material structure. The thermal strains of a channel wall are nearly equal biaxial strains in a transverse and longitudinal direction. The thermal strains of a tubular construction are biaxial, but are not equal in a transverse and longitudinal direction. This can be realized by the fact that part of the transverse thermal strain of a tubular nozzle is relieved by the flexing of the tube hot surface which is unrestrained. The latter mechanical strain contributes significantly to the physical barrier adherance.
3. The application of a graphite liner to a tubular construction is impractical and ceramic coating application may be limited.

The fluid thermal barriers considered for cooling enhancement were film cooling, transpiration cooling, and zoned combustion. All three fluid barriers were allotted a 3% performance loss. For reason No. 1 noted above, the associated nozzle designs were not enhanced.

A design matrix of the regenerative cooling analyses conducted for the enhanced designs is presented in Table 5 . The gas generator cycle was utilized for these designs since there is no significant difference between it and the staged combustion cycle for this study. The gas generator cycle operates at lower coolant inlet pressures where the coolant properties are better known.

TABLE 5. COOLING ENHANCEMENT ENGINE DESIGN MATRIX

Propellants	RP-1						CH_4						C_3H_8					
Thrust, NEWTONS (LBF)	89,000 (20,000)		667,000 (150,000)		2,669,000 (600,000)		89,000 (20,000)		667,000 (150,000)		2,669,000 (600,000)		89,000 (20,000)		667,000 (150,000)		2,669,000 (600,000)	
P_{in}/P_c	1.8	2.25	1.8	2.25	1.8	2.25	1.8	2.25	1.8	2.25	1.8	2.25	1.8	2.25	1.8	2.25	1.8	2.25
Fluid Barriers																		
Film Cooling	□	○	○	○	□	○	○	○	□	○	□	○	□	○	○	○	□	○
Transpiration							○	○	□	○	□	○	□	○	○	○	□	○
Zoned Combustion	□	○	○	○	□	○	○	○	□	○	□	○	□	○	○	○	□	○
Physical Barriers																		
Carbon Layer	□	○	○	○	□	○	□	○	□	○	□	○	□	○	○	○	□	○
Ceramic Coating	□	○	○	○	□	○	○	○	□	○	□	○	□	○	○	○	□	○
Liner	□	○	○	○	□	○	○	○	□	○	□	○	□	○	○	○	□	○
Other	□	○	○	○	□	○	○	○	□	○	□	○	□	○	○	○	□	○
Sensitivity Studies																		
Cyclic Life											□							
RP-1 T_{wc}					□													

□ Detailed Regenerative Cooling Analysis Conducted to Establish Increase in Max P_c

○ Max P_c Estimated by Scaling Results from Detailed Regenerative Cooling Analysis

CARBON LAYER

A carbon coating was selected as the renewable physical thermal barrier.

Assessment

Reference 7 describes the interior of an O_2/RP-1 chamber after firing as having the appearance of being freshly painted black. Inspection reveals that the outer surface of the layer is sooty and can be easily removed by light rubbing. Underneath this soot layer is a harder graphite-like layer that can also be removed, but is more tenatious.

The mechanism of deposition of the carbon layer on the wall is not fully understood. The elemental carbon is formed by cracking of the fuel. Evidence exists from thermocouple measurements (Ref. 7) that the carbon layer builds up during the first few seconds of operation and then undergoes periodic spalling due to thermal and dynamic stresses until an equilibrium value is achieved. Unfortunately, these fluctuations are most pronounced in the throat region, which is usually the critical area from a thermal design standpoint.

A number of factors appear to influence the amount of carbon layer buildup. Among them are:

- Chamber pressure
- Mixture ratio
- Type of fuel
- Injector design
- Amount of film cooling
- Wall temperature

Reference 8 contains combustion chamber heat load data for FLOX/methane, FLOX/propane, and FLOX/butene-1 propellants over a range of mixture ratios. These data have been reviewed to determine if the effect of fuel type and mixture ratio on the carbon layer can be quantitatively correlated. These data are presented in Table 6. From the predicted and measured heat load data in Table 6, the average carbon layer resistance for each test was calculated in the following manner:

1. The predicted average heat flux in the combustion chamber was calculated by dividing the predicted heat load by the chamber surface area (calculated to be 3003 cm^2, 465.5 $in.^2$).

2. A predicted average heat transfer coefficient was calculated by dividing the average heat flux by an assumed hot gas-to-wall average ΔT of 2778 K (5000 F).

3. From the ratio of measured to predicted heat load and the average heat transfer coefficient, the average carbon layer resistance (x/k) was determined from the following equation:

$$\frac{\text{Measured } Q}{\text{Predicted } Q} = \frac{\left(\frac{\bar{x}}{k} + \frac{1}{\bar{h}_g}\right)^{-1} A \ \Delta\bar{T}}{\bar{h}_g \ A \ \Delta\bar{T}} \qquad (25)$$

These results are given in Table 6 . It was found that the carbon layer resistance correlated best with the carbon atom fraction in the combustion gas, as shown in Fig. 17. A least-squares parabolic curve fit to the data is shown. By correlating with the carbon atom fraction the carbon layer resistance can be determined for any hydrocarbon fuel at any mixture ratio. The injectors for the study presented in Table had fuel coolant holes around the periphery through which approximately 5% of the fuel flowed. The effect this has on the carbon layer cannot be determined from the data.

The tests in Table 6 were all run at a chamber pressure of approximately 69 N/cm^2 (100 psia). The average mass velocity in the combustion chamber is approximately 0.015 kg/cm^2-sec (0.21 $lbm/in.^2$-sec). Rocketdyne has developed a correlation for carbon layer resistance as a function of the combustion gas mass velocity (Ref. 3). This correlation is shown in Fig. 18 (the dashed line). The test data in Fig. 18 are for O_2/RP-1 propellants. Additionally, a large amount of film cooling (>10%) was used during the tests. The carbon layer resistance for each of the three propellant combinations at their respective mixture ratios is taken from Fig. 17 and plotted in Fig. 18 at a mass velocity of 0.015 kg/cm^2-sec (0.21 $lbm/in.^2$-sec). Lines are then extended from these three points parallel to the Rocketdyne-developed curve. The Rocketdyne experimental carbon layer resistances are believed to be high because of the excessive amount of film coolant. In equation form, the correlations from Fig. 18 are:

- O_2/RP-1, MR = 2.8 $x/k = e^{(11.7 - 7.26G)}$
- O_2/C_3H_8, MR = 3.1 $x/k = e^{(10.9 - 7.26G)}$
- O_2/CH_4, MR = 3.5 $x/k = e^{(9.6 - 7.26G)}$

where G is in kg/cm^2-sec and x/k is in cm^2-sec-K/kcal. In the English system of units,, the equations are:

- O_2/RP-1, MR = 2.8 $x/k = e^{(9.0 - 0.51G)}$
- O_2/C_3H_8, MR = 3.1 $x/k = e^{(8.2 - 0.51G)}$
- O_2/CH_4, MR = 3.5 $x/k = e^{(6.9 - 0.51G)}$

where G is in $lbm/in.^2$-sec and x/k is in $in.^2$-sec-R/Btu.

There is a considerable amount of uncertainty in these equations, particularly when they are applied at high chamber pressures. However, until addtional data become available, the solid lines of Fig. 18 represent the best available measure of the effectiveness of carbon layers.

TABLE 6. PRATT & WHITNEY CARBON LAYER DATA

Test No.	Injector	Fuel	Mixture Ratio	% F_2 in Oxidizer	Carbon Atom Fraction	Predicted Q (Kcal/Sec)	Meas. Q / Pred. Q	Predicted $\overline{Q/A}$ (Kcal/cm^2-Sec)	Predicted $\bar{h}_g$ (10^{-5} Kcal/cm^2-Sec-K)	Carbon Layer Resistance (cm^2-Sec-K/Kcal)
6	S(1)	Methane	6.26	82.6	0.0958	221	0.941	0.0736	2.65	2370
7	"	"	5.87	"	0.0990	225	0.866	0.0749	2.70	5730
11	"	"	5.98	"	0.0980	183	1.050	0.0609	2.19	-2170
2UA	R(1-C)	"	4.54	"	0.1117	201	0.895	0.0669	2.41	4870
3UA	"	"	5.16	"	0.1054	186	0.910	0.0619	2.23	4440
4UA	"	"	4.17	"	0.1159	198	0.847	0.0659	2.37	7620
5UA	"	"	3.81	"	0.1203	205	0.707	0.0683	2.46	16850
6UA	"	"	3.57	"	0.1234	213	0.637	0.0709	2.55	22350
7UA	"	"	3.85	"	0.1198	184	0.758	0.0613	2.21	14450
8UA	"	"	3.67	"	0.1221	188	0.728	0.0626	2.25	16610
9UA	"	"	4.00	"	0.1179	205	0.716	0.0683	2.46	16120
10UA	"	"	4.96	"	0.1074	193	0.712	0.0643	2.31	17510
11UA	"	"	5.99	"	0.0980	161	0.845	0.0536	1.93	9500
2	S(1)	Propane	3.99	76.0	0.1563	275	0.438	0.0916	3.30	38880
3	"	"	3.88	"	0.1472	246	0.448	0.0819	2.95	41770
4	"	"	4.09	"	0.1436	218	0.516	0.0726	2.61	35940
5	"	"	4.92	"	0.1310	179	0.654	0.0596	2.15	24610
63	R(1-C)	Butene-1	5.15	70.4	0.1427	133	0.644	0.0443	1.59	34770
65	"	"	3.85	"	0.1668	236	0.294	0.0786	2.83	84850
66	"	"	3.21	"	0.1819	209	0.264	0.0696	2.51	111070
69	"	"	2.88	"	0.1908	214	0.256	0.0713	2.57	113080

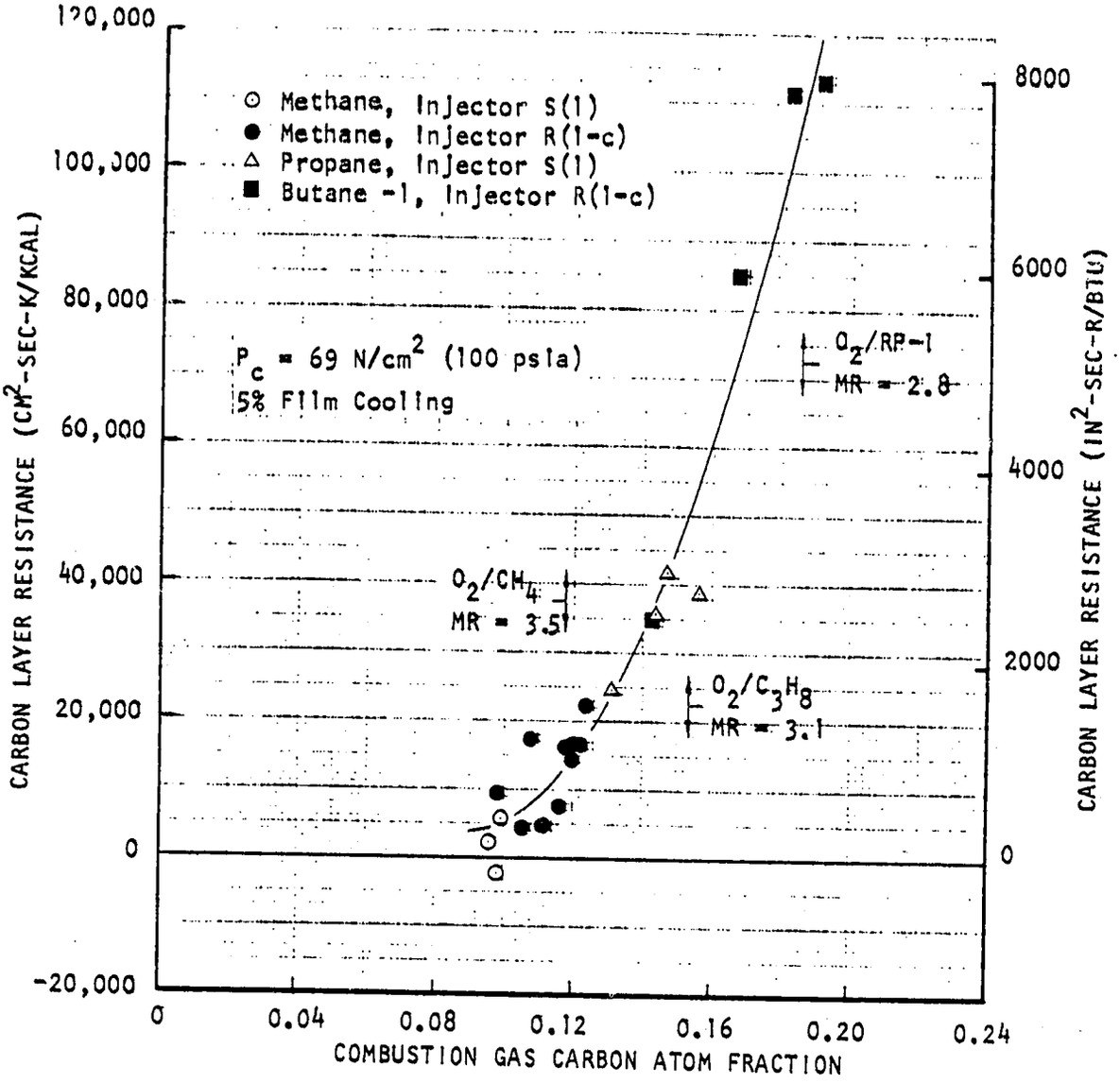

Figure 17. Effect of Fuel on Carbon Layer Resistance

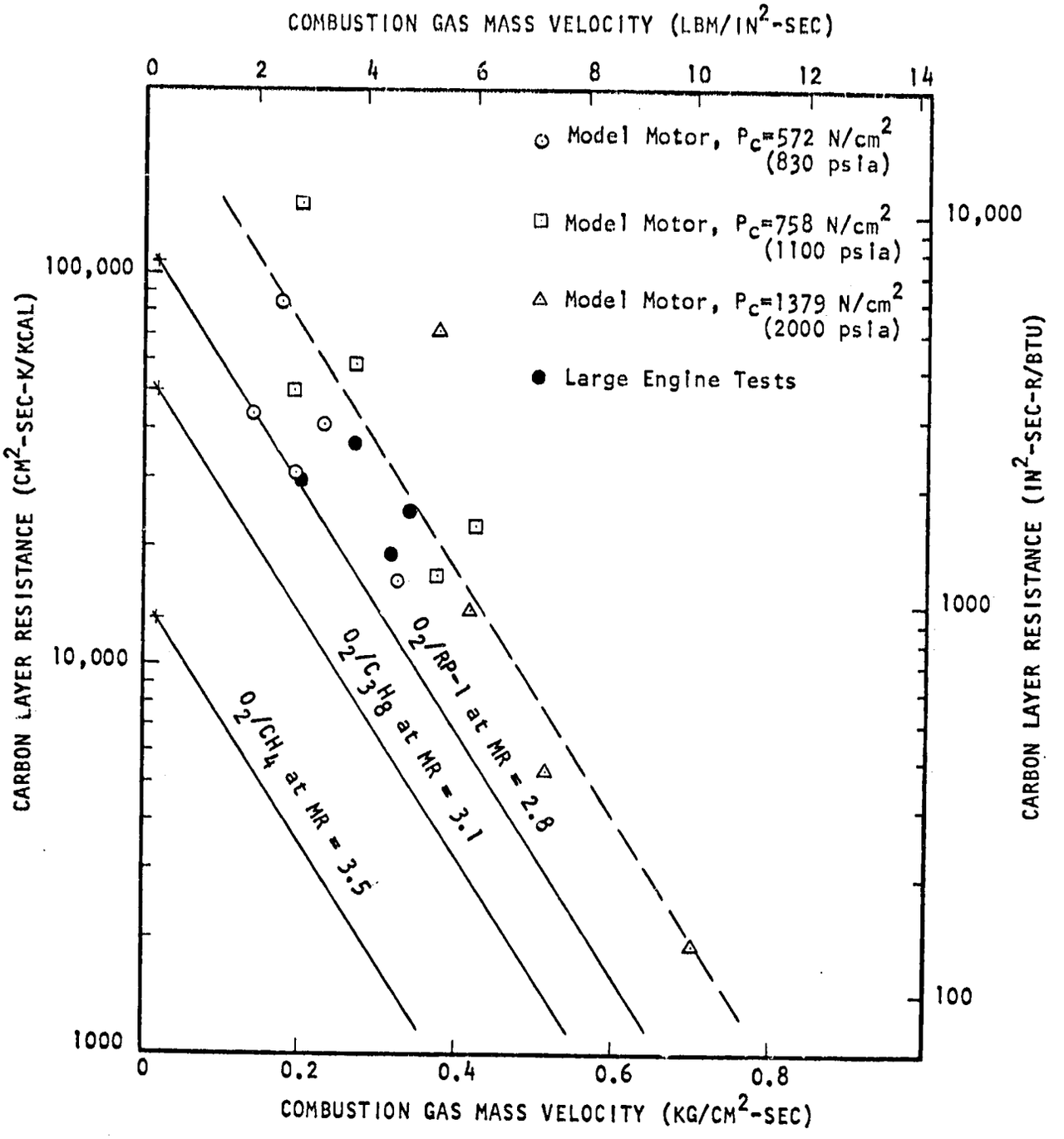

Figure 18. Carbon Layer Resistance Correlations

Design Analysis

A carbon layer, to some degree, will always exist on the hot-gas wall of a thrust chamber using hydrocarbon fuels. For these analyses, it is assumed the carbon layer is tenacious and adheres to the combustion chamber wall. For reasons previously mentioned, compatible nozzle designs did not utilize a carbon layer, excluding the 89,000 N (20,000 lbf) thrust nozzle which requires a nozzle carbon layer to allow $T_{wc} \leq 589$ K (1060 R).

As shown in Fig. 18, the carbon layer thermal resistance (x/k) is greatly dependant on hot-gas mass velocity (Gg) and propellant combination. This means the carbon layer thermal resistance is large in the combustion chamber and supersonic regions compared to the higher heat flux throat region. Therefore, the enhancement benefit to be attained requires enlarging the coolant passages in the regions upstream and downstream of the throat to provide a higher coolant mass velocity (mass flux) in the throat region. This tradeoff requires adjusting the unenhanced designs to provide greater cooling of the throat region. Coolant channel geometry adjustments consist of increasing the channel widths and heights upstream and downstream of the throat while decreasing the channel height in the throat. The carbon layer thermal resistance also allows the bi-width channel transitions to be located closer to the throat. There is a multitude of channel geometry variations considered to meet cyclic life, structural criteria, and fuel decomposition temperature limits. Therefore, specific designs of certain propellant combinations may differ slightly from the above general approach.

The carbon layer enhanced design analyses parameters are summarized in Table 7 and compared to the unenhanced chamber pressure. Descriptive graphical presentations of these designs are presented in Fig. 93 through 106 of Appendix D. Comparison of the unenhanced P_c to carbon layer enhanced P_c of Table 7 shows negligible increase in chamber pressure for the carbon layer enhanced O_2/CH_4 and O_2/C_3H_8 designs. However, there is an outstanding chamber pressure increase for the O_2/RP-1 "Short Chamber" design. This can be seen in Fig. 18 where the thermal resistance for O_2/RP-1 is an order of magnitude greater than O_2/CH_4. The thermal resistance of these two propellant combinations is shown in Fig. 19 as a function of chamber axial length. The RP-1 carbon layer resistance is significantly greater than CH_4, as denoted in Fig. 18.

The maximum chamber pressure of the carbon layer enhanced designs is compared to the unenhanced designs as a function of thrust level in Fig. 20. All of these designs used a P_{inlet}/P_c of 1.8, as noted in Table 7. Only the 89,000 N (20,000 lbf) thrust O_2/CH_4 design marginally exceeded the chamber pressure guideline limit of 2860 N/cm^2 (4150 psia). A very minimal reduction in P_{inlet}/P_c could be ascertained for a chamber pressure limit design.

The overpowering affect of the RP-1 carbon thermal resistance can be seen in a chamber pressure increase from the unenhanced 2,669,000 N (600,000 lbf) thrust "short chamber" design at 896 N/cm^2 (1300 psia) to a carbon enhanced design at 2275 N/cm^2 (3300 psia) for the T_{wc} limit of 589 K (1060R). The significance of using a "short chamber" for O_2/RP-1 is extremely notable. The carbon-

TABLE 7. SUMMARY OF HIGH-PRESSURE HYDROCARBON FUELED ENGINE REGENERATIVE COOLING LIMITS

(FOR CARBON LAYER ENHANCED COMBUSTION CHAMBER)

Propel. Comb.	Thrust N (lbf)	P_{in}/P_c	Max P_c Unenh. N/cm^2 (psia)	Max P_c Enh. N/cm^2 (psia)	P_c Limiting Factor	Cooling Circuit	Chamber To Nozzle ε	Min LW cm (in)	Channel Width cm (in)	Channel Wall Thickness cm (in)	Nozzle Min UTD cm (in)	Nozzle Min Wall Thickness cm (in)
O_2/C_3H_8	89,000 (20,000)	1.8	2068 (3000)	2172 (3150)	Life	Series	10:1	.076 (.03)	.102/.076 (.04/.03)	.064 (.025)	.152/.434 (.06/.171)	.023/.076 (.009/.03)
O_2/C_3H_8	2,669,000 (600,000)	1.8	1586 (2300)	1896 (2750)	Life	Split	5:1	.076 (.03)	.140/.076/.140 (.055/.03/ .055)	.102/.064 (.04/.025)	.203 (.08)	.025 (.01)
O_2/CH_4	89,000 (20,000)	1.8	2758 (4000)	2861 (4150)	Life	Series	12:1	.076 (.03)	.102/.076 (.04/.03)	.064 (.025)	.178/.432 (.07/.17)	.020/.076 (.008/.03)
O_2/CH_4	667,000 (150,000)	1.8	2620 (3800)	2758 (4000)	Life	Series	10:1	.076 (.03)	.140/.089/.140 (.055/.035/ .055)	.089/.064 (.035/.025)	.267/.434 (.1052/ .171)	.025/.051 (.01/.02)
O_2/CH_4	2,669,000 (600,000)	1.8	2144 (3110)	2189 (3175)	Life	Split	5:1	.076 (.03)	.229/.140 (.09/.055)	.114/.064 (.045/.025)	.203 (.08)	.020/.028 (.008/.011)
O_2/RP-1 Short Chamber	2,669,000 (600,000)	1.8	896 (1300)	2275 (3300)	T_{wc} Life	Split	5:1	.076 (.03)	.229/.140 (.090/.055)	.114/.076 (.045/.030)	.203 (.080)	.025 (.01)
O_2/RP-1 Long Chamber	2,669,000 (600,000)	1.8	1179 (1710)	1179 (1710)	Life T_{wg},T_{wc}*	Split	5:1	.076 (.03)	.229/.140 (.09/.055)	.102/.064 (.04/.025)	.203 (.08)	.025 (.01)
O_2/RP-1 Long Chamber	89,000 (20,000)	1.8	<690 (1000)	1378 (2000)	T_{wc} Life	Split	10:1	.076 (.03)	.127/.076/.127 (.05/.03/.05)	.076 (.030)	.152 (.060)	.023 (.009)

*CRITERIA DISREGARDED (T_{wc} EXCEEDED GUIDELINES)

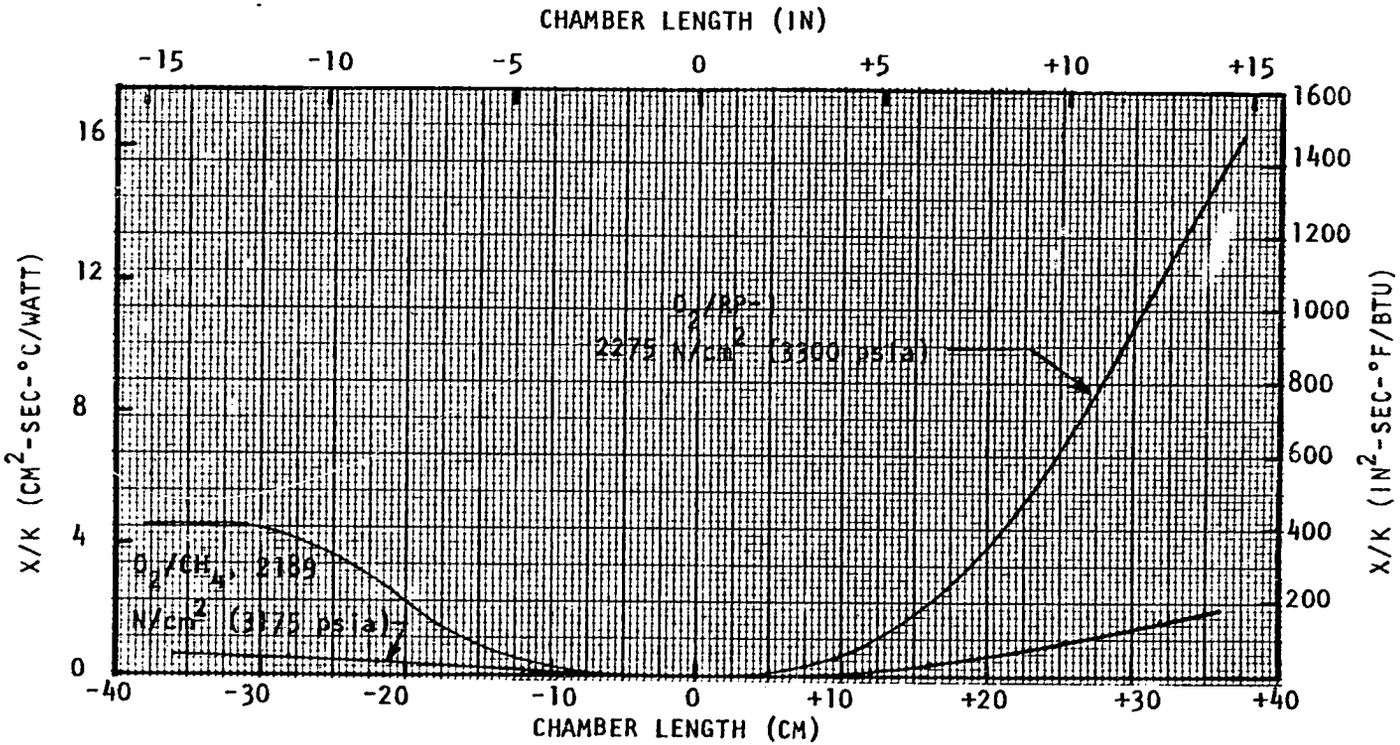

Figure 19. Comparison of Carbon Layer Thermal Resistances for O_2/RP-1 and O_2/CH_4 Designs

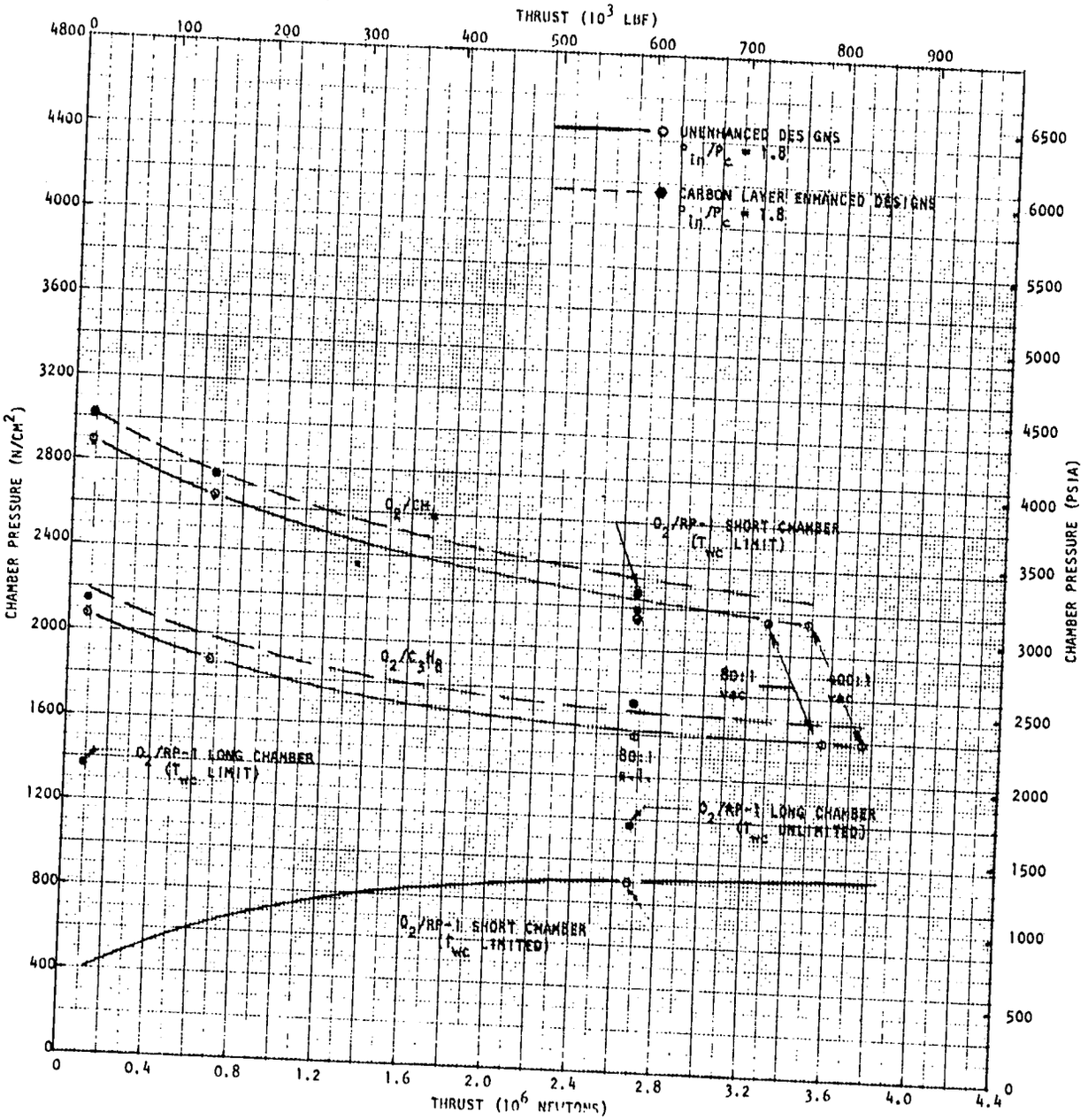

Figure 20. Effect of Thrust on Regenerative Cooling Limit for Carbon Layer Enhanced Designs Compared to Unenhanced Designs

enhanced 2,669,000 N (600,000 lbf) thrust "long chamber" could not meet the T_{wc} limit at 1700 P_c, approximately 111 K (200 R) above the T_{wc} limit.

CERAMIC COATING

Zirconium oxide (ZrO_2) was selected as the ceramic coating for a physical thermal barrier.

Assessment

Zirconium oxide is a low thermal conductivity material (Guideline Table III). This low thermal conductivity provides an excellent thermal barrier. However, because of this fact, and the fact that it is a low ductility material, the use of its application is limited to thin thicknesses for high chamber pressure. To maintain the surface temperature limit <1944 K (3500 R), the thicknesses employed were between 0.0025 cm (0.001 in.) and 0.0127 cm (0.005 in.). This is within reasonable control. The large thermal gradients across the coating thickness means large thermal strains. This also dictates the surface temperature limit. It is the most utilized ceramic coating for reducing hot-gas wall temperatures in high heat flux rocket engines.

Design Analysis

The cyclic life of ZrO_2 coatings enhances the life of the parent combustor NARloy-Z material. The cyclic life of the ZrO_2 coating is undefinable at this time. It is most likely that the ceramic coating will have to be replenished a number of times during the life of the NARloy-Z chamber. For reasons previously mentioned, compatible nozzle designs did not employ a ceramic coating.

The ceramic-coated O_2/CH_4 and O_2/C_3H_8 designs provide a significant increase in chamber pressure as compared to the unenhanced designs. The results of these analyses are summarized in Table 8, and the descriptive graphic presentations are shown in Fig. 107 through 117 in Appendix D. The 89,000 N (20,000 lbf), thrust O_2/RP-1 "long chamber" design (for liquid/liquid injection) was within the decomposition temperature limit (T_{wc}) for 680 N/cm^2 (1000 psia) chamber pressure. However, the large bulk temperature rise of the chamber plus nozzle would require an enhanced nozzle design to stay within the coolant wall temperature limit.

The chamber pressure benefits attainable with ceramic coating are shown in Fig. 21. As noted in Table 8 and Fig. 21, two of these designs were at reduced P_{inlet}/P_c to stay within the chamber pressure guidelines. These were the 89,000 N (20,000 lbf) thrust O_2/C_3H_8 and the 667,200 N (150,000 lbf) thrust O_2/CH_4 designs.

The O_2/RP-1 "short-chamber' benefits are for a T_{wc} limit of 589 K (1060 R) instead of life limited. This accounts for the reversed chamber pressure trend as a function of thrust level.

TABLE 8. SUMMARY OF HIGH PRESSURE HYDROCARBON-FUELED ENGINE REGENERATIVE COOLING LIMITS (FOR ZrO_2 CERAMIC COATING ENHANCED COMBUSTION CHAMBERS)

Propel. Comb.	Thrust N (lbf)	Max P_c Unenh. N/cm^2 (psia)	Max P_c Enh. N/cm^2 (psia)	P_c Limiting Factor	Cooling Circuit	Chamber to Nozzle ε	Min LW cm (in)	Channel Width cm (in)	Channel Wall Thick cm (in)	Coolant P_{in}/P_c	Nozzle Min UTD cm (in)	Nozzle Min Wall Thick cm (in)	Coating Thickness cm (in)
O_2/C_3H_8	89,000 (20,000)	2068 (3000)	2758 (4000)	Life T_{wc}	Series	10	.076 (.03)	.114/.076 (.045/.03)	.069/.064 (.027/.025)	1.64*	.127/.434 (.05/.171)	.018/.076 (.007/.03)	.0030/.0048 (.0012/.0019)
O_2/C_3H_8	2,669,000 (600,000)	1586 (2300)	2758 (4000)	Life T_{wc}	Split	7.4	.076 (.03)	.140/.102 .140 (.055/.04/ .055)	.089/.064 .074 (.035/.025 .029)	1.8	.193 (.076)	.018 (.007)	(.0013/.0017)
O_2/CH_4	667,000 (150,000)	2620 (3800)	3447 (5000)	T_{wcc}	Series	10	.076 (.03)	.140/.089 .140 (.055/.035 .055)	.104/.086 (.041/.034)	1.67	.229/.434 (.09/.171)	.020/.030 .025 (.008/.012 .01)	.003/.0043 (.001/.0017)
O_2/CH_4	2,669,000 (600,000)	2144 (3110)	3344 (4850)	Life T_{wcc}	Split	9.5	.076 (.03)	.203/.140 (.08/.055)	.155/.099 (.061/.039)	1.8	.178 (.07)	.018/.025 (.007/.01)	.003/.0046 (.001/.0018)
O_2/RP-1 Long Chamber	89,000 (20,000)	689 (1000)**	689 (1000)**	T_{wc}*	Series	10	.076 (.03)	.076 (.03)	.064 (.025)	1.8	.152 (.06)	.023 (.009)	.013 (.005)
O_2/RP-1 Short Chamber	2,669,000 (600,000)	896 (1300)	1516 (2200)	T_{wc}	Split	5	.076 (.03)	.229/.140 (.09/.055)	.152/.094 (.060/.037)	1.8	.165 (.065)	.025 (.010)	.0088/.013 (.0035/.005)

* CRITERIA DISREGARDED
** REFERENCE CASE

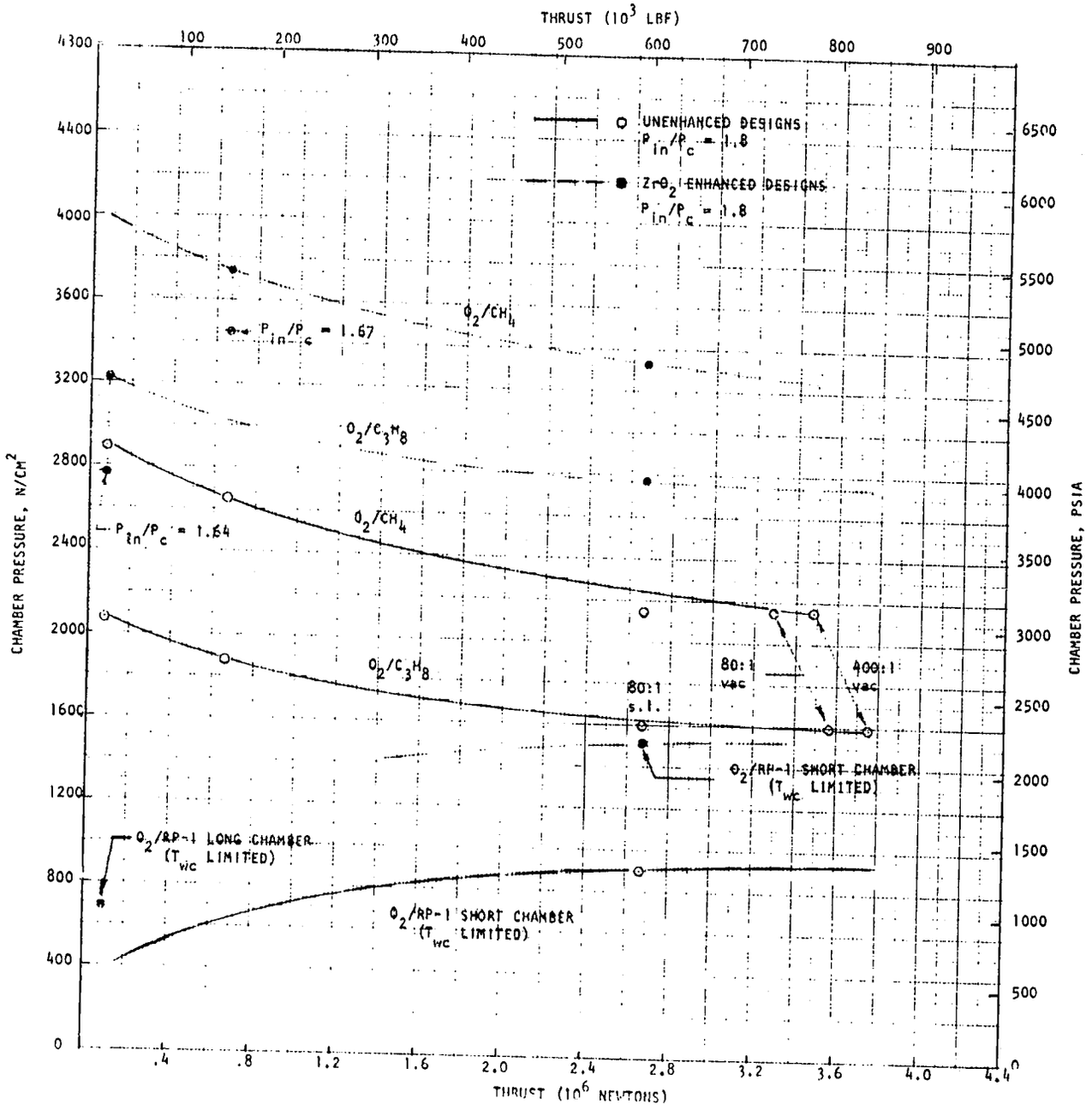

Figure 21. Effect of Thrust on Regenerative Cooling Limits for ZrO_2 Ceramic-Coated Enhanced Designs Compared to Unhanced Designs

Typical ZrO_2 combustion chamber designs resulted in an increased nozzle attachment area ratio because of the higher chamber pressure with an unenhanced nozzle. The ceramic coating of the nozzle was allotted a bi-thickness similar to the bi-thickness of the combustion chamber wall to stay within the guideline ZrO_2 surface temperature limits. This is noted in Table 8, and the graphic design presentation figures in Appendix D.

GRAPHITE LINER

ATJ Graphite was recommended for the graphite liner physical thermal barrier.

Assessment

The recommended constraints were 0.1 in. minimum thickness with a maximum hot-gas surface temperature of 1644 K (2960 R). It is Rocketdyne's experience that ATJ graphite is superior to ATJ at elevated temperature. Neither does Rocketdyne's experience support a 1644 K (2960 R) operation of either material in oxygen-bearing propellant combinations.

The graphite liner analysis guidelines utilized ATJ graphite at a maximum surface temperature of 1644 K (2960 R) and a manufacturers wall thickness of 0.254 to 1.27 cm (0.100 to 0.500 in.). The wall thickness limits were a function of chamber diameter. The thicker liner was for the larger thrust engines. These thickness were recommended based on information from Union Carbide, the manufacturer. Union Carbide was consulted several times to further establish the feasibility of a graphite liner for thermal control. With the design guideline of up to 12-inch-diameter injector end chamber with a conventional convergent and divergent throat section for a total length up to 18 inches, the minimum practical ATJ thickness would be 1.28 cm (0.5 in.) for a 2,669,000 N (600,000 lbf) thrust chamber. Anythin less than that would result in machining problems and service cracks. Even with the 1/2-inch thickness, the liner may have to be made up of cemented segments. Furthermore, it was confirmed that the maximum recommended temperature is 922 K (1660 R) in an oxidizing environment, which is less than the guideline temperature utilized.

As will be shown later, the use of ATJ was not feasible at these high chamber pressures; therefore, other graphite liner prospects were reviewed, i.e., pyrolitic graphite and "graphoil-laminate" graphite. These types of graphites can be applied in thinner layers (>5 mils). However, the thermal conductivity perpendicular to the hot wall results in thermal conductances greater than an order of magnitude beyond those of ATJ graphite, being near the thermal resistance of ZrO_2. Although these types of graphite allows a reduced liner thickness, the increase in thermal conductivity perpendicular to the wall negates their ability to be applied as thinner layers within manufacturing guidelines.

Figure 22 compares the conductivity of ATJ graphite to the conductivities of pyrolitic graphite and "grafoil" laminate. Because of the decreased conductivities of pyrolitic graphite materials, their liner thickness must be on the order of several thousandths of an inch thick for high chamber pressures. Pyrolitic graphite can be deposited with a vapor deposition process in fairly thin films, but the high vapor depositing temperature itself would make it unfeasible to deposit the film directly onto the combustion chamber wall without degrading

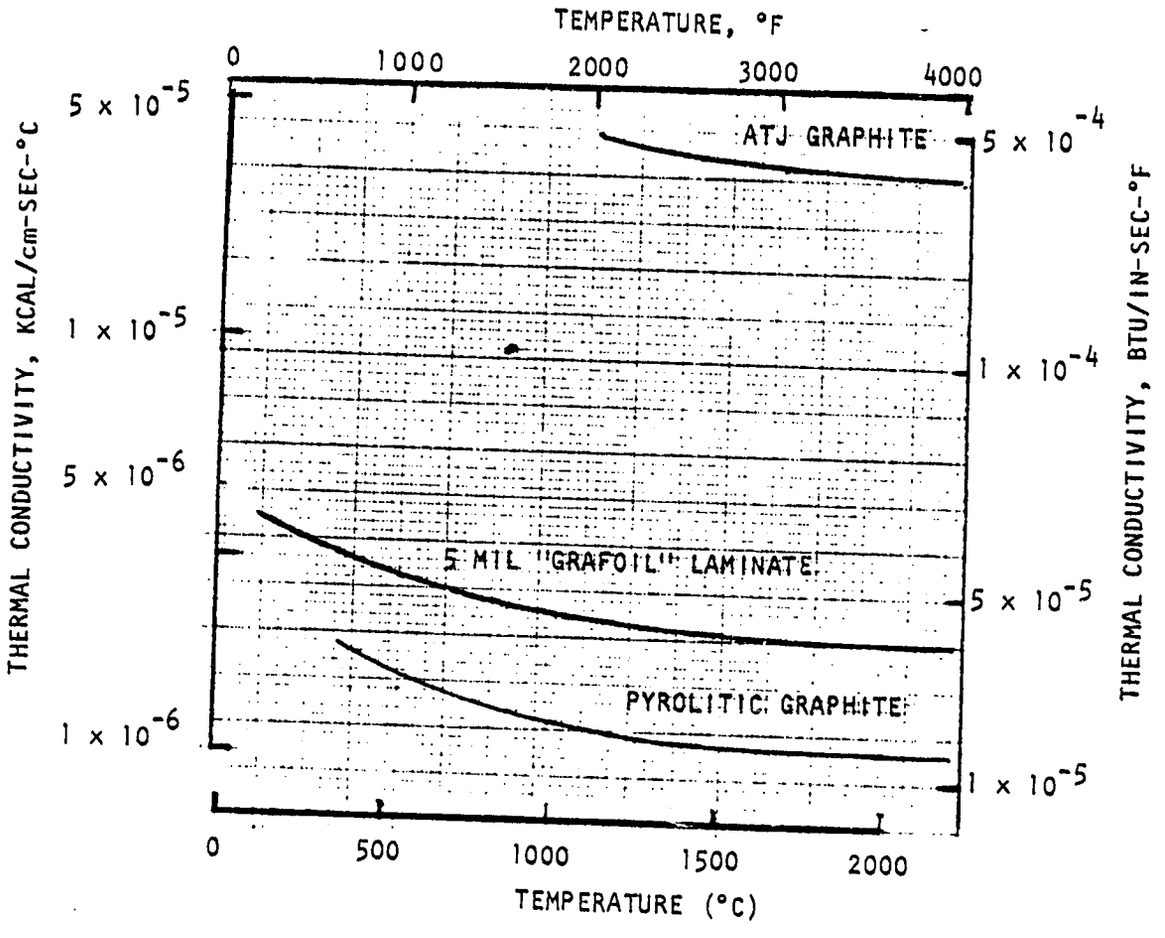

Figure 22. Comparison of Thermal Conductivity of Graphic Liners

material properties of the NARloy-Z. Preformed pyrolitic graphite liners would be extremely difficult to handle and install and it would be impractical to expect them to withstand the extreme thrust chamber conditions. Forming a liner by cementing jointed segments together only a few thousandths of an inch thick is possible, but impractical.

The 5-mil "grafoil" laminate is bonded to a surface in the form of a thin tape. This graphite liner technique is inferior to the two previously described liners because of its inherently weak structural integrity. In addition, the thermal resistances of the "grafoil" laminate and the pyrolitic graphite would exceed that of the 0.1-inch ATJ liner.

Design Analysis

A comparative assessment indicated that the graphite liner thickness specified by the manufacturer and the guideline surface temperature were incompatible. However, several designs were analyzed to provide greater insight to the problem.

An initial analysis was made utilizing an ATJ graphite liner with a minimum guidelines thickness of 0.254 cm (0.10 in.) on the O_2/CH_4, F = 2,669,000 N (600,000 lbf), P_c = 2144 N/cm^2 (3110 psia) combustion chamber. The purpose of this analysis was to determine the benefit of the graphite liner attached to the combustor hot wall of an unenhanced design with minimum guideline thickness. The result of this analysis shows that the ATJ graphite liner is strongly limited in its use at high heat fluxes as a cooling enhancer by its hot-gas surface temperature. In this case, the ATJ surface temperature reached 2665 K (4779 R). Although all other design criteria can be improved from the unenhanced chamber case by the use of the ATJ liner at the cooling pressure limit of the unenhanced case, the surface temperatures attained within any acceptable thickness range of the graphite liner requires the chamber pressure to be reduced below the unenhanced limit.

In order to make a comparison between the graphite liner and ceramic coating, ATJ graphite was considered on an otherwise unaltered ceramic coated enhanced case. The ATJ lining was applied to the O_2/C_3H_8, 89,000 N (20,000 lbf), P_c = 2758 N/cm^2 (4000 psia) design. In order to maintain a maximum liner hot-gas surface temperature of 1644 K (2960 R) the thermal resistance x/k was reduced by 18% less than for the ZrO_2 case. This required an ATJ thickness of 0.04 cm (0.016 in.) upstream from the attachment point through the throat. The ATJ liner thickness in the combustion zone was 0.06 cm (0.024 in.). The result was a sharp decrease in cycle life due to fatigue. The ATJ surface temperature reached 1792 K (3226 R) in the throat region. For this comparison, the graphite liner thickness was held to a value much less than possible for manufacturing criteria, and the liner surface temperature reached levels that would cause rapid oxidation of the ATJ liner.

The above design analysis shows that even a graphite throat insert would need be considerably thinner than the design guideline.

This study shows that graphite liners are really only applicable for space-engine type low heat flux combustion chambers. This is particularly true of

pyrolitic graphite applied as an INTEREGEN heat sink chamber barrier, since they have an axial x/k equivalent to copper with a very low perpendicular x/k.

FILM COOLING

Film cooling was selected as one of the three thermal fluid barriers. It has been extensively used to some degree in most liquid propellant rocket engines. For this study a 3% performance loss is accepted.

Assessment

A number of film-cooling heat transfer models were evaluated. Most of the existing analytical models assume that the presence of the film does not affect the heat transfer coefficient between the wall and film, and concentrate on prediction of the effective film temperature as a function of distance from the injection point. These models utilize a "dry wall" heat transfer coefficient and assume no mixing of the free stream main core flow with the film cooling. The Hatch and Pappell model (Ref. 9) and the Tribus-Klein model (Ref. 10) use this approach. These are two commonly used models for assessing film cooling effects of rocket engines.

A more accurate approach to compute the heat transfer rate between a gaseous film coolant and wall is to predict both a heat transfer coefficient and an effective film temperature. This is particularly true when the film-coolant properties are different from the free stream gas. One such correlation for predicting the film heat transfer coefficient was developed at Rocketdyne (Ref. 11) and assumes equal Mach numbers of film and free stream gases to relate the heat transfer coefficient of the film to the "dry wall" heat transfer coefficient as:

$$\frac{h_f}{h_g} = \frac{C_{p_f}}{C_{p_g}} \left(\frac{P_{r_g}}{P_{r_f}} \right)^{2/3} \left[\frac{\gamma_g M_f T_f}{\gamma_f M_g T_f} \right]^{1/2} \qquad (26)$$

This approach accounts for a mass balance in the film where the concentration difference is expressed as a ratio of flow rates and injection mass fluxes:

$$\frac{\partial}{\partial x} \frac{w_f}{p} = G \frac{\partial \Delta}{\partial x} + Le \frac{h_g}{C_{p_g}} \left(\frac{m_f w_c}{m_c w_f} \right) \qquad (27)$$

The entrainment of the free stream gas into the film is accountable by impingement (the first term) and by diffusion (the second term).

The film thickness (Δ) is related to the zero film cooling thermal thickness as derived from the integral energy balance equation and assumes the velocity

profile through the film does not change in shape with distance:

$$G_\Delta \frac{\partial \Delta}{\partial x} = K \frac{h_g}{C_{p_g}} \left[\frac{T_{aw} - T_w}{T_o - T_w} \right] \tag{28}$$

For subsonic flow, the temperature ratio is unity, and Eq. 27 becomes:

$$\frac{\partial}{\partial x} \left(\frac{w_f}{p} \right) = \left[K + Le \left(\frac{w_c \, m_f}{w_f \, m_c} \right) \right] \frac{h_g}{C_{p_g}} \tag{29}$$

The subsonic flow heat transfer coefficient for an adiabatic flat plate is:

$$h_g = 0.0296 \frac{C_{p_g} \, G^{0.8}}{Pr_g^{2/3}} \left(\frac{\mu_g}{x} \right)^{0.2} \tag{30}$$

The variables are separated in Eq. 29 and integrated after substitution of Eq. 30 from the end of the wall jet region, x_1, to the location x to give the film flowrate as:

$$\frac{w_f}{w_c} = 1 + 0.037 \, (K + Le) \frac{\mu_g \, p}{w_c \, Pr_g^{2/3}} \left(Re_x^{0.8} - Re_{x_1}^{0.8} \right) \tag{31}$$

Assuming no coolant is lost from the film allows the film temperature ratio to be expressed in terms of the film flowrate as:

$$\frac{1}{\eta} = \frac{T_g - T_c}{T_g - T_f} = 1 + \frac{C_{p_g}}{C_{p_c}} \left(\frac{w_f}{w_c} - 1 \right) \tag{32}$$

Combining Eq. 31 and 32 gives:

$$\frac{1}{\eta} = 1 + 0.037 \, (K + Le) \frac{C_{p_g}}{C_{p_c}} \frac{\mu_g \, p}{w_c \, Pr_g^{2/3}} \left(Re_x^{0.8} - Re_{x_1}^{0.8} \right) \tag{33}$$

The analytical model film temperature ratio should, therefore, be a linear function of the parameter B* which is similar to the parameters used by other investigators and is defined as:

$$B^* \quad \frac{C_{p_g}}{C_{p_c}} \frac{\mu_g \, p \, Re_x^{0.8}}{w_c \, Pr_g^{2/3}} \tag{34}$$

Therefore, an equation of the general form:

$$\frac{1}{\eta} = 1 + \xi(B^* - B^*_o) \tag{35}$$

was used to evaluate test data. The Lewis number and, hence, the slope, β, were evaluated based on a slot Reynolds number as suggested by Hatch and Pappell.

$$\beta = a + b \, Re_s^n \tag{36}$$

The correlation equation for the slope that gave the minimum data scatter to predict the end of the wall jet region is:

$$\beta = 0.037 \, (K + Le) = 0.04 + 0.004 \, Re_s^{0.4} \tag{37}$$

Data fit of Eq. 36 indicates that K is of the order of unity.

In developing these correlations, it was observed that a large part of the data scatter was apparently due to a coolant injection velocity effect. This type of effect was noted by Hatch and Pappell for coolant injection velocities approximately equal to the free stream velocity where the coolant efficiency exhibits a local maximum. In addition to this effect, it was noted during this study that the coolant efficiency also exhibited a local minimum at a value of 0.4 for the slot coolant parameter, B^*_s. Thus, for the range of conditions covered by the test data ($U_c < U_g$), the best correlation for the slope of the temperature ratio was:

$$\beta = 0.04 + 0.041 \, Re_s^{0.4} \quad \frac{B^*_s}{(1 + B^*_s)^{3.5}} \tag{38}$$

Combining Eq. 37 and 38

$$Le = 1.1 + 1.2 \, (Re_s)^{0.4} \frac{B^*_s}{(1 + B^*_s)^{3.5}} \tag{39}$$

The film-cooling data of Ref. 9 and 12 through 14 are correlated in Fig. 23. The data of Hatch and Pappell (Ref. 9) is shown to correlate well with slot sizes and film-coolant flowrate in Fig. 24. Correlation of data from Ref. 15 is shown in Fig. 25 for nitrogen film cooling of a JP-4/CO_2 thrust chamber. Figure 26 shows the correlation of a Rocketdyne APS O_2/H_2 hydrogen film-cooled chamber.

The primary equations used in the film-cooling computer program are Eq. 26, 34, and 39. The entrainment of core gas in the coolant film by diffusion is accountable by the Lewis number. The entrainment by impingement G $\partial\Delta/\partial x$ was correlated to be unity as noted by K of Eq. 37. Therefore, the heat transferred to the film coolant by mixing is by the correlating diffusion and impingement relationships. The coolant properties are adjusted by subsonic flow relationships to obtain the film properties. The coolant film convective heat transfer coefficient is obtained from Eq. 26. A film heat flux to the wall is then obtained by the product of the h_f and $(T_f - T_{wall})$. For use in the regenerative cooling program, the h_f and T_f are input at each axial station in place of the h_g and T_{aw} used for dry wall calculations.

The film cooling efficiency used for the O_2/CH_4 designs and O_2/C_3H_8 designs is 0.20. This is compatible with design considerations and efficiencies of other experimenters, accounting for molecular weight sensitivity and slot injection characteristics.

Design Analysis

The film-cooling efficiency used for these designs was 20%. This is compatible with design considerations and efficiencies used by other experimenters considering the slot injection characteristics and working fluid properties. The film-cooling characteristics are defined by a film-cooling mathematical model previously described which defines the film convective heat transfer coefficient, hg, and the film boundary temperature, T_f, as a function of chamber contour. These values are then utilized in the regenerative cooling analysis to generate the cooling geometry of the main combustion chamber.

The amount of film cooling used relates to a specific impulse loss of 3%. The combustion gas temperature was corrected from the theoretical to the guideline specified energy release efficiency (η_{c*}) of 98% as follows:

$$T_{o\ \text{Actual}} = T_{o\ \text{Theoretical}} \times (\eta_{c*})^2 \qquad (40)$$

Although the allocated film cooling reduces the total performance to 95%, the actual efficiency of the adjacent hot-gas core is operating at 98% energy release efficiency.

Film-cooling characteristics were evaluated for several slot injection geometries and assumed efficiencies within practical application. The results indicate negligible effects in the film boundary except for the first 2 in. near the point of injection. Typical slot widths used were between 0.152 cm (0.060 in.) and 0.304 cm (0.120 in.). Except for large variations, the film-coolant

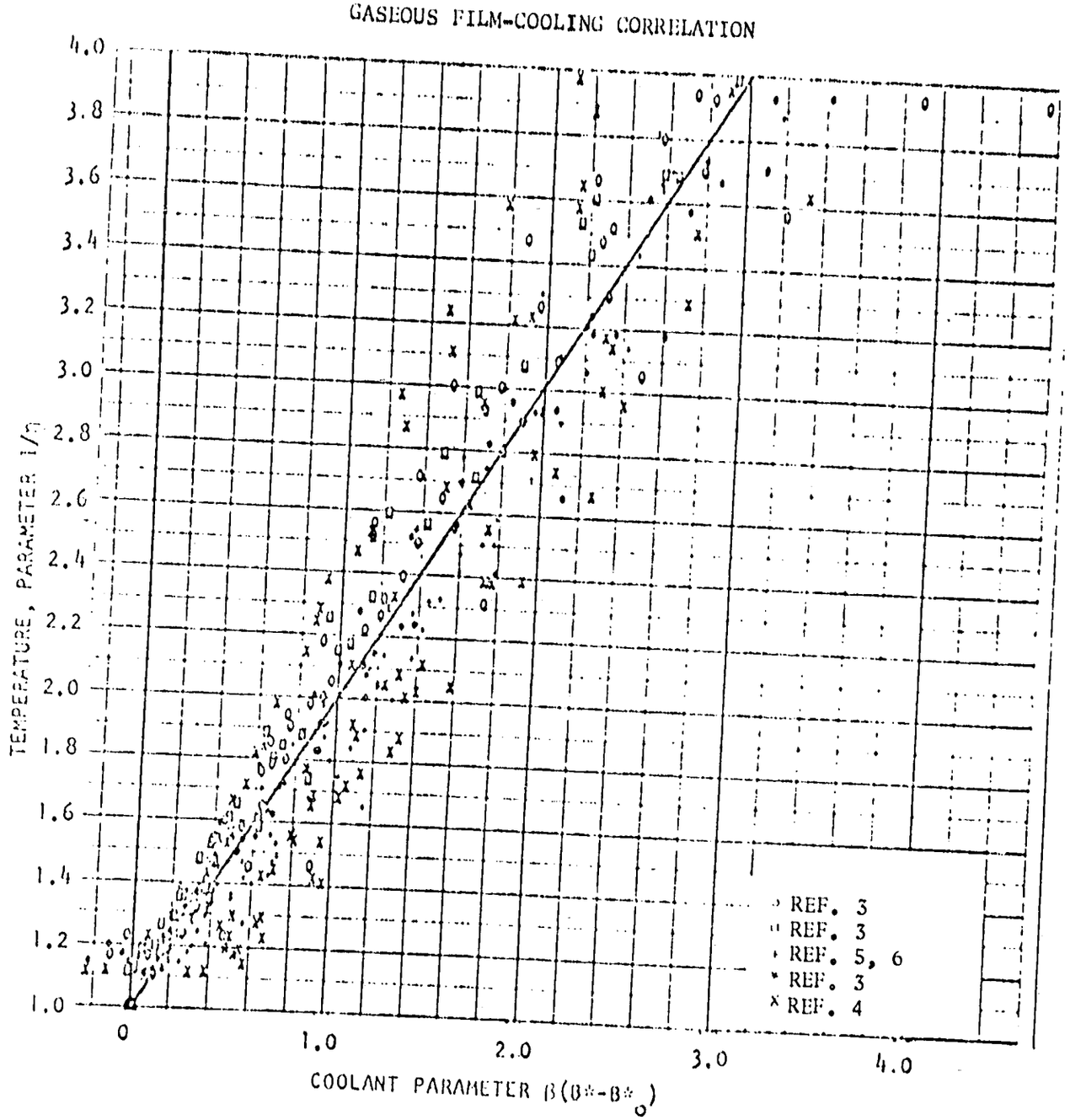

Figure 23. Modified Correlation of Adiabatic Flat Plate Film-Cooling Data

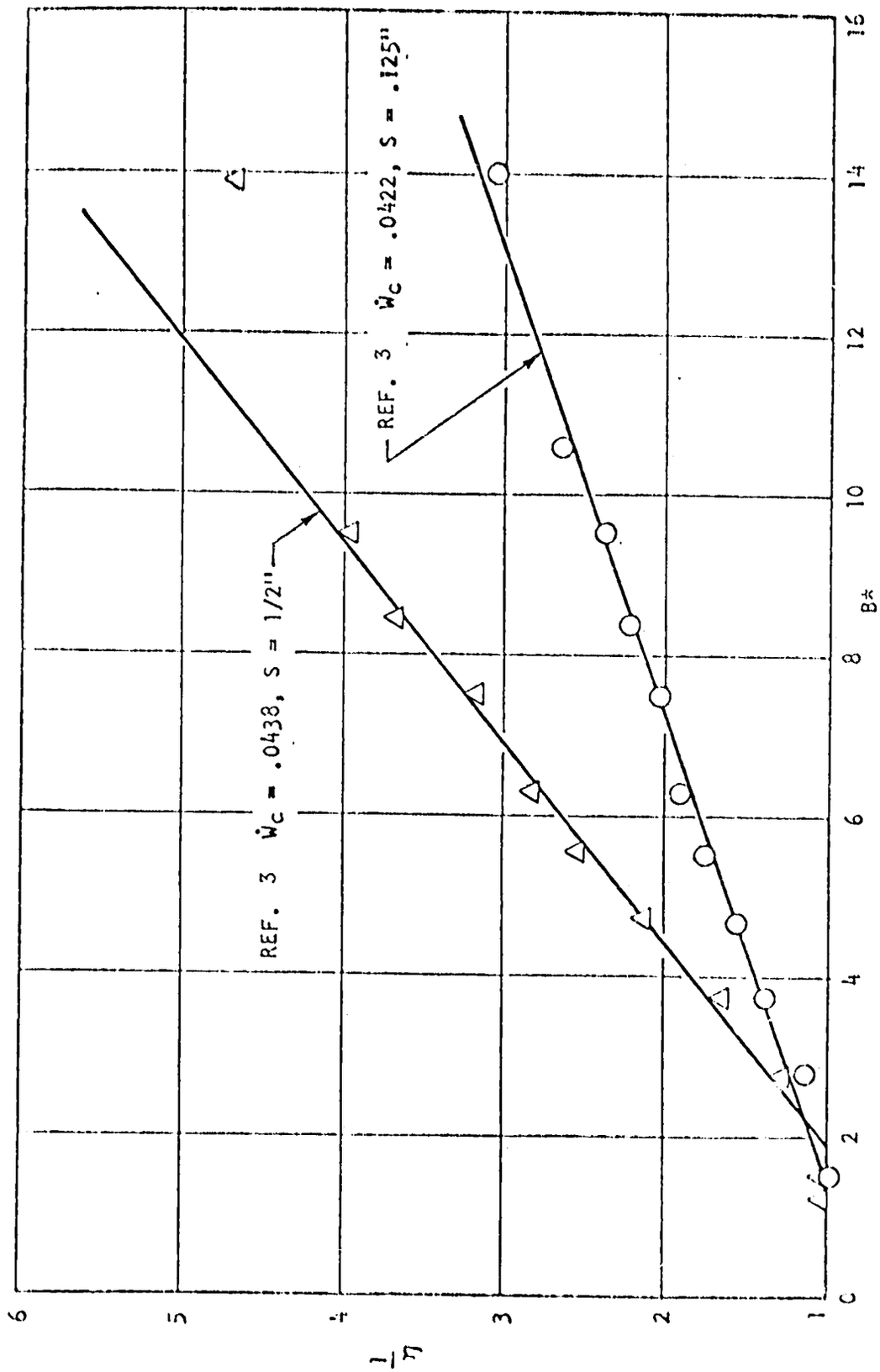

Figure 24. Comparison of Test Data With Linear Model for Temperature Rise

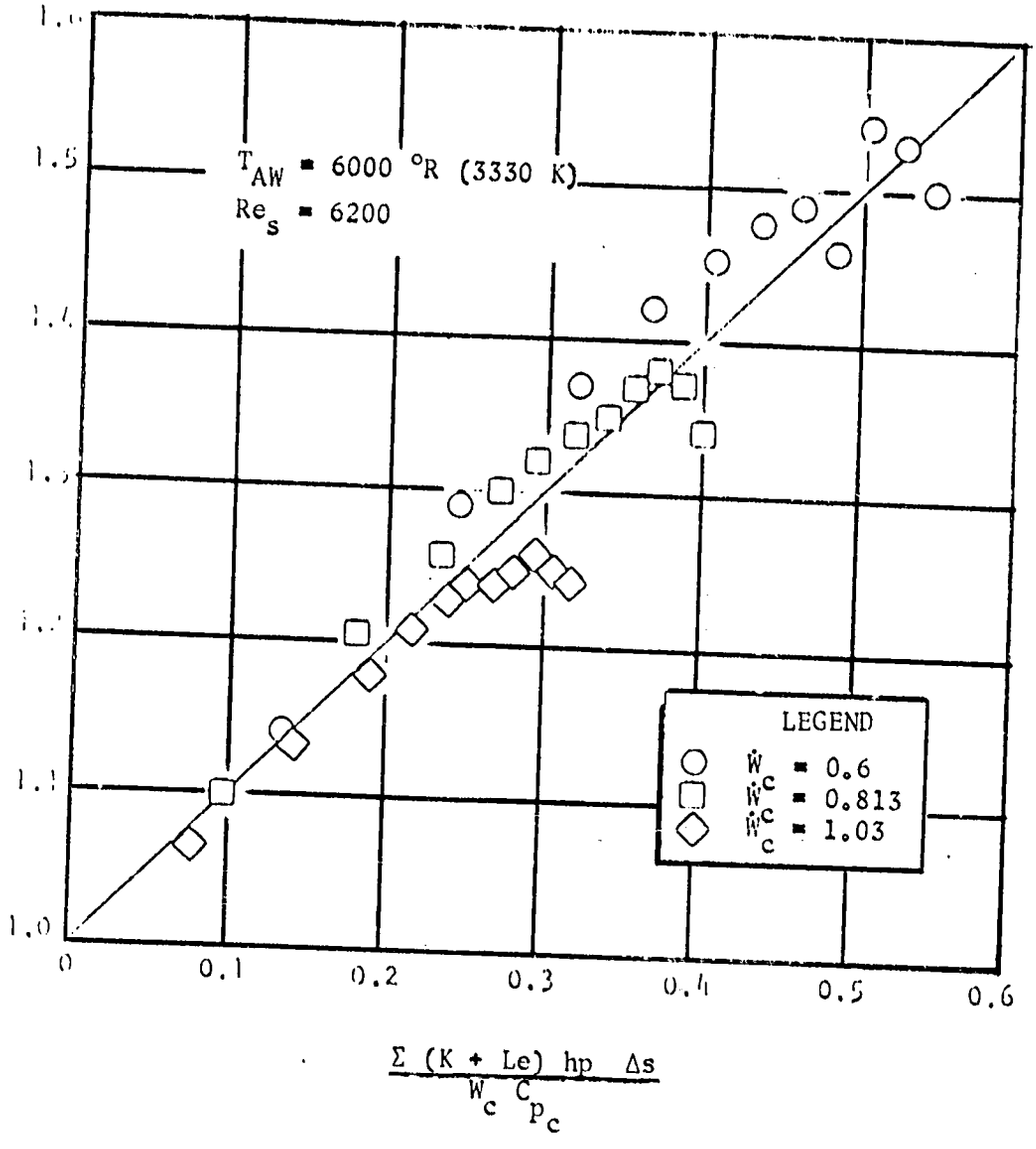

Figure 25. Variation of 1/η With Coolant Parameter

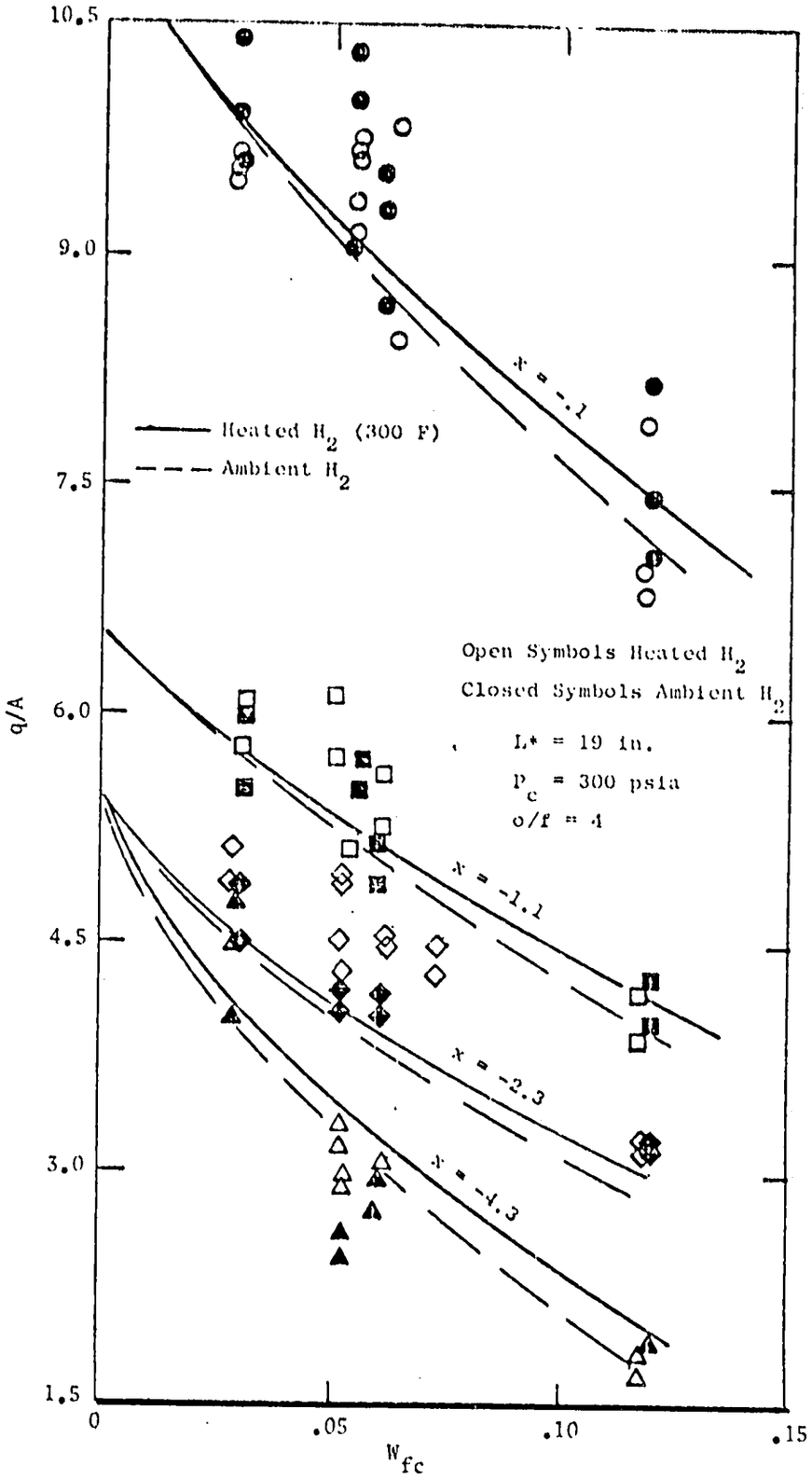

Figure 26. Comparison of Transient Heat Transfer Rates With Film Cooling Model Predictions

flowrate (or effective efficiency) did not significantly impact the chamber design. This is realized by the fact that the larger flowrate reflects a lower film temperature and, correspondingly, a higher heat transfer coefficient as a function of chamber length.

The results of these analyses are depicted in Table 9 and Fig. 27 and compared to the unenhanced chamber pressure. The descriptive graphic presentations of these designs are shown in Fig. 118 through 128 in Appendix D. All film-cooling designs utilized an unenhanced nozzle design with the chamber-to-nozzle attach point and nozzle tube unformed tube diameter changed appropriately for adequate cooling of the unenhanced nozzle to meet life. A P_{in}/P_c ratio of 1.8 was used for all designs to establish a maximum P_c trend for enhanced cooling. This resulted in the O_2/CH_4 667,000 N (150,000 lbf) and the O_2/C_3H_8 89,000 N (20,000 lbf) thrust designs exceeding the chamber pressure guidelines.

The coolant passage geometry changes relative to the unenhanced designs nearly parallel those of the ceramic-coated combustion chambers. This is primarily attributed to the fact that the hot-wall heat flux profile is nearly constant throughout the combustor, except for the first several inches downstream of the injector. As the film cooling progresses down the combustor, the (film hg/dry wall hg) decreases and the film temperature increases. This results in a near uniform heat flux reduction, which is typically 20% to 30% below the unenhanced designs for all propellant combinations. These trends are typically shown in Fig. 28. RP-1 provides the greatest film-cooling benefit. This is attributed to a lower specific heat (C_p) which results in a lower film temperature as a function of axial length.

TABLE 9. SUMMARY OF HIGH-PRESSURE HYDROCARBON-FUELED ENGINE REGENERATIVE COOLING LIMITS (FOR FILM-COOLED ENHANCED COMBUSTION CHAMBERS)

Propel. Comb.	Thrust N (lbf)	Max P_c Unenh. N/cm^2 (psia)	Max P_c Enh. N/cm^2 (psia)	P_c Limiting Factor	Cooling Circuit	Chamber to Nozzle ε	Min LW cm (in)	Channel Width cm (in)	Channel Wall Thickness cm (in)	Coolant P_{in}/P_c	Nozzle Min UTD cm (in)	Nozzle Min Wall Thickness cm (in)
O_2/C_3H_8	89,000 (20,000)	2068 (3000)	3034+ (4400)	Life	Series	12	.076 (.030)	.102/.076 (.040/.030)	.064 (.025)	1.8	.152 (.060)	.018 (.007)
O_2/C_3H_8	2,669,000 (600,000)	1586 (2300)	2137 (3100)	Life	Split	5	.081 (.032)	.229/.140 (.090/.055)	.114/.064 (.045/.025)	1.8	.203 (.080)	.018 (.007)
O_2/CH_4	667,000 (150,000)	2620 (3800)	3723+ (5400)	Life	Series	10	.081 (.032)	.127/.086/.127 (.050/.034/.050)	.089/.064/.071 (.035/.025/.028)	1.8	.152 (.060)	.025 (.010)
O_2/CH_4	2,669,000 (600,000)	2144 (3110)	2896 (4200)	Life	Split	7	.074 (.029)	.229/.140 (.090/.055)	.132/.069 (.052/.027)	1.8	.203 (.080)	.018 (.007)
O_2/RP-1 Short Chamber	2,669,000 (600,000)	896 (1300)	1516 (2200)	T_{wc}	Split	5	.076 (.030)	.229/.140 (.090/.055)	.089/.068 (.035/.027)	1.8	.165 (.065)	.025 (.010)

+ P_c GUIDELINE LIMIT EXCEEDED

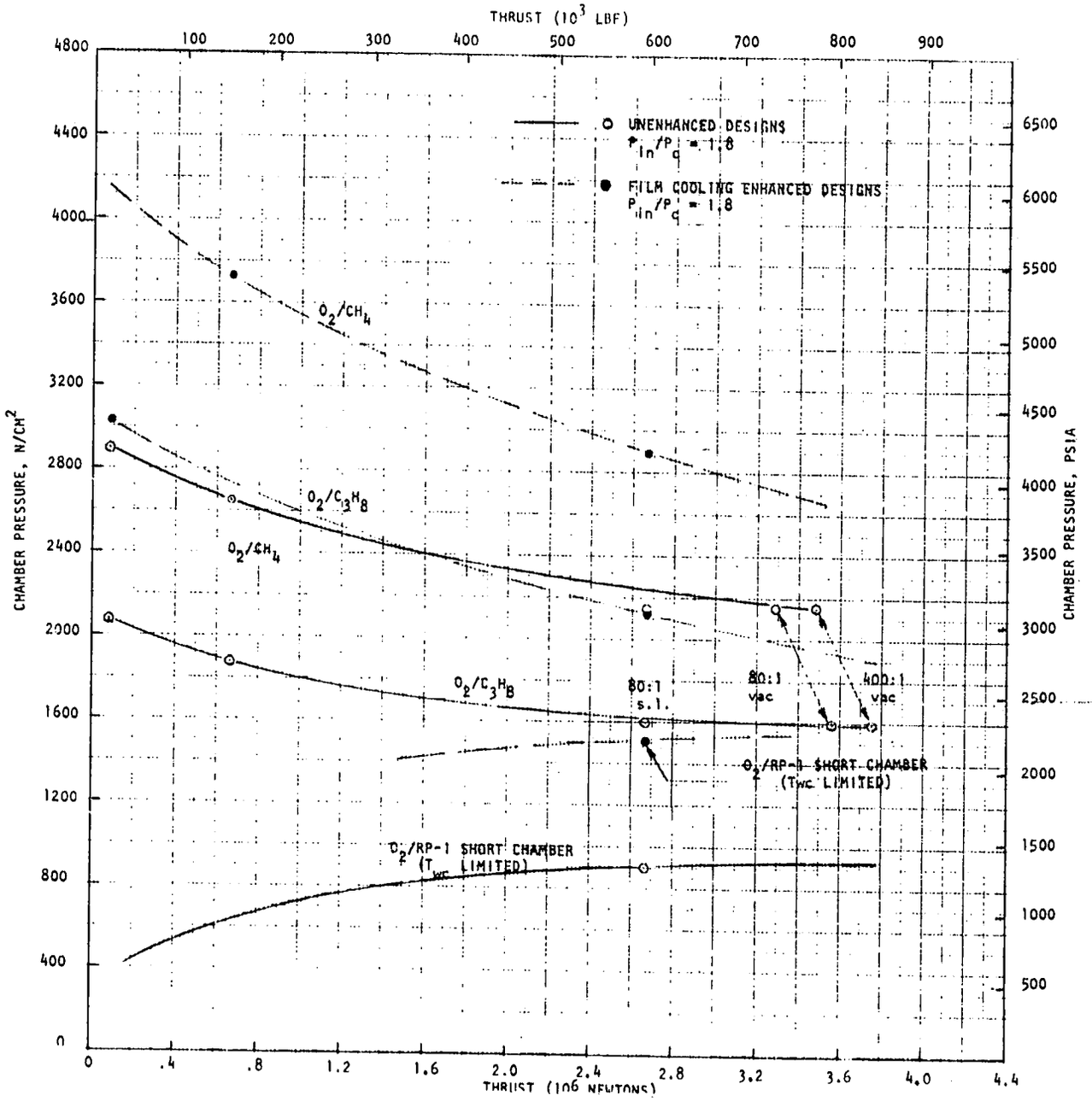

Figure 27. Effect of Thrust on Regenerative Cooling Limits for Film Cooling Enhanced Designs Compared to Unenhanced Designs

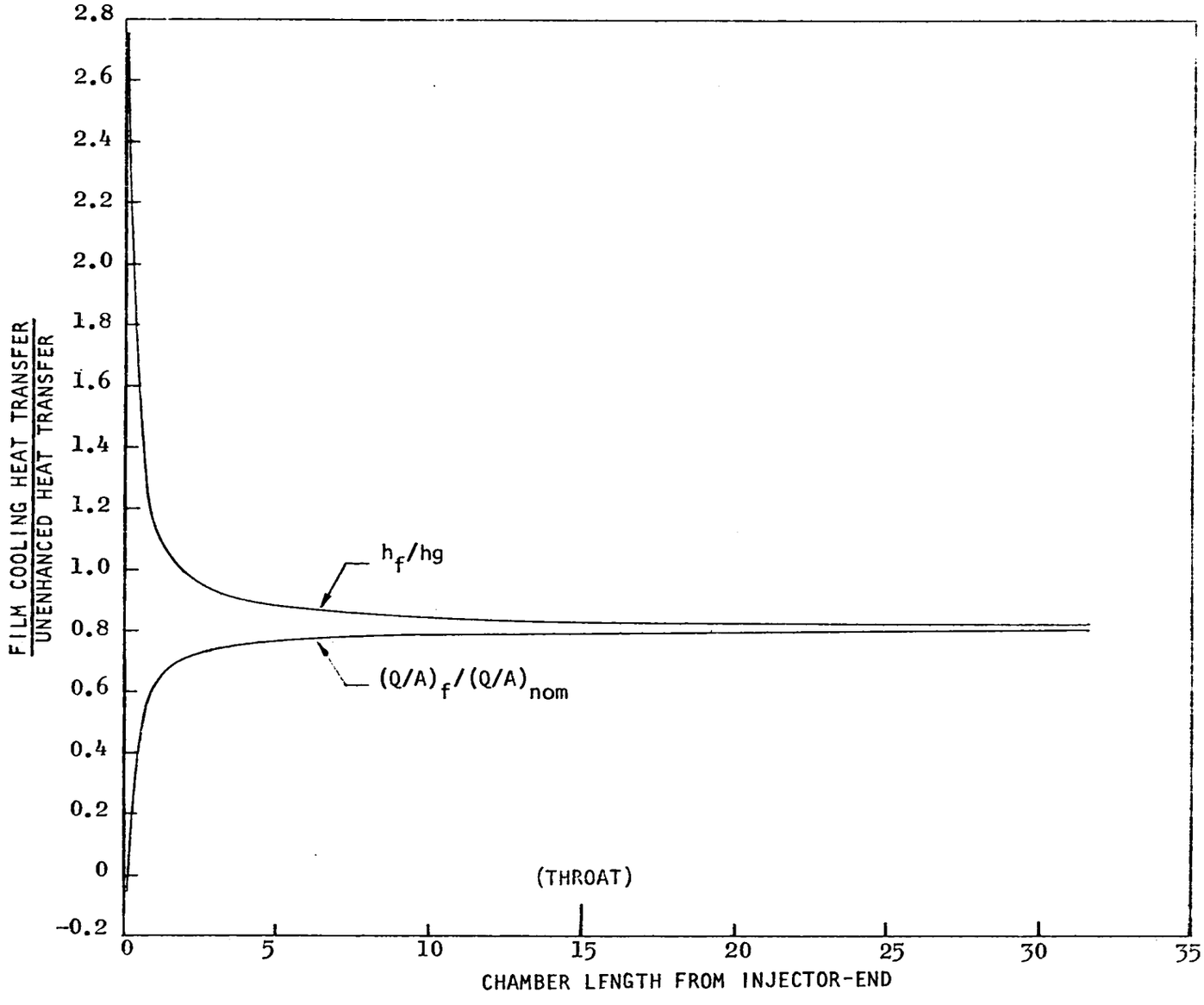

Figure 28. Typical Film-Coolant Heat Transfer Trends [2,668,800 N (600,000 lbf) O_2/CH_4 Chamber]

TRANSPIRATION COOLING

Transpiration cooling is applied by removing a regenerative-cooled section of the throat and replacing it with a section that inputs some fuel coolant through slots or a porous material. The optimum type of transpiration cooling is a wafer-type which also benefits from convective cooling and conduction as the transpiration coolant is injected through slots to the hot-gas wall. However, this study considers only the conventional type of transpiration cooling. It is assumed that the coolant is injected through a porous-type material and there are no convective or conduction benefits. Also, only CH_4 and C_3H_8 are considered because of the potential coking problems with RP-1 fuel.

Assessment

Considerable analytical and experimental effort has been expended in past years in the area of transpiration cooling. Most analyses, however, considered laminar flow systems, largely because this type is more amenable to solution. There has been some work in the area of turbulent flow.

The successful turbulent correlation of the Rannie equation for similar gas injection (Ref.16) suggested that his approach has a reasonably firm basis for extension to foreign gas injection. The original equation derived by Rannie is:

$$\frac{T_{aw}-T_c}{T_{wg}-T_c} = \left[1+\frac{C_{pc}}{C_{pg}}(1.18\ Re_b^{0}-1)(1-e^{-37\frac{G_c}{G_g}Re_b^{0.1}})\right].e^{-37\frac{G_c}{G_g}Re_b^{0.1}Pr} \qquad (41)$$

where the ratio C_{pc}/C_{pg} reflects one of the properties differences between the injected coolant and primary gases. A more accurate analysis would use enthalpy rather than temperature differences. Using this concept in a derivation similar to Rannie's, one obtains the following relation (Ref. 5):

$$\frac{H_g-H_c}{H_w-H_c} = \left[1+(1.18\ Re_b^{0.1}-1)(1-e^{-37\frac{G_c}{G_g}(\frac{\mu_w}{\mu_*})Re_b^{0.1}})\right].e^{37\frac{G_c}{G_g}(\frac{\mu_w}{\mu_*})Re_b^{0.1}Pr} \qquad (42)$$

A viscosity ratio correction (μ_w/μ_*) has been included to account for the change across the sublayer. The asterisk denotes an appropriate mean value of

a parameter in the sublayer. The enthalpy at the wall (H_w) refers to the enthalpy of the mixture at the wall and is, therefore, not readily obtained without consideration of the concentration profile of the injected gas. An equilibrium concentration profile exists whenever a foreign gas is injected into the flow of a primary gas. Knowledge of this profile is necessary not only for evaluating the enthalpy of the mixture at the wall, but, also, for use in determining mean sublayer values of various parameters. The calculation of this profile can be accomplished in the same manner that Rannie develops for his basic transpiration relation and is given below:

$$\frac{C_{1g}-1}{C_{1w}-1} = \left[1+\frac{Sc_*}{Sc}\frac{\mu_\delta}{\mu_*}\left(1.18\ Re_b^{0.1}-1\right)\left(1-e^{-37\frac{G_c}{G_g}\frac{\mu_w}{\mu_*}Re_b^{0.1}}\right)\right].e^{37\frac{G_c}{G_g}\frac{\mu_w}{\mu_*}Re_b^{0.1}Sc_*} \qquad (43)$$

Equation 43 relates the mainstream and wall concentration of the injected gas as a function of various parameters. To determine the wall concentration, it is necessary to specify the concentration of the injected gas in the mainstream (C_{1g}). The usual assumption is that $C_{1g}=0$, thereby implying that all of the injected gas remains in the boundary layer. Having selected a value for C_{1g}, Eq. 43 may be solved for C_{1w}:

$$C_{1w} = 1 - \frac{1}{\phi} \qquad (44)$$

where ϕ = righthand side of Eq. 43

The relation (Eq. 44) above, used in conjunction with Eq. 42, represents the solution to the problem of transpiration cooling using foreign gas injection. The actual solution requires the use of a digital computer because of the iterative process involved. To perform the necessary calculations, the variation of viscosity, Schmidt number, and Prandtl number with concentration must be known.

Calculations for hydrogen injection into air were performed using the preceeding analytical technique, and were compared with results based on the original form of the Rannie equation. The variation of the parameters of interest with concentration were obtained from Ref. 17. The results of the analysis are presented in Fig. 29, where the usual temperature ratio term $\eta = (T_{aw} - T_c/T_{wg} - T_c)$ is presented as a function of the coolant to gas flow ratio requirements. It is apparent that the modified analysis presented herein predicts considerably less coolant flow required to maintain a given wall termperature than does the Rannie equation.

The validity of the modified analysis is strengthened if a simple heat balance is considered. If it is assumed that the Stanton number (St) is unaffected by the coolant injection, there results from a simple heat balance the linear relation:

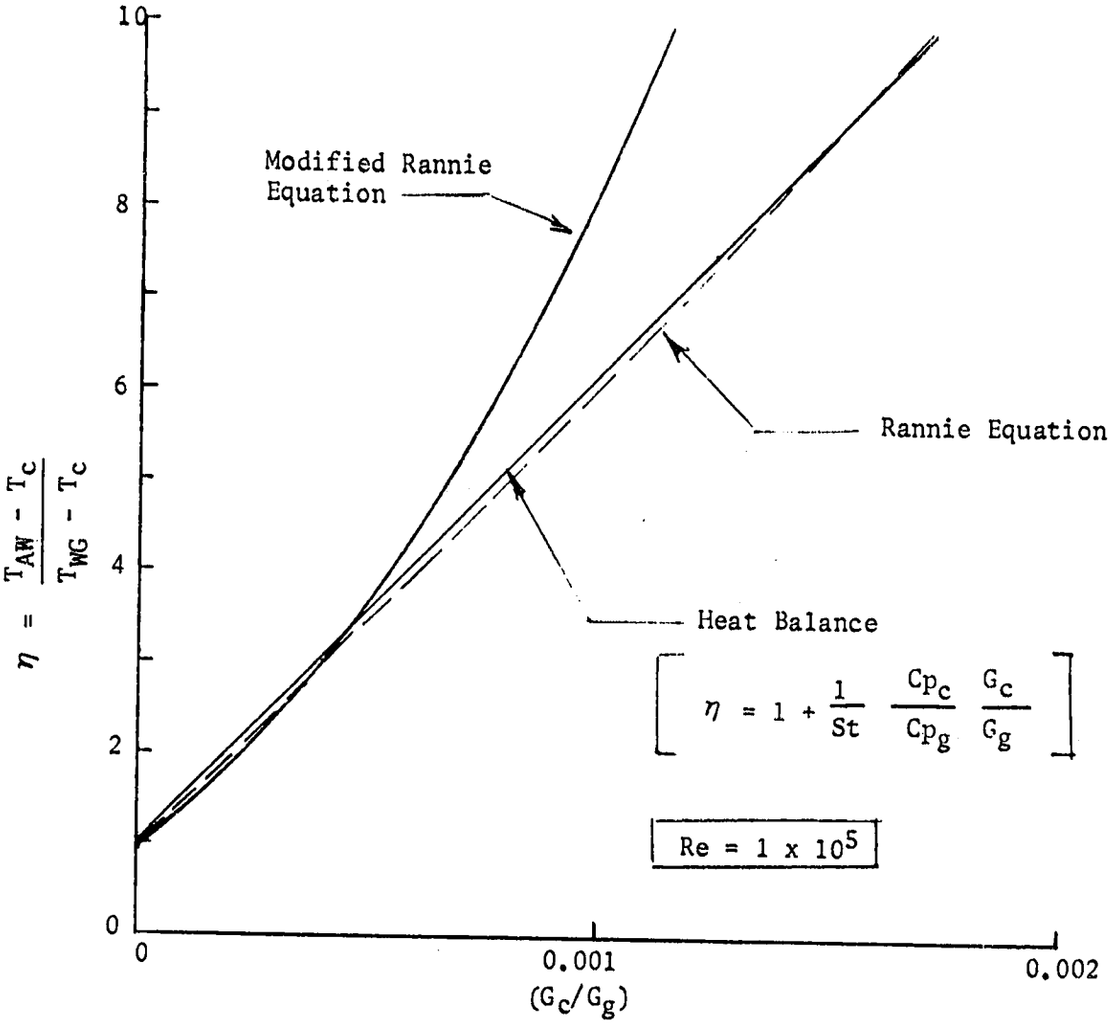

Figure 29. Comparison of the Modified Analysis for Foreign Gas Injection With the Rannie Equation for Hydrogen Injection Into Air

$$\frac{T_{aw}}{T_{wg}} = 1 + \frac{1}{St}\frac{C_{pc}}{C_{pg}}\frac{G_c}{G_g} \tag{45}$$

which is also plotted in Fig. 29 using the standard relation for Stanton number:

$$St_x = \left(\frac{h_g}{G_g\ C_{pg}}\right)_x \tag{46}$$

It is apparent in Fig. 29 that the Rannie relation and the heat balance relation are nearly identical. It is known, however, that the effect of "blowing" is to reduce the Stanton number and, thereby, the coolant flowrate requirements so that the modified analysis appears more appropriate. However, because of the simplicity of the heat balance relationship, it will be used in this study for the transpiration cooling analyses.

Combining Eq. 45 and 46:

$$G_c = \frac{hg_x}{C_{pc}}\left(\frac{T_{aw} - T_c}{T_{wg} - T_c} - 1\right) \tag{47}$$

Therefore, the transpiration cooled area is:

$$A_{TC} = \frac{\dot{\omega}_{TC}\ C_{pc}}{\left(\frac{T_{aw} - T_c}{T_{wg} - T_c}\right)-1\quad hg_x} \tag{48}$$

Design Analysis

In determining the effect of transpiration cooling in conjunction with regenerative cooling on the design chamber pressure limits, several assumptions must be made. The required hot-gas wall temperature, T_{wg}, was established as 589 K (1060R) to meet cycle life, ϕ has been a restricting factor. Second, the transpiration coolant flowrate will nominally be 3.5% of the total propellant mass flowrate to meet the 3% performance loss criteria.

These previous correlations represent transpiration cooling efficiencies of 100%. The actual hot-gas wall area cooled with transpiration cooling departed from this value with the assumption of an 85% cooling efficiency.

The regenerative cooling circuit chosen for this analysis is an uppass circuit which bypasses the throat and combustion chamber surface area to be transpiration cooled. The transpiration coolant flow enters at the same temperature as the regenerative coolant flow. The coolant is manifolded around a porous wall through which the coolant transpires through the hot-gas wall and forms a film that mixes with the boundary layer. The cooling is basically derived from the heat capacitance of the coolant. Figure 30 illustrates the cooling design analyzed for the O_2/CH_4 and O_2/C_3H_8 propellant combination. While it is realized that the transpiration coolant must have a variable pressure along the injection surface of the porous wall to accommodate the variable hot-gas flow conditions, parameters are averaged over the cooling surface area. The reduced efficiencies are assumed to account for maldistribution of the cooling. O_2/RP-1 was not considered for transpiration cooling because of the probability of RP-1 coking and plugging the pores of the wall material.

The transpiration cooled design results are summarized in Table 10 and compared to the unenhanced chamber pressure limits. The chamber designs are graphically presented in Fig. 129 through 132 of Appendix D. The nozzle designs are identical to those for other thermal barriers as graphically presented in Fig. 108, 112, 137, and 140 of Appendix D. All transpiration cooled designs were at the guideline chamber pressure limits with the exception of the 2,669,000 N (600,000 lbf) thrust O_2/C_3H_8.

The chamber geometry reflecting the transpiration-cooled areas and regeneratively cooled areas is summarized in Table 11. The transpiration-cooled area (A_{TC}) was defined by Eq.48. The transpiration-cooled insert was terminated just downstream of the geometric throat. The attractiveness of this approach to increase chamber pressure limits is dependent on recovering most of the very high regenerative velocity head at both discharge regions. This would require some very unique designs in these regions. Practical designs would not suffice. However, design optimization of the regenerative-cooled discharge regions and possibly the use of a more optimum wafer-type transpiration-cooled region should reflect the design limits established by this study.

ZONED COMBUSTION

Zoned combustion (mixture ratio bias) is a means of normally reducing the wall heat flux by running the outer perimeter of injector elements at a mixture ratio below nominal (where the nominal mixture ratio is below stoichiometric) while running the core elements at a mixture ratio above nominal. In theory, this provides a reduced temperature combustion gas along the wall with a high temperature core flow. From a cooling standpoint, the most effective case of zoned combustion would be the limiting case of film cooling where the outer zone mixture ratio, in effect, becomes zero.

Assessment

One method of normally reducing combustor wall heat flux is the use of low mixture ratio zones in the elements adjacent to the wall. This is closely akin to film cooling except, instead of directing fuel streams on or adjacent to wall, the outer row of elements is reduced in mixture ratio. This reduces the

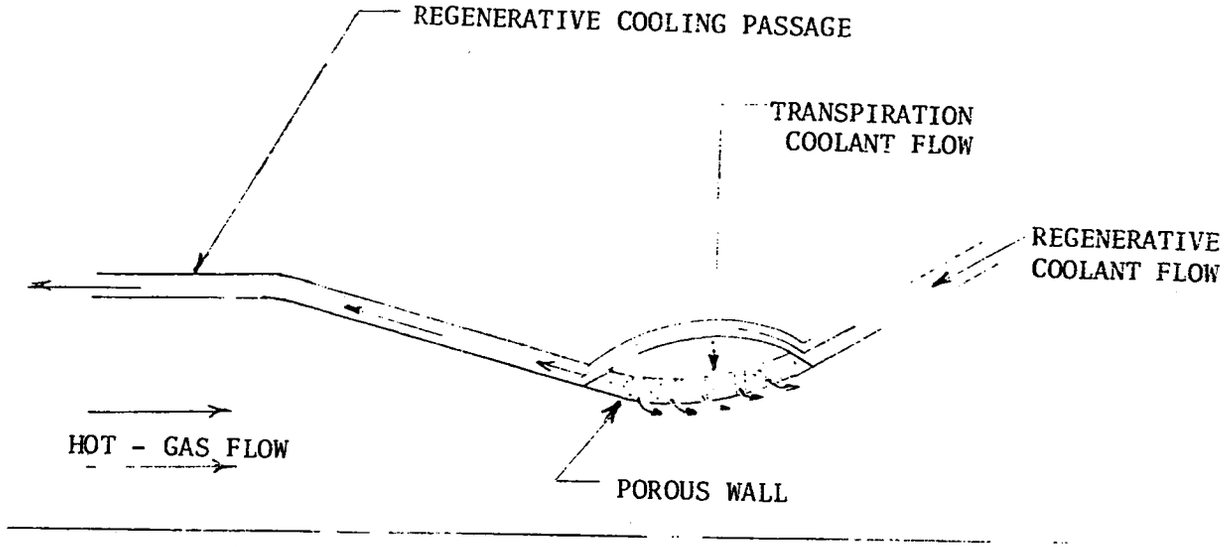

Figure 30. Combination Regenerative/Transpiration Cooling Method

TABLE 10. SUMMARY OF HIGH-PRESSURE HYDROCARBON-FUELED ENGINE
(TRANSPIRATION COOLING ENHANCED COMBUSTION CHAMBER)
REGENERATIVE COOLING LIMITS

METRIC UNITS

Propellant Combination	Thrust (Newtons)	Coolant P_{in}/P_c	Max P_c (N/cm^2)	P_c Limiting Factor	Cooling Circuit	Chamber-To-Nozzle ϵ	Minimum LW (cm)	Channel Width (cm)	Channel Wall Thickness (cm)	Nozzle Min. ITD (cm)	Nozzle Min. Wall Thickness (cm)
O_2/C_3H_8	89,000 vac	1.8	2654	T_{wg}, T_{wc}, Life	Series	10:1	0.076	0.137/0.102/ 0.076	0.102/0.074	0.127/0.434*	0.018/0.076
O_2/C_3H_8	2,669,000 s.l.	1.8	3240	T_{wg}, Life	Split	9.5:1	0.076	0.178/0.127/ 0.076	0.14/0.097/ 0.064	0.203 **	0.018 **
O_2/CH_4	667,000 vac	1.6	3450	Life	Series	10:1	0.076	0.152/0.081/ 0.076/0.102	.112/.064/ 0.071	0.229/0.434*	0.02/0.03/ 0.025*
O_2/CH_4	2,669,000 s.l.	1.55	4140	T_{wg}, Life	Split	9.5:1	0.076	0.229/0.127/ 0.102	0.188/0.094 0.069/0.064	0.203 **	0.018 **

* ZIRCONIUM OXIDE NOZZLE DESIGNS
** COMBINED ENHANCEMENT DESIGNS

TABLE 10. (Concluded)

ENGLISH UNITS

Propellant Combination	Thrust (lbf)	Coolant P_{in}/P_c	Max P_c (psia)	P_c Limiting Factor	Cooling Circuit	Chamber-To-Nozzle ε	Minimum LW (in)	Channel Width (in)	Channel Wall Thickness (in)	Nozzle Min. uTD (in)	Nozzle Min. Wall Thickness (in)
O_2/C_3H_8	20,000 vac	1.8	3850	T_{wg},T_{wc} Life	Series	10:1	.03	.054/.04/ .03	.04/.029/ .025	.05/.171*	.007/.33*
O_2/C_3H_8	600,000 s.l.	1.8	4700	T_{wg},Life	Split	9.5:1	.03	.07/.05/.03	.055/.038/ .025	.08**	.007**
O_2/CH_4	150,000 vac	1.6	5000	Life	Series	10:1	.03	.06/.032/ .03/.04	.044/.025 .028	.09/.171*	.008/.012 .01*
O_2/CH_4	600,000 s.l.	1.55	6000	T_{wg},Life	Split	9.5:1	.03	.09/.05/ .04	.074/.037/ .027/.025	.08 **	.007 **

* ZIRCONIUM OXIDE NOZZLE DESIGNS
** COMBINED ENHANCEMENT DESIGNS

TABLE 11. TRANSPIRATION COOLED COMBUSTION CHAMBER GEOMETRY AND SURFACE AREAS

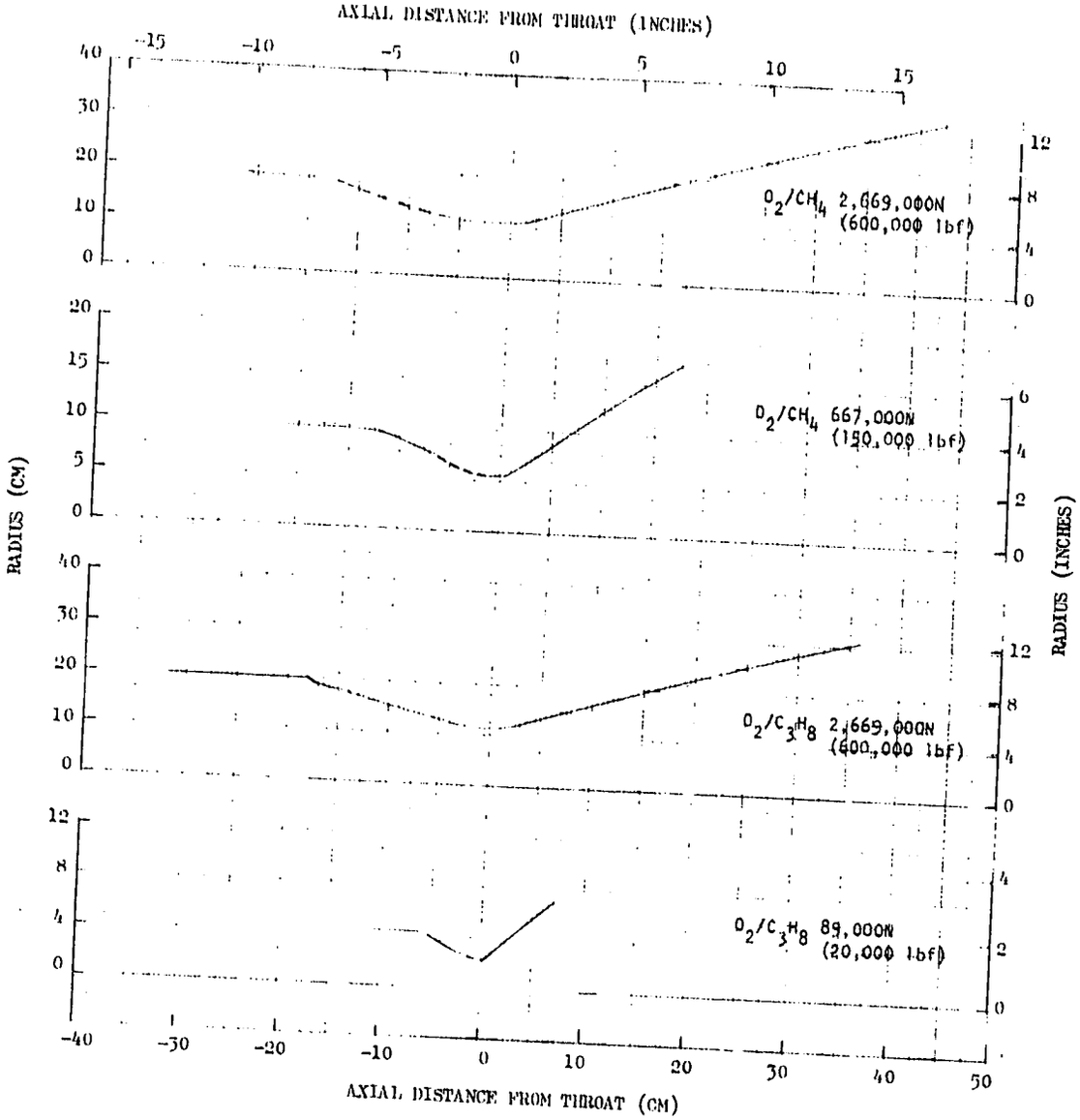

Propellant	Thrust N	Thrust (lbf)	P_c N/cm^2	P_c (psia)	Coolant P_{in}/P_c	A_{mcc} cm^2	A_{mcc} (in^2)	A_{T_c} cm^2	A_{T_c} (in^2)	X_{inj} cm	X_{inj} (in)	X_{T_c} cm	X_{T_c} (in)
O_2/CH_4	2,669,000	(600K)	4140	(6000)	1.55	2755	(427)	1632	(253)	26.2	(10.3)	16.5	(6.5)
	667,000	(150K)	3450	(5000)	1.6	1187	(184)	265	(41)	21.8	(8.6)	6.6	(2.6)
O_2/C_3H_8	2,669,000	(600K)	3240	(4700)	1.8	3673	(569)	1448	(224)	31.7	(12.5)	15.2	(5.96)
	89,000	(20K)	2760	(3850)	1.8	391	(60.5)	32.6	(5.1)	15.4	(6.1)	2.0	(0.80)

local flame temperature, and the average gas flow temperature through a fairly thick layer adjacent to the wall. The disadvantage of this system is that the outer row of injection elements typically involve a high percentage of the injected mass. This is especially true for smaller engines where this outer zone exceeds half the total flow.

The outer row mass flow was determined for the three typical engine sizes in the range of interest for this study. Several items go into the estimate for each of these sizes. For example, the smallest engine was 89,000 N (20,000 lbf) thrust engine with a 10.16-cm (4-in.) combustion chamber diameter. The first 0.51 cm (0.20 in.) radial distance at the injector face was assumed to be acoustic cavity for providing damping for combustion stability. An estimate was then made of the manifold size and element spacing that would be expected in an injector of this size and flowrate. The outer zone was taken as the area outside a median line between the outer element location and the second row of injection elements all the way to the combustor wall (including that area utilized for the acoustic cavity). The median line between the outer and the second row of elements was estimated to be 6.60 cm (2.6 in.) in diameter, the area outside of that line being 58% of the total combustor face area. Uniform injection mass flux was assumed, which means that 58 percent of the total mass flow should likewise be injected in this zone.

The other injector examples are treated in a similar manner. The larger injectors will require a wider acoustic cavity, and physically larger manifolds. This means that the mean line between the outer row and the second row will be radially further from the wall in a larger chamber, but the percent of area in the outer zone will decrease. An example, the mean line for a 25.40 cm (10-in.) diameter chamber is estimated to be 20.8 cm (8.2 in.) chamber). The outer zone percentage for this size chamber is 33% of the total. A similar technique results in an outer zone area of 21% for a 63.5 cm (25 in.) chamber.

These values are typical for ordinary fabrication techniques, and it is possible to provide somewhat smaller zones with special attention to design and fabrication. Also, different element types result in differing spacing with elements such as coaxial or triplets requiring wider spaces than the doublet configuration assumed in this study. Deliberate interzone mixing also can be introduced to limit the mass percentage involved with the outer wall zone. Also, an element row can be designed, which has a mixture ratio bias within the element zone to reduce the mass fraction involved at the low ratio. Typical of this approach is the use of edge-impinging fans in like-impinging doublet systems, with fan offset in the outer row (Fig. 31). All of these techniques have been applied in previous injector designs with varying degrees of success. The reduction in cooling effectiveness by transverse mixing is difficult to predict, and becomes even more unpredictible as these alternate techniques are used to provide thinner low mixture ratio sections. These type of designs would require use of the Rocketdyne film-cooling model to determine their effectiveness.

Specific impulse performance looses and shifts in mixture ratio were determined for a zoned injector combustor. Criteria for the zoned design were based on practical hardware injector impingement area cross sections. For the three thrust levels, Table 12 summarizes typical chamber and zone dimensions and percentage of total chamber flowrates.

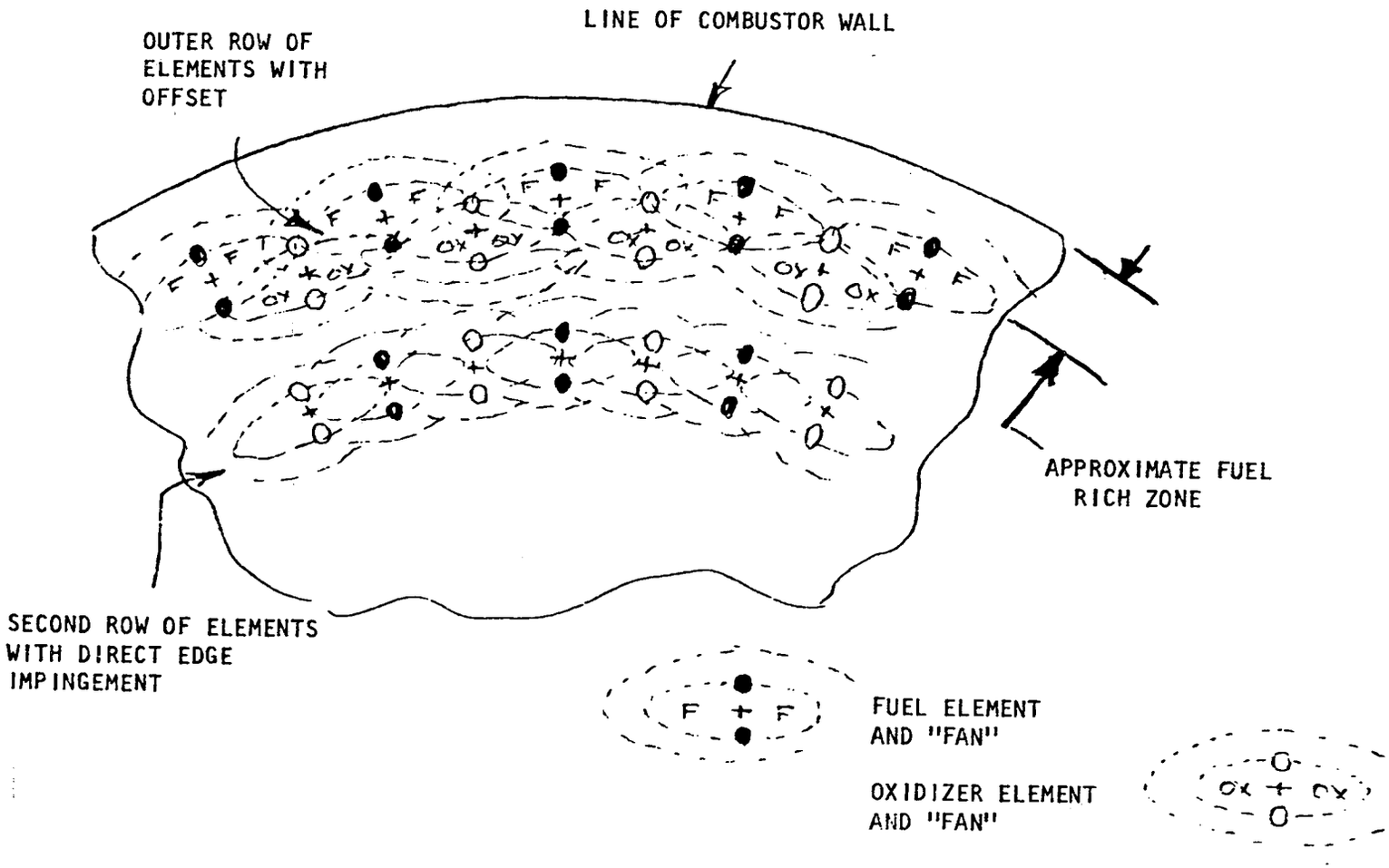

Figure 31. View of Typical Like-Impinging Injector Face Showing Element Offset in Outer Row To Provide Fuel Rich Zone Adjacent to Wall

TABLE 12. ZONED COMBUSTION INJECTOR MODEL DESIGN CONSTRAINTS

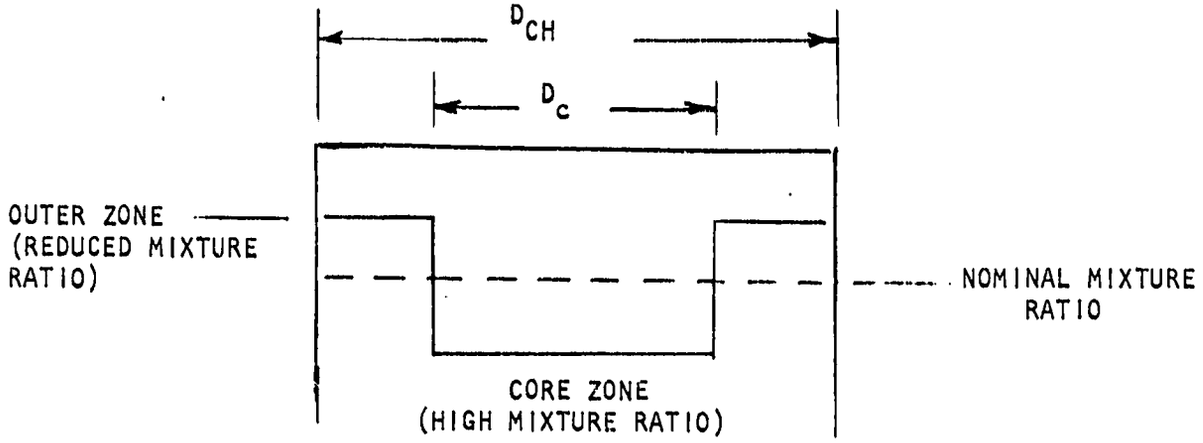

THRUST, N (lbf)	CHAMBER DIAMETER D_{CH} cm	INCHES	ZONE DIAMETER D_c cm	(INCHES)	PERCENTAGE OF TOTAL FLOW RATE IN OUTER ZONE
89,000 (20,000)	10.2	(4)	6.6	(2.6)	58
667,000 (150,000)	25.4	(10)	20.8	(8.2)	33
2,669,000 (600,000)	63.5	(25)	56.6	(22.3)	20.4

Table 12 data are applicable for all three propellant combinations (O_2/RP-1, O_2/CH_4, O_2/C_3H_8). Relative zonal flowrates shown in Table 12 were established using the criteria afforded by minimum stream boundary mixing within the chamber. This was satisfied by selecting equal stream mass velocities, ($\rho v = w/A$). The mathematical relationships governing mixture ratio shifts, (core and outer zone) are given by the following equations:

$$A + \frac{MR_{eng} - MR_{\substack{Outer \\ Zone}}}{1 + MR_{\substack{Outer \\ Zone}}} \left(\frac{D_{CH}^2 - D_{Core}^2}{D_{Core}^2} \right) \tag{49}$$

$$MR_{Core} = \frac{MR_{Eng} + A}{1 - A} \tag{50}$$

$$I_{\substack{Eng \\ Vac}} + \frac{I_{\substack{Core \\ vac}} + \left(\frac{D_{CH}^2 - D_{Core}^2}{D_{Core}^2} \right) I_{\substack{Outer\ Zone \\ Vac}}}{1 + \left(\frac{D_{CH}^2 - D_{Core}^2}{D_{Core}^2} \right)}$$

Zonal specific impulse was generated using the JANNAF One-Dimensional Kinetics (ODK) Computer program. Reaction rate data used were those published on 10 January 1977 and represents the latest selected by the JANNAF Performance Standardization Working Group. Computations were made for a range of area ratios. However, for comparative studies, a single area ratio was selected, e.g., 400 to 1. Kinetic specific impulse is dependent on engine size relatively a weak function with slight improvements with higher thrust.

Performance analysis results are shown in Fig. 32 through 34. For selected percentages of I_s vacuum losses, the curves may be used to determine operational core and outer zone mixture ratios. The general nature of the curves does show larger performance losses for a fixed outer zone mixture ratio with higher amounts of outer zone flowrates. Performance sensitivity decreases with smaller amounts of outer zone film-cooling requirements.

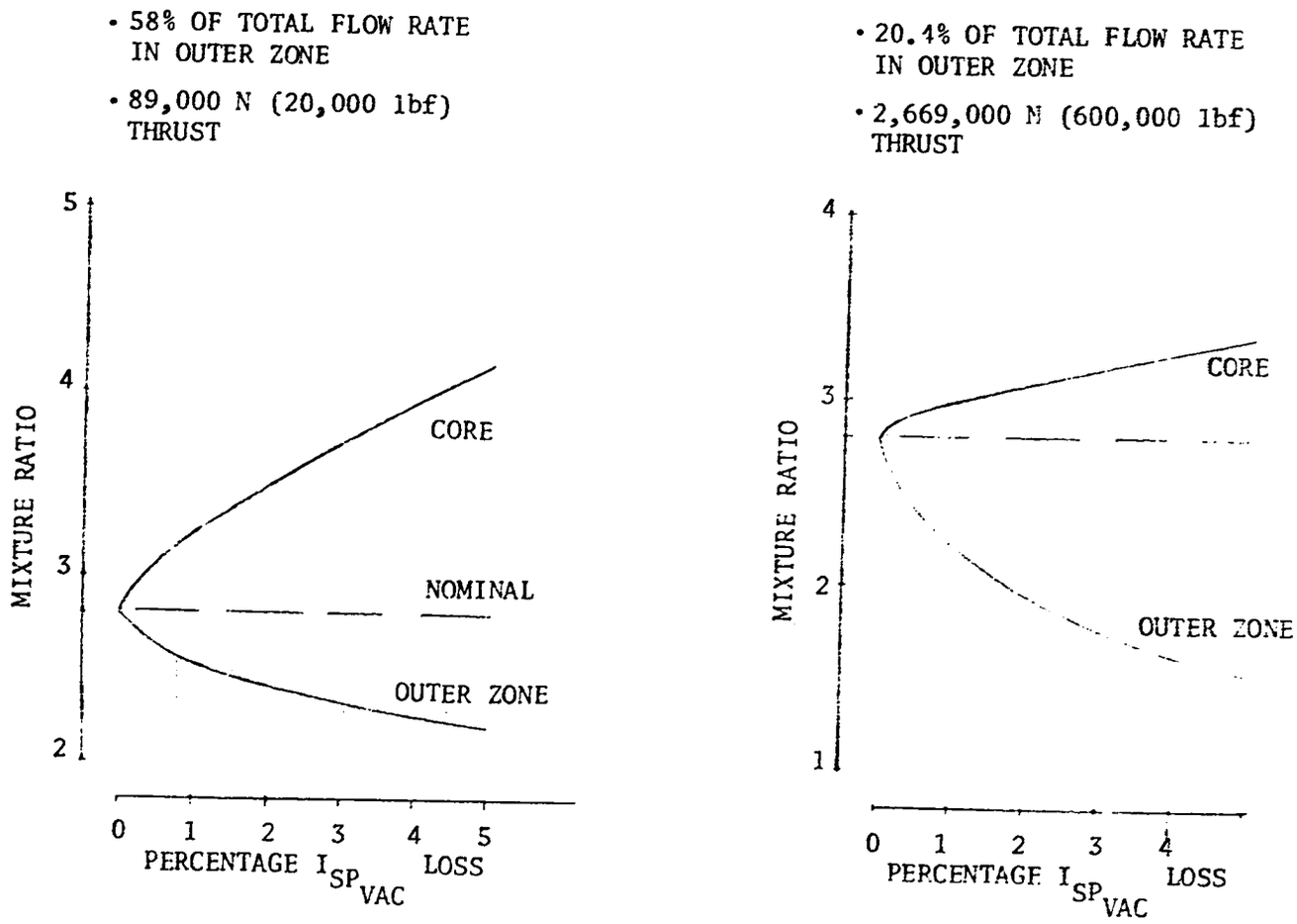

Figure 32. O_2/RP-1 Zoned combustion Core and Outer Zone Mixture Ratio Influence on Performance Loss for Constant Mass Flux

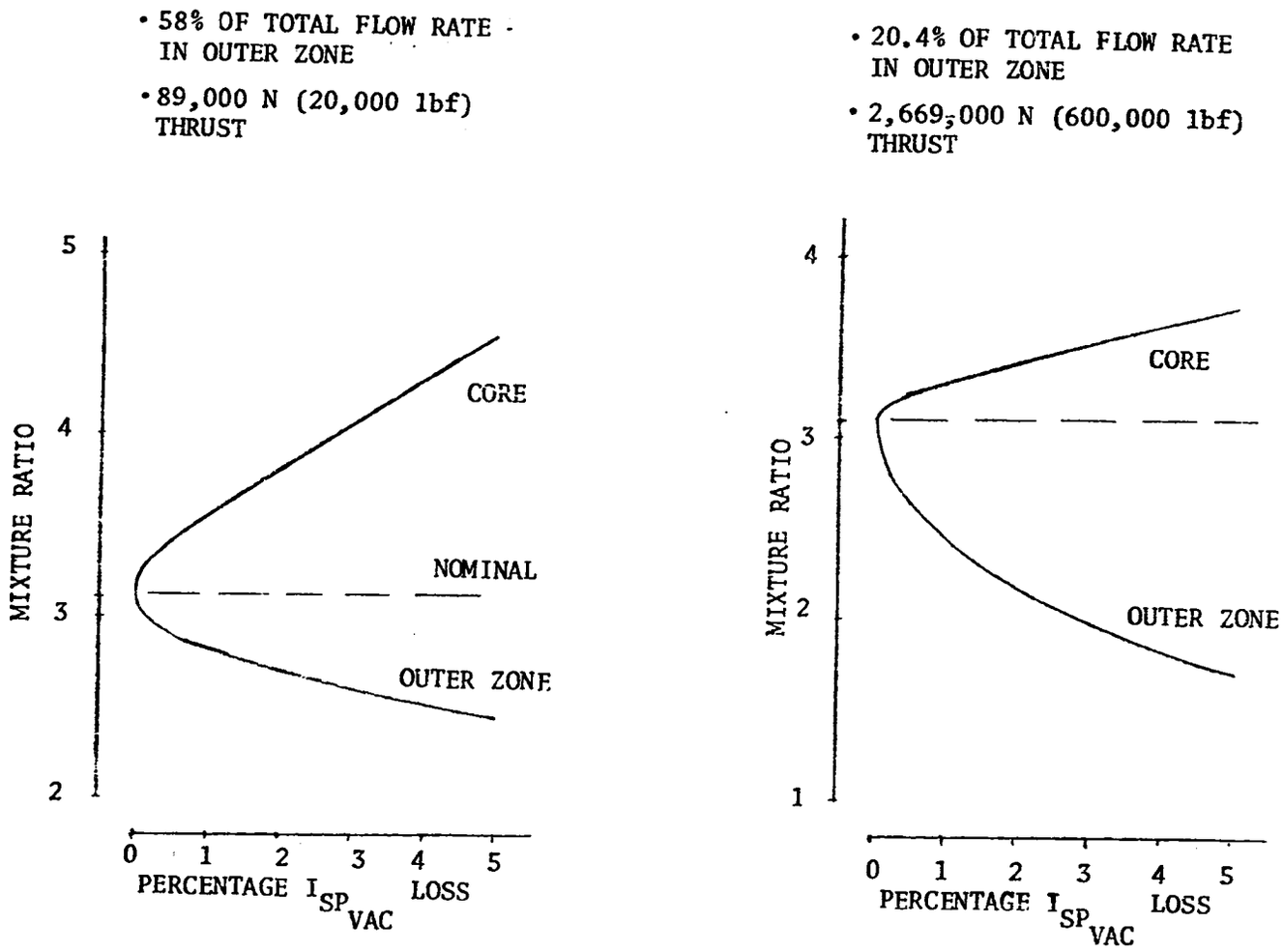

Figure 33. O_2/C_3H_8 Zoned Combustion Core and Outer Zone Mixture Ratio Influence on Performance Loss for Constant Mass Flux

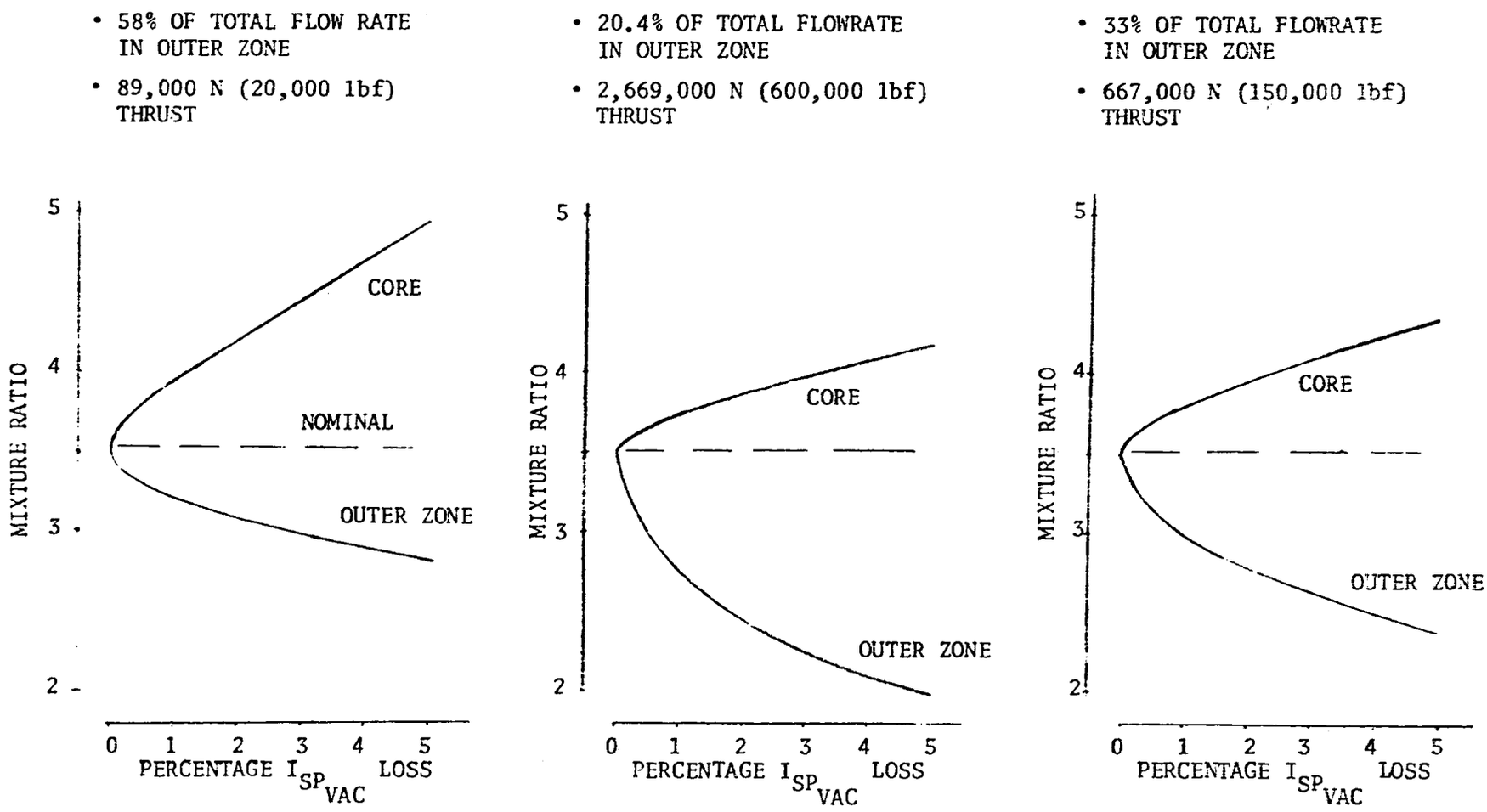

Figure 34. O_2/CH_4 Zoned Combustion Core and Outer Zone Mixture Ratio Influence on Performance Loss for Constant Mass Flux

Design Analysis

The zoned combustion chamber design analysis utilized a performance loss of 3%. The zoned combustion mixture ratio and core mixture ratio are depicted in Fig. 35 for the the three propellant combinations and thrust levels. The thermal analysis utilized the convective heat transfer coefficient and adiabatic wall temperature associated with the reduced zone mixture ratio. The chamber and nozzle surface and throat areas were for the nominal mixture ratio. In general, it was handled as a low mixture ratio case.

The zoned combustion outer zone and core mixture ratio also were based on a constant injection ρV and overall nominal mixture ratio. The allocated 3% performance loss is related to the theoretical performance of the zoned mixture ratio of the core and outer zone. The theoretical performance for the three propellant combinations is shown in Fig. 36 as a function of propellant mixture ratio. These values are based on the JANNAF One-Dimensional Kinetics (ODK) computer program. The nominal mixture ratio used for this study is denoted for each propellant combination.

The zoned combustion approach is graphically presented in Fig. 37 for the three thrust levels for the O_2/CH_4 propellant combination. The guideline 3% performance loss is shown by a 3% vertical displacement from the peak performance (nominal mixture ratio). The outer zone and core mixture ratio for a constant injection ρV is a straight line intersecting the 3% vertical offset. The slope of this line is determined by the percentage of outer zone mass flowrate to the total mass flowrate, as depicted for the three thrust levels. It can be seen in Fig.37 that the 3% performance loss is associated with the reduced performance core and outer zone mixture ratio. Therefore, it can be rationalized that the characteristic velocity efficiency (ηc^*) of the zonal mixture and core mixture are at the nominal guideline efficiency of 98% as controlled by the injector/chamber design. This means that the theoretical combustion temperature of the outer zone would, accordingly, be reduced to reflect 98% ηc^*. However, the actual characteristic velocity (c^*) for sizing the chamber throat is 3% lower than used for the nominal mixture ratio instead of the actual c^* presented in the propellant properties figures (Appendix B). The actual c^* presented in the propellant properties figures reflects an overall mixture ratio equal to the outer zone mixture ratio.

The hot-gas-side convective heat transfer coefficient (h_g) profile used a boundary layer analysis for the six design cases noted in Table 5. As might be expected, the h_g increases for the reduced mixture ratio of the outer zone near the wall. The boundary layer convective heat transfer coefficient is a function of the transport properties at the designated chamber pressure, as noted below:

$$h_g \alpha \frac{\mu^{0.2} C_P}{Pr^{0.6}} \qquad (52)$$

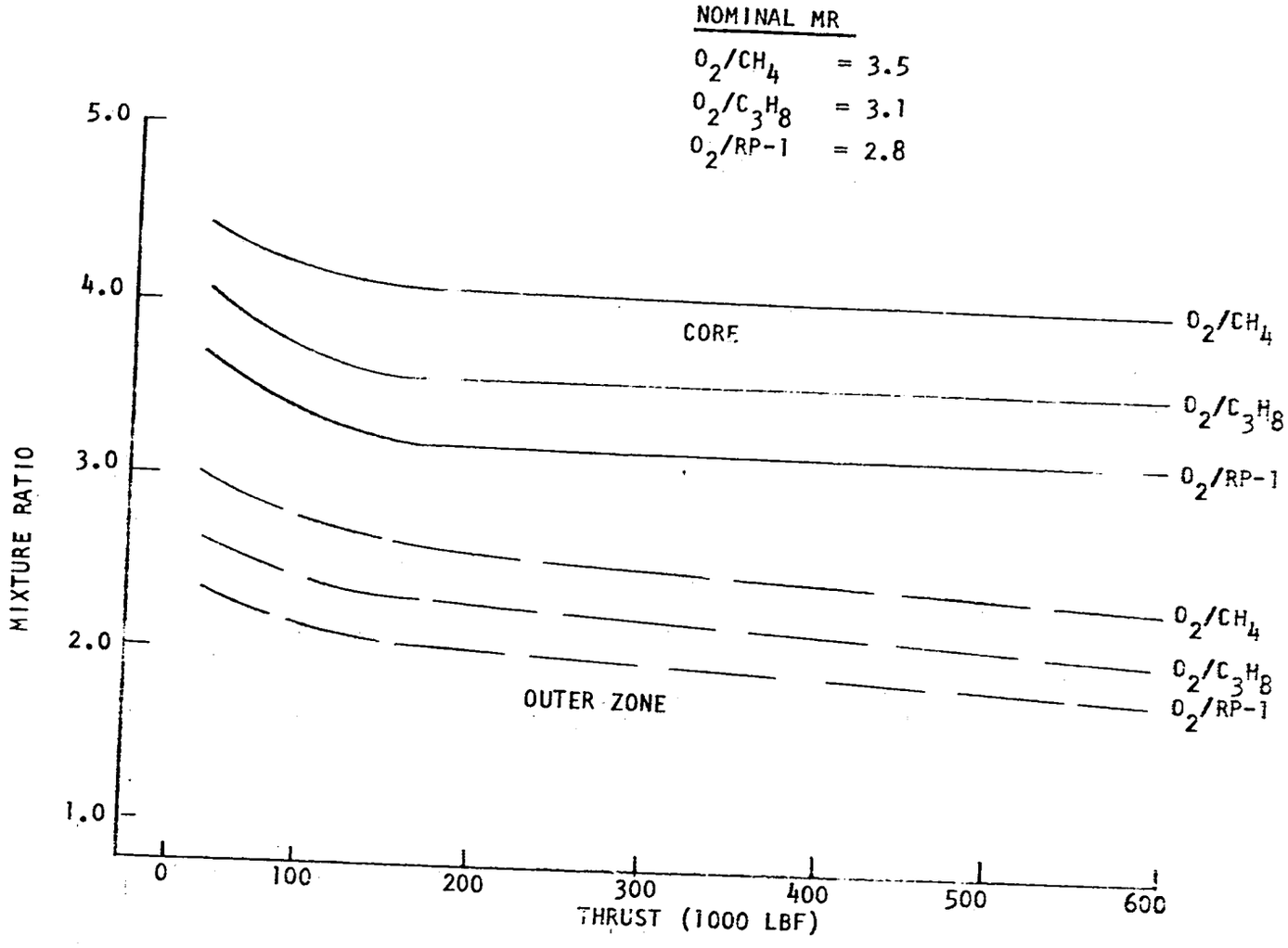

Figure 35. Zoned Combustion Core and Outer Zone Mixture Ratio as a Function of Thrust Level and Propellant Combination for 3% Performance Loss

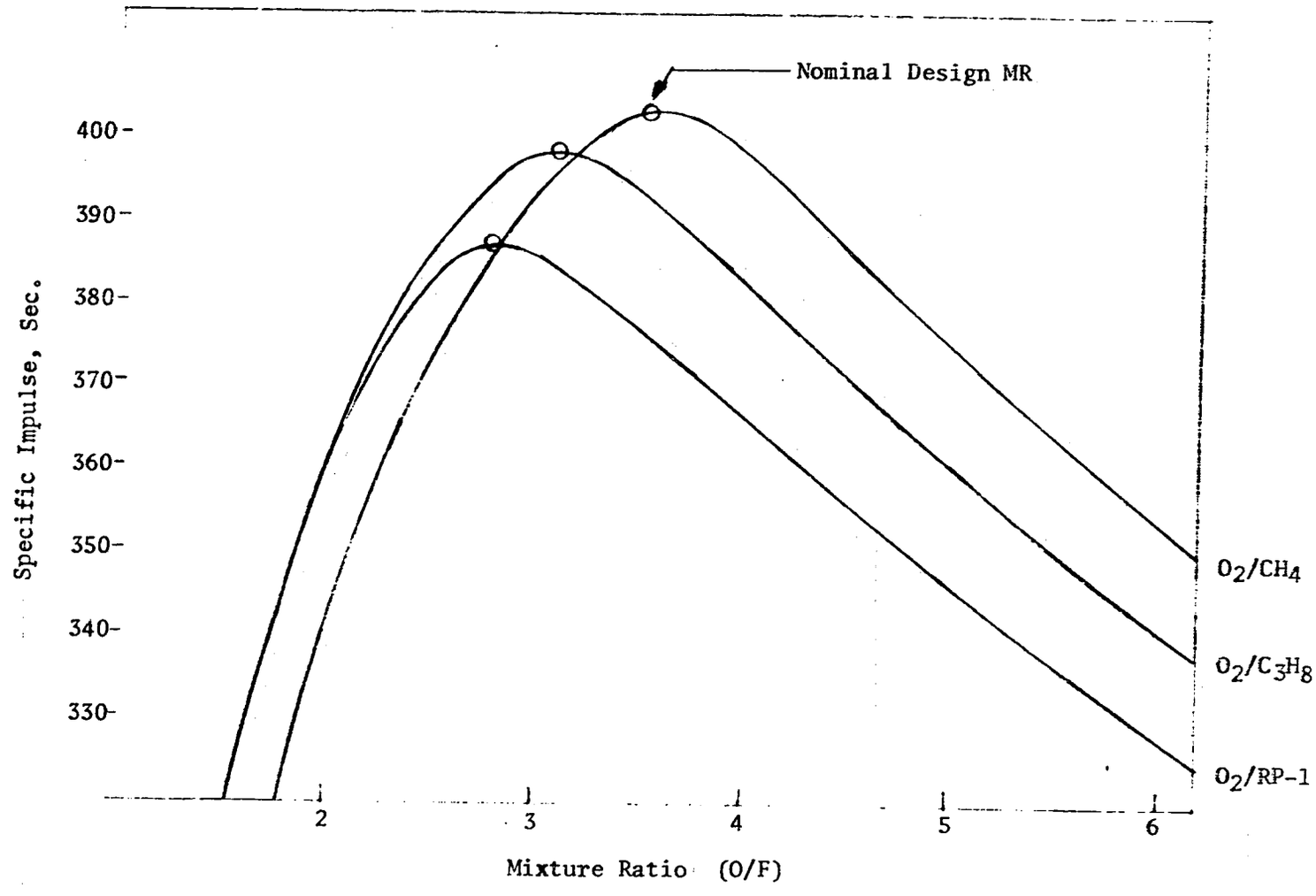

Figure 36. One-Dimensional Kinetic (ODK) Specific Impulse versus Mixture Ratio for the Three Propellant Combinations

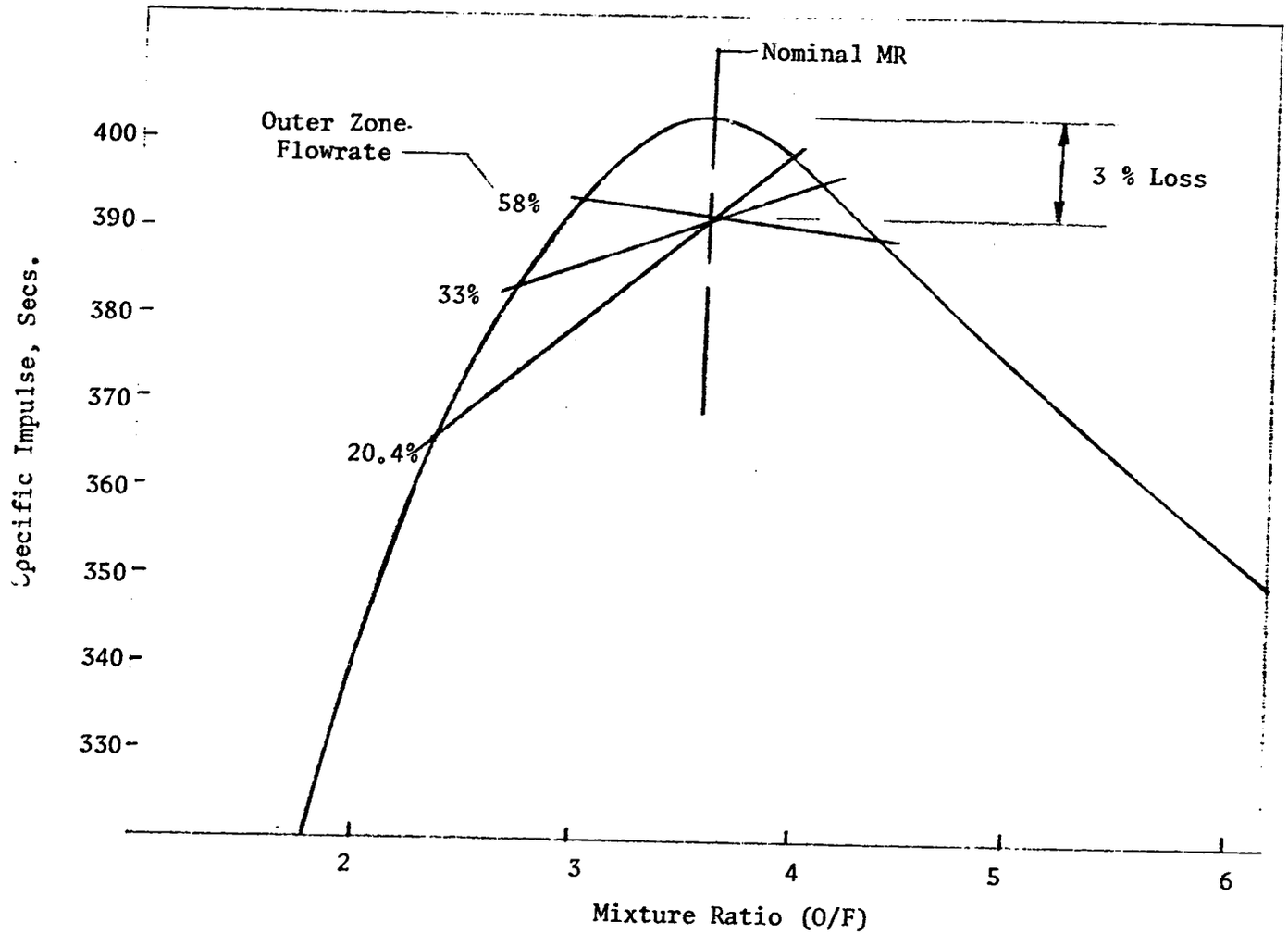

Figure 37. Zoned Combustion Graphical Approach for the Three Thrust Levels for O_2/CH_4 Propellant Combination

The local heat flux is

$$Q/A = h_g (T_{aw} - T_{wg}) \tag{53}$$

The zoned combustion heat flux can be compared to the nominal mixture ratio heat flux by:

$$\frac{(Q/A)_{Zone}}{(Q/A)_{Nom.}} = \left(\frac{\mu_{Zone}}{\mu_{Zone}}\right)^{0.2} \left(\frac{c_{p_{Zone}}}{c_{p_{Nom.}}}\right) \left(\frac{Pr_{Nom.}}{Pr_{zone}}\right)^{0.6} \frac{(T_{aw} - T_{wg})_{zone}}{(T_{aw} - T_{wg})_{Nom.}} \tag{54}$$

Although the adiabatic wall temperature (T_{aw}) is substantially reduced for the zoned mixture ratio, the zoned heat flux provides little or no benefit toward increasing the chamber pressure. This trend is shown in Fig. 38 for the respective mixture ratio and chamber pressure for each propellant combination at the noted thrust level. The chamber pressure of the zoned combustion design to attain a life of (250 x 4) cycles is related to the nominal unenhanced design by:

$$\frac{P_{c_{zoned\ comb.}}}{P_{c_{unenhanced}}} = \left[\frac{(Q/A)_{Nom.}}{(Q/A)_{Zoned}}\right]^{1.25} \tag{55}$$

This results in the unenhanced O_2/CH_4 design chamber pressure being increased from 2144 N/cm^2 (3110 psia) to 2344 N/cm^2 (3400 psia). Graphic presentation of this design is presented in Fig.133 and 134, Appendix D. The only other propellant combination and thrust level that would attain a higher chamber pressure would be the 89,000 N (20,000 lbf) thrust O_2/RP-1 design. However, the 89,000 N (20,000 lbf) thrust O_2/RP-1 unenhanced design could not meet the coolant wall criterion (589 K, 1060 R). Therefore, it was not deemed necessary to evaluate this zoned combustion design.

Undoubtably, one would expect a reduced heat flux for a lower mixture ratio as denoted by zoned combustion. However, as previously noted, the outer zone operates at a η_{c^*} = 98% as designed for a constant injection ρV. Therefore, the analysis is representative of a chamber designed to operate at this mixture ratio as though it were a constant overall mixture ratio. A theoretical heat flux plateau exists for all propellant combinations for the mixture ratio dome region of maximum energy release efficiency. There are Rocketdyne experimental O_2/H_2 data that tend to support this trend over a mixture ratio range of 5.0 to 7.0 for a constant injection overall mixture ratio.

There are also experimental O_2/H_2 zoned combustion data that contradict this analysis. However, these data are primarily for injectors that were designed for nominal mixture ratio and later modified for reduced outer zone mixture ratio to alleviate combustor wall hot spots as a function of circumferential position. These latter injector designs do not operate at a constant injector ρV. It is believed that zoned combustion provides a heat flux reduction greater than theoretically predicted because it actually suppressses the local heat fluxes associated with the nonuniformity of local injection mass fluxes and

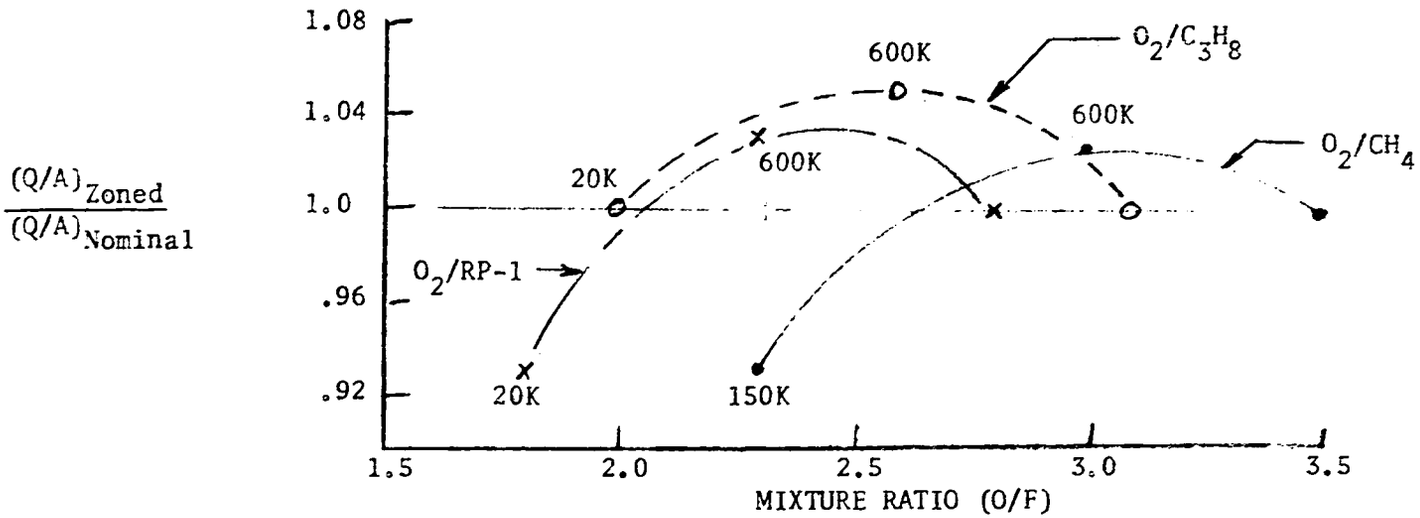

Figure 38. Comparison of Zoned Combustion Chamber Heat Flux to Unenhanced Chamber Heat Flux at Nominal Mixture Ratio

mixture ratio variations off nominal. Besides, it is difficult to believe that zoned combustion has less effect in reducing the heat flux than a nonoptimum nominal mixture ratio injector with a similar performance loss where:

$$T_{aw} \alpha (\eta_c^*)^2 \tag{56}$$

and

$$Q/A \alpha (T_{aw} - T_{wg}) \tag{57}$$

This reduction in heat flux has been experimentally verified as a function of performance loss. Therefore, a 3% performance loss of a less efficient nominal mixture ratio injector represents an 11% reduction in heat flux, which is considerably greater than theoretically reflected by zoned combustion. This is one area that needs experimental verification for O_2/hydrocarbon-fueled engines.

"OTHER" THERMAL BARRIERS

A combination physical and fluid thermal barrier was selected. There were several combinations considered. Transpiration cooling and film cooling were the contenders as fluid barriers, each with a 3% performance loss. Zoned combustion did not show promising aspects. Ceramic (ZrO_2) coating and carbon layer were the physical barrier contenders. The graphite liner did not show any promising aspects. It was also determined from design analyses of single thermal barriers that the combination barrier for O_2/CH_4 and O_2/C_3H_8 would differ from that for O_2/RP-1. The combination of two fluid barriers was not considered because of the large performance loss. Although transpiration cooling showed the greatest chamber pressure increase potential, it was not selected because of inherent design and fabrication problems and extended development required to make it operational. It is also a high-risk design because of potential flow blockage of the micro-injection holes.

Combined Thermal Barriers (O_2/CH_4 and O_2/C_3H_8)

ZrO_2 ceramic coating plus film cooling was selected as the combined thermal barrier to provide maximum benefits for increased chamber pressure of the O_2/CH_4 and O_2/C_3H_8 designs. The addition of a carbon layer would provide negligible benefits since the selected combination already pushes the channel height to its maximum limit in the regions where a carbon layer would be beneficial. At these high chamber pressures, the carbon layer thickness of these two propellant combinations is basically zero in the high mass flux region (convergence zone and throat).

The O_2/CH_4 and O_2/C_3H_8 designs are summarized in Table 13. All designs were at guideline chamber pressure limits and used reduced P_{inlet}/Pc. Unenhanced nozzle designs were used with adjustments to the attachment area ratio and unformed tube diameter to accommodate the high chamber pressure. The lower thrust nozzle designs for the ZrO_2 enhanced chambers, which were at their respective P_c limits, were used for the combined thrmal barrier chamber designs. The graphic presentation of these chamber and nozzle designs is shown in Fig. 135 through 140 of Appendix D. The ceramic-coating (ZrO_2) thickness was nearly

TABLE 13. SUMMARY OF HIGH-PRESSURE HYDROCARBON-FUELED ENGINE REGENERATIVE COOLING LIMITS (FOR COMBINED THERMAL BARRIERS OF ZrO_2 AND FILM COOLING OF CHAMBER)

Propel. Comb.	Thrust N (lbf)	Max P_c Uneh. N/cm (psia)	Max P_c Enh. N/cm (psia)	P_c Limiting Factor	Cooling Circuit	Chamber to Nozzle ε	Min. LW cm (in)	Channel Width cm (in)	Channel Wall Thickness cm (in)	Coolant Pin/P_c	Nozzle Min UTD cm (in)	Nozzle Min. Wall Thickness cm (in)
O_2/C_3H_8	89,000 (20,000)	2068 (3000)	2758 (4000)	LIFE	Series	10.0	.076 (.030)	.122/.102 (.048/.040)	.076/.064 (.030/.025)*	1.37	.127/.434* (.05/.171)	.018/.076* (.007/.03)
O_2/C_3H_8	2,669,000 (600,000)	1586 (2300)	4137 (6000)	LIFE	Split	9.5	.076 (.030)	.229/.140 (.090/.055)	.165/.097 (.065/.038)	1.52	.203 (.08)	.018 (.007)
O_2/CH_4	667,000 (150,000)	2620 (3800)	3448 (5000)	LIFE	Series	10.0	.076 (.030)	.152/.102/ .152 (.060/.040/ .060)	.102/.08/ .086 (.040/.032/ .034)	1.44	.229/.434* (.09/.171)	.020/.030/ .025* (..08/.012/ .01)
O_2/CH_4	2,669,000 (600,000)	2144 (3110)	4137 (6000)	LIFE	Split	9.5	.076 (.030)	.229/.140 (.090/.055)	.165/.097 (.065/.038)	1.42	.203 (.08)	.018 (.007)
O_2/RP-1** "SHORT CHAMBER"	2,669,000 (600,000)	896 (1300)	3448 (5000)	T_{wc}	Split	5:1	.076 (.030)	.229/.140 (.090/.055)	.152/.094 (.060/.037)	1.80	.229/.434 (.09/.171)	.020/.030/ .025 (.08/.013/ .01)

* ZIRCONIUM OXIDE NOZZLE DESIGNS USED FOR COMBINED THERMAL BARRIERS
** COMBINED BARRIERS ARE CARBON LAYER AND ZIRCONIUM OXIDE (FIRST 1/3 NOZZLE REQUIRES THERMAL BARRIER)

identical to those previously used for the ZrO_2 designs. This is realized by the fact that the additional increase in chamber pressure for the combined thermal barrier is associated with the addition of film cooling. As previously shown, the film cooling produces a near uniform heat flux reduction along the chamber length. Therefore, nearly the same ceramic coating thicknesses are required for the guideline ZrO_2 surface temperature limit.

Combined Thermal Barrier (O_2/PR-1)

A carbon layer thermal barrier is extremely overpowering for the O_2/RP-1 propellant combination, as previously noted. The next most efficient thermal barrier is a ZrO_2 ceramic coating, as defined for the other two propellant combinations. Therefore, a carbon layer plus ZrO_2 ceramic coating was selected for the combined O_2/RP-1 thermal barrier. This combination represents the best thermal barrier(s) for the O_2/RP-1 designs. This combination has a great benefit over the combined thermal barriers of the other propellant combinations since it represents no performance loss. The O_2/RP-1 barriers are both physical thermal barriers.

A "short chamber", 2,669,000 N (600,000 lbf), thrust chamber was evaluated for this study. The ZrO_2 ceramic coating was applied between the injector end and chamber throat. The thickness was 0.0030 cm (0.0012 in.) in the throat region and high heat flux convergent region. The lower heat flux region utilized 0.0046 cm (0.0018 in.). These ceramic coating thicknesses are typical of those used for the previous ceramic coating studies. These thicknesses represent optimum thicknesses for the guideline ceramic coating surface temperature limit.

At high chamber pressures, the carbon layer thickness diminishes in the throat region. The maximum chamber pressure that could be cooled was 3448 N/cm^2 (5000 psia). This is lower than the other two propellant combination limits, but is quite spectacular since the unenhanced design Pc limit was 896 N/cm^2 (1300 psia). This design is shown in Fig. 141 of Appendix D. Because of the high chamber pressure, the nozzle design requires a carbon layer or ceramic coating thermal barrier for approximately one-third of the nozzle length starting at the attachment to the combustion chamber. The coolant flow split between the chamber and nozzle was 50/50%, typical of other split flow designs.

ENHANCED DESIGN COMPARISON

Each of the seven enhanced techniques were presented independently. A comparison of each enhancement as related to the maximum increased chamber pressure for the propellant combination is presented in Table 14. The enhancements represent (4 x 250) cycles and are compared to the unenhanced chamber pressure.

The best enhancement is the combined thermal barriers. These are ZrO_2 ceramic coating and film cooling for the O_2/CH_4 and O_2/C_3H_8 propellant combination and ZrO_2 ceramic coating and carbon layer for the O_2/RP-1. The second best enhancement is transpiration cooling for the O_2/CH_4 and O_2/C_3H_8 propellant combination and carbon layer for the O_2/RP-1 propellant combination. It should be noted that each fluid thermal barrier represents a 3% performance loss.

A comparison is shown in Fig. 39 and 40 for the ZrO_2 ceramic-coated designs and the carbon layer designs. In summary, a carbon layer thermal barrier provides a significant increase in P_c for the O_2/RP-1 designs, where a ZrO_2 barrier has little impact on the designs. A ZrO_2 coating provides a significant increase in P_c for the O_2/CH_4 and O_2/C_3H_8 designs, where a carbon layer has a negligible effect.

The ZrO_2 ceramic coating provides the third best and film cooling provides the fourth best thermal barriers for all propellant combinations. Transpiration cooling, which is the second best thermal barrier for O_2/CH_4 and O_2/C_3H_8, is not applicable for O_2/RP-1 because of coking temperature limitations. As analyzed, transpiration cooling requires development of very special designs and may be less effective than analyzed because of the coolant velocity head loss potential. However, a wafer-type transpiration-cooled design may result in typical ratings, as noted.

The rating of enhanced cooling (thermal barriers) for each propellant combination is shown below (a rating of 1 represents the best enhancement and 7 represents the least effective enhancement):

Enhancement	Rating for Maximum P_c		
	O_2/CH_4	O_2/C_3H_8	O_2/RP-1
Physical Barrier			
Carbon Layer	5	5	2
ZrO_2 Ceramic Coating	3	3	3
Graphite Liner	7	7	7
Fluid Barrier (3% performance Loss)			
Film Cooling	4	4	4
Transpiration Cooling	2	2	DNA
Zoned Combustion	6	6	6
Other			
Combined Barriers			
ZrO_2/Film Cooling	1	1	--
Carbon/ZrO_2	--	--	1

TABLE 14. HIGH-PRESSURE HYDROCARBON-FUELED ENGINE REGENERATIVE COOLING LIMITS (SUMMARY)

		Unenhanced		Carbon Layer		ZrO_2 Ceramic Coating		Film Cooling		Transpiration Cooling		Zoned Combustion		Graphite Liner	"Other" Combined Thermal Barriers		
Propel. Comb.	Thrust N (lbf)	Coolant P_{in}/P_c	Max P_c N/cm² (psia)	Coolant P_{in}/P_c	P_c	P_{in}/P_c	P_c	P_{in}/P_c	P_c	P_{in}/P_c	P_c	P_{in}/P_c	P_c		P_{in}/P_c	P_c	Combined Barriers
O_2/C_3H_8	89,000 (20,000)	GG 1.8	2068 (3000)	1.8	2172 (3150)	1.64	2758 (4000)	1.8	3034 (4400)	1.63	2758 (4000)				1.37	2758 (4000)	
		SC 2.25	2137 (3100)														
	667,000 (150,000)	GG 1.8	1855 (2690)														ZrO_2 + Film Cooling
		SC 2.25	1896 (2750										N/A	N/A			
	2,669,000 (600,000)	GG 1.8	1586 (2300)	1.8	1896 (2750)	1.8	2758 (4000)	1.8	2137 (3100)	1.8	3790 (5500)				1.52	4137 (6000)	
		SC 2.25	1613 (2340)														
O_2/CH_4	89,000 (20,000)	GG 1.8	2826 (4100)	1.8	2861 (4150)												
		SC 2.25	2791 (4050)														
	667,000 (150,000)	GG 1.8	2620 (3800)	1.8	2758 (4000)	1.67	3447 (5000)	1.8	3723 (5400)	1.5	3450 (5000)				1.44	3448 (5000)	ZrO_2 + Film Cooling
		SC 2.25	2565 (3720)														
	2,669,000 (600,000)	GG 1.8	2144 (3110)	1.8	2189 (3175)	1.8	3344 (4850)	1.8	2896 (4200)	1.5	4140 (6000)	1.8	2344 (3400)	N/A	1.42	4137 (6000)	
		SC 2.25	2068 (3000)														
$O_2/RP-1$ Long Chamber	89,000 (20,000)	GG 1.8	689* (1000)	1.8	1378 (2000)												
		SC 2.25	(Ref. Case)														
Short Chamber	2,669,000 (600,000)	GG 1.8	896 (1300)	1.8	2275 (3300)	1.8	1516 (2200)	1.8	1516 (2200)		N/A		N/A	N/A	1.8	3448 (5000)	ZrO_2 + Carbon Layer
		SC 2.25															
Long Chamber	2,669,000 (600,000)	GG 1.8	1179 (1710)*	1.8	1179 (1710)*												
		SC 2.25															
Short Chamber	2,669,000 (600,000)	1.8	1585 (2300)*														

* - DID NOT MEET T_{wc} LIMIT

N/A - NOT APPLICABLE OR NO BENEFITS ATTAINABLE

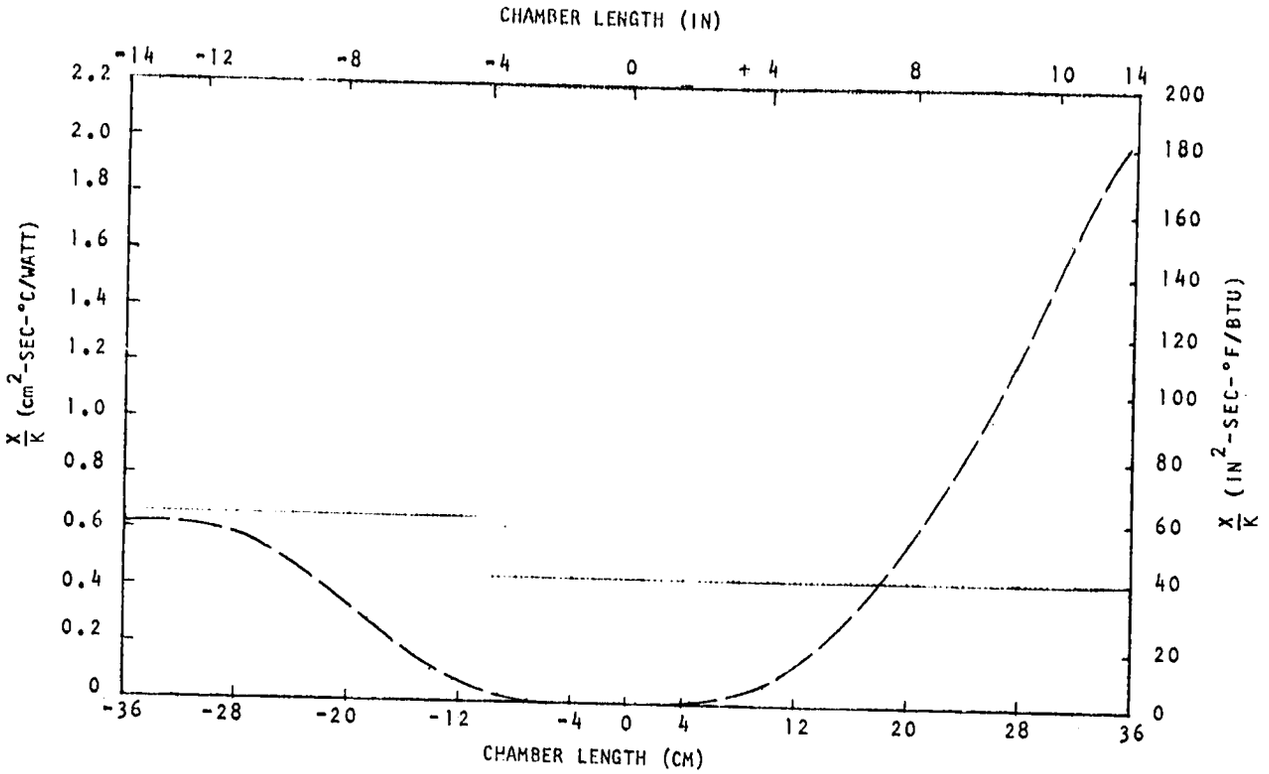

Figure 39. Comparison of O_2/CH_4 2,669,000 N (600,000 lbf) Barrier Thermal Resistance vs Axial Length

—— Zr/O_2 (P_c = 4850 PSIA)

— — CARBON LAYER (P_c = 3175 PSIA)

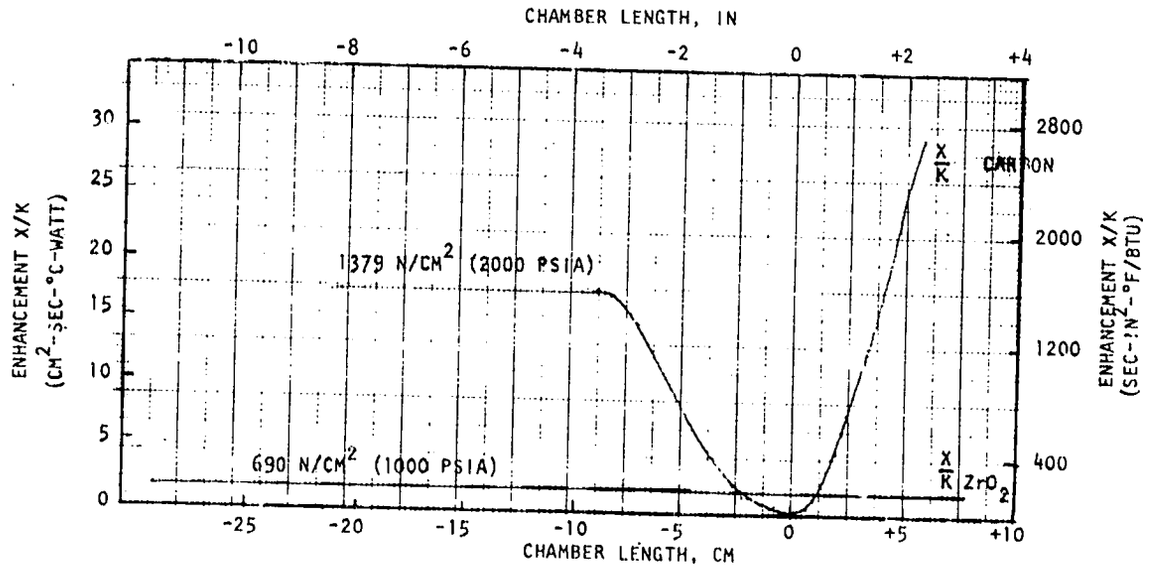

Figure 40. Comparison of Thermal Resistance Values for O_2/RP-1, 20,000 lbf MR = 2.8, P_{in}/P_c - 1.8, MCC (Long Chamber)

Film cooling is the fourth best thermal barrier for all propellant combinations. Carbon layer is fifth best for O_2/CH_4 and O_2/C_3H_8 designs, providing negligible benefits. However, carbon layer is the No. 1 single thermal barrier for O_2/RP-1, being second only to a combined thermal barrier.

Theoretically, zoned combustion has negligible or no enhancement benefits. A graphite liner is not applicable for high heat flux (high chamber pressure) designs from a fabrication and installation standpoint.

Many of the enhanced designs are at their chamber pressure limits with reduced (P_{inlet}/P_c) ratio. Therefore, a representative maximum chamber pressure as a function of thrust cannot be presented graphically.

SENSITIVITY STUDIES

These sensitivity studies evaluated cyclic life as a function of chamber pressure and RP-1 decomposition temperature impact on chamber pressure limits.

LIFE SENSITIVITY

A life sensitivity study was conducted to define the influence of the cyclic fatigue life ground rule on maximum chamber pressure. The 2,669,000 N (600,000 lbf) O_2/CH_4 unenhanced chamber design was selected for this study. The (Pc_{nf}/Pc_{1000Nf}) of this design should be typical of that attainable for the other propellant combinations and thrust levels.

The 1000 cycle (4 x 250) baseline unenhanced design maximum pressure was 2144 N/cm^2 (3110 psia). Life sensitivity analyses were conducted at chamber pressures of 2482 N/cm^2 (3600 psia), 2895 N/cm^2 (4200 psia), 3102 N/cm^2 (4500 psia), and 3309 N/cm^2 (4800 psia). The increased chamber pressure designs utilized reduced channel heights. The wall thickness was increased for each design to accommodate a higher operating pressure stress level. The wall thickness, maximum gas-side wall temperature, strain range, and cycle life are shown in Table 15. All designs reflect a $P_{inlet}/P_c = 1.8$ and approximately 50/50% coolant flowrate split between the chamber and nozzle. The chamber pressure to cyclic life relationship is shown in Fig. 41. This trend should be typical for the other propellant combinations and thrust level (ignoring RP-1 T_{wc}) since the baseline 1000 cycle designs represent similar gas-side wall temperatures (T_{wg}), and the nozzle ΔP of series flow designs are insignificant.

The life of the higher chamber pressure designs is questionable at NARloy-Z surface temperatures (T_{wg}) above 867 K (1560 R). Although it is not recommended to operate above this temperature, the low cycle fatigue curve for NARloy-Z was extended to accommodate the higher surface temperatures at the higher chamber pressures, as noted in Fig. 42. This 922 K (1660 R) curve is based on limited data obtained from isothermal uniaxial fatigue specimens.

O_2/RP-1 DECOMPOSITION SENSITIVITY STUDY

Respectable chamber pressures were not attained for the O_2/RP-1 unenhanced and enhanced "long chamber" designs. This is primarily attributed to: (1) the low coolant wall temperature required to negate coking and (2) the long chamber length typically associated for gas generator cycle liquid/liquid injection systems to meet performance criteria with conventional type injectors. Therefore, it was difficult to compare the cooling capabilities of RP-1 to the other hydrocarbon-fueled engines using CH_4 and C_3H_8.

Reviewing the O_2/RP-1 analyses for "long chambers" reflect unfavorable operating conditions for all unenhanced and enhanced designs except for the 89,000 N (20,000 lbf) thrust design with a carbon layer. The RP-1 carbon layer provides a large thermal resistance throughout the chamber length except for the local high mass flux throat region. This allowed the 89,000 N (20,000 lbf) thrust chamber to meet the coolant wall temperature criterion of 589 K (1060 R) at a chamber pressure of 1379 N/cm^2 (2000 psia) although the unenhanced design could not meet this criterion at 690 N/cm^2 (1000 psia). The larger thrust enhanced

TABLE 15. SUMMARY OF CYCLIC LIFE SENSITIVITY STUDY
(UNENHANCED O_2CH_4 2,669,000 N (600,000 lbf) THRUST CHAMBER)
$P_{INLET}/P_c = 1.8$

Chamber Pressure N/cm^2 (psia)	Chamber to Nozzle ε	Channel Wall Thickness cm (in)	Maximum Wall Temperature °K (°R)	Strain Range (Percent)	Life (Cycles)
2144 (3110)	5.1	.114/.064 (.045/.025)	692 (1245)	2.0	250 x 4
2482 (3600)	6.8	.132/.071 (.052/.028)	781 (1405)	2.4	120 x 4
2896 (4200)	6.8	.145/.084 (.057/.033)	914 (1645)	3.0	60 x 4
3103 (4500)	6.8	.152/.091 (.060/.036)	950 (1710)	3.3	45 x 4
3310 (4800)	6.8	.183/.127 (.072/.050)	1017 (1830)	3.5	30 x 4

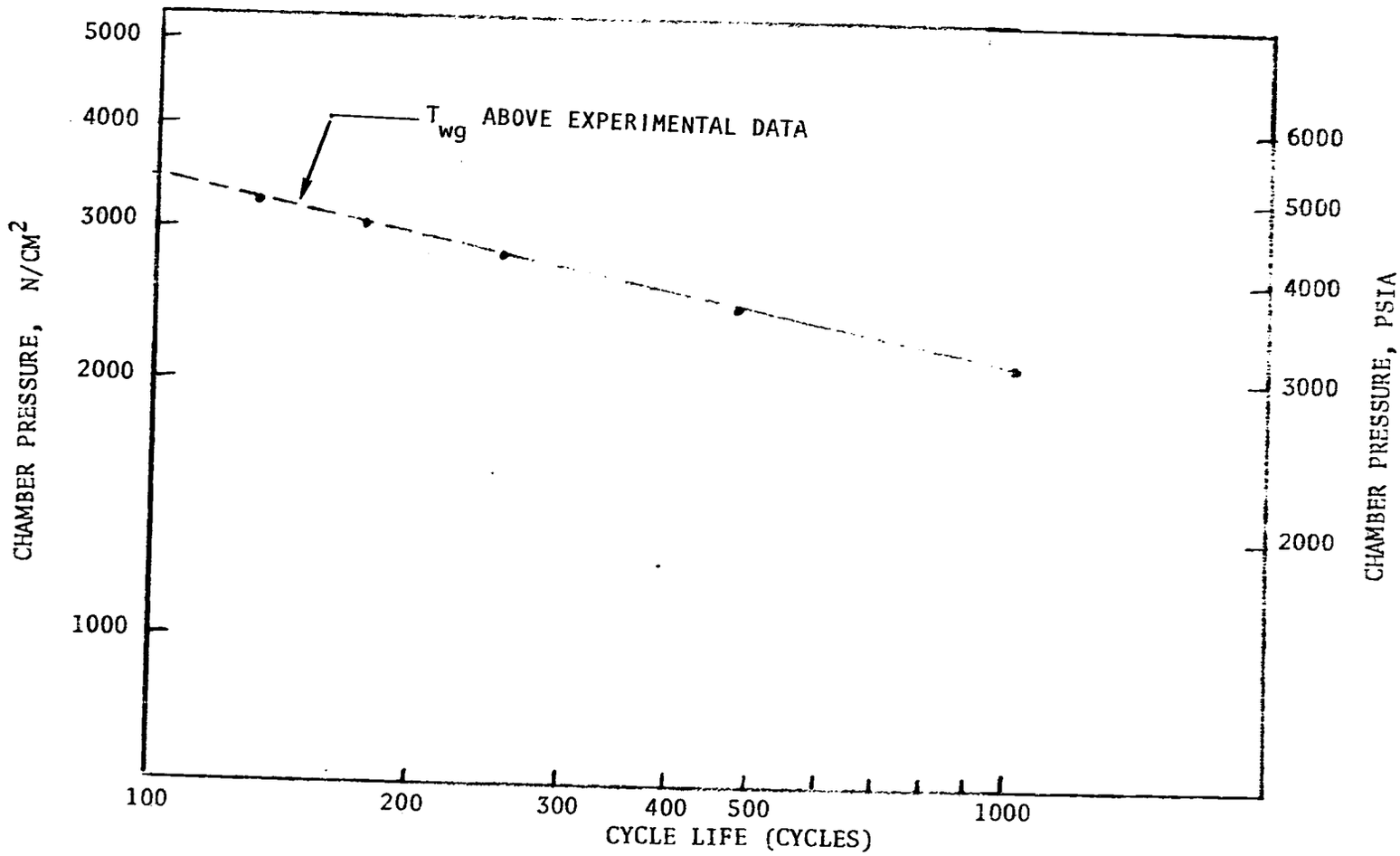

Figure 41. Life Sensitivity 2,669,000 N (600,000 lbf) O_2/CH_4 Chamber

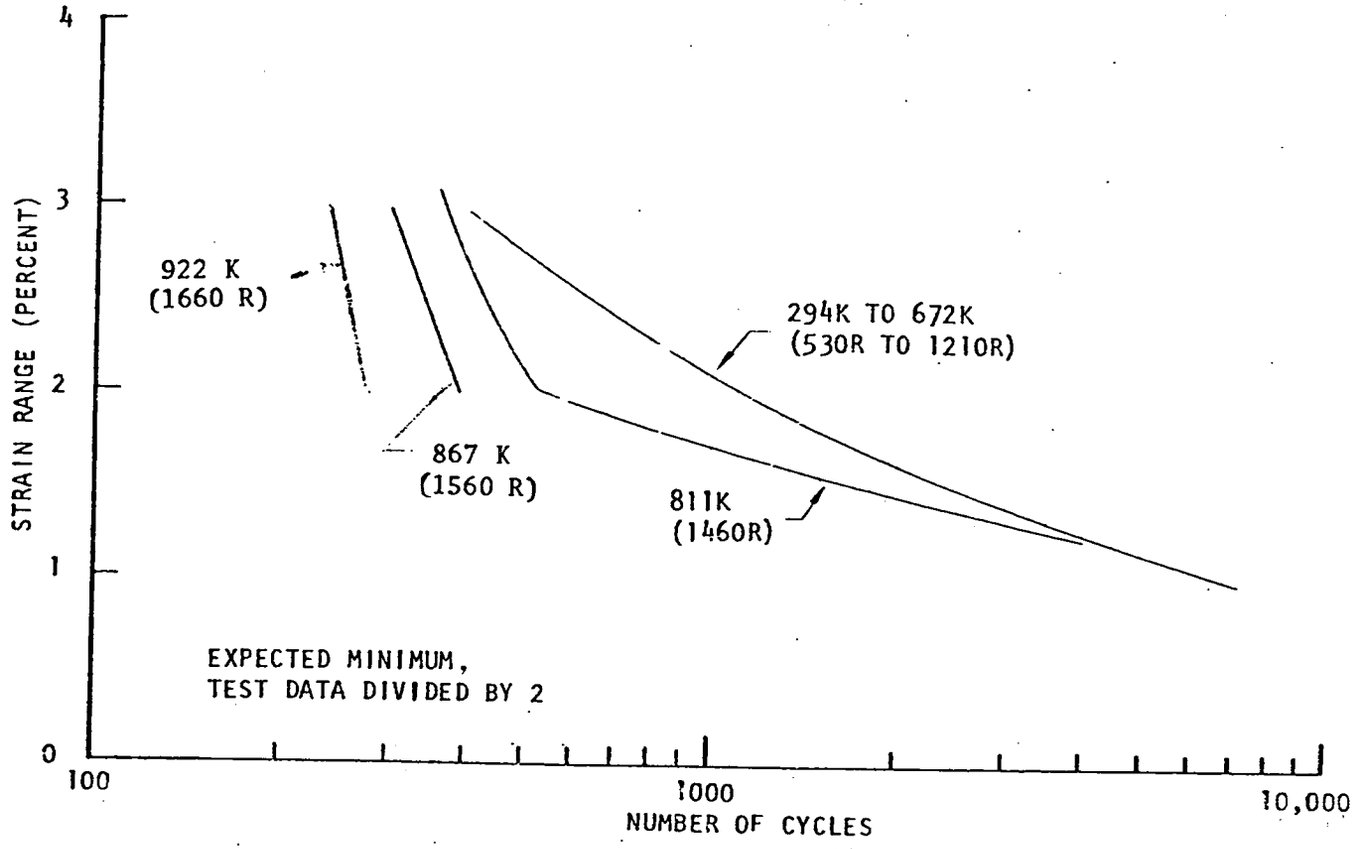

Figure 42. Low Cycle Fatigue Curves for Wrought NARloy-Z

design could not meet this criterion at considerably lower chamber pressure. This is attributed to the fact that the larger thrust chamber length (injector to throat) was three times longer than the lower thrust chamber length. This additional length retards the cooling capability associated with an increased injector-end bulk temperature and a reduced coolant mass flux for a fixed P_{inlet}/P_c ratio.

The O_2/RP-1 gas generator cycle sensitivity analyses utilized gas-gas injection chamber contours typical of the O_2/CH_4 and O_2/C_3H_8 designs. It assumed that 98% energy release efficiency can be obtained with the short chamber utilizing a micro-orifice type of injector. This injector would require development but is a possibility for a liquid-liquid gas generator cycle system. The 2,669,000 N (600,000 lbf) thrust level design was selected for analysis because of its potential booster application and the additional design benefits provided by a split flow chamber/nozzle system for an O_2/RP-1 gas generator cycle engine. The sensitivity study defined the chamber pressure limits for an unenhanced design and an enhanced carbon layer design as a function of coolant wall temperature, as shown in Fig. 43.

Pertinent design analysis parameters are shown in Table 16. Off-set design points were established for an energy release efficiency of 96% by accounting for the reduced combustion temperature. This represents design points for a typical type liquid-gas injector. The large thermal resistance of the carbon drives the channel height to its maximum for two-thirds of the chamber length.

Graphic design presentations are shown in Fig. 142 and 143 for the 1172 N/cm^2 (3500 psia) unenhanced chamber and nozzle, and in Fig. 144 and 145 for the 2413 N/cm^2 (1700 psia) carbon layer enhanced combustion chamber with an unenhanced nozzle.

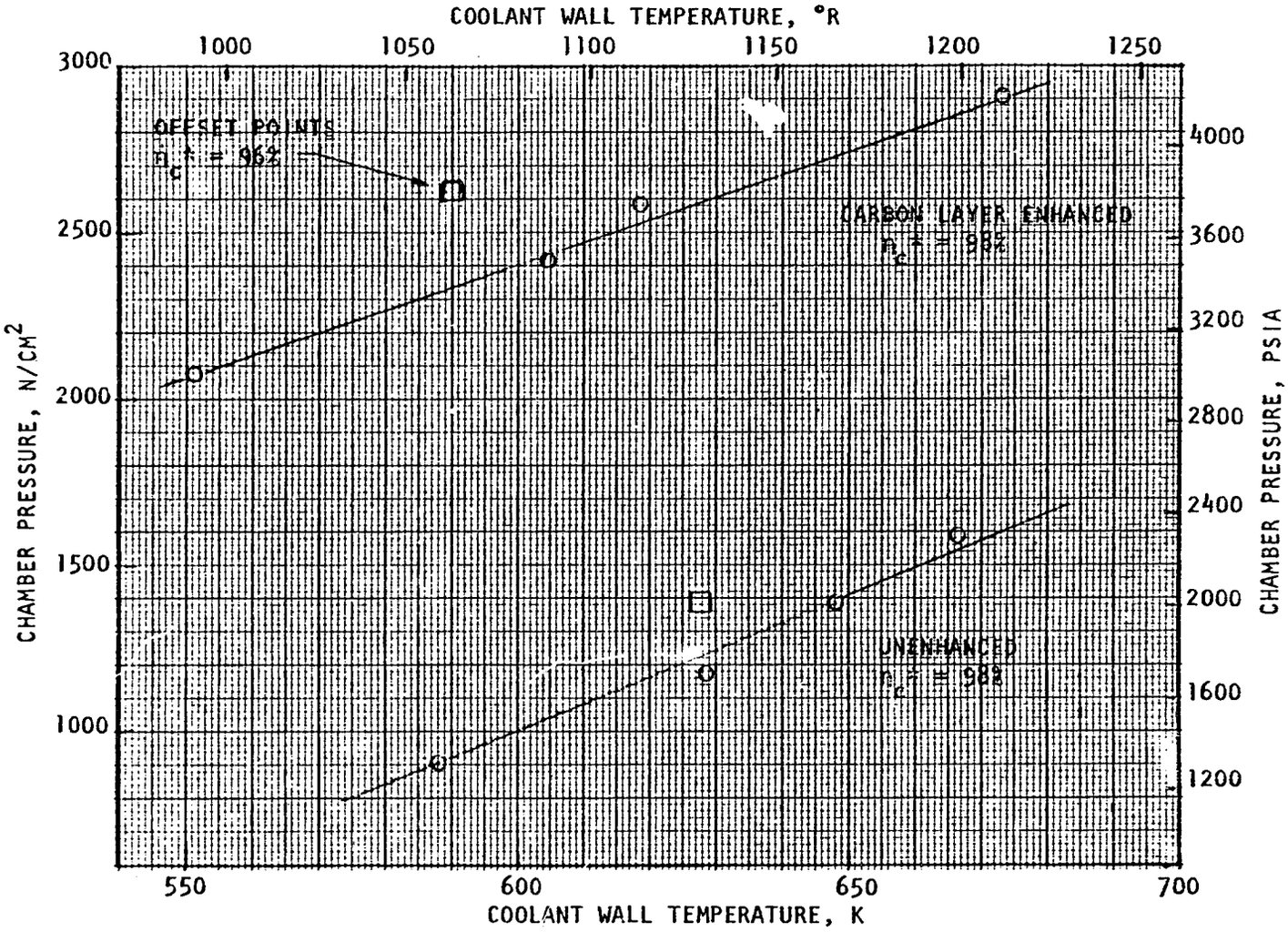

Figure 43. O_2/RP-1 Coolant Wall Temperature (Decomposition Temperature) Sensitivity Study

TABLE 16. SUMMARY OF O_2/RP-1 SENSITIVITY STUDY
(2,669,000 N (600,000 lbf) THRUST SHORT CHAMBER
$P_{inlet}/P_c = 1.8$

P_c, N/cm^2 (psia)	T_{wc}, K (°R)	T_{wg}, K (°R)	Cycle Life	Maximum Strain Range	Enhancement	η_c^* Percent
896 (1300)	587 (1056)	634 (1142)	4850	.01172	Unenhanced	98
1172 (1700)	628 (1131)	711 (1279)	2260	.01505	Unenhanced	98
1379 (2000)	648 (1166)	753 (1356)	1300	.01708	Unenhanced	98
1379 (2000)	628 (1131)	728 (1311)	1740	.01609	Unenhanced	96 (Offset)
1586 (2300)	667 (1200)	777 (1399)	1020	.01836	Unenhanced	98
2068 (3000)	551 (992)	712 (1282)	1700	.01658	Carbon Layer	98
2413 (3500)	605 (1089)	754 (1357)	1100	.01810	Carbon Layer	98
2629 (3800)	619 (1114)	804 (1447)	580	.02038	Carbon Layer	98
2620 (3800)	589 (1061)	777 (1398)	830	.01916	Carbon Layer	96 (Offset)
2896 (4200)	674 (1213)	866 (1559)	260	.02327	Carbon Layer	98

TECHNOLOGY IDENTIFICATION

Recommended technology items to be considered for follow-on work are summarized below. These suggested areas requiring experimental investigation are based on the results of this analytical study.

1. Carbon Layer Deposition (O_2/RP-1

   This is particularly important since the O_2/RP-1 chamber must rely on a carbon layer to be cooled at competitive chamber pressures of other hydrocarbon-fueled engines.

2. RP-1 Coking Temperature Limit

   The chamber pressure limit is very sensitive to the maximum allowable coolant wall surface temperature. Coking limits also should be evaluated with additives to increase the coking temperature limit.

3. Ceramic Coating (ZrO_2)

   This provides a substantial increase in chamber pressure when applied to the combustion chamber. For high chamber pressures, a thickness less than 0.005 cm (0.002 in.) is required. Application of extremely thin coatings and hot-fire testing is merited.

4. Film Cooling

   Performance degradation and cooling efficiencies need be experimentally determined.

5. Zoned Combustion

   Analytically, this provides an insignificant increase in chamber pressure. This needs experimental evaluation of performance loss and thermal characteristics.

CONCLUSIONS

Both the unenhanced and enhanced designs reflect an increase in chamber pressure for a decreased thrust level when cyclic life is the primary fixed criterion. Another contributor to this trend is the shorter length and larger contraction area ratio of the low thrust designs for a 98% energy release efficiency. This chamber pressure to thrust trend is reversed for the O_2/RP-1 designs where the coolant wall temperature is the limiting criterion (to meet the coking temperature limit) instead of life-limited.

The greatest increase in chamber pressure can be attained by a combined thermal barrier. This combination is a ZrO_2 ceramic coating with film cooling for the O_2/CH_4 and O_2/C_3H_8 propellant combination, and a ZrO_2 ceramic coating with a carbon layer for the O_2/RP-1 propellant combination.

The best single heat barrier is transpiration cooling for the O_2/CH_4 and O_2/C_3H_8 propellant combination and a carbon layer for the O_2/RP-1 propellant combination.

The highest chamber pressures can be attained for the O_2/CH_4 propellant combination. The O_2/RP-1 propellant combination reflects the lowest cooling limits which is primarily attributed to a low RP-1 decomposition temperature. Another limitation for the O_2/RP-1 propellant combination is development of a high performance liquid-gas micro-orifice injector to allow use of a "short chamber" typical of the other two propellant combination. The O_2/RP-1 unenhanced designs are only competitive for a "short chamber" and if an inhibitor is used to increase the coking temperature limit.

The gas generator cycle engine system provides a slight chamber pressure benefit over the staged combustion cycle engine assuming the same energy release efficiency can be obtained for either cycle.

A ceramic coating and film cooling are admirable heat barriers. The nozzle can be adequately cooled within engine system pressure drop allocations without any thermal barriers for the enhanced thermal barrier combustion chambers.

APPENDIX A

COMBUSTION CHAMBER AND NOZZLE MATERIAL PROPERTIES

The combustion chamber and nozzle material properties are presented in this appendix. These properties were used for the life analysis and structural design of this study. The basis for the selection of these materials was previously presented. NARloy-Z was selected for the combustion chamber liner, which used an electroformed nickel closeout structure. Inconel 718 was the load-carrying structure for the combustion chamber and nozzle. A-286 was used for the nozzle tube material. The above materials are identical to those currently being used on the Space Shuttle Main Engine (SSME).

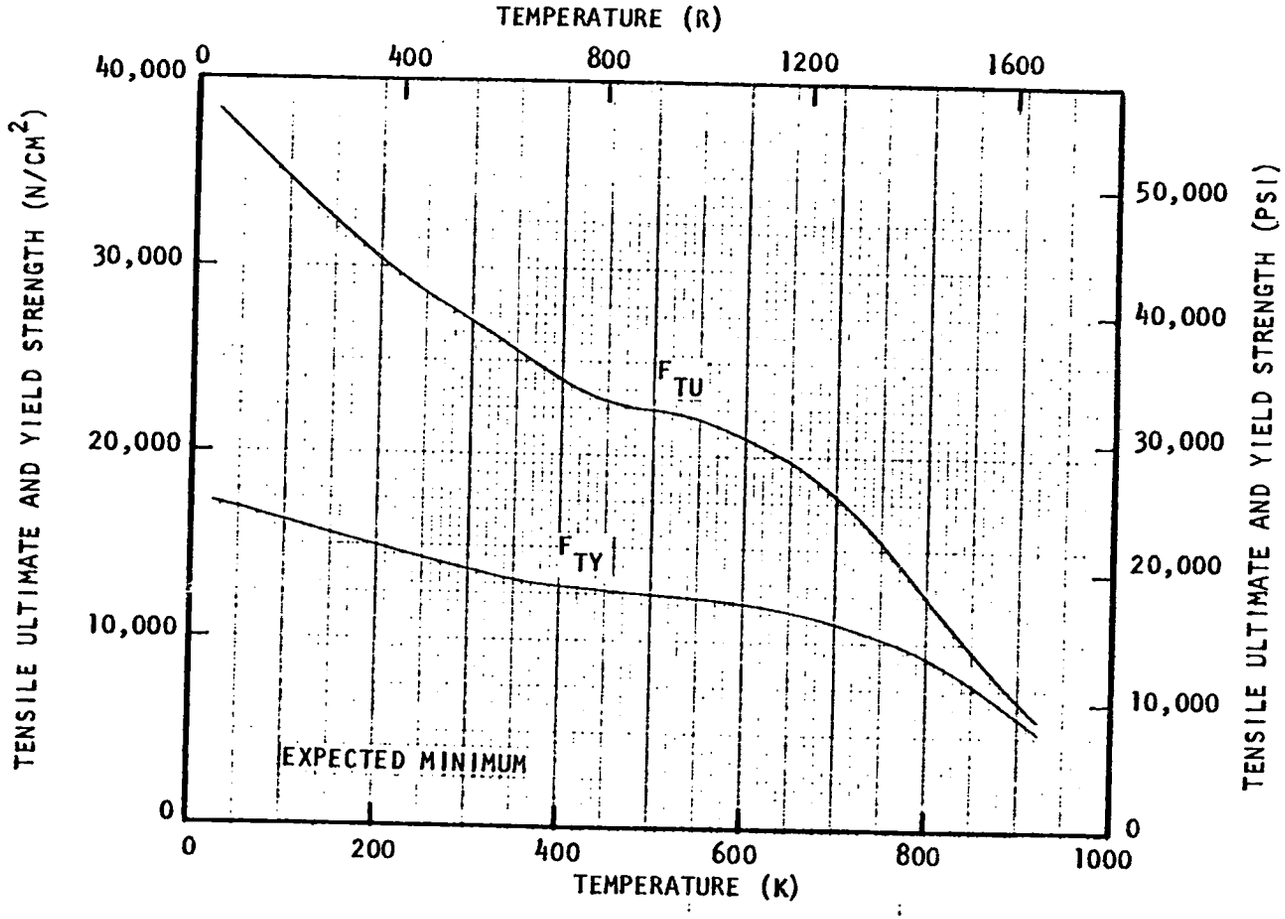

Figure 44. Tensile Ultimate and Yield Strength for Wrought NARloy-Z

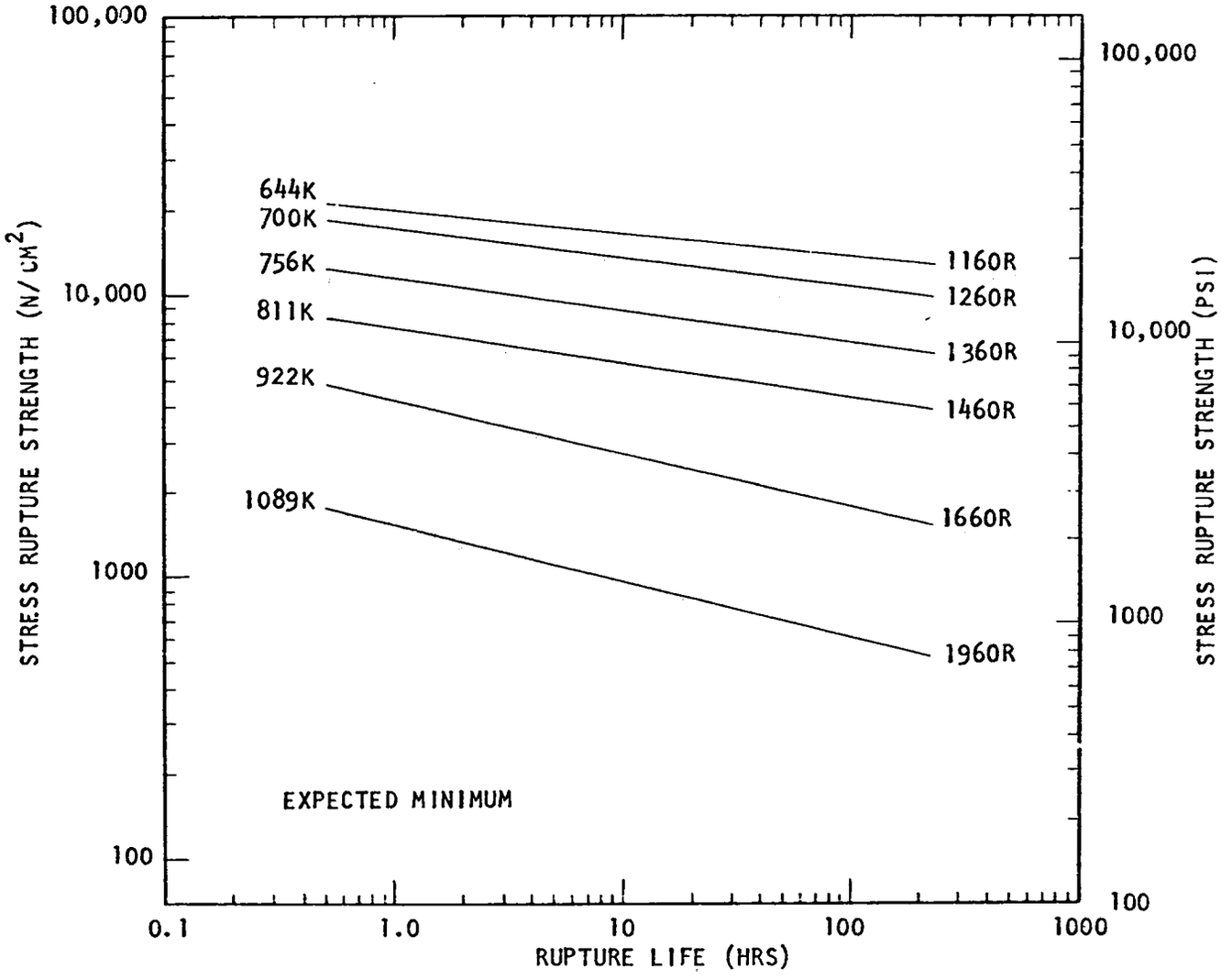

Figure 45. Stress Rupture Curves for Wrought NARloy-Z

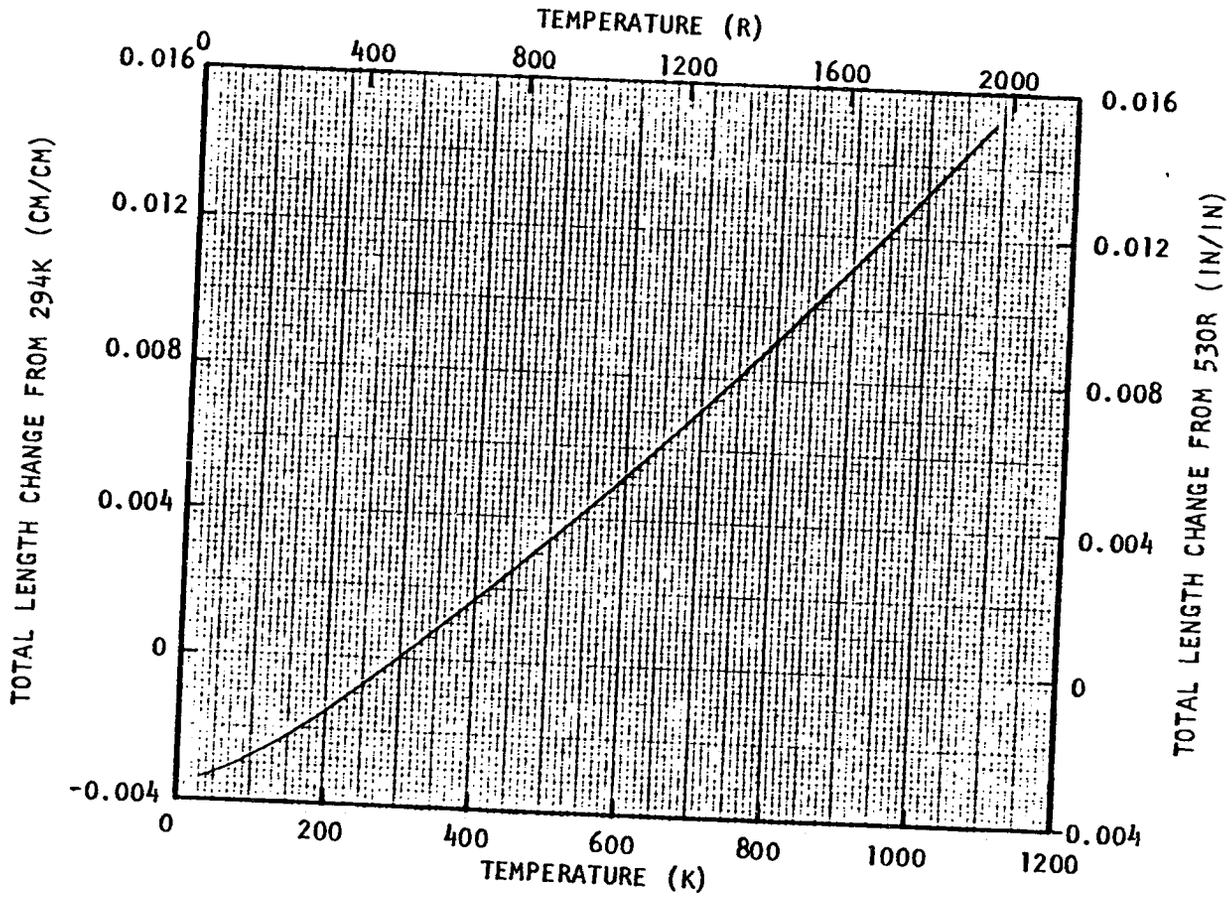

Figure 46. Thermal Expansion for Wrought NARloy-Z

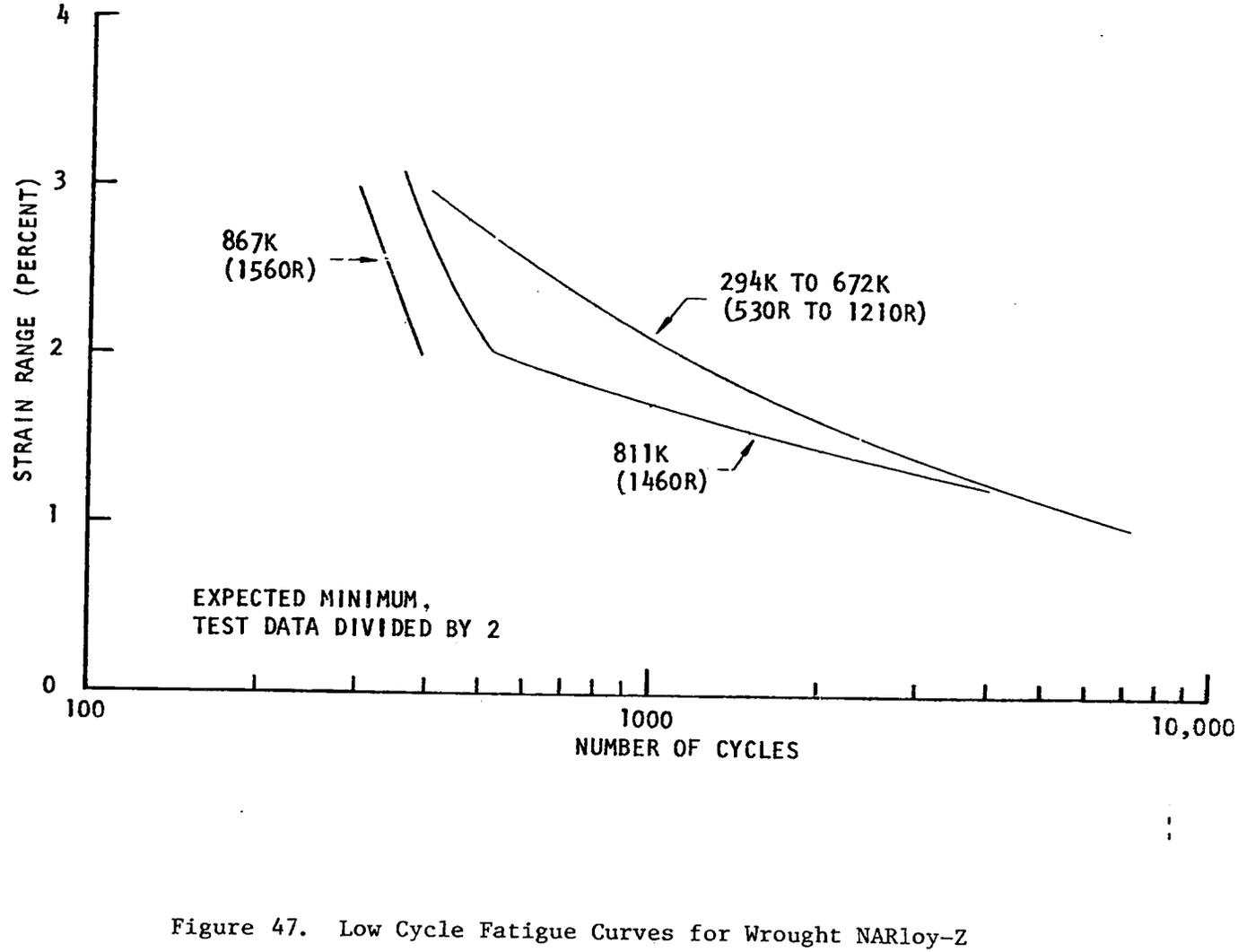

Figure 47. Low Cycle Fatigue Curves for Wrought NARloy-Z

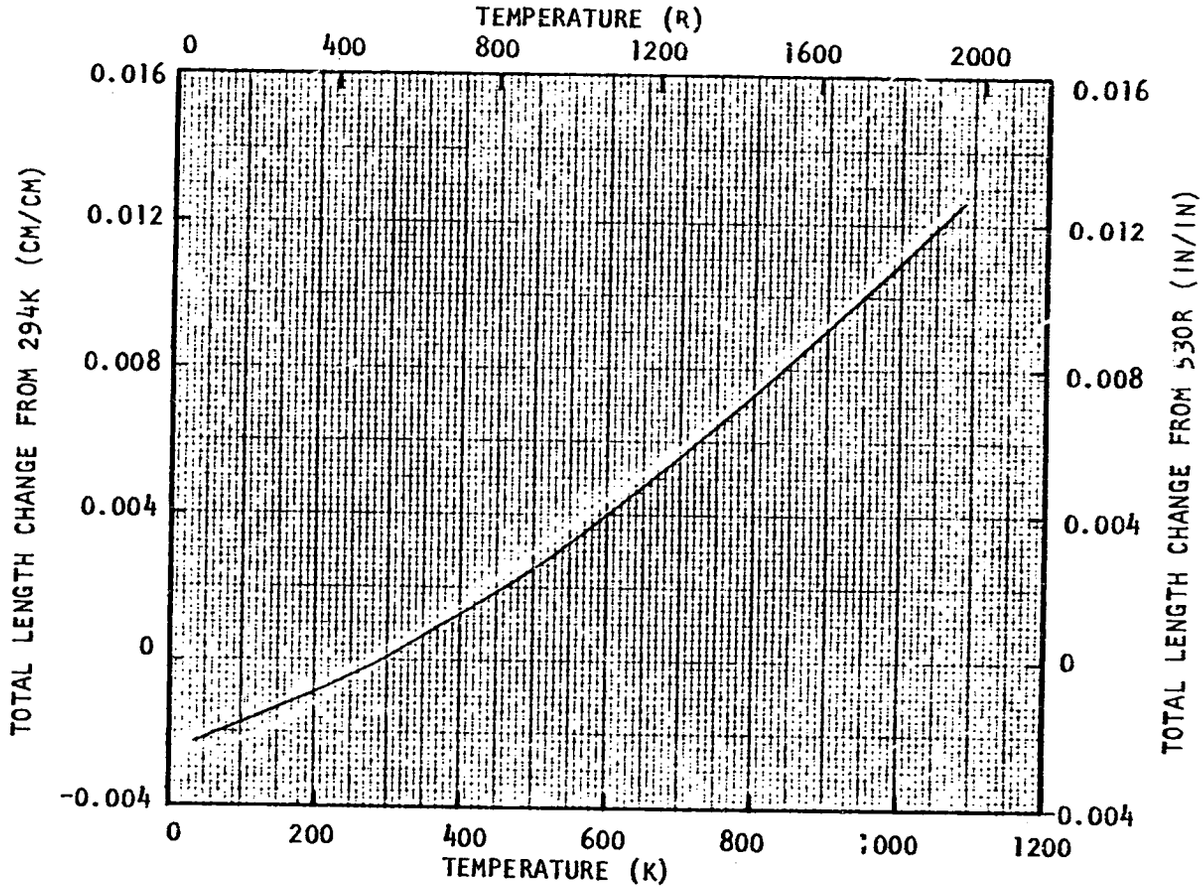

Figure 48. Thermal Expansion for Electroformed Nickel

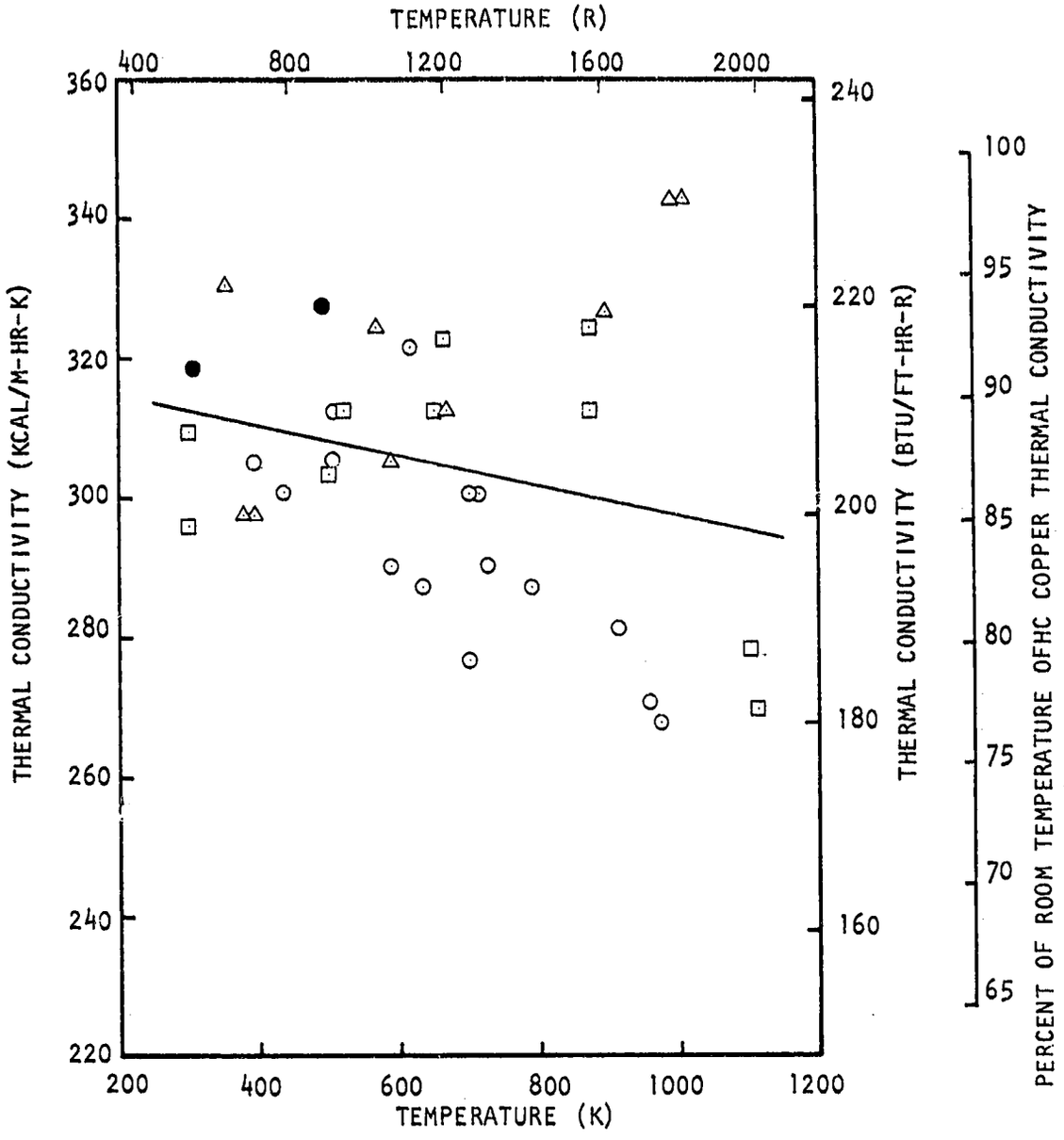

Figure 49. Thermal Conductivity of NARloy-Z

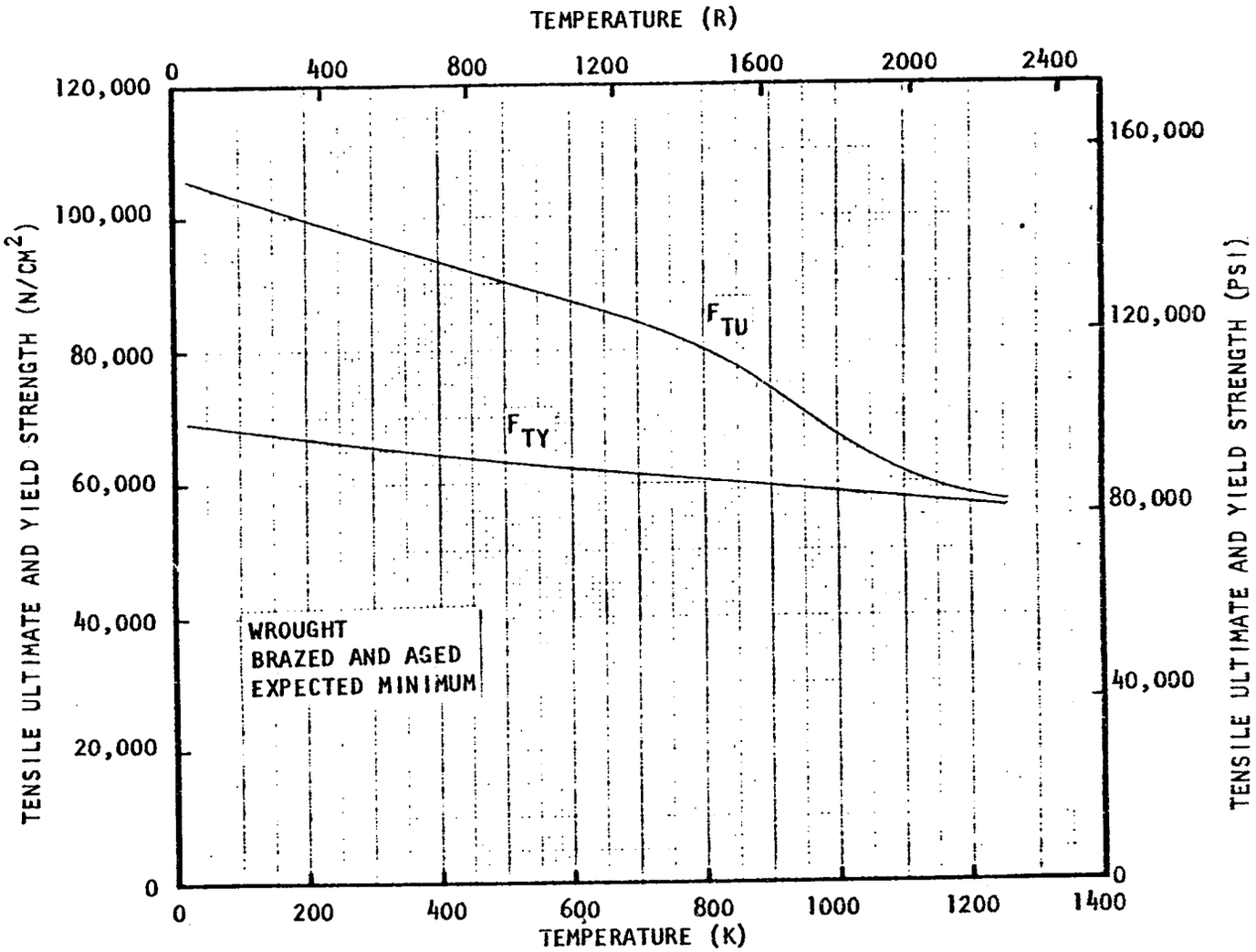

Figure 50. Tensile Ultimate and Yield Strength for A-286

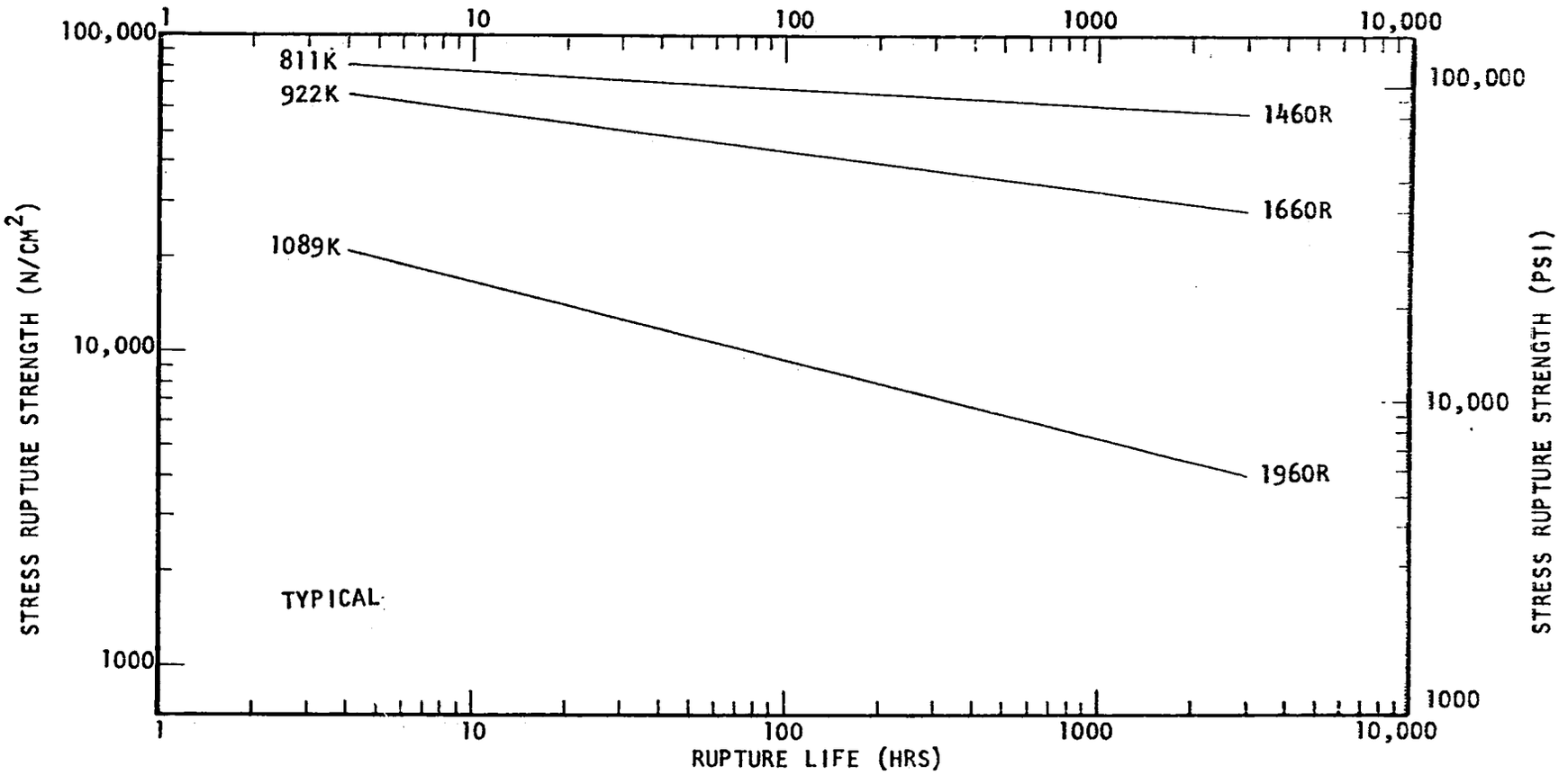

Figure 51. Stress Rupture Curves for Wrought A-286

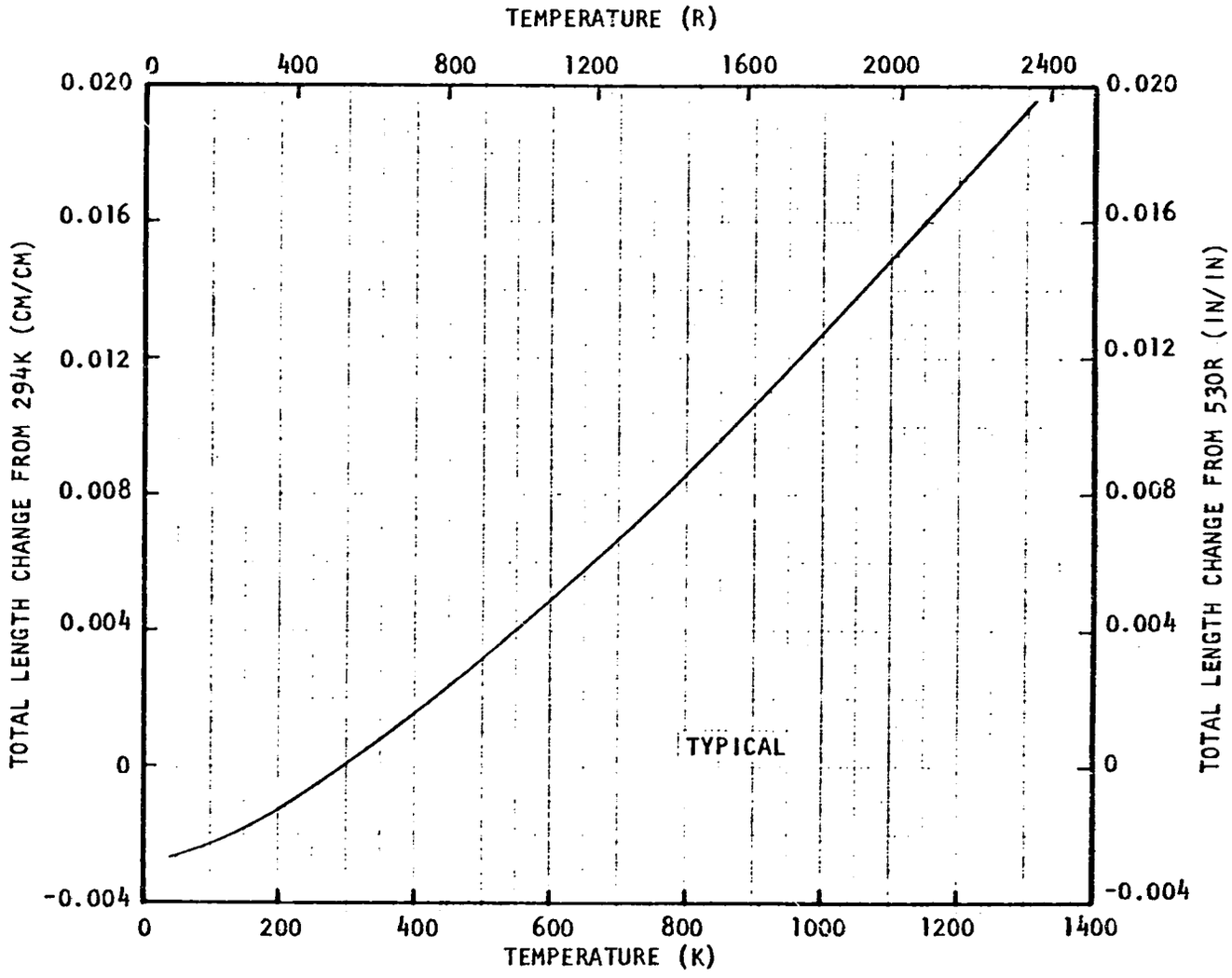

Figure 52. Thermal Expansion for Wrought A-286

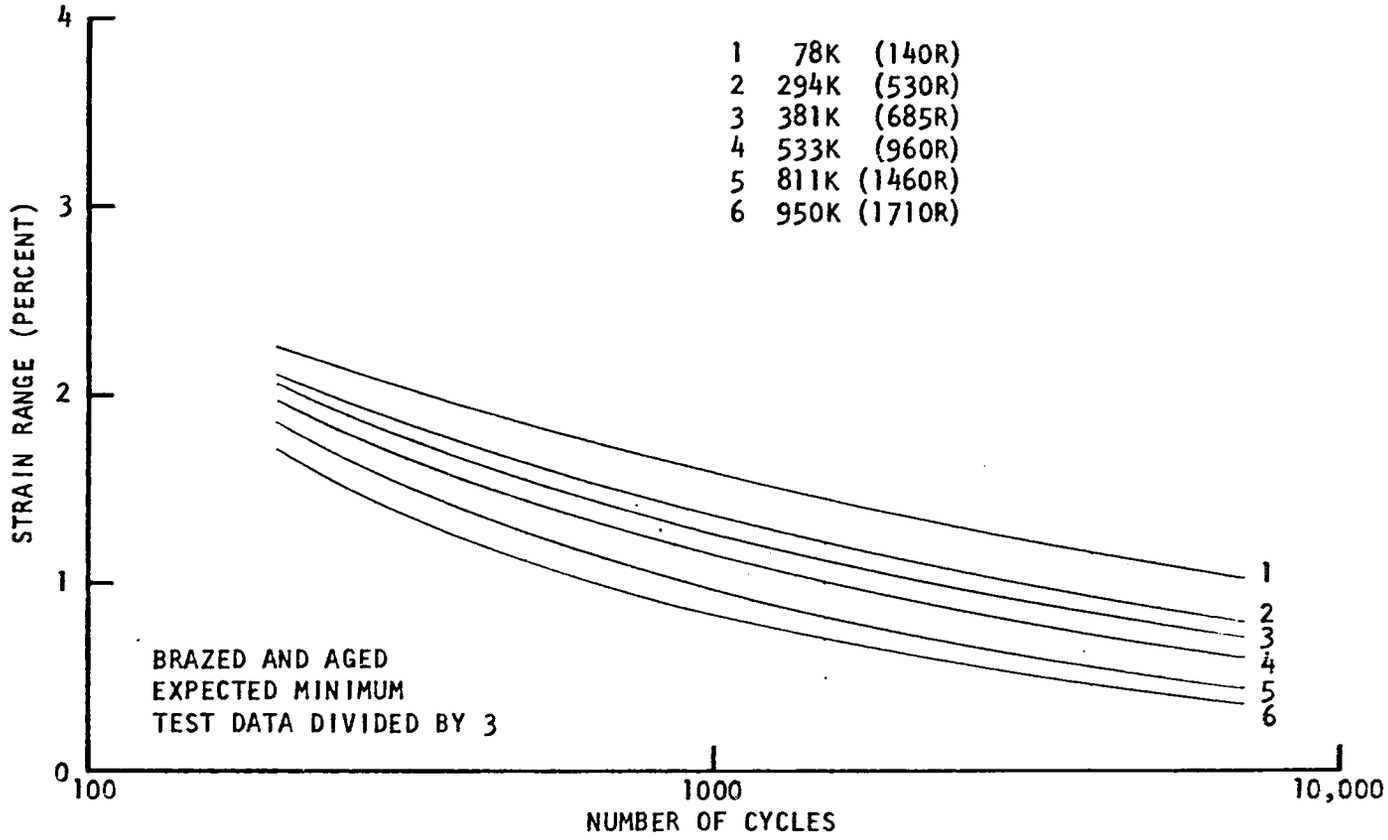

Figure 53. Low-Cycle Fatigue Data for Wrought A-286

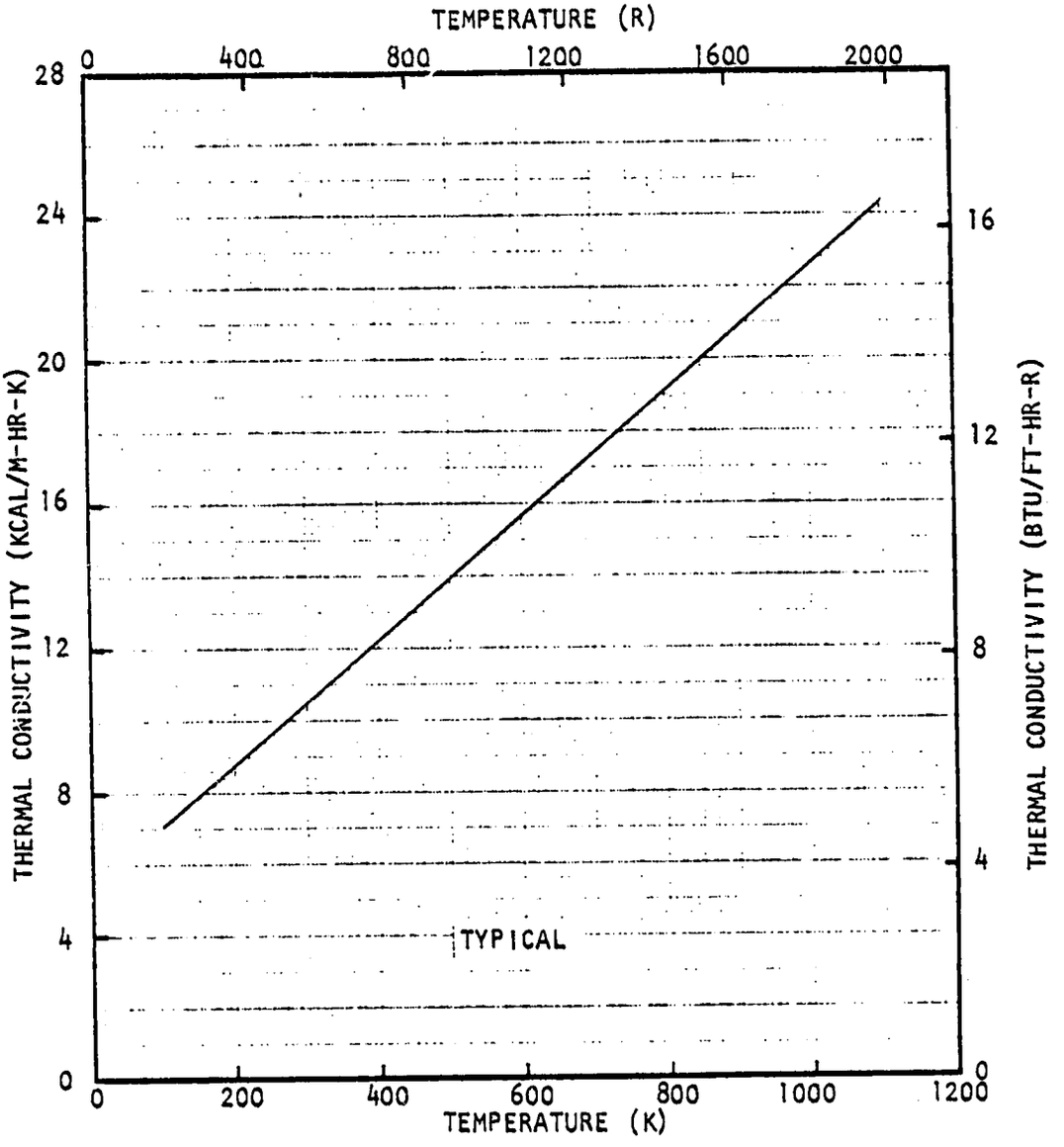

Figure 54. Thermal conductivity of Wrought A-286

APPENDIX B

COMBUSTION HOT-GAS PROPELLANT PROPERTIES

Combustion gas properties and performance were generated for the propellant combinations considered in this study. Rocketdyne's Free-Energy Program uses an up-to-date JANNAF flame species data file and has been found to yield results in agreement with NASA's program and the JANNAF ODE program. Flame properties computed in the combustion chamber, at the throat, and at specified nozzle stations included: temperature, enthalpy, entropy, heat capacities (shifting and frozen), gammas (shifting and frozen), effective molecular weight, density, viscosity, thermal conductivity, Prandtl number, and composition.

A sample computer program printout of data available for LOX/CH_4 propellants is shown in Table 17. The first part of this table indicates the full shifting characteristic velocity for the operating conditions. The second part contains the gas physical and thermodynamic properties and composition in the combustion chamber and at every expansion area ratio station selected. The third part summarizes performance parameters such as thrust coefficient and specific impulse for each expansion area ratio chosen, at vacuum, and at design altitude. It also summarizes exit temperature and pressure conditions for each expansion area ratio.

Combustion gas properties for the propellant combinations at nominal mixture ratio (O_2/RP-1 at MR = 2.8:1, O_2/O_3H_8 at MR = 3.1:1, and O_2/CH_4 at MR = 3.5:1) are shown as functions of chamber pressure in Fig. 55 and 56. The combustion gas properties evaluated for zoned mixture ratio enhancement are presented in Fig. 57 through 62.

The combustion gas temperature was corrected from the theoretical value by using the study guidelines specified energy release efficiency (η_{c*}) of 98% in the following manner:

$$T_{o_{actual}} = T_{o_{theory}} \times (\eta_{c*})^2$$

The characteristic velocity (c*) also was corrected for η_{c*}. In generating the combustion gas properties, the following fuel temperatures were used for calculating the heat of formation:

RP-1:	461 K (830 R)
C_3H_8:	344 K (630 R)
CH_4:	390 K (700 R)

Results from the Free-Energy Program where the RP-1 fuel temperature was varied showed that the property variations with change in the fuel temperature are insignificant (less than 1%) for the ranges of this study.

TABLE 17. FREE ENERGY PROGRAM OUTPUT PRINTOUT

EXIT CONDITIONS ** SHIFTING COMPOSITION

PROPELLANT	RELATIVE MASS IN MIXT	OF MIXT	MASS FRACTION
O2, 90K	1.0000		
OXIDIZER		3.5000	0.7778
METHANE LNBP	1.0000		
FUEL		1.0000	0.2222

PC = 5000 PSIA
MR = 3.500
DENSITY = 0.8325

SHIFTING CSTAR = 6120 FT/SEC

	PC/PE	P PSIA	T DEG. K	GAMMA SHIFTING	EPSILON	CF-VAC	I-VAC LB-SEC/LB	θ	CF-OPT	I-OPT LB-SEC/LB
	1.00	4999.996	3785.3	1.138	0.0	0.0	0.0	0.0	0.0	0.0
THROAT	1.73	2887.745	3587.3	1.135	1.000	1.2328	234.47	0.04	0.6552	124.62
	7.57	660.312	3110.3	1.131	2.000	1.4703	279.65	0.08	1.2061	229.41
	13.58	368.238	2934.3	1.133	3.000	1.5679	298.22	0.11	1.3470	256.20
	20.14	248.310	2816.0	1.137	4.000	1.6281	309.67	0.15	1.4295	271.89
	34.56	144.674	2650.8	1.146	6.000	1.7034	324.00	0.23	1.5298	290.98
	50.39	99.230	2531.8	1.155	8.000	1.7512	333.08	0.30	1.5924	302.88
	67.38	74.206	2437.5	1.163	10.000	1.7854	339.59	0.38	1.6370	311.36
	90.00	55.553	2342.1	1.170	12.500	1.8175	345.69	0.48	1.6786	319.27
	123.86	40.367	2236.1	1.177	16.000	1.8505	351.97	0.61	1.7213	327.40
	165.17	30.272	2141.1	1.183	20.000	1.8784	357.28	0.76	1.7573	334.25
	278.02	17.984	1973.7	1.190	30.000	1.9248	366.10	1.14	1.8169	345.57
	340.23	14.696	1910.9	1.192	35.129	1.9414	369.27	1.34	1.8382	349.63
	401.59	12.450	1860.4	1.194	40.000	1.9546	371.77	1.52	1.8550	352.82
	672.75	7.432	1709.6	1.198	60.000	1.9928	379.04	2.28	1.9036	362.08
	968.69	5.162	1609.2	1.200	80.000	2.0175	383.74	3.04	1.9345	368.03
	1284.22	3.893	1535.0	1.202	100.000	2.0354	387.14	3.80	1.9575	372.33
	3073.12	1.627	1323.7	1.207	200.000	2.0848	396.54	7.61	2.0197	384.16
	5109.15	0.979	1212.8	1.209	300.000	2.1099	401.30	11.41	2.0511	390.13
	7322.11	0.683	1139.6	1.210	400.000	2.1262	404.41	15.22	2.0716	394.02
	12148.68	0.412	1043.4	1.212	600.002	2.1472	408.41	22.82	2.0978	399.02
	17390.83	0.288	979.7	1.214	800.004	2.1609	411.01	30.43	2.1149	402.26
	22967.75	0.218	932.7	1.216	1000.004	2.1709	412.91	38.04	2.1274	404.63

TABLE 17. (Concluded)

PRESSURE (PSIA)	4999.996	2887.745	660.312	368.238	248.310	144.674	99.230	74.206
TEMPERATURE (DEG R)	6813.5	6457.1	5598.6	5281.7	5068.7	4771.9	4557.2	4387.5
H (BTU/LB)	5272.3	4951.0	4183.4	3914.3	3742.8	3520.5	3374.3	3266.5
S (BTU/LB-DEG R)	2.742	2.742	2.742	2.742	2.742	2.742	2.742	2.742
CP,SH. (BTU/LB-DEG R)	1.406	1.375	1.181	1.052	0.955	0.804	0.711	0.652
CP,FR. (BTU/LB-DEG R)	0.549	0.546	0.538	0.535	0.532	0.528	0.524	0.521
GAMMA, SHIFTING	1.138	1.135	1.131	1.133	1.137	1.146	1.155	1.163
GAMMA, FROZEN	1.193	1.191	1.188	1.187	1.187	1.188	1.188	1.189
VISCOSITY,CENTIPOISE	0.1026	0.0989	0.0897	0.0861	0.0836	0.0801	0.0775	0.0755
VISCOSITY (LB/HR-FT)	0.2482	0.2394	0.2170	0.2083	0.2022	0.1939	0.1876	0.1826
K,FR. (BTU/HR-FT-F)	0.2153	0.2056	0.1815	0.1725	0.1664	0.1579	0.1517	0.1469
K,SH. (BTU/HR-FT-F)	0.5515	0.5176	0.3982	0.3393	0.2971	0.2405	0.2059	0.1838
PRANDTL NUMBER	0.6326	0.6359	0.6434	0.6456	0.6467	0.6478	0.6481	0.6480
M,FRZ. (LB/LB-MOLE)	22.382	22.654	23.331	23.562	23.658	23.851	23.930	23.975
DENSITY (LB/FT3)	1.53057	0.94412	0.25644	0.15308	0.10818	0.06735	0.04856	0.03779
VELOCITY (FT/SEC)	0.0	4009.5	7381.0	8242.8	8747.8	9361.9	9744.5	10017.8
MACH NO, SHIFTING	0.0	1.000	2.009	2.319	2.516	2.773	2.947	3.080
MACH NO, FROZEN	0.0	0.976	1.961	2.266	2.462	2.724	2.905	3.046
EPSILON	0.0	1.00	2.00	3.00	4.00	6.00	8.00	10.00

THERMODYNAMIC AND TRANSPORT PROPERTIES IN THE ABOVE TABLE ARE THEORETICAL ESTIMATES.
PERFORM USING FOR HARDWARE DESIGN PURPOSES. PLEASE CONTACT ORIGINATING UNIT.

COMPOSITION - GRAM MOLES PER 100 GRAMS PROPELLANT

H	0.06749	0.05689	0.03290	0.02504	0.02021	0.01421	0.01053	0.00804
O	0.03545	0.02704	0.01033	0.00601	0.00381	0.00172	0.00084	0.00044
OH	0.27597	0.22990	0.12232	0.08683	0.06545	0.04026	0.02623	0.01774
H2	0.30382	0.29388	0.23905	0.22672	0.22076	0.21676	0.21742	0.21993
H2O	2.29469	2.34901	2.45366	2.48767	2.50674	2.52033	2.53452	2.53750
CO	0.72571	0.68556	0.59061	0.54306	0.52035	0.49387	0.47881	0.46894
CO2	0.65931	0.69952	0.80454	0.84210	0.86477	0.89130	0.90636	0.91622
O2	0.10536	0.08933	0.04264	0.02676	0.01758	0.00826	0.00409	0.00211

EXPANSIONS WITH LIMITED SHIFTING COMPOSITION

EXPANSION TO ONE ATMOSPHERE

PC/PE	P PSIA	T DEG. K	CSTAR FT/SEC	T DEG. K	EXIT CONDITIONS GAMMA	EPSILON	I-OPT LB-SEC/LB
1.0000	4999.996	3785.3	6010.				
FULL SHIFTING			6120.	1371.5	1.239	29.28	329.54
				1910.9	1.192	35.12	349.62
					DENSITY IMPULSE =		291.08

EXPANSION TO EPSILON = 40

PC/PE	P PSIA	T DEG. K	P PSIA	T DEG. K	EXIT CONDITIONS GAMMA	I-OPT LB-SEC/LB	I-VAC LB-SEC/LB
1.000	4999.996	3785.3					
FULL SHIFTING			9.7429	1265.9	1.245	335.83	353.35
			12.4505	1860.4	1.194	352.82	371.77

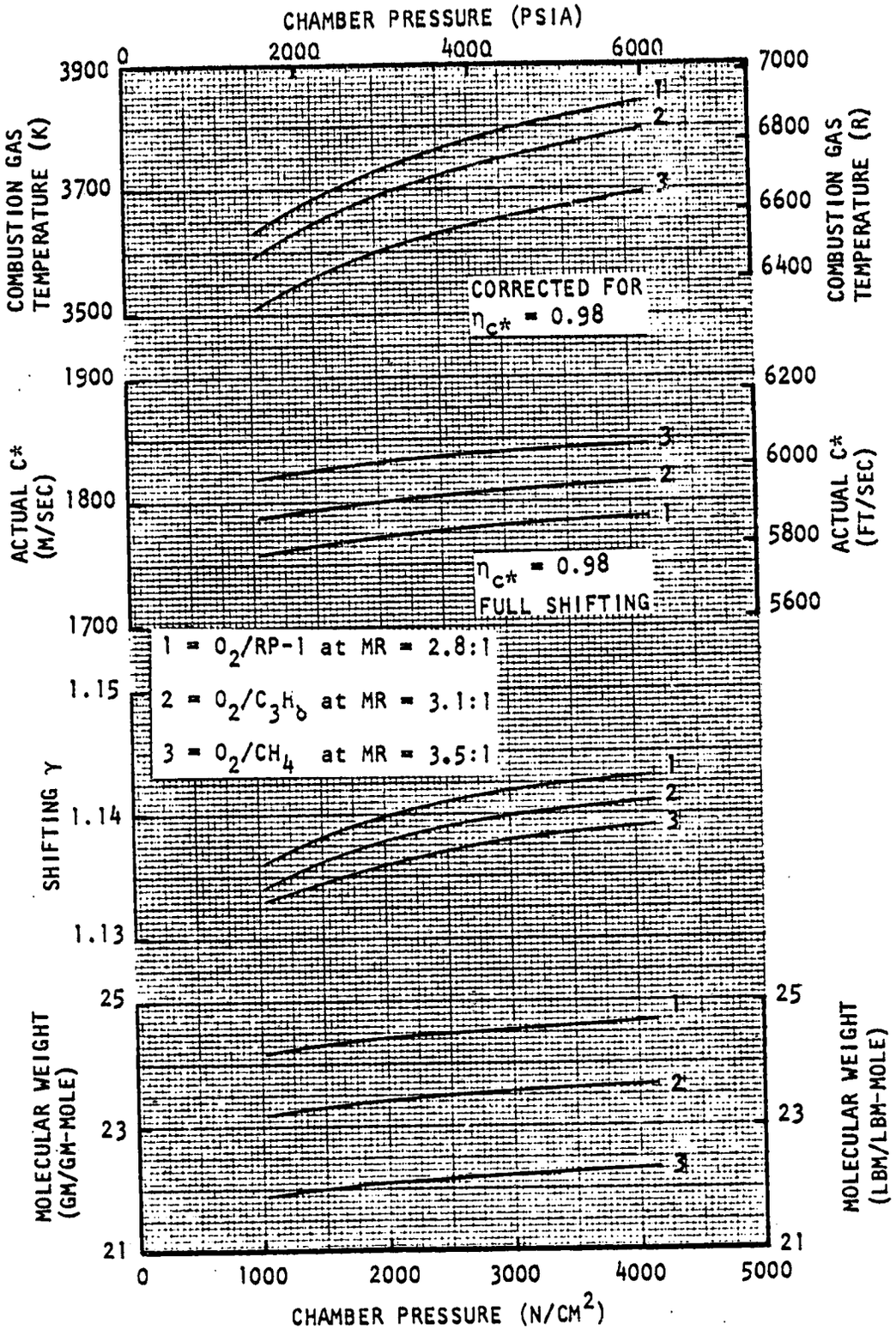

Figure 55. Properties of O_2/RP-1, $O_2/C_3/H_8$, and O_2/CH_4 Combustion Gases

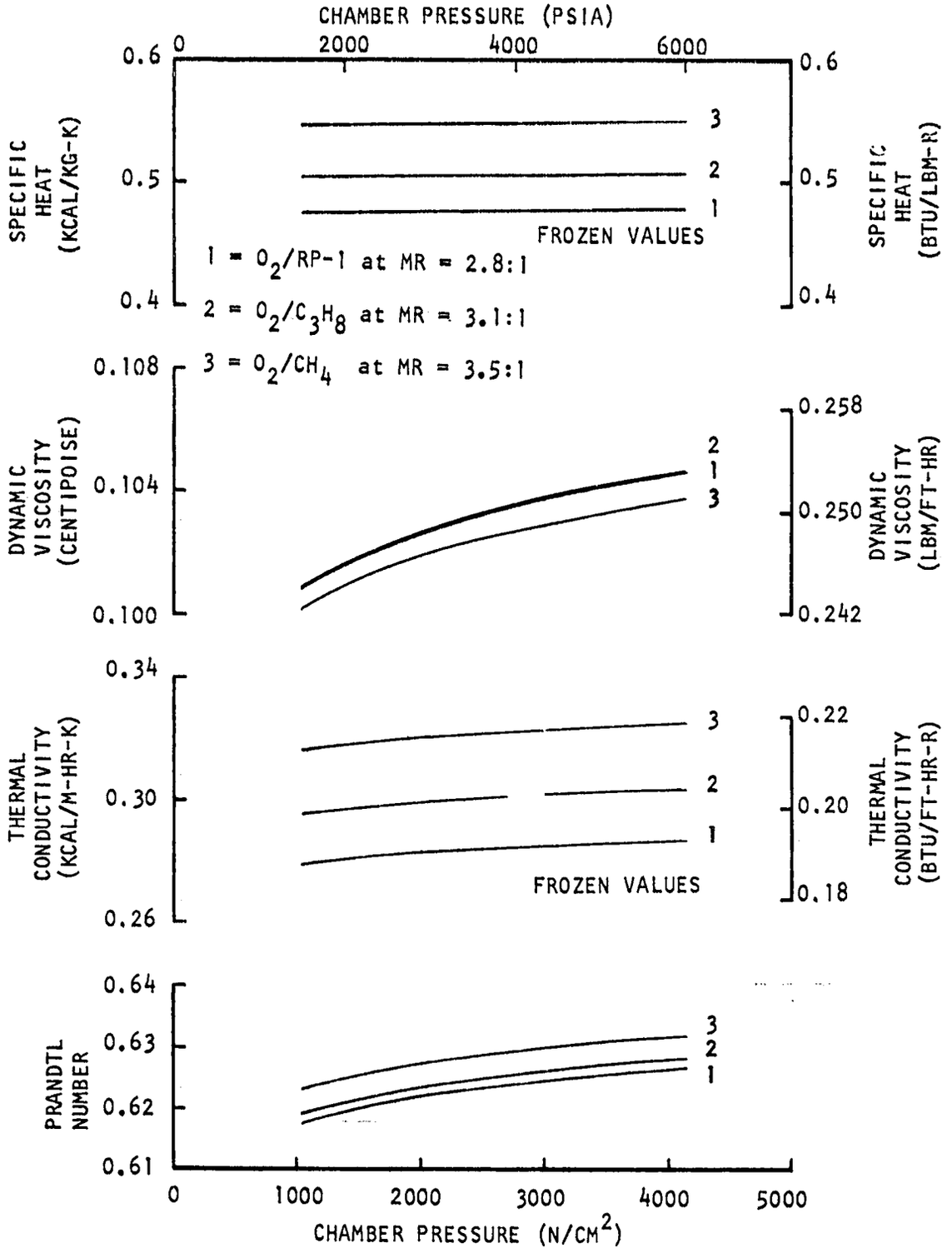

Figure 56. Properties of O_2/RP-1, O_2/C_3H_8, and O_2/CH_4 Combustion Gases

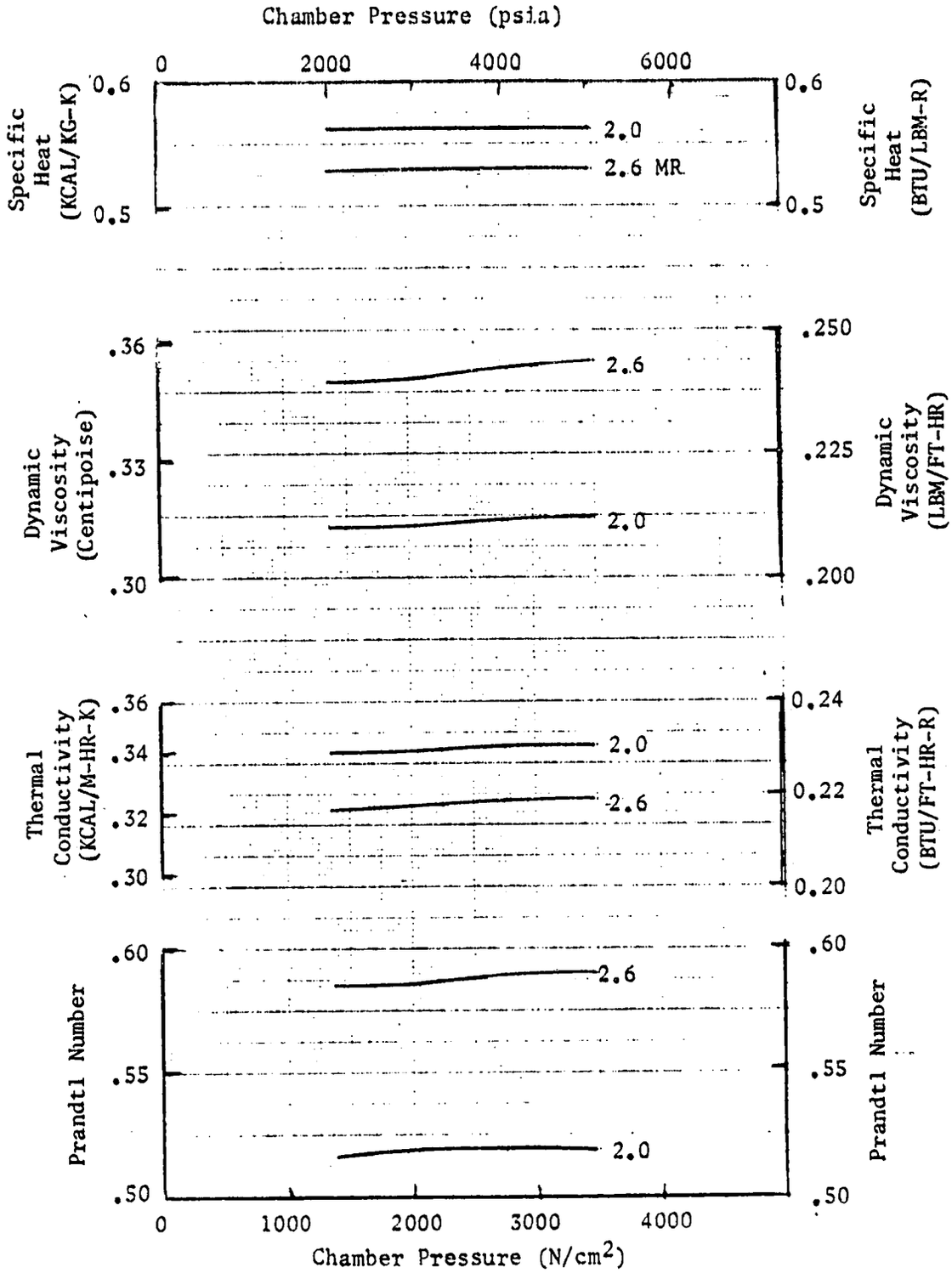

Figure 57. O_2/C_3H_8 Zoned Combustion Gas Properties

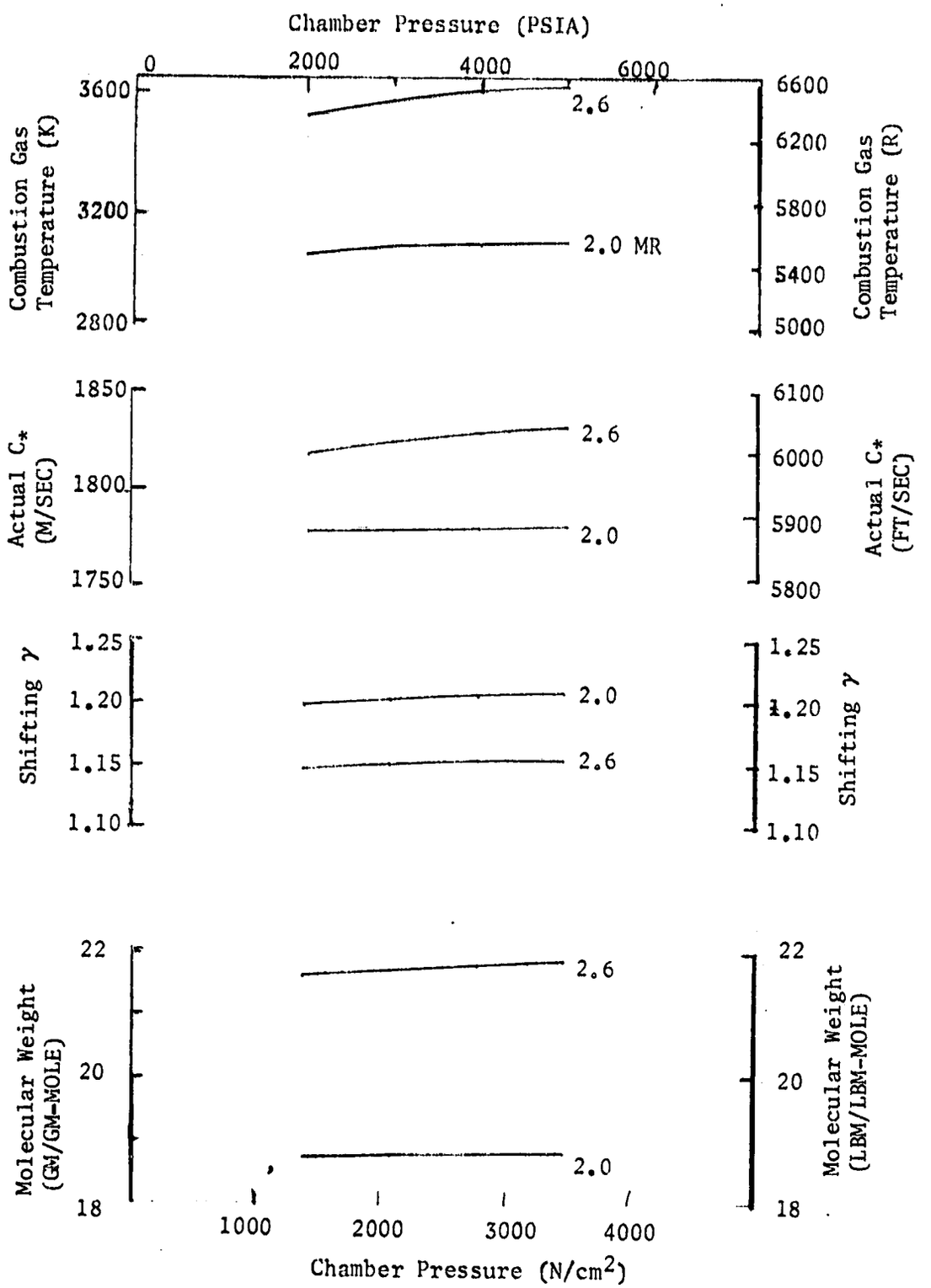

Figure 58. O_2/C_3H_8 Zoned Combustion Gas Properties

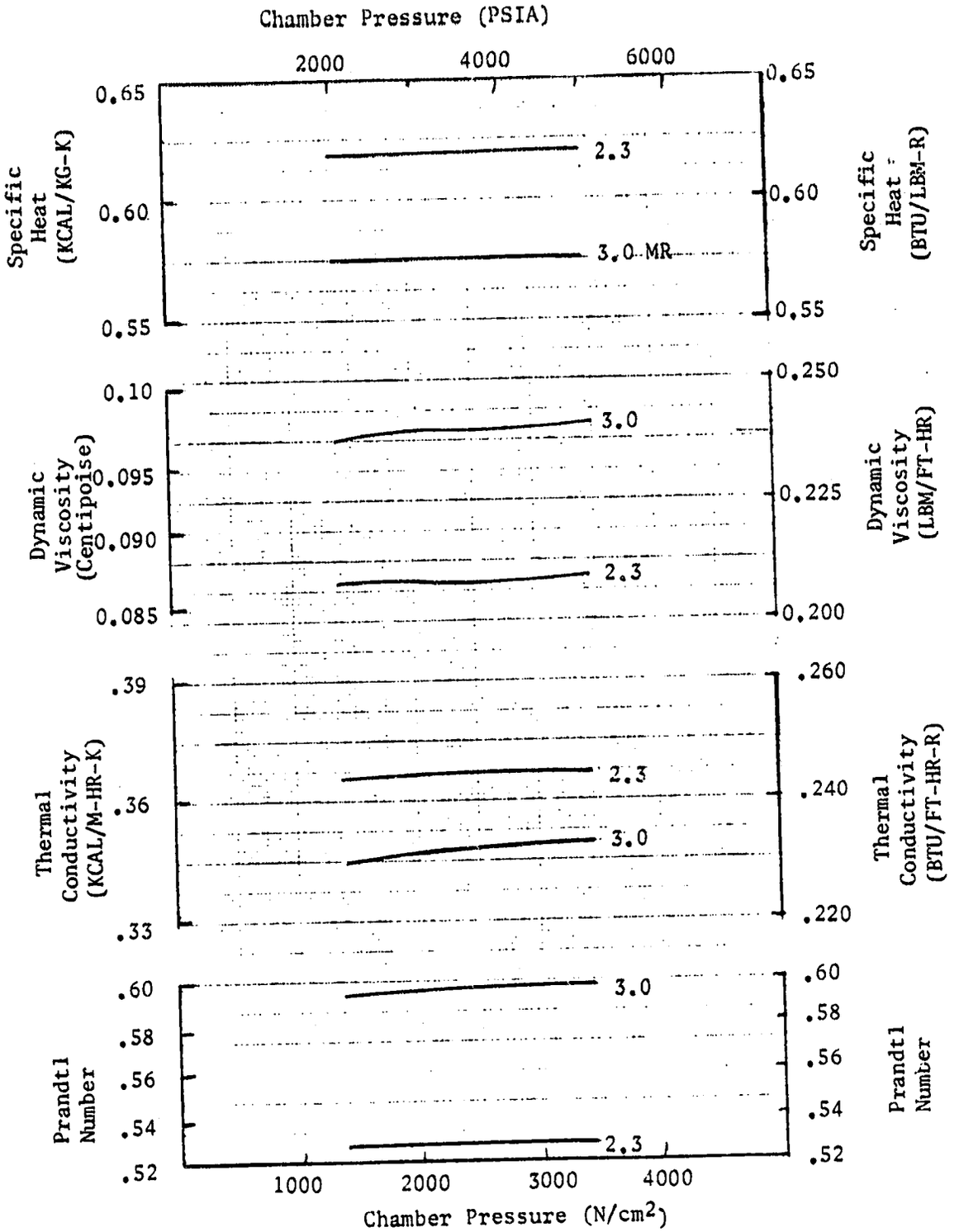

Figure 59. O_2/CH_4 Zoned Combustion Gas Properties

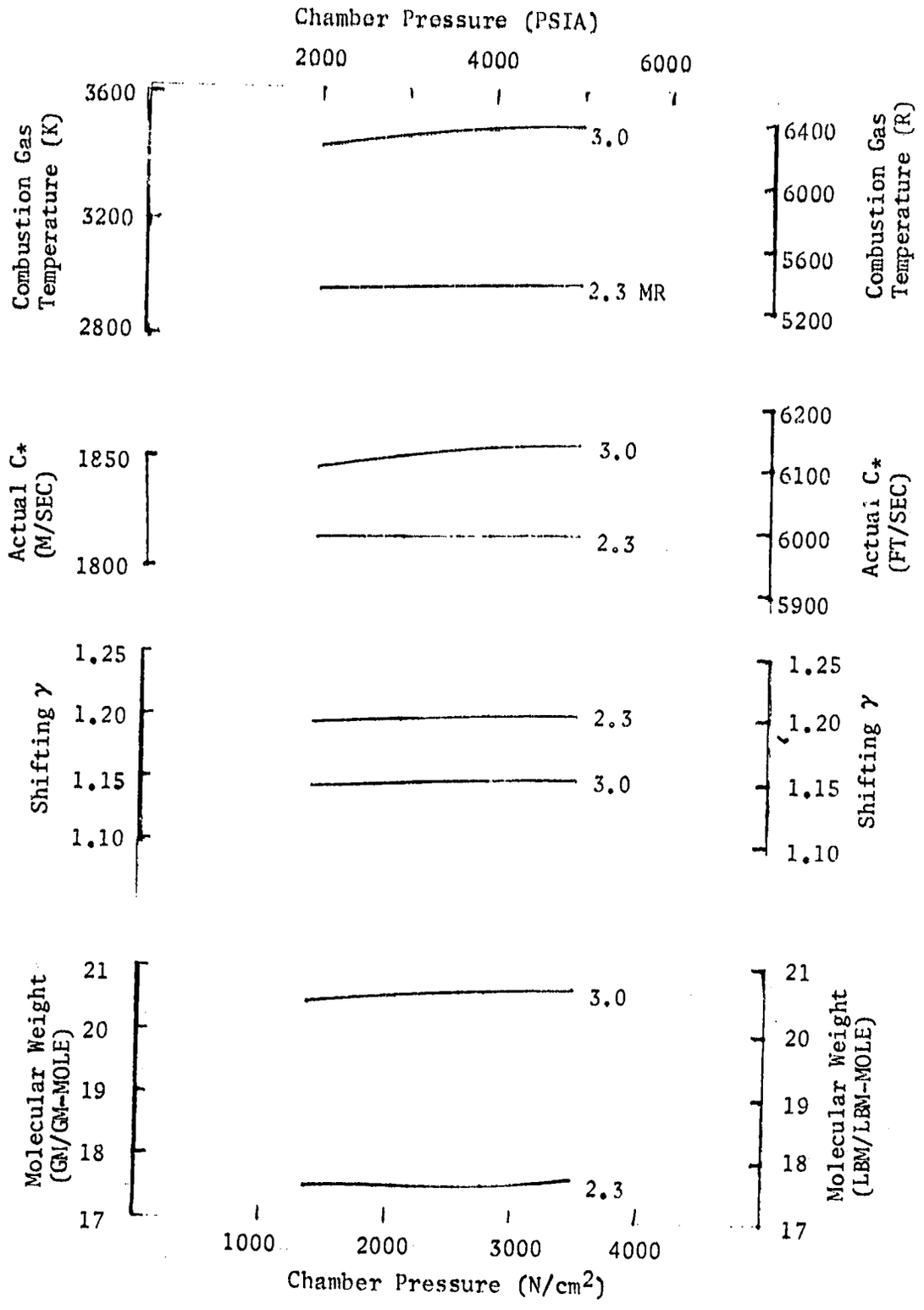

Figure 60. O_2/CH_4 Zoned Combustion Gas Properties

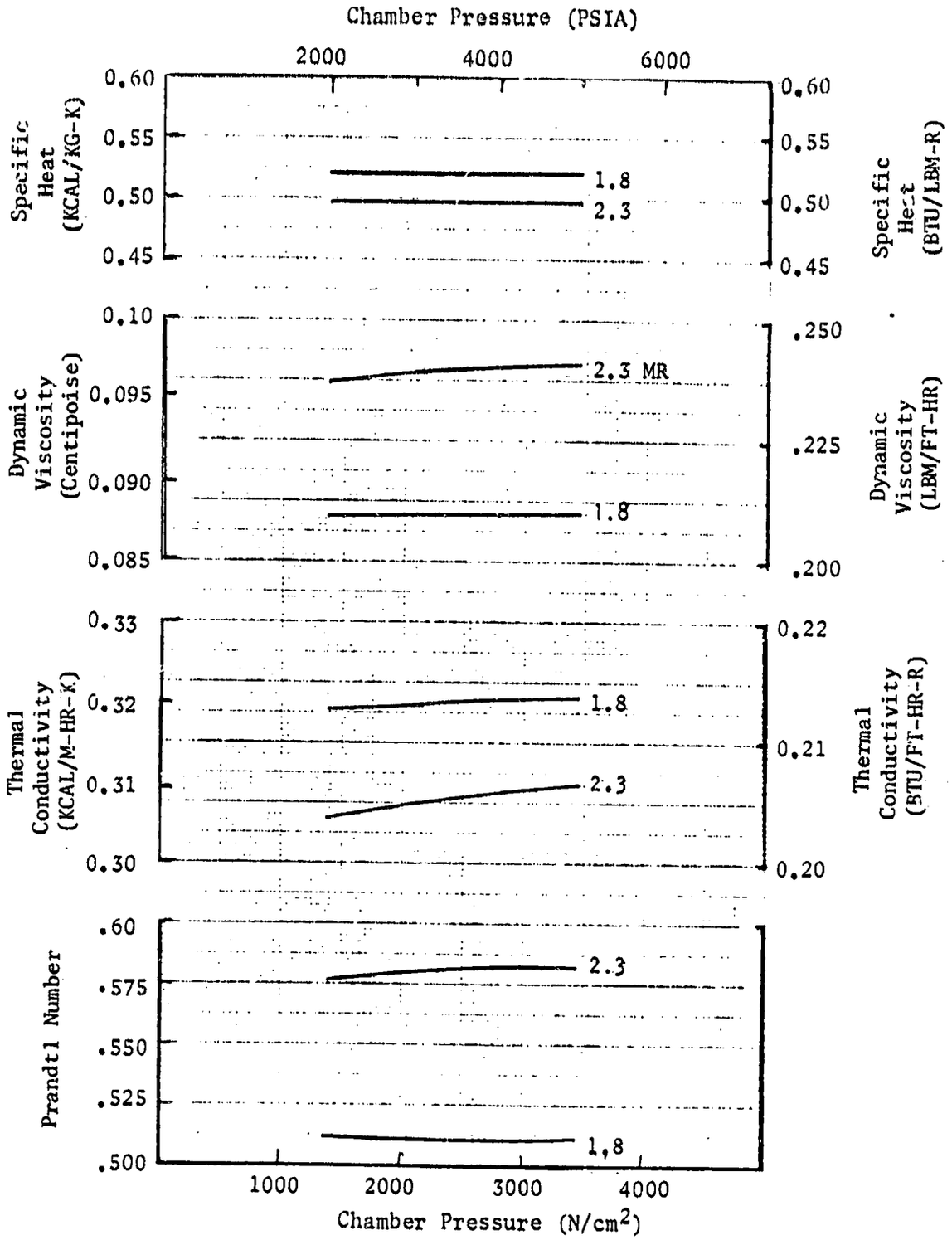

Figure 61. O_2/RP-1 Zoned Combustion Gas Properties

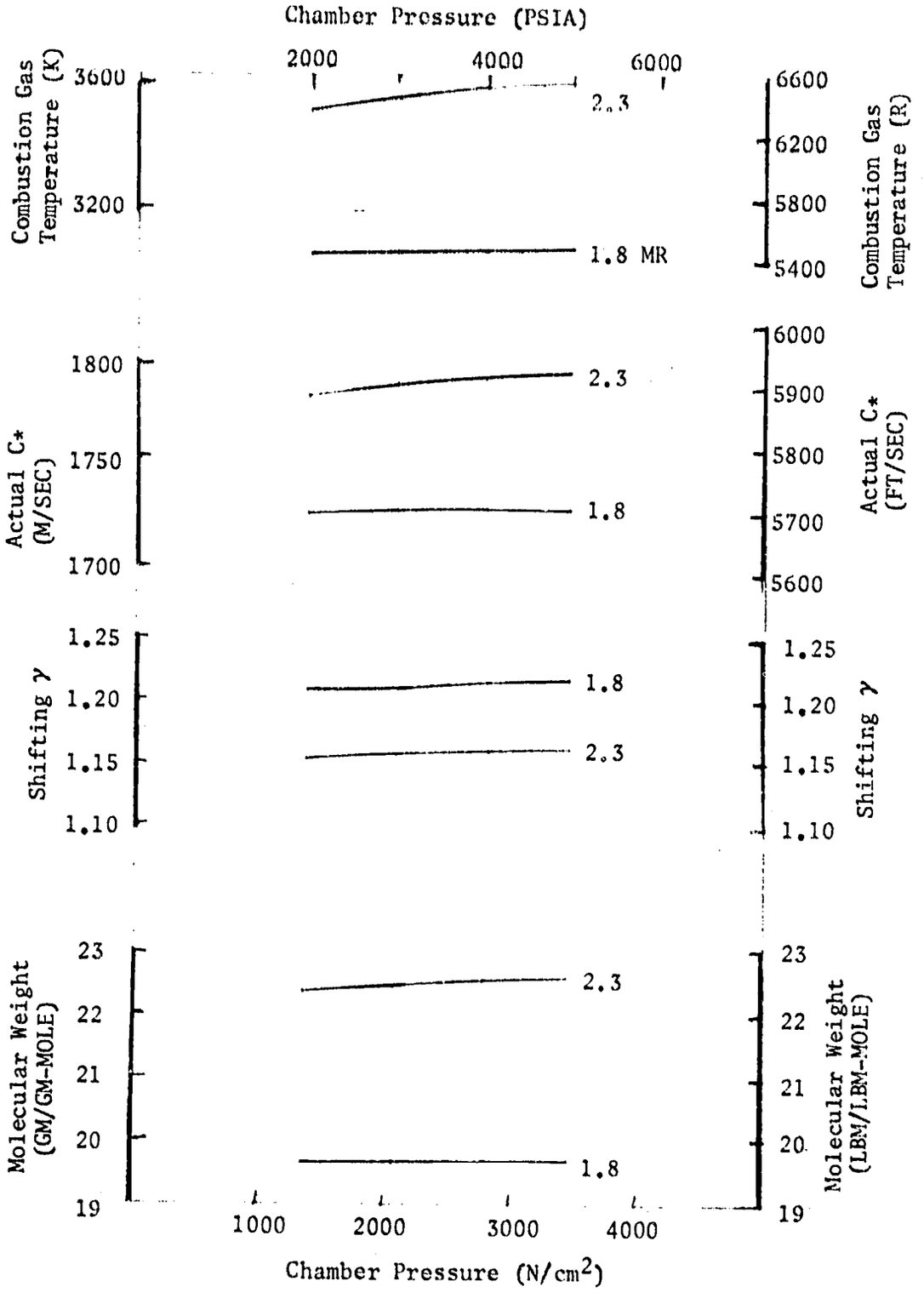

Figure 62. O_2/RP-1 Zoned Combustion Gas Properties

APPENDIX C

GRAPHIC PRESENTATION OF UNENHANCED COMBUSTION CHAMBER AND NOZZLE DESIGNS

The detailed combustion chamber and nozzle design analyses are presented in this appendix. Graphic presentations describe the operating parameters, coolant passage geometry, hot-gas wall geometry, and heat transfer characteristics.

The combustion chamber and nozzle designs are presented in the sequence noted in Table 4 under Design Results in the Unenhanced Design Cooling Analysis and Results section in the main body of the report.

PAGE 134 INTENTIONALLY BLANK

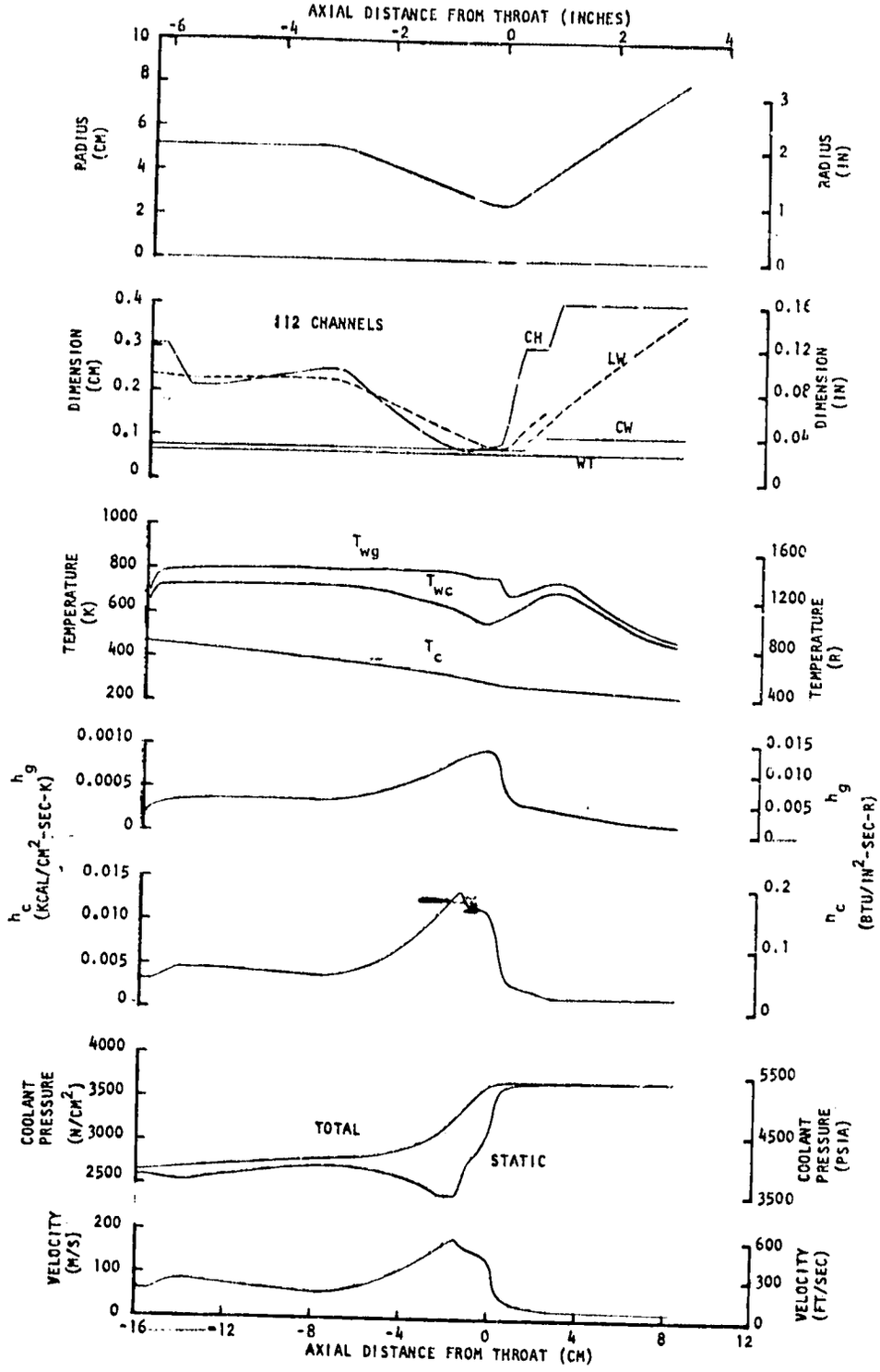

Figure 63. Parameters of the O_2/C_3H_8, MR = 3.1, F=89,000 N (20,000 lbf), Coolant P_{in_2}/P_c = 1.8 Combustion Chamber at P_c = 2068 N/cm^2 (3000 psia)

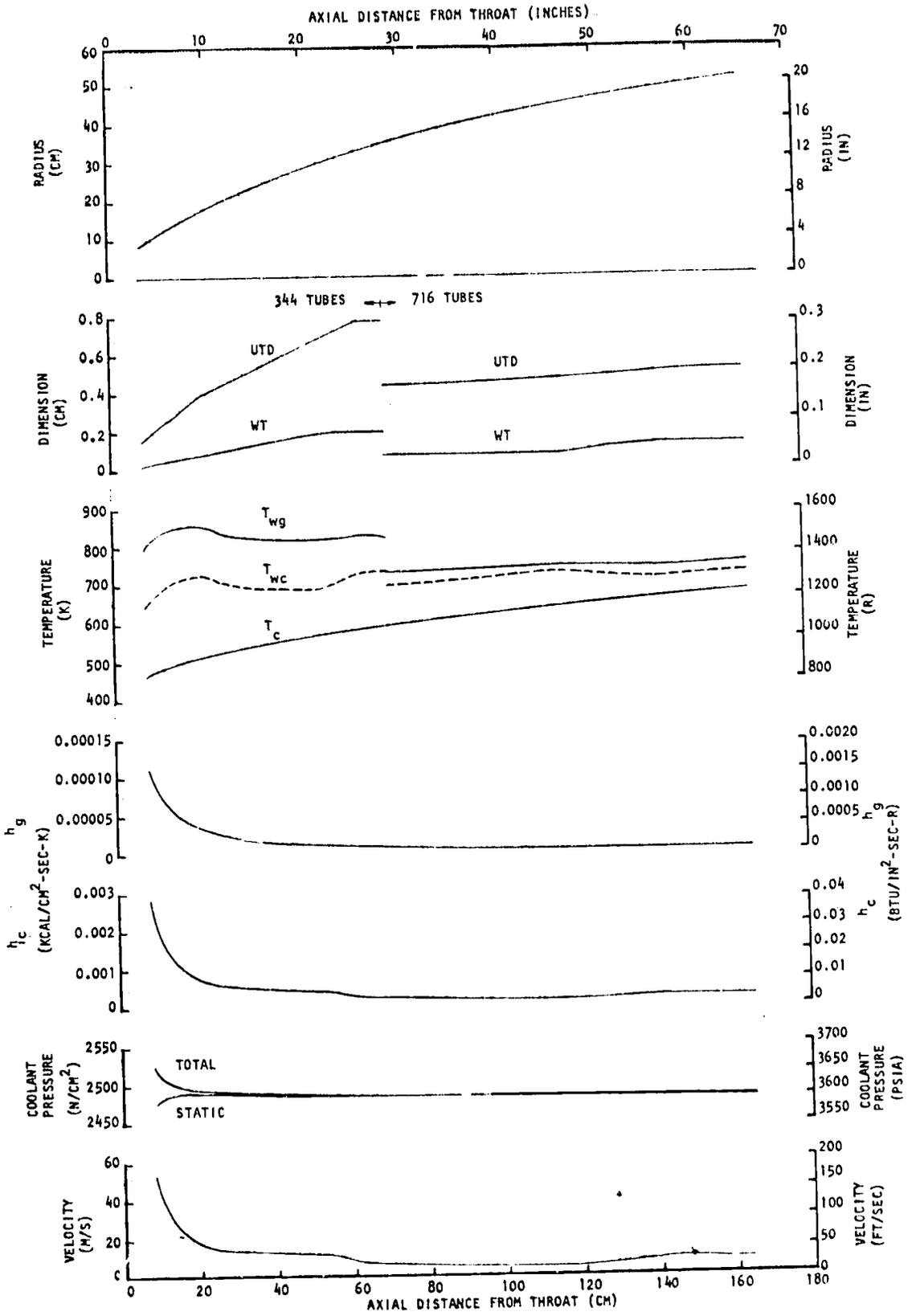

Figure 64. Parameters for the O_2/C_3H_8, MR = 3.1, F = 89,000 N (20,000 lbf), Coolant P_{in}/P_c = 1.8 Nozzle at P_c = 2068 N/cm^2 (3000 psia)

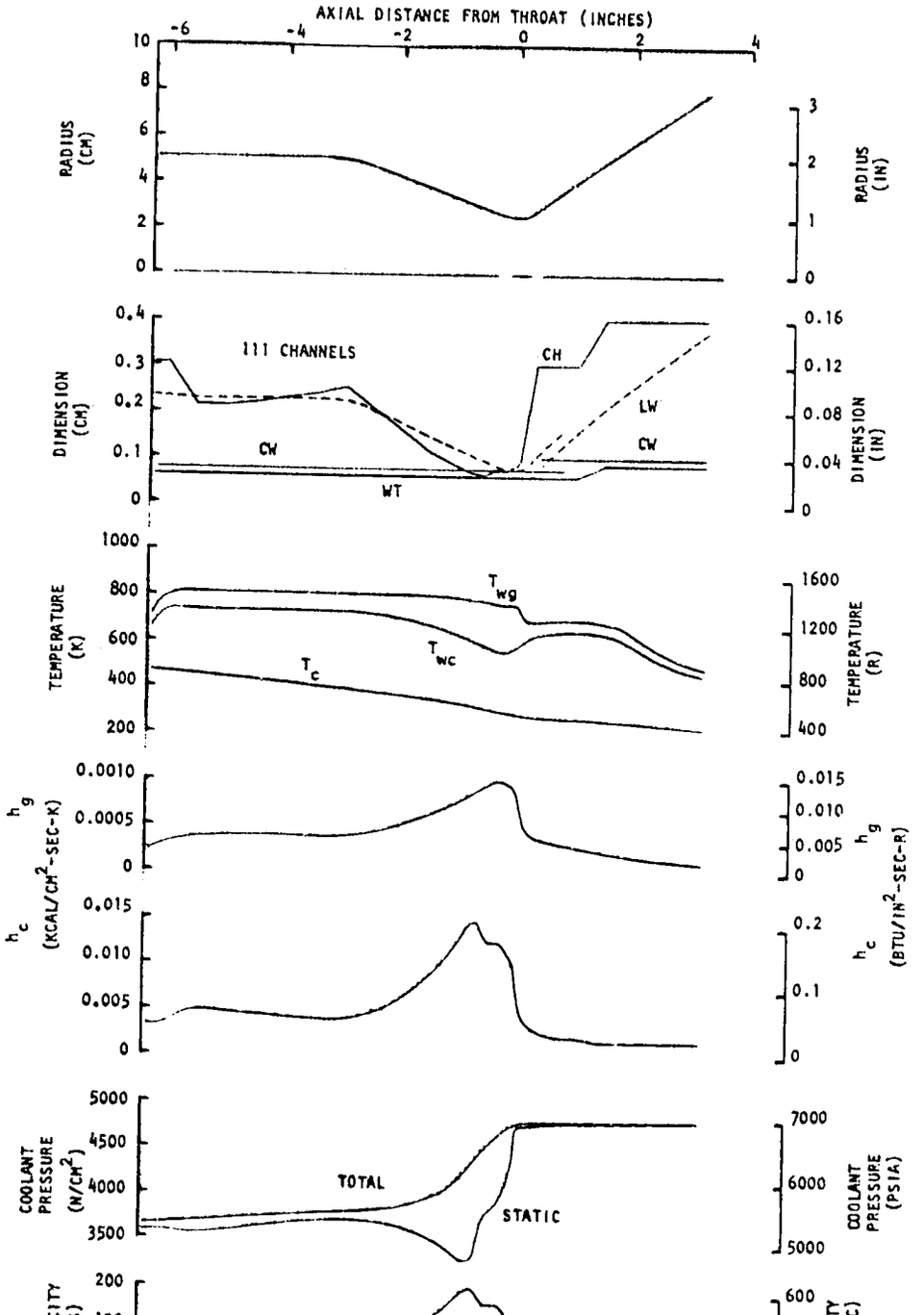

Figure 65. Parameters for the O_2/C_3H_8, MR = 3.1, F = 89,000 N (20,000 lbf), Coolant P_{in}/P_c = 2.25 Combustion Chamber at P_c = 2137 N/cm^2 (3100 psia)

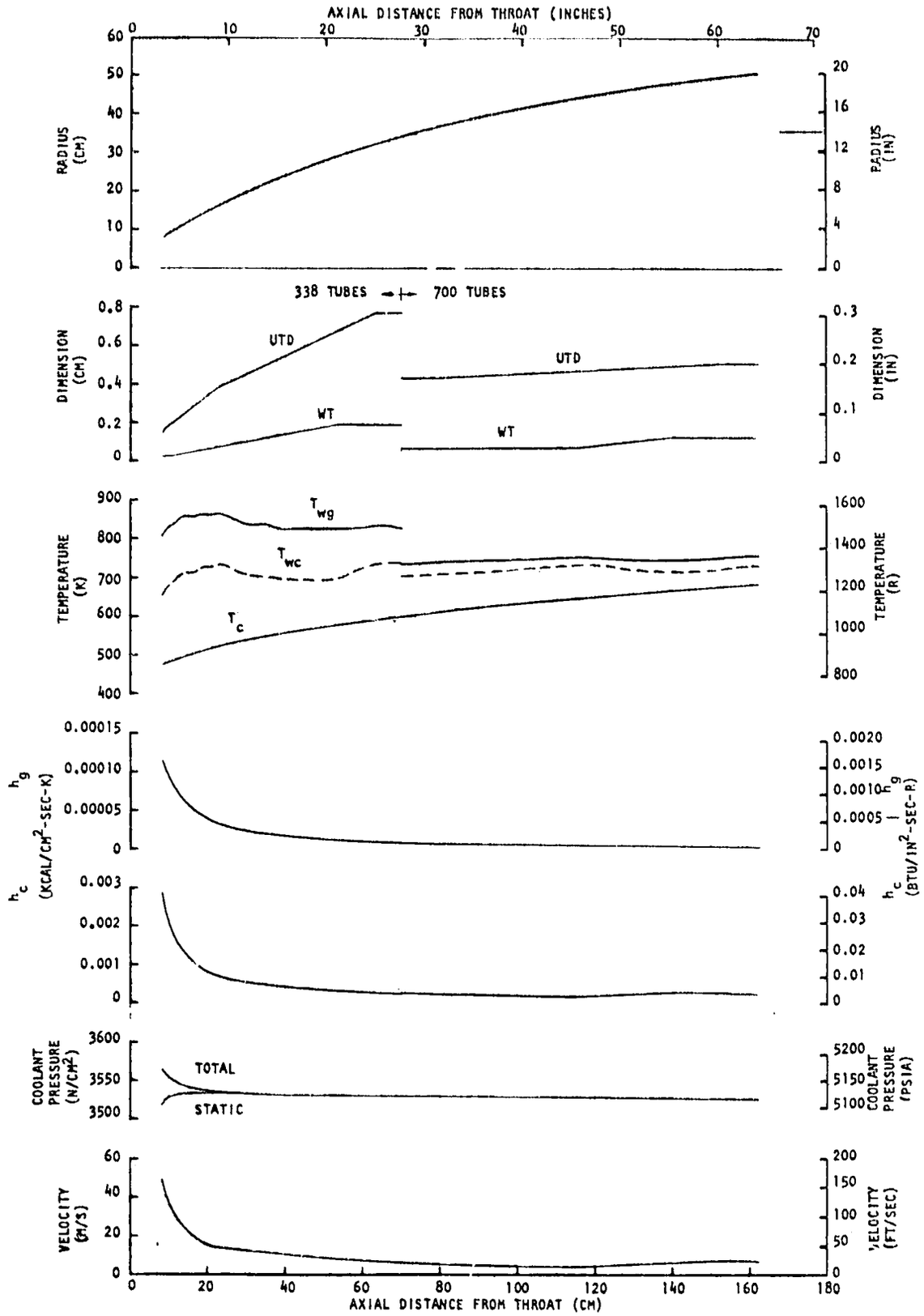

Figure 66. Parameters for the O_2/C_3H_8, MR = 3.1, F = 89,000 N (20,000 lbf), Coolant P_{in}/P_c = 2.25 Nozzle at P_c = 2137 N/cm^2 (3100 psia)

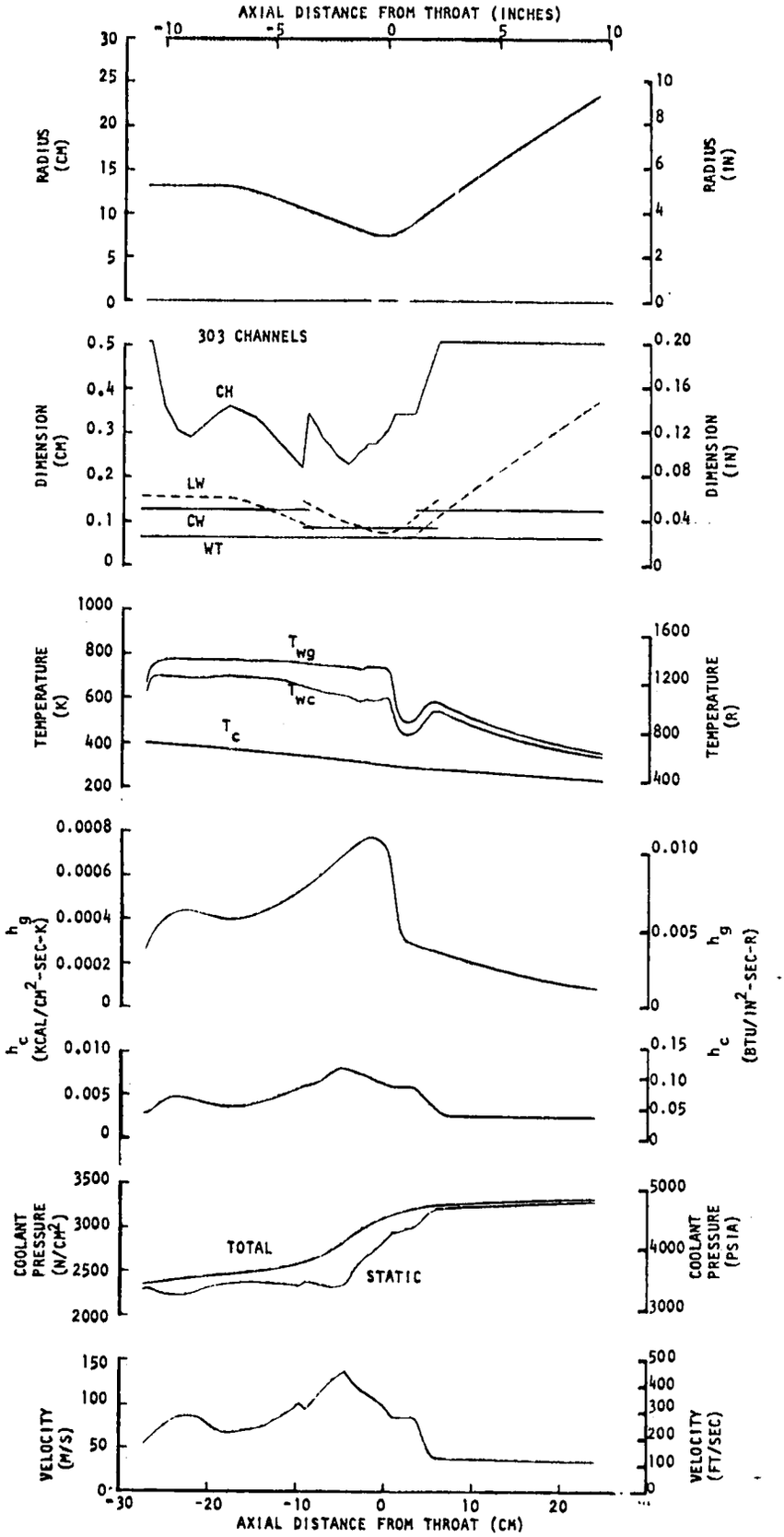

Figure 67. Parameters for the O_2/C_3H_8, MR = 3.1, F - 667,000 N (150,000 lbf) Coolant P_{in}/P_c = 1.8 Combustion Chamber at P_c = 1855 N/cm^2 (2690 psia)

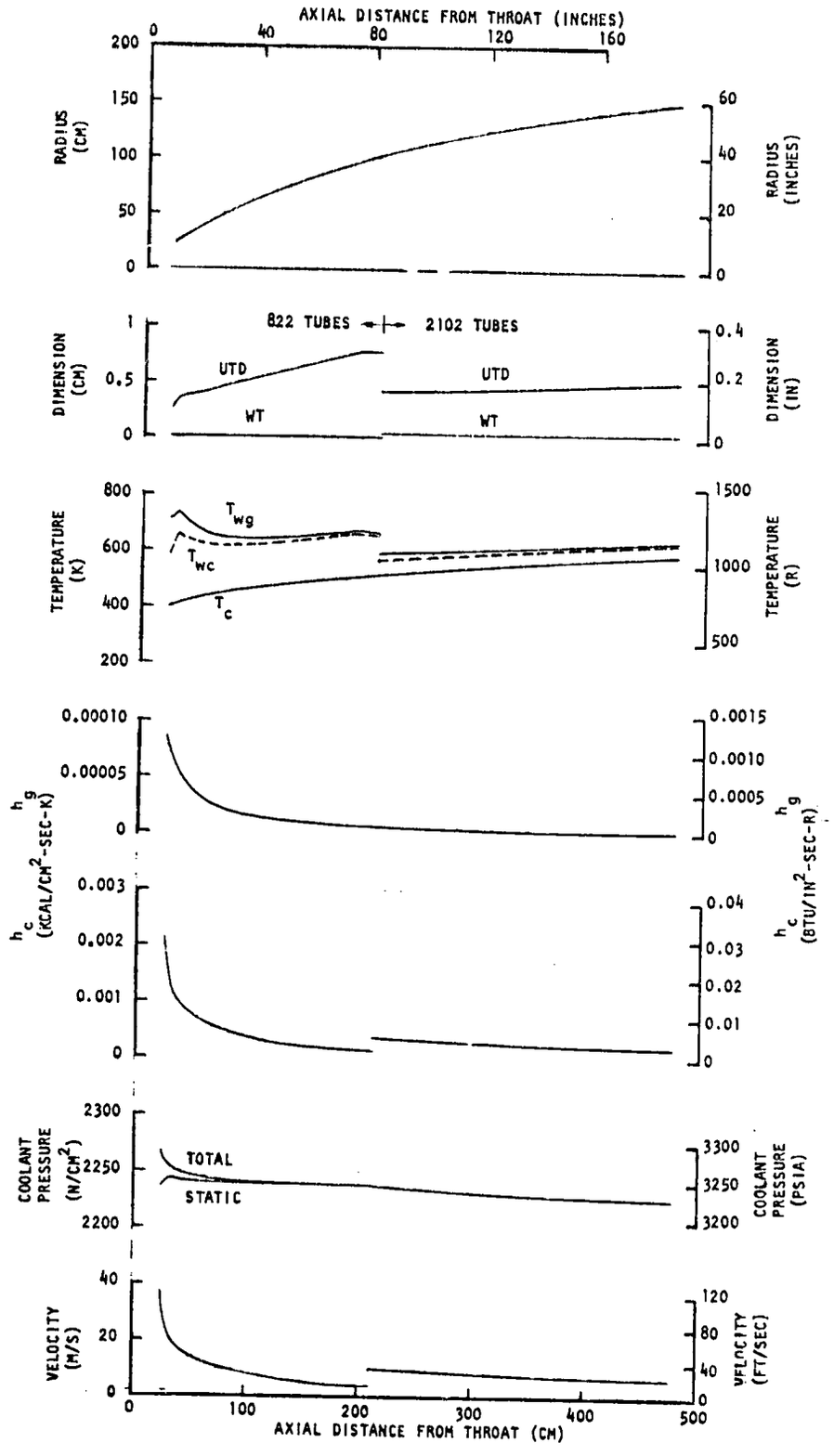

Figure 68. Parameters for the O_2/C_3H_8, MR = 3.1, F = 667,000 N (150,000 lbf), Coolant P_{in}/P_c = 1.8 Nozzle at P_c = 1855 N/cm^2 (2690 psia)

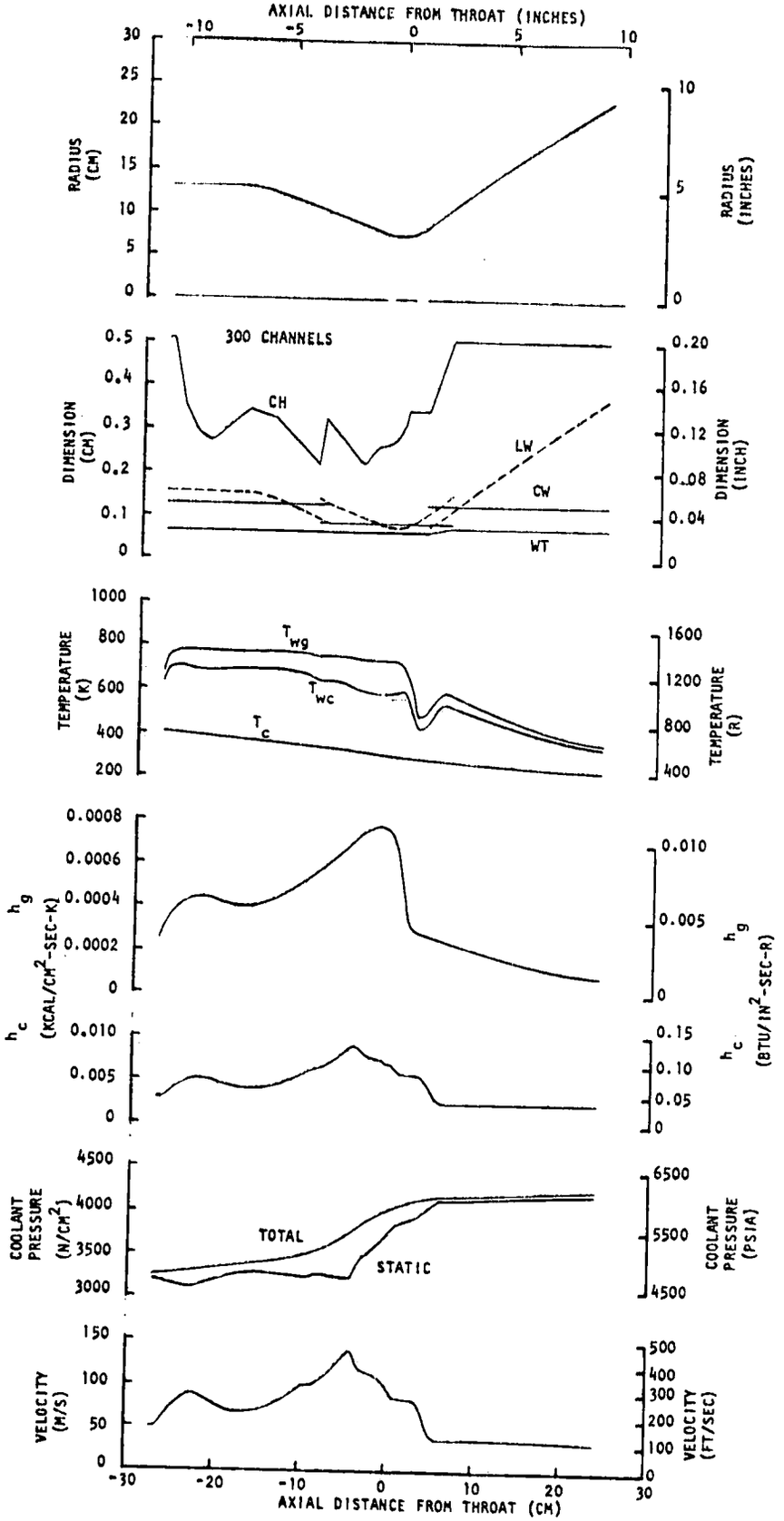

Figure 69. Parameters for the O_2/C_3H_8, MR = 3.1, F = 667,000 N (150,000 lbf), Coolant P_{in}/P_c = 2.25 Combustion Chamber at P_c = 1896 N/cm^2 (2750 psia)

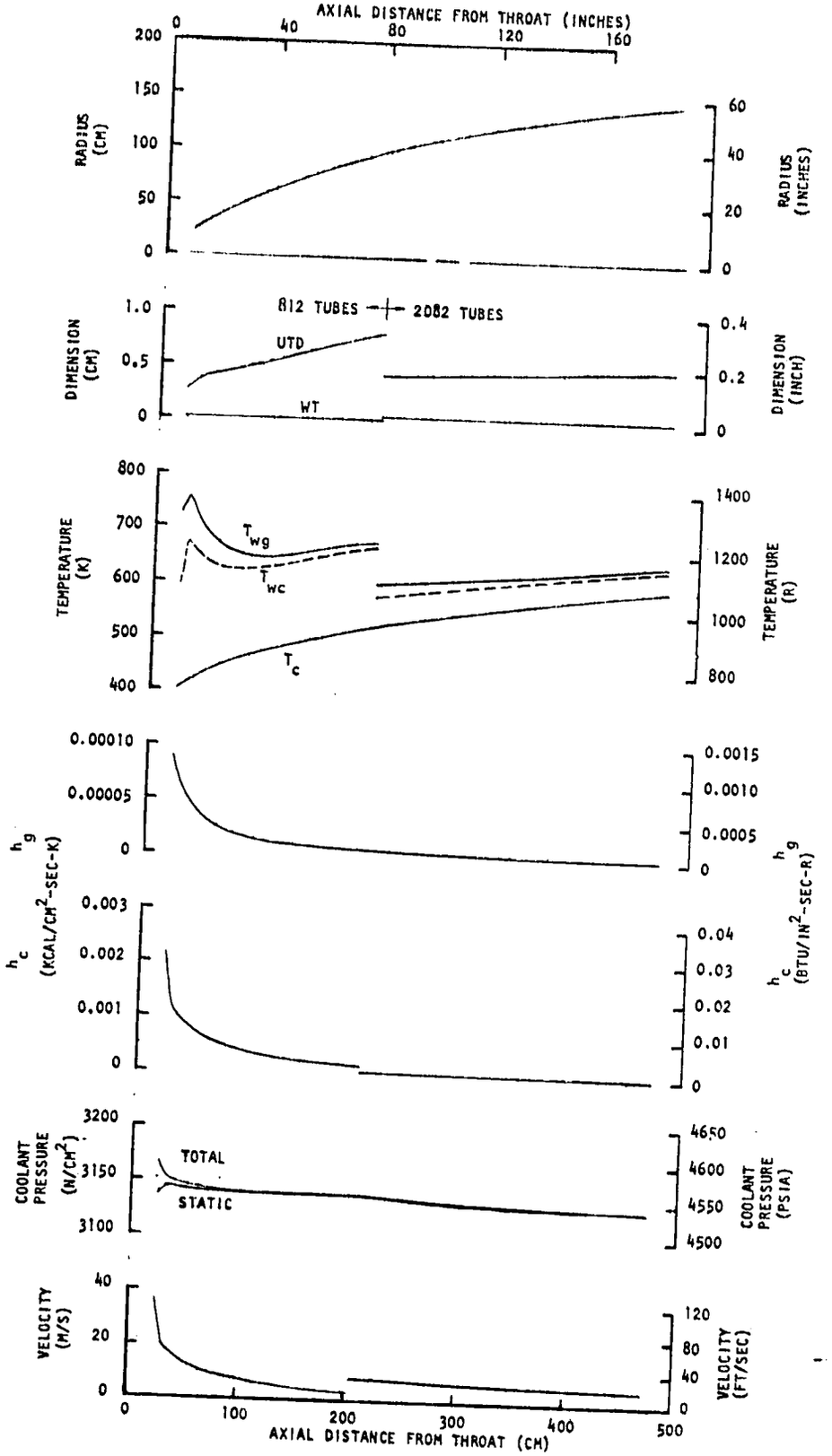

Figure 70. Parameters for the O_2/C_3H_8, MR = 3.1, F = 667,000 N (150,000 lbf), Coolant P_{in}/P_c = 2.25 Nozzle at P_c = 1896 N/cm^2 (2750 psia)

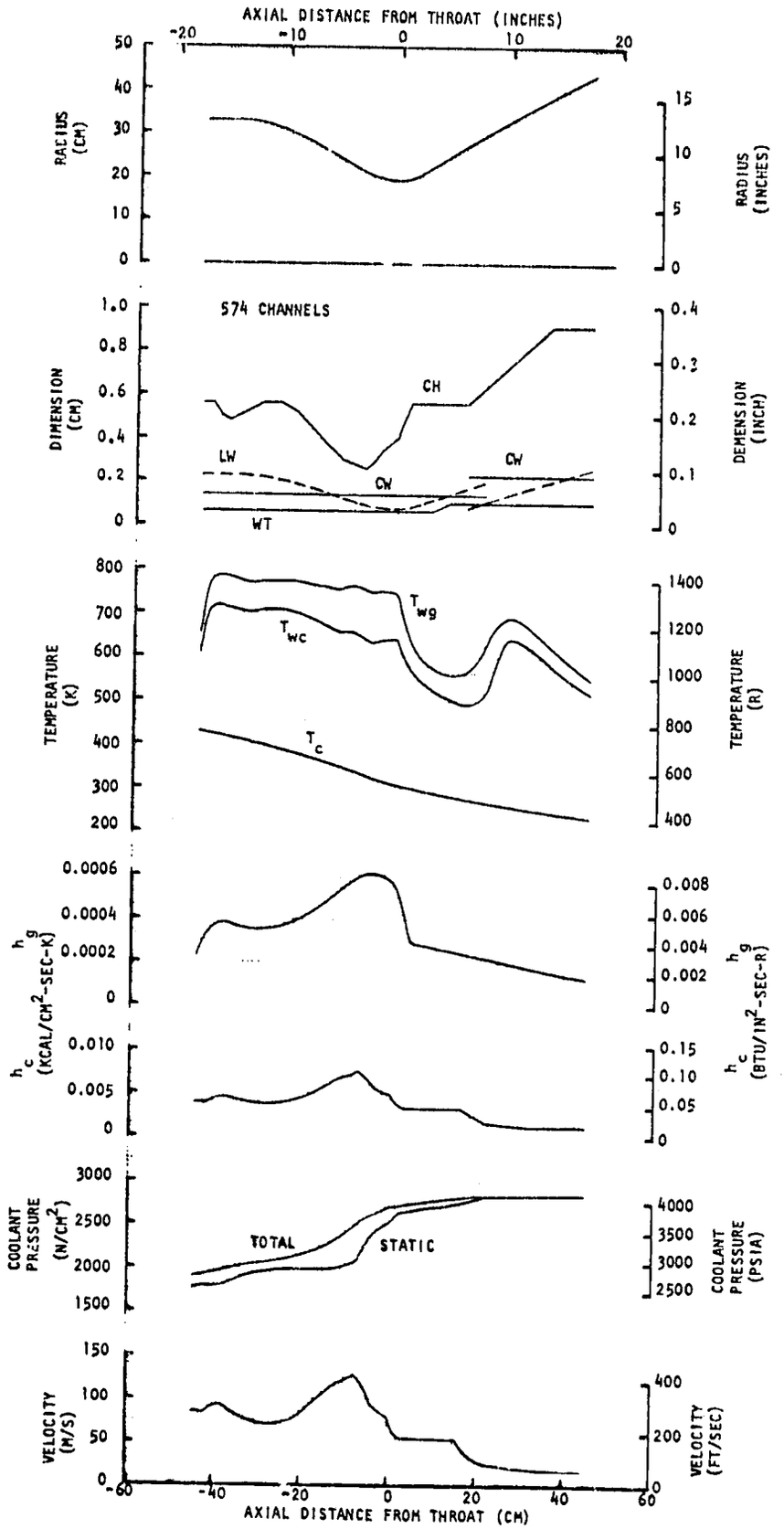

Figure 71. Parameters for the O_2/C_3H_8, MR = 3.1, F = 2,669,000 N (600,000 lbf), Coolant P_{in}/P_c = 1.8 Combustion Chamber at P_c = 1586 N/cm^2 (2300 psia)

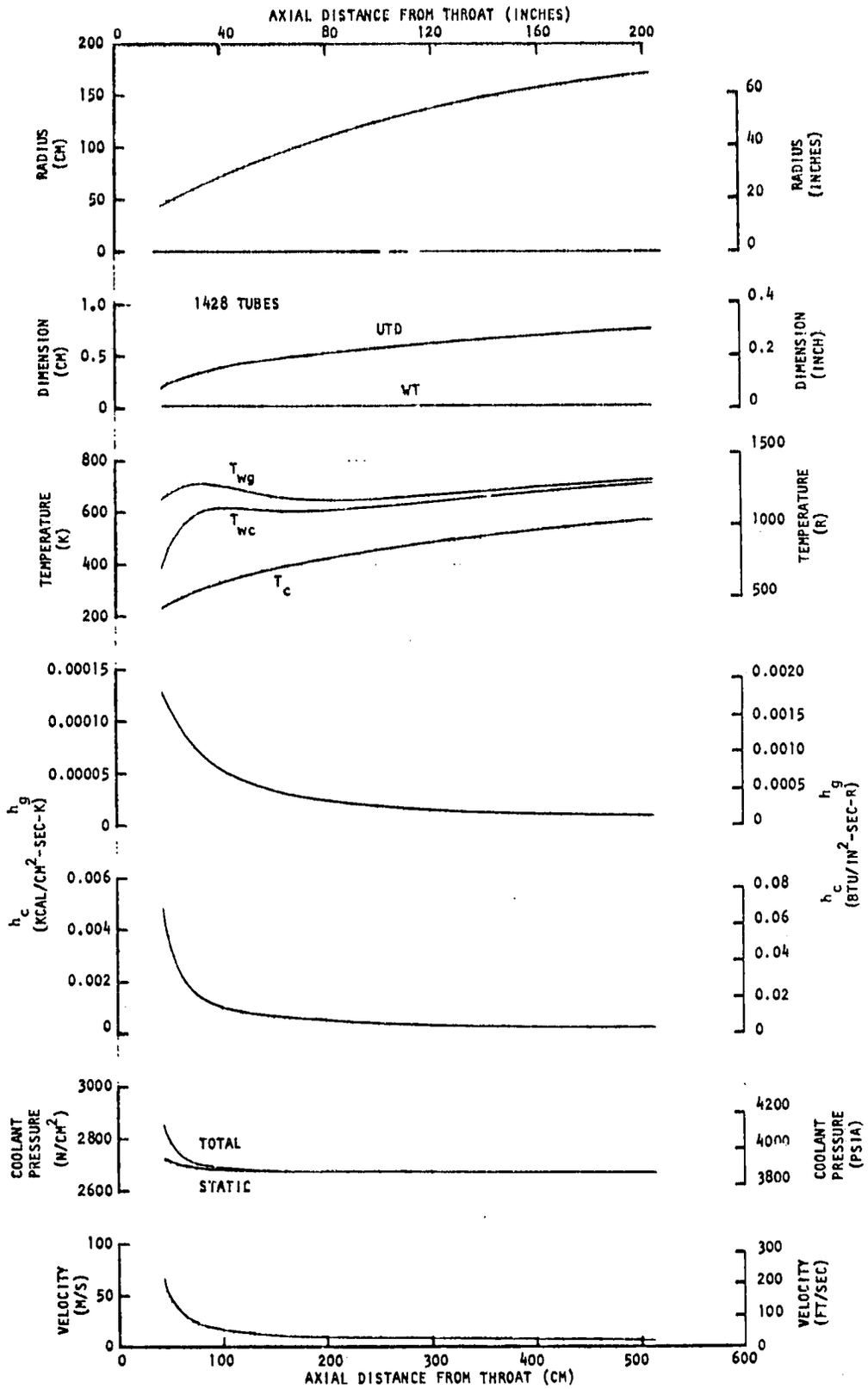

Figure 72. Parameters for the O_2/C_3H_8, MR = 3.1, F = 2,669,000 N (600,000 lbf), Coolant P_{in}/P_e = 1.8 Nozzle at P_c = 1586 N/cm^2 (2300 psia)

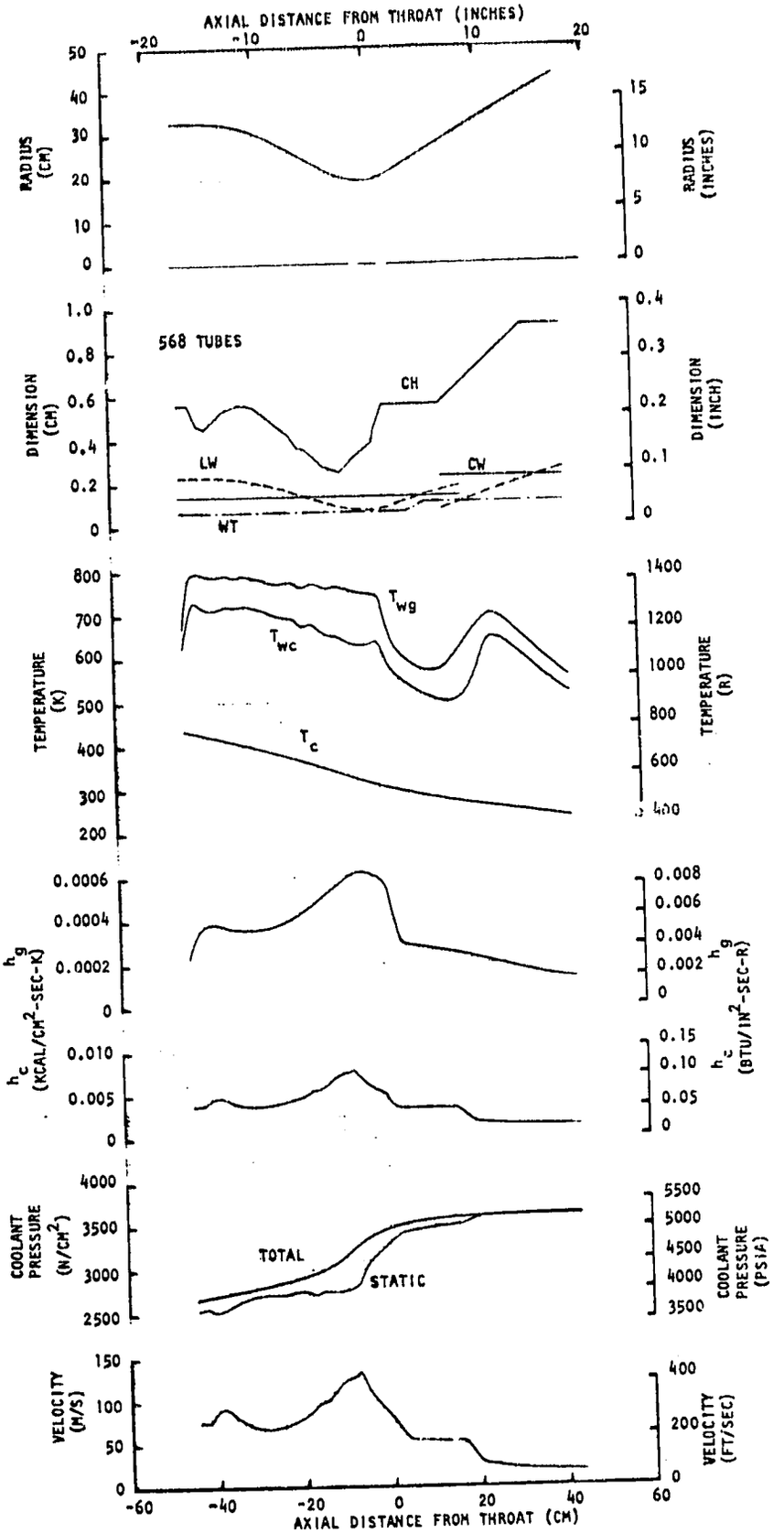

Figure 73. Parameters for the O_2/C_3H_8, MR = 3.1, F = 2,669,000 N (600,000 lbf), Coolant P_{in}/P_c = 2.25 Combustion Chamber at P_c = 1613 N/cm^2 (2340 psia)

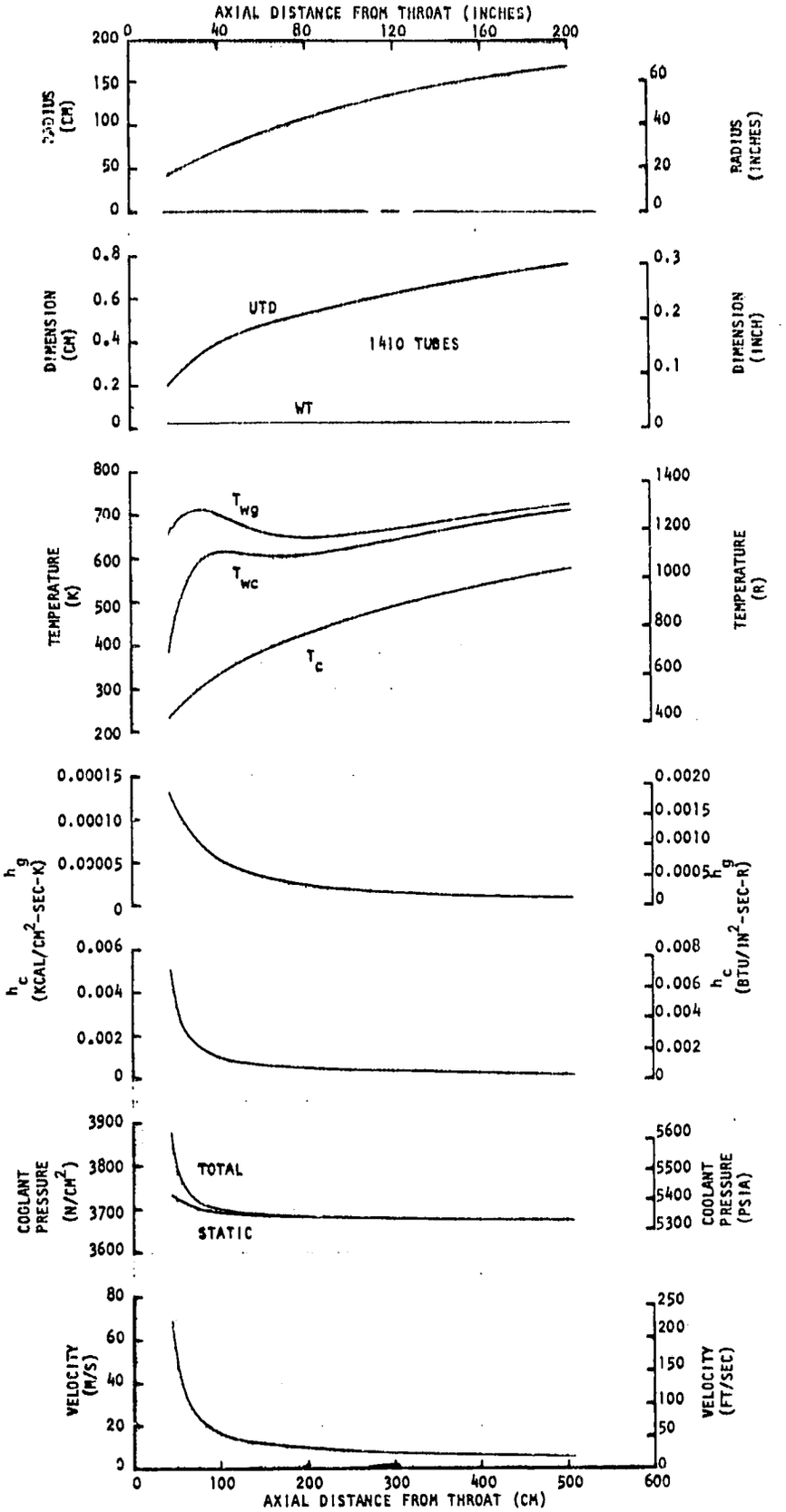

Figure 74. Parameters for the O_2/C_3H_8, MR = 3.1, F = 2,669,000 N (600,000 lbf), Coolant P_{in}/P_c = 2.25 Nozzle at P_c = 1613 N/cm^2 (2340 psia)

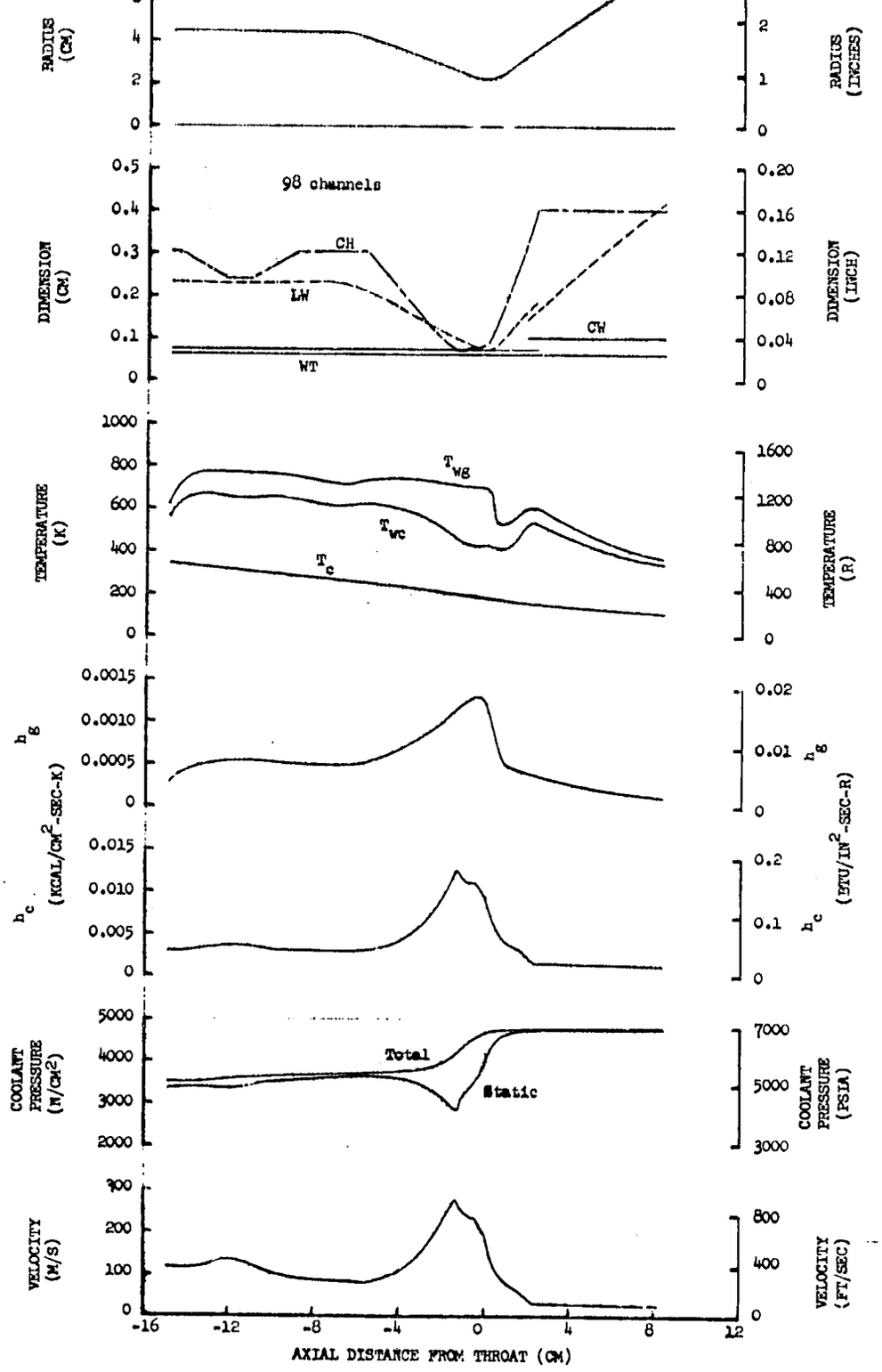

Figure 75. Parameters for the O_2/CH_4, MR = 3.5, F = 89,000 N (20,000 lbf), Coolant P_{in}/P_c = 1.74 Combustion Chamber at P_c = 2758 N/cm^2 (4000 psia)

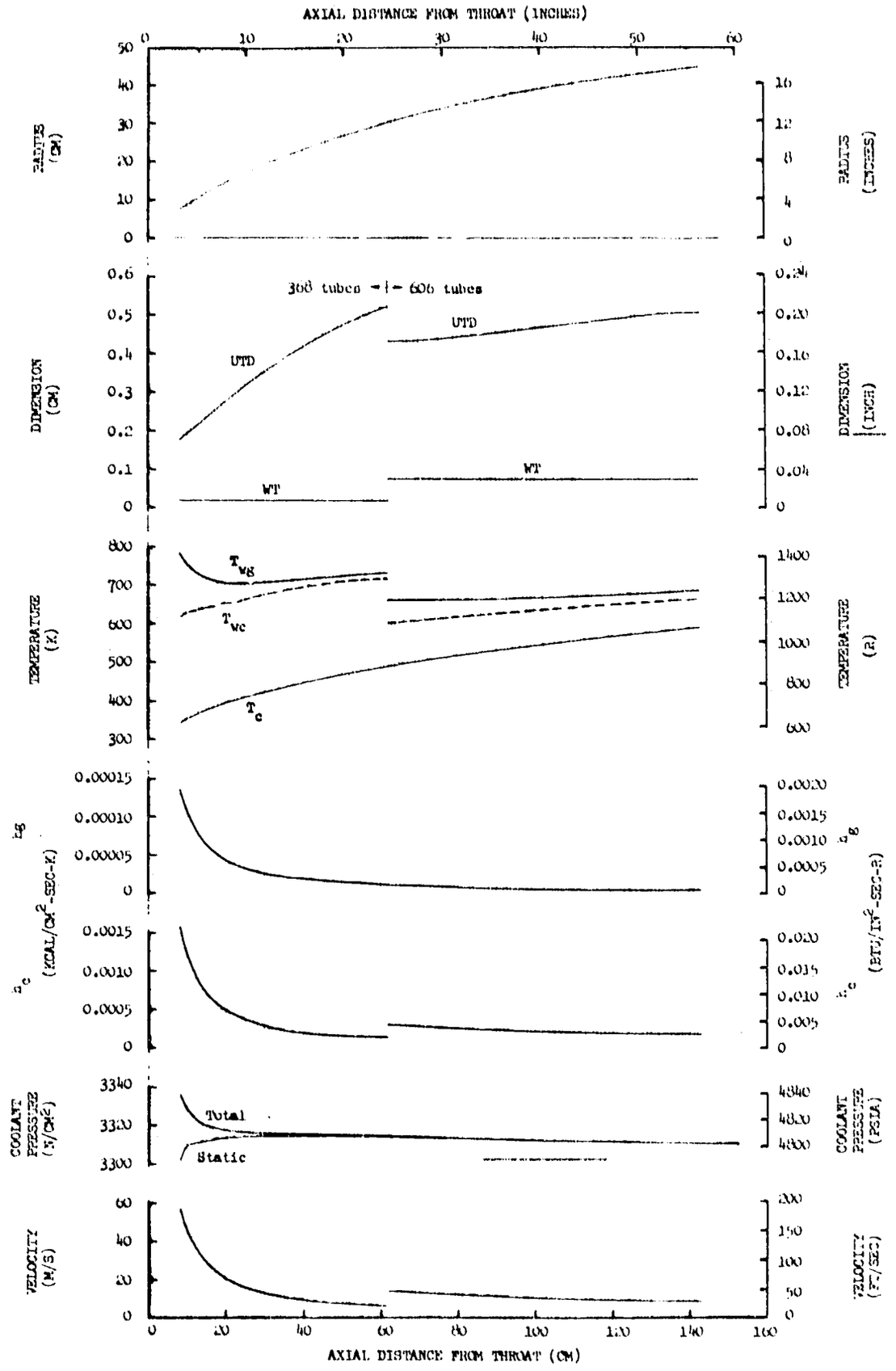

Figure 76. Parameters for the O_2/CH_4, MR = 3.5, F = 89,000 N (20,000 lbf), Coolant P_{in}/P_c = 1.74 Nozzle at P_c = 2758 N/cm^2 (4000 psia)

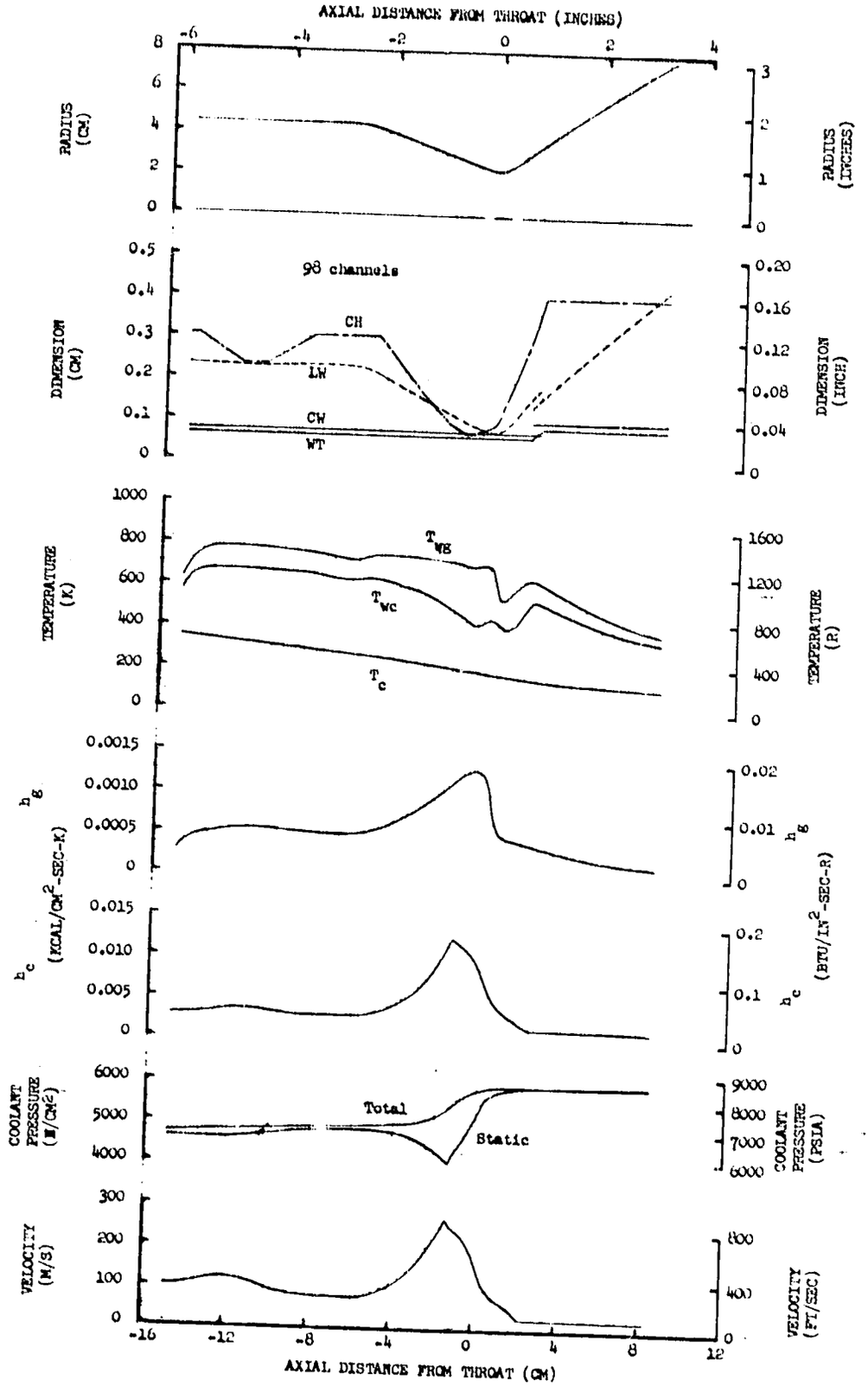

Figure 77. Parameters for the O_2/CH_4, MR = 3.5, F = 89,000 N (20,000 lbf), Coolant P_{in}/P_c = 2.15 Combustion Chamber at P_c = 2758 N/cm^2 (4000 psia)

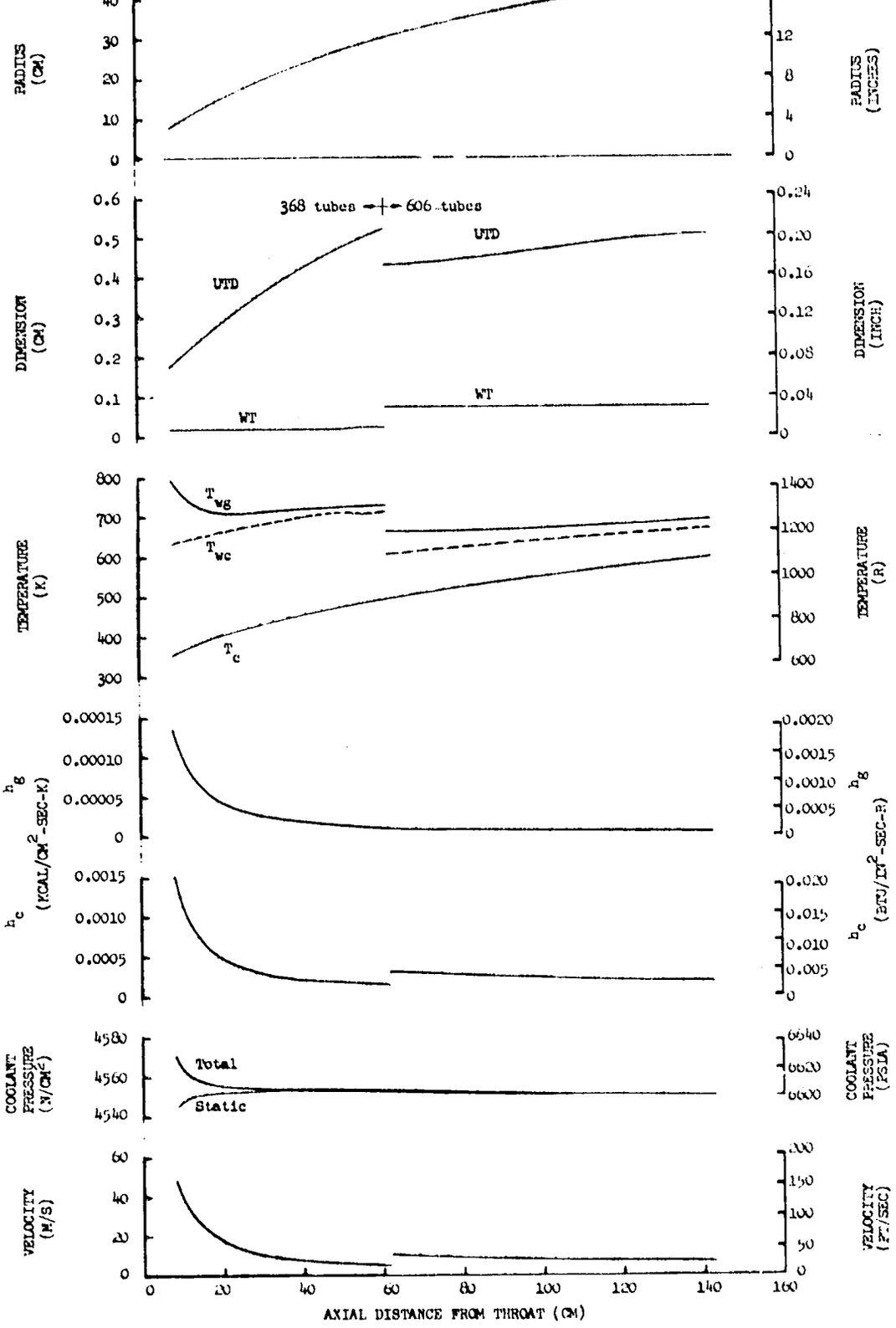

Figure 78. Parameters for the O_2/CH_4, MR = 3.5, F = 89,000 N (20,000 lbf), Coolant P_{in}/P_c = 2.15 Nozzle at P_c = 2758 N/cm^2 (4000 psia)

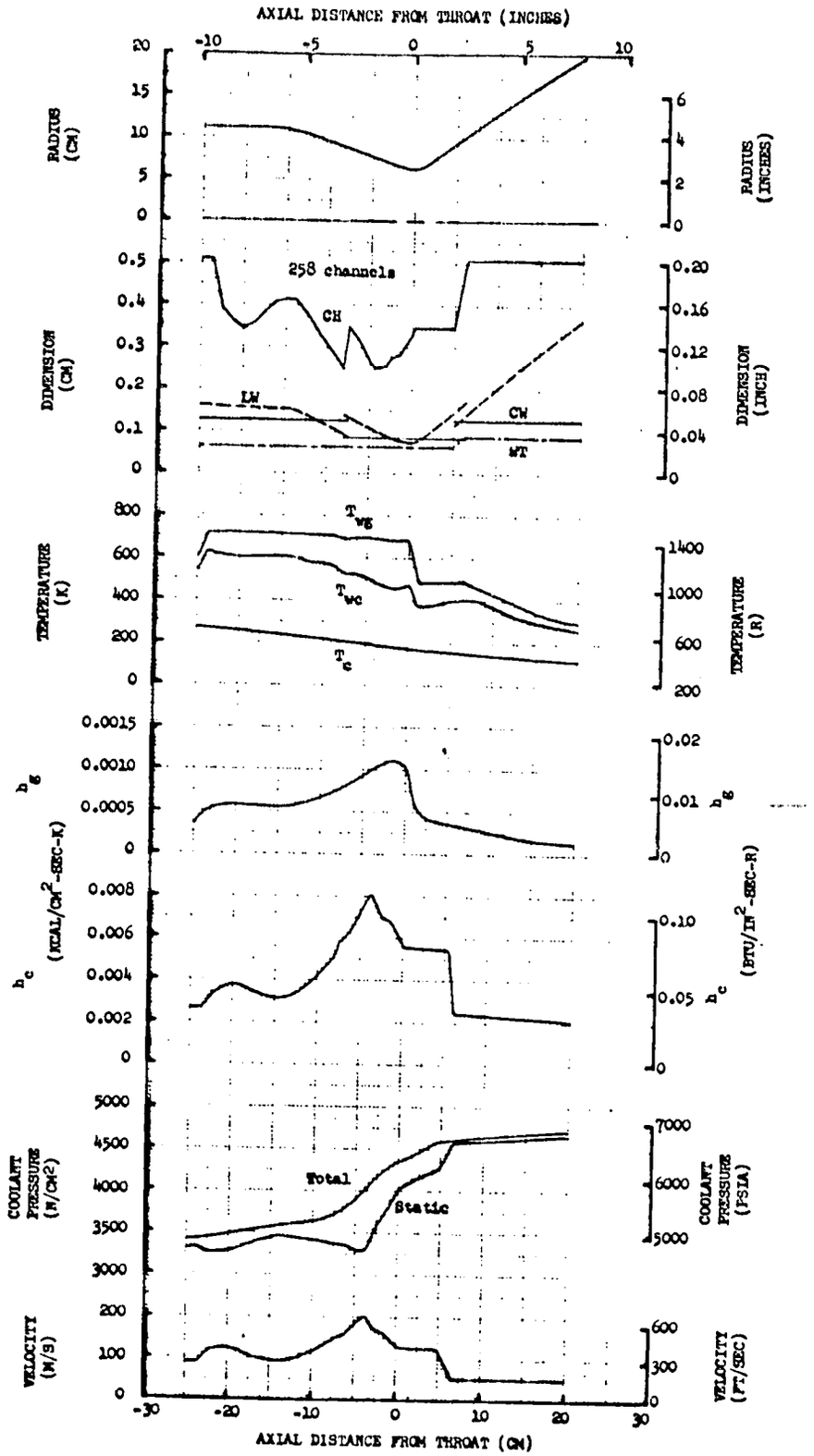

Figure 79. Parameters for the O_2/CH_4, MR = 3.5, F = 667,000 N (150,000 lbf), Coolant P_{in}/P_c = 1.8 Combustion Chamber at P_c = 2620 N/cm^2 (3800 psia)

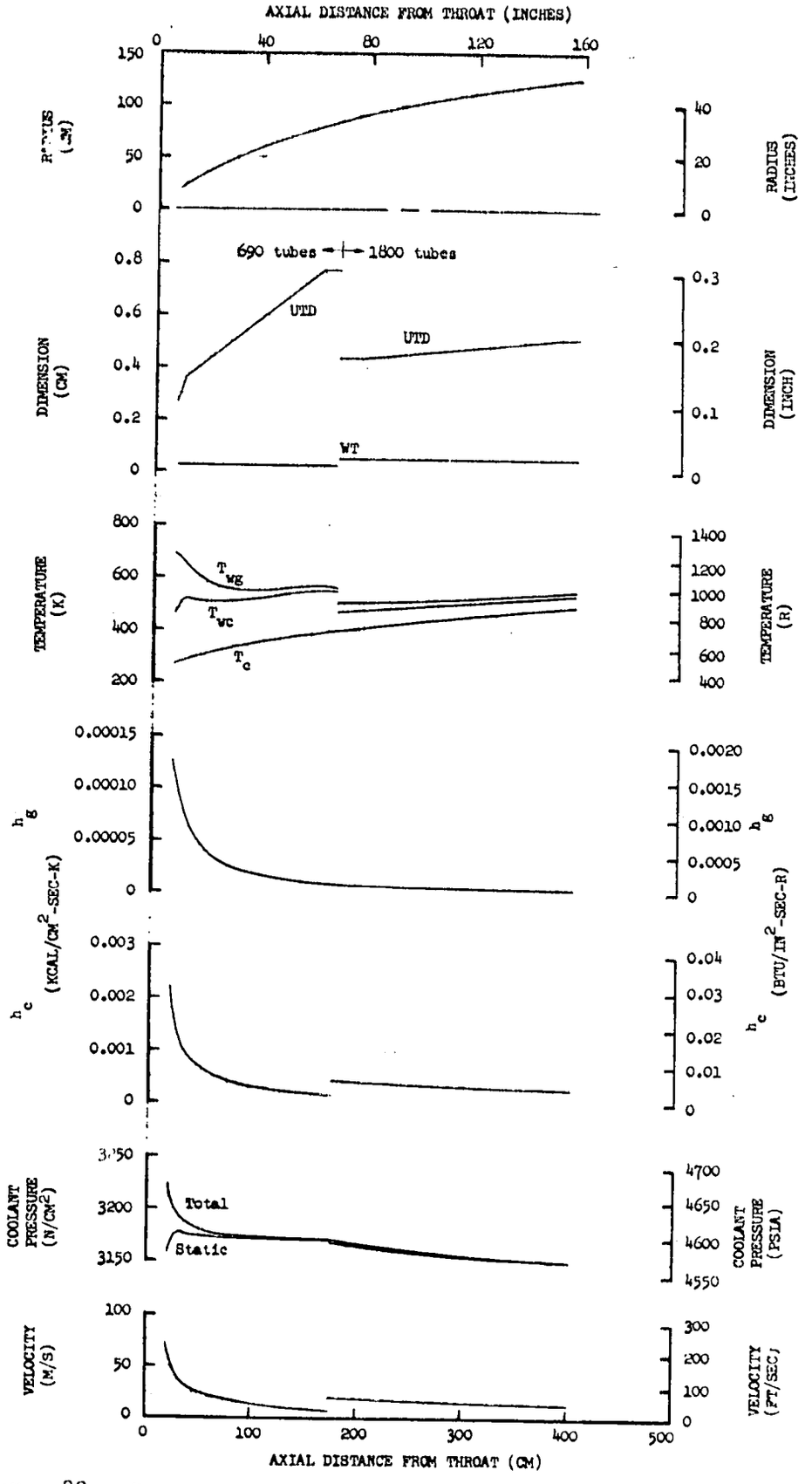

Figure 80. Parameters for the O_2/CH_4, MR = 3.5, F = 667,000 N (150,000 lbf), Coolant P_{in}/P_c = 1.8 Nozzle at P_c = 2620 N/cm^2 (3800 psia)

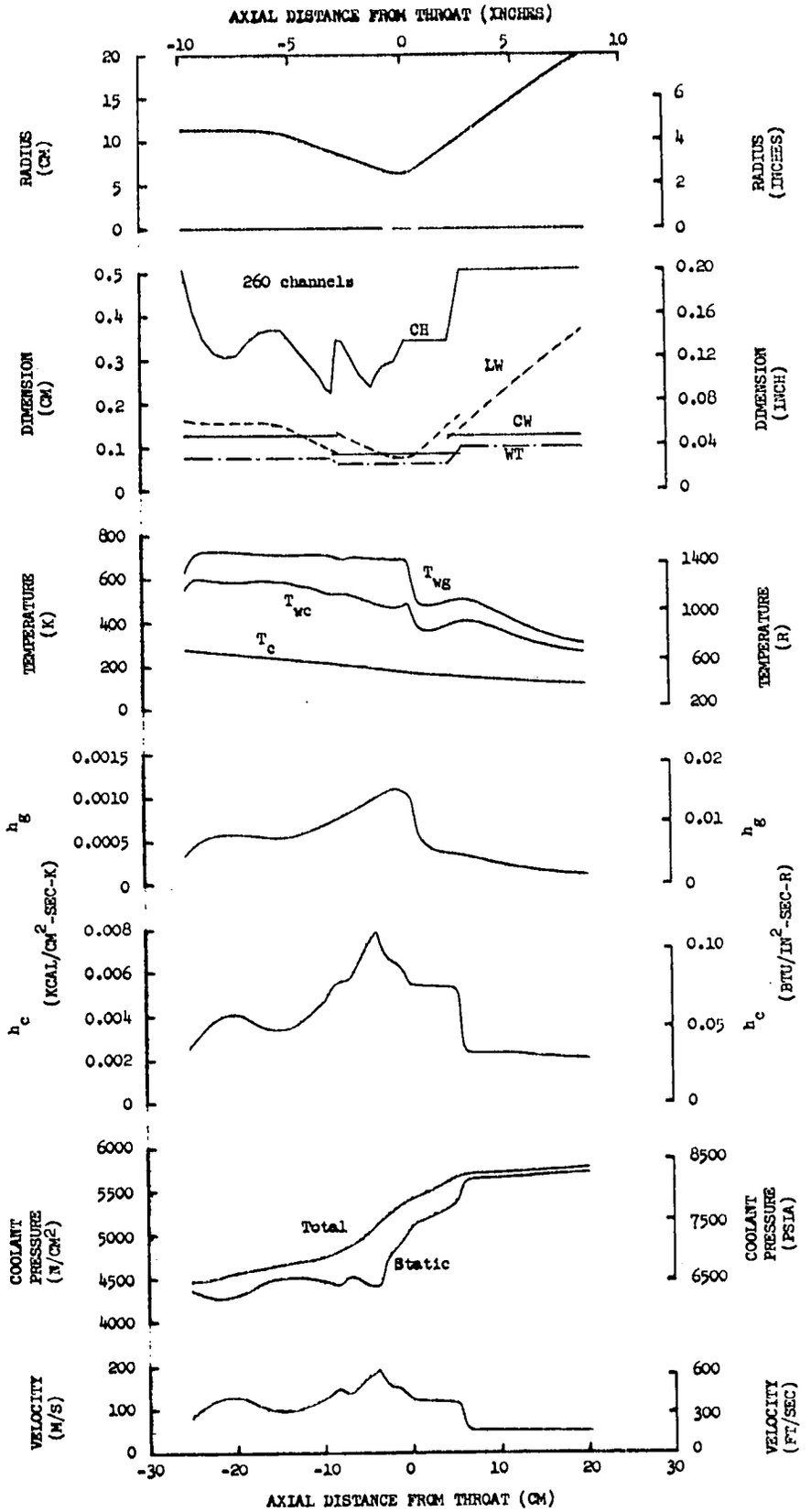

Figure 81. Parameters for the O_2/CH_4, MR = 3.5, F = 667,000 N (150,000 lbf), Coolant P_{in}/P_c = 2.25 Combustion Chamber at P_c = 2565 N/cm^2 (3720 psia)

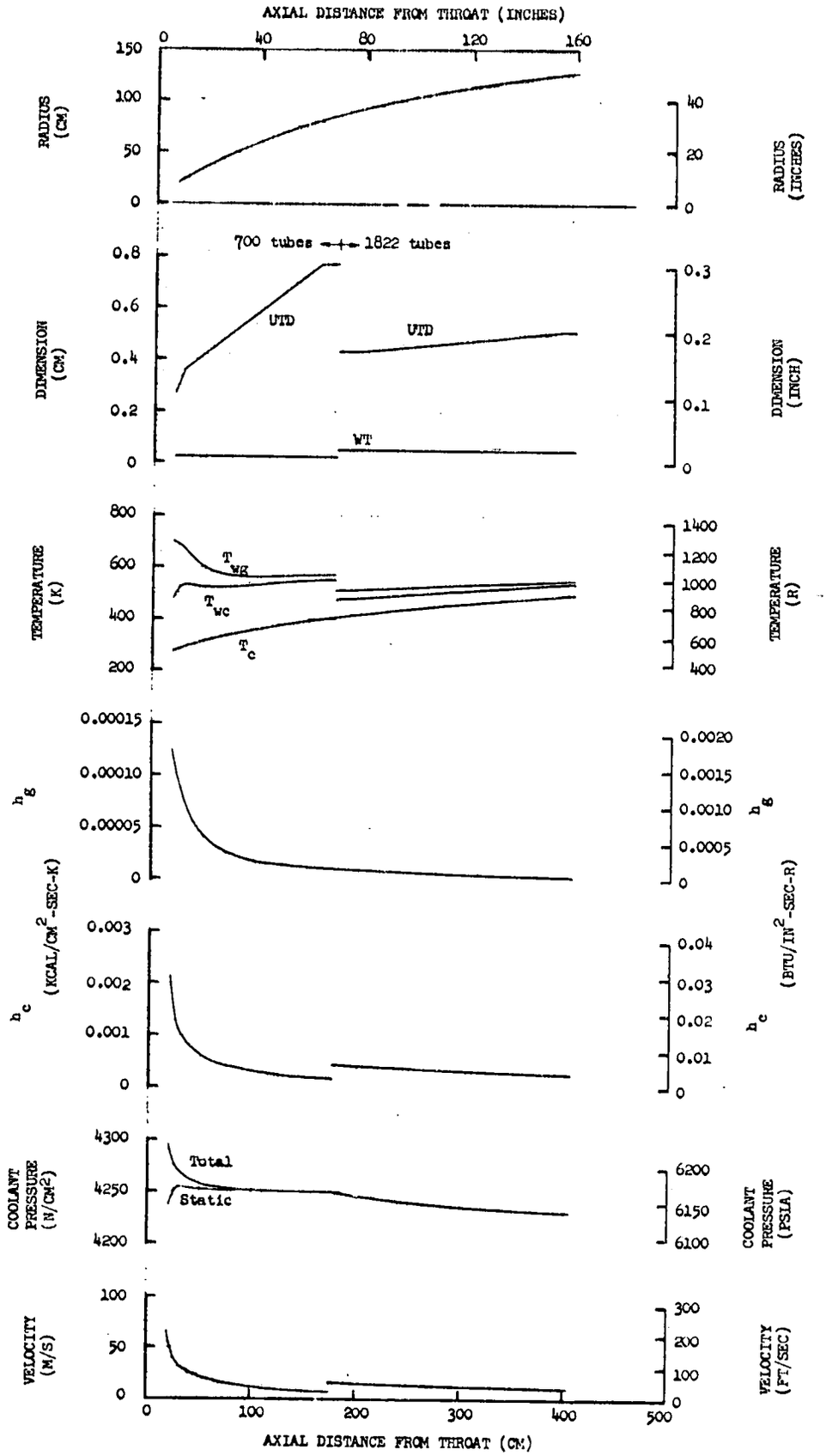

Figure 82. Parameters for the O_2/CH_4, MR = 3.5, F = 667,000 N (150,000 lbf), Coolant P_{in}/P_c = 2.25 Nozzle at P_c = 2565 N/cm^2 (3720 psia)

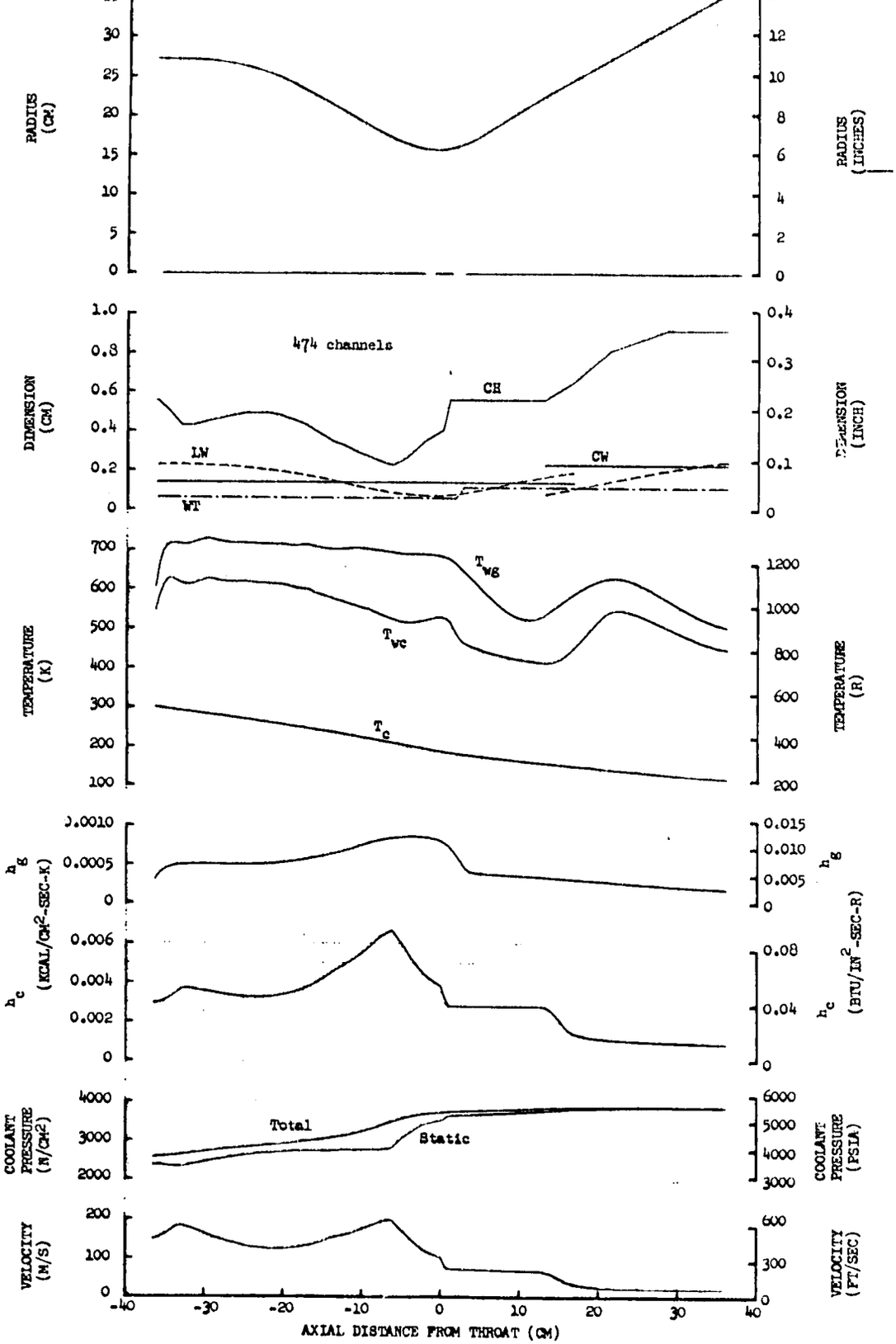

Figure 83. Parameters for the O_2/CH_4, MR = 3.5, F = 2,669,000 N (600,000 lbf), Coolant P_{in}/P_c = 1.8 Combustion Chamber at P_c = 2144 N/cm^2 (3110 psia)

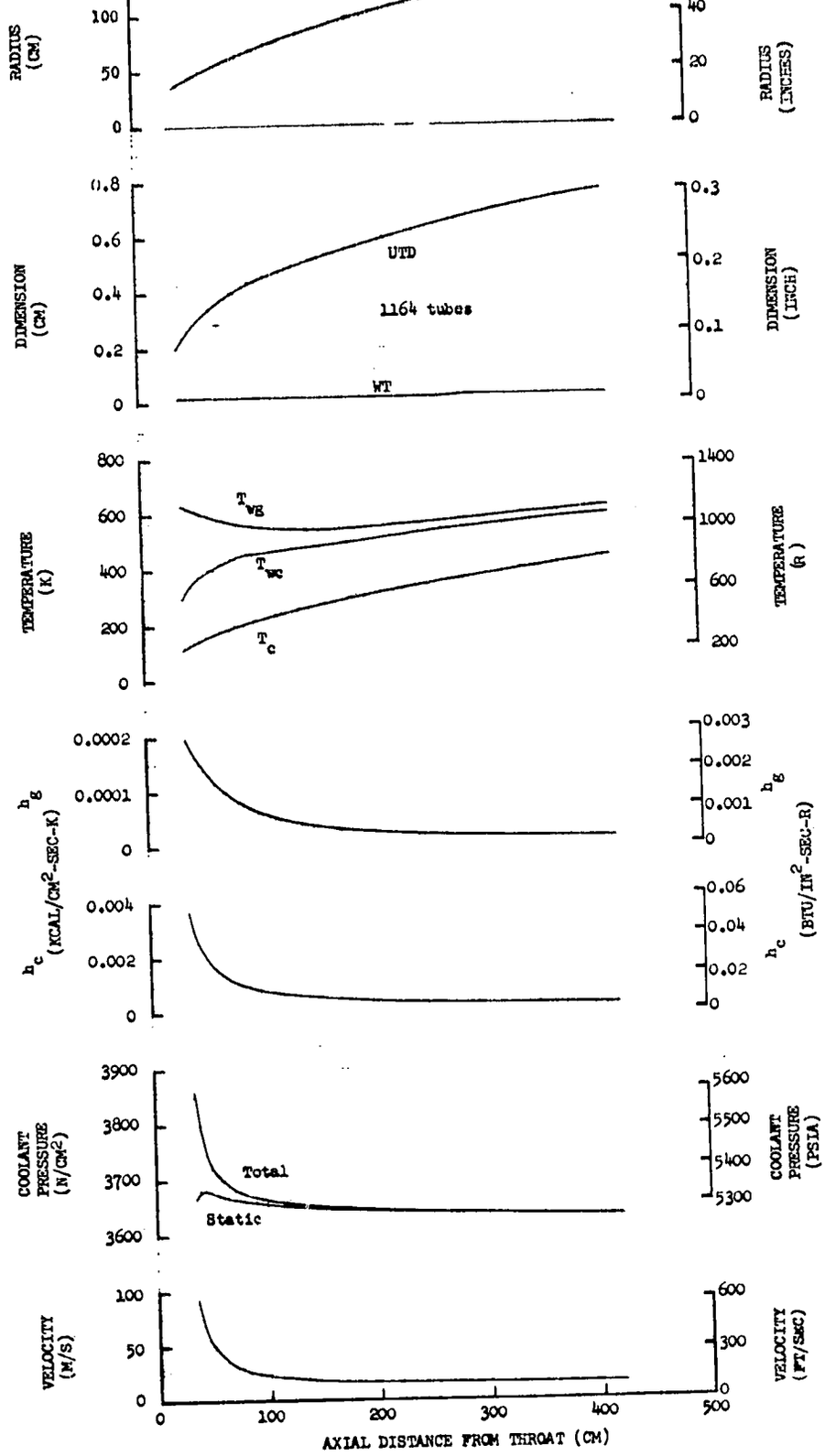

Figure 84. Parameters for the O_2/CH_4, MR = 3.5, F = 2,669,000 N (600,000 lbf), Coolant P_{in}/P_c = 1.8 Nozzle at P_c = 2144 N/cm^2 (3110 psia)

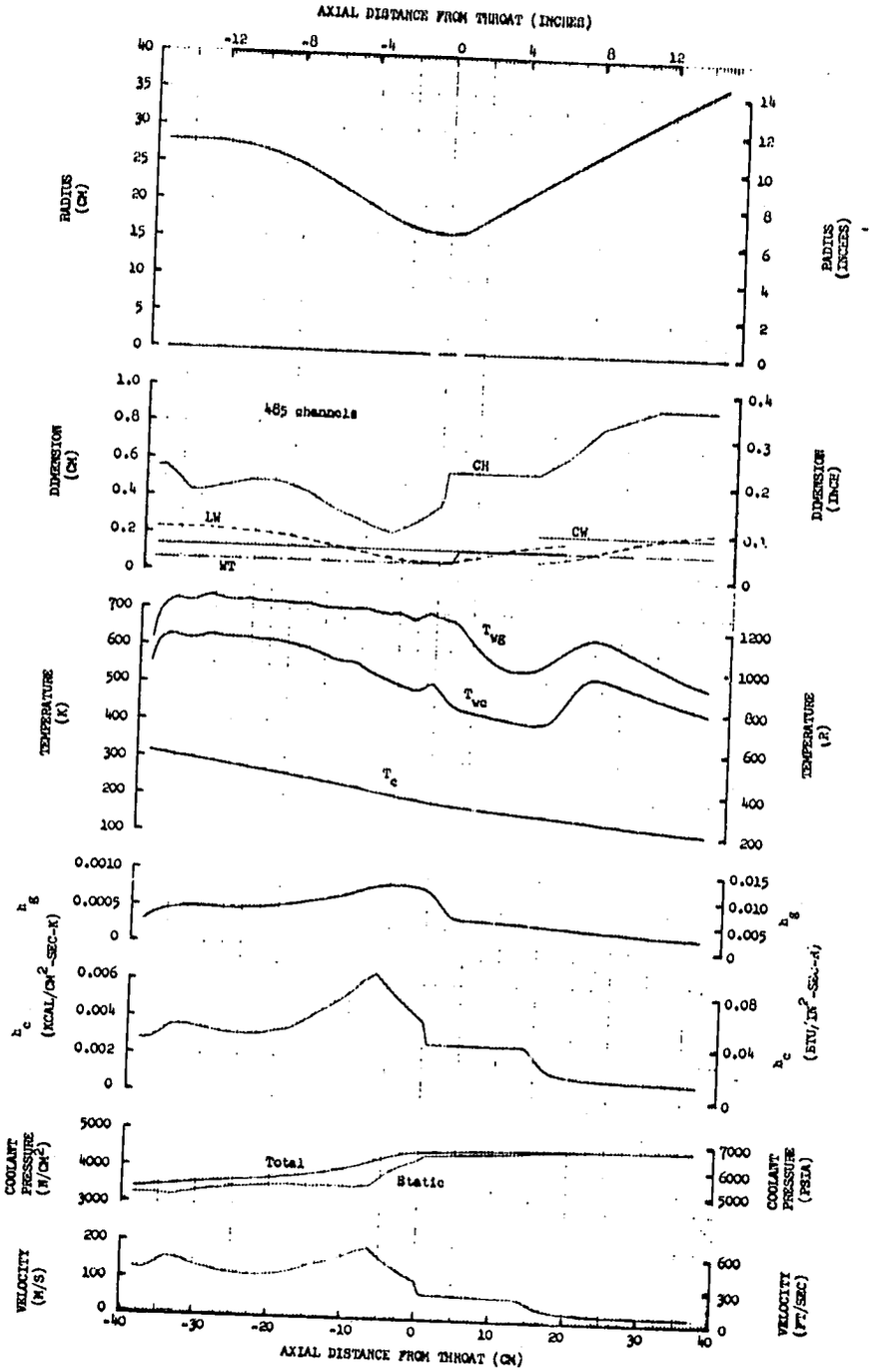

Figure 85. Parameters for the O_2/CH_4, MR = 3.5, F = 2,669,000 N (600,000 lbf), Coolant P_{in}/P_c = 2.25 Combustion Chamber at P_c = 2068 N/cm^2 (3000 psia)

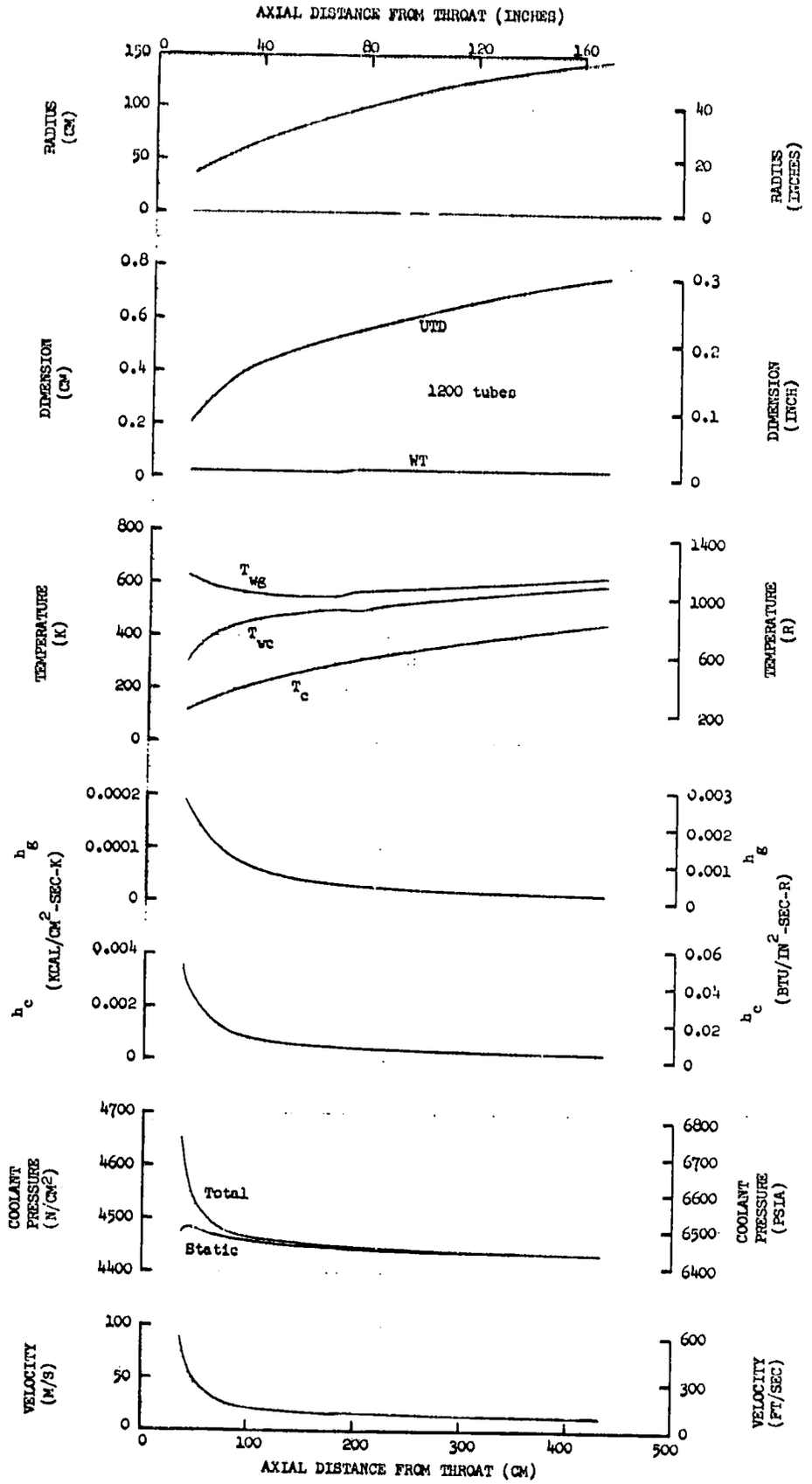

Figure 86. Parameters for the O_2/CH_4, MR = 3.5, F = 2,669,000 N (600,000 lbf), Coolant P_{in}/P_c = 2.25 Nozzle at P_c = 2068 N/cm^2 (3000 psia)

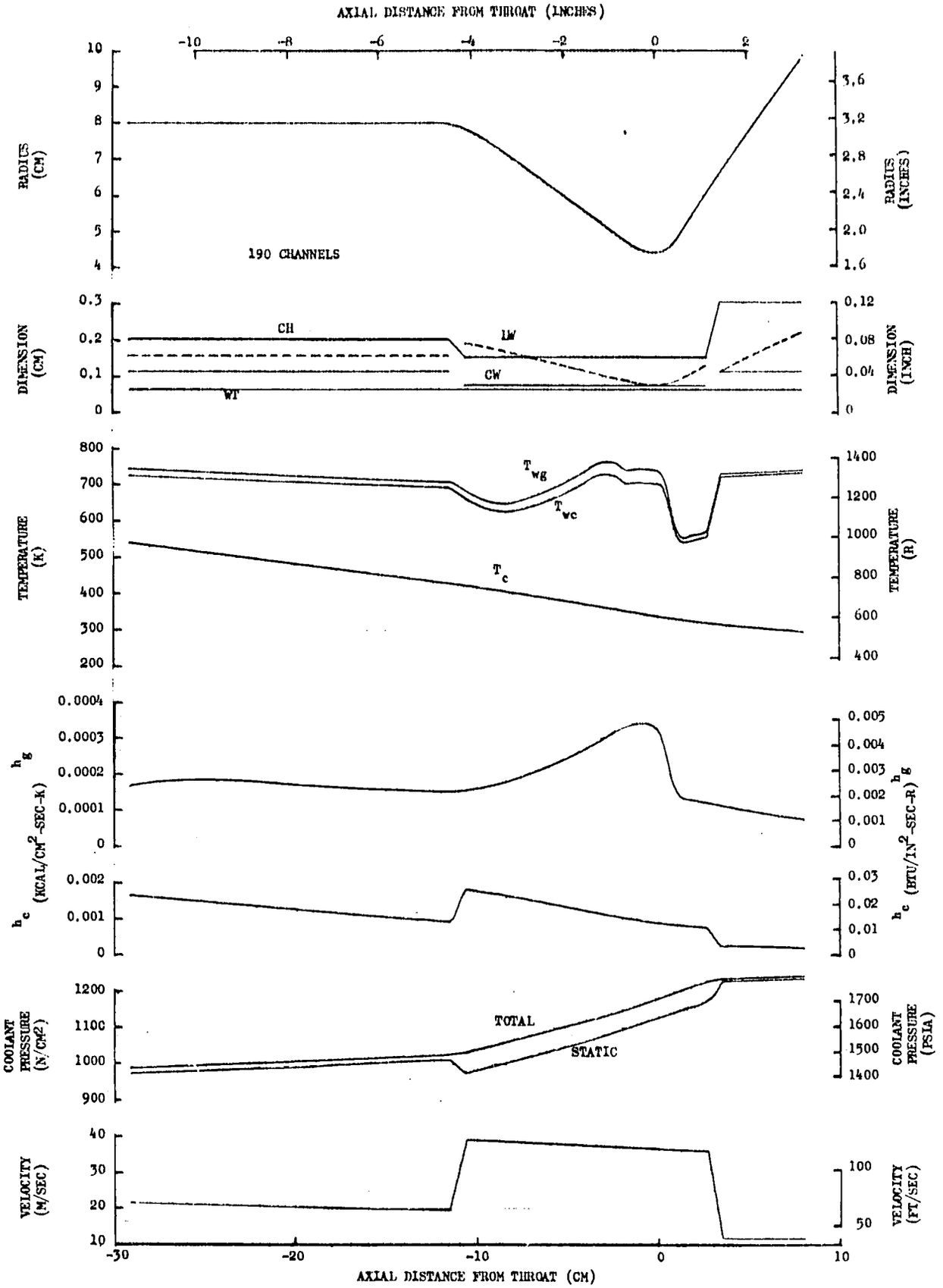

Figure 87. Parameters for the O_2/RP-1, MR = 2.8, F = 89,000 N (20,000 lbf), Coolant P_{in}/P_c = 1.8, Combustion Chamber at P_c = 689 N/cm^2 (1000 psia) (Reference Case Only)

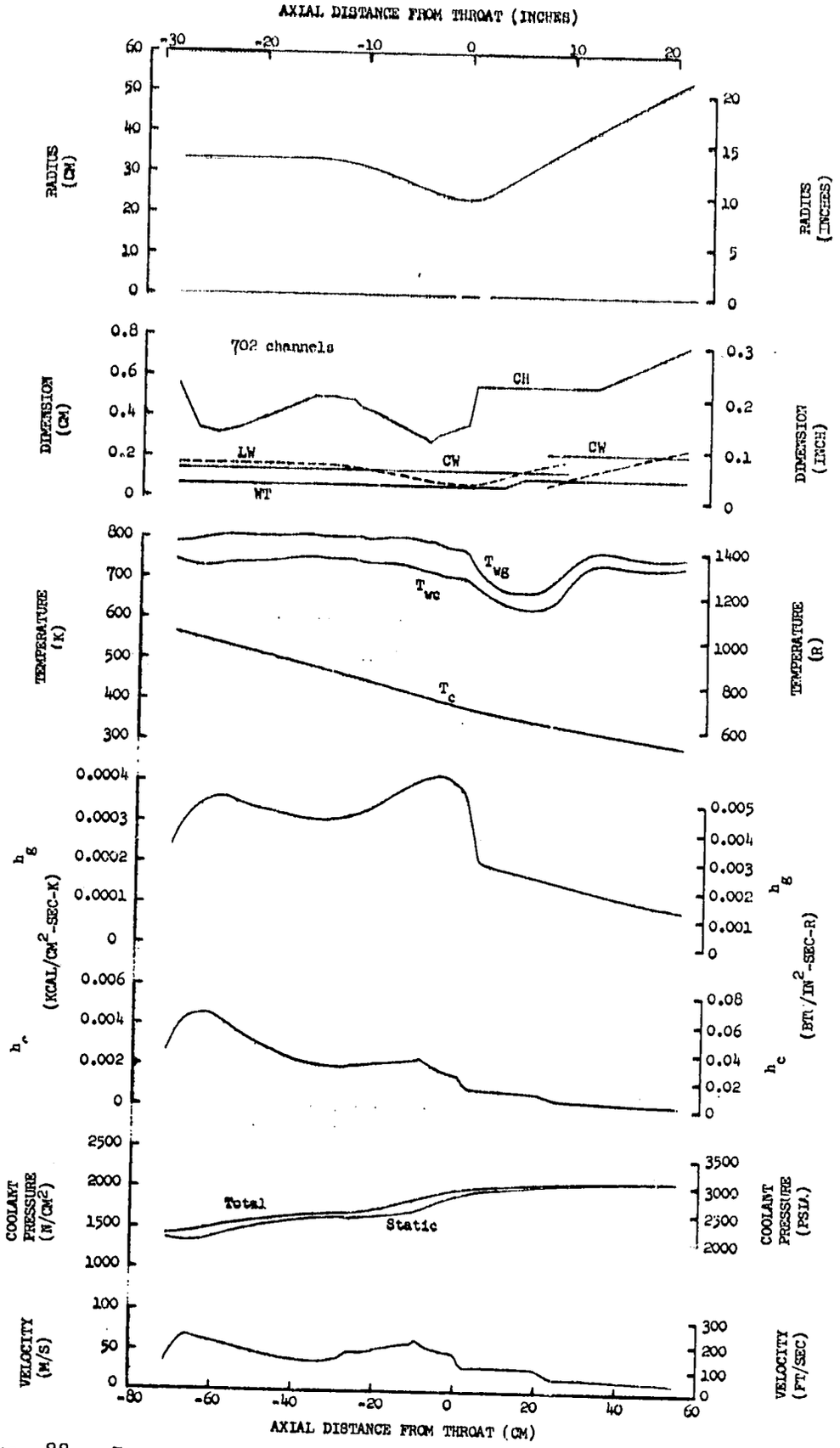

Figure 88. Parameters for the O_2/RP-1, MR = 2.8, F = 2,669,000 N (600,000 lbf), Coolant P_{in}/P_c = 1.8 Combustion Chamber at P_c = 1179 N/cm2 (1710 psia)

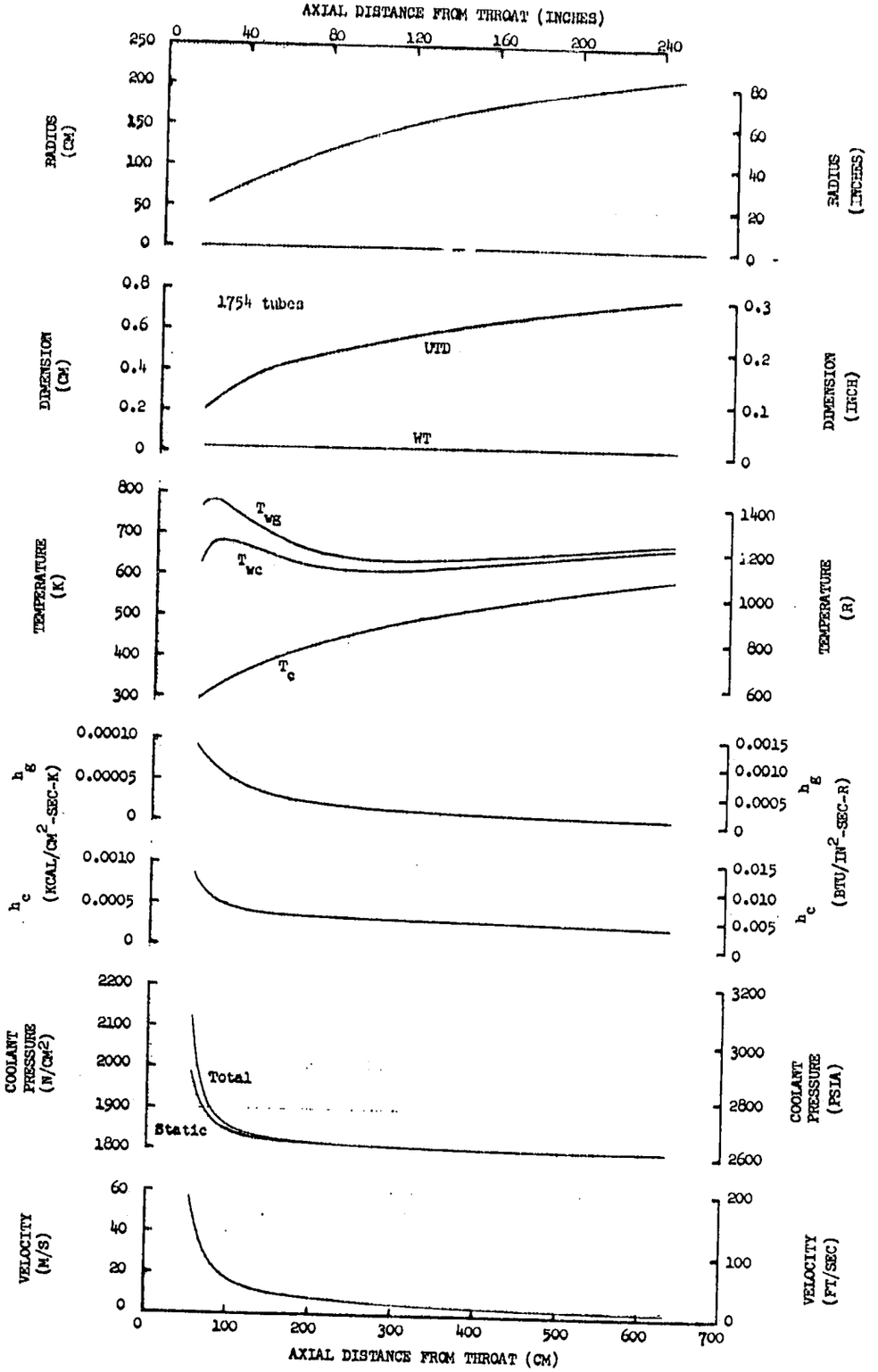

Figure 89. Parameters for the O$_2$/RP-1, MR = 2.8, F = 2,669,000 N (600,000 lbf), Coolant P_{in}/P_c = 1.8 Nozzle at P_c = 1179 N/cm^2 (1710 psia)

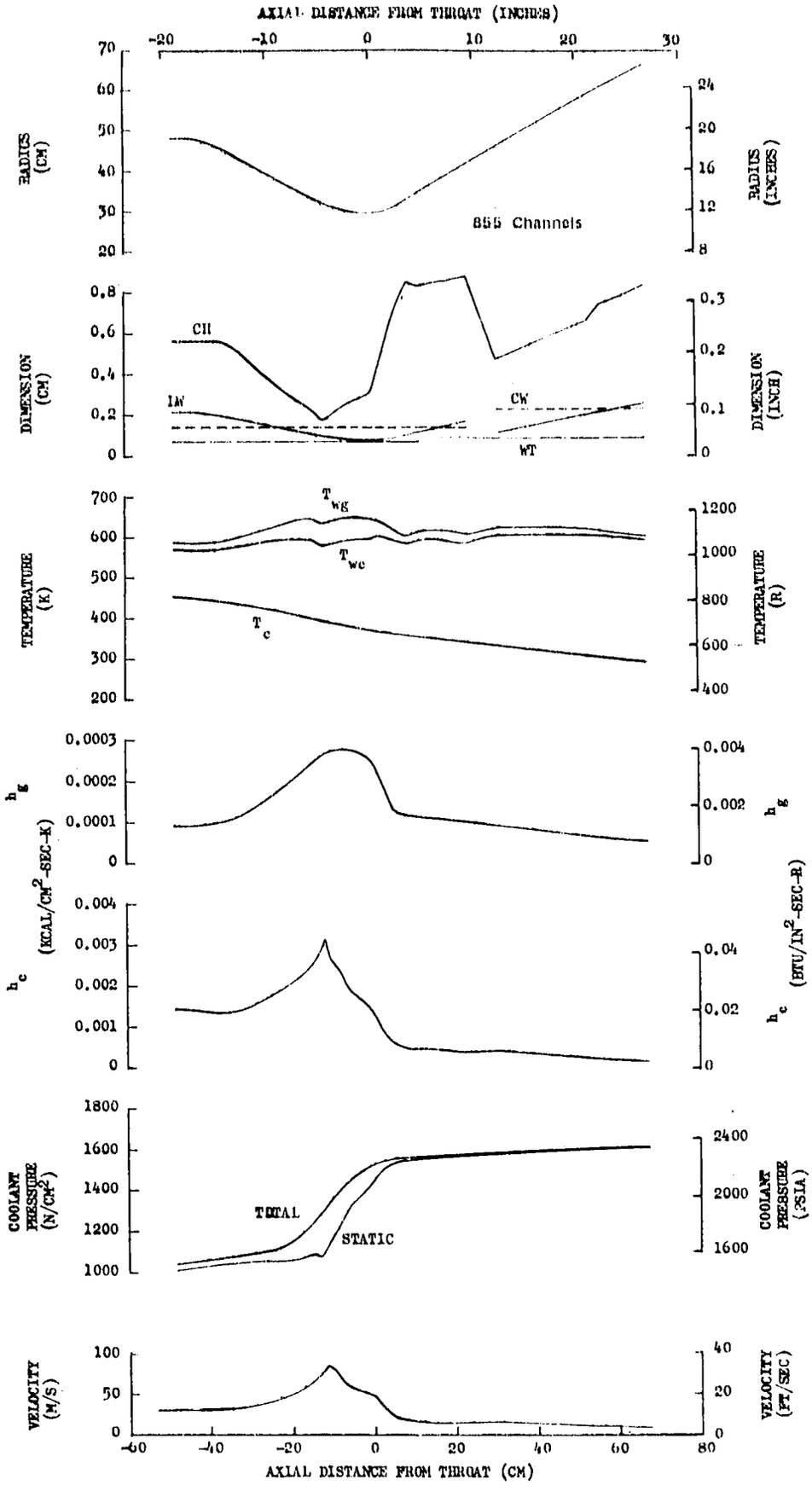

Figure 90. Parameters for the O_2/RP-1, MR = 2.8, F = 2,669,000 N (600,000 lbf), Coolant P_{in}/P_c = 1.8, Combustion Chamber at P_c = 896 N/cm^2 (1300 psia) Short Chamber (Unenhanced)

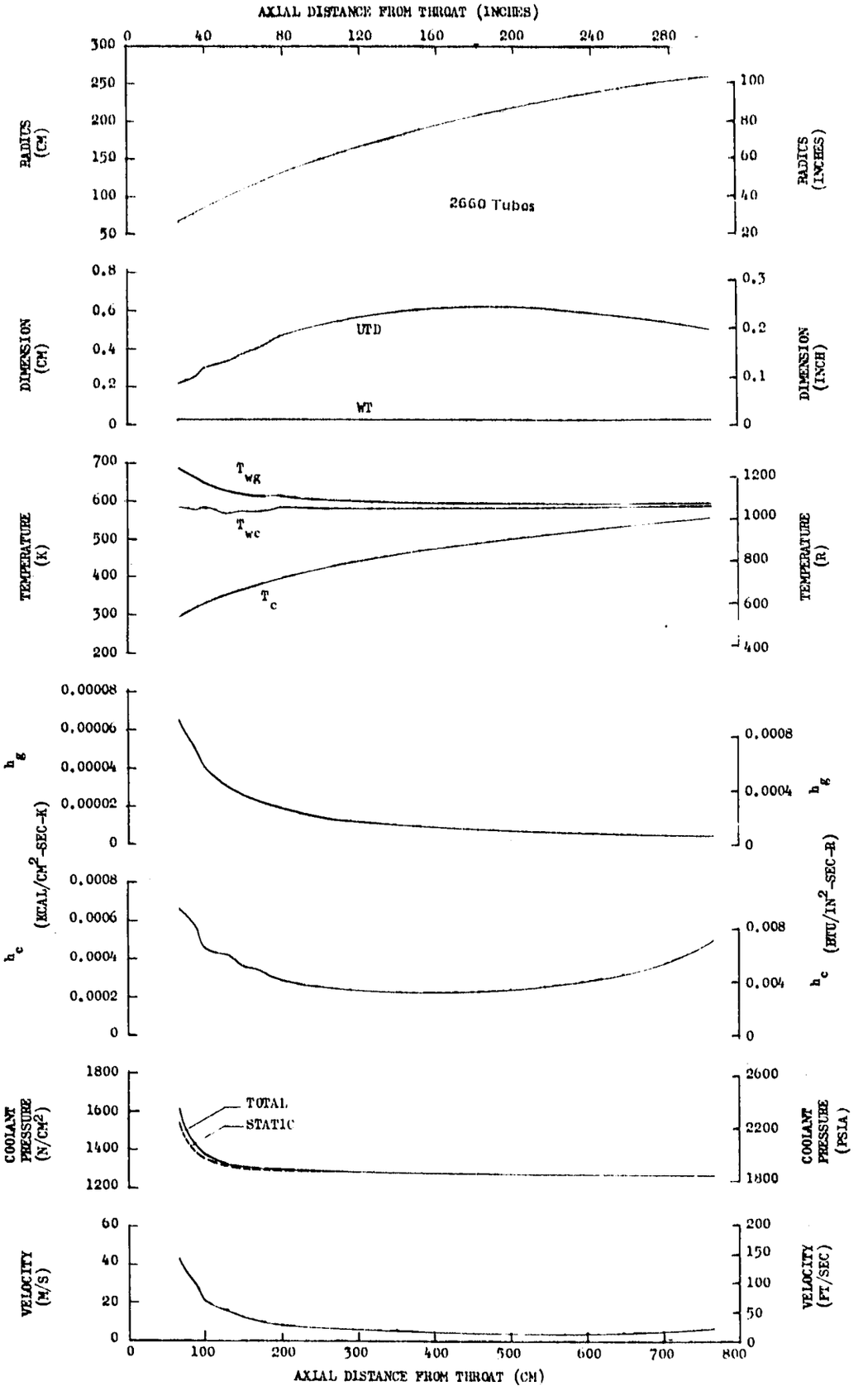

Figure 91. Parameters for the O_2/RP-1, MR = 2.8, F = 2,669,000 N (600,000 lbf), Coolant P_{in}/P_c = 1.8, Nozzle at P_c = 896 N/cm^2 (1300 psia), Short Chamber (Unenhanced)

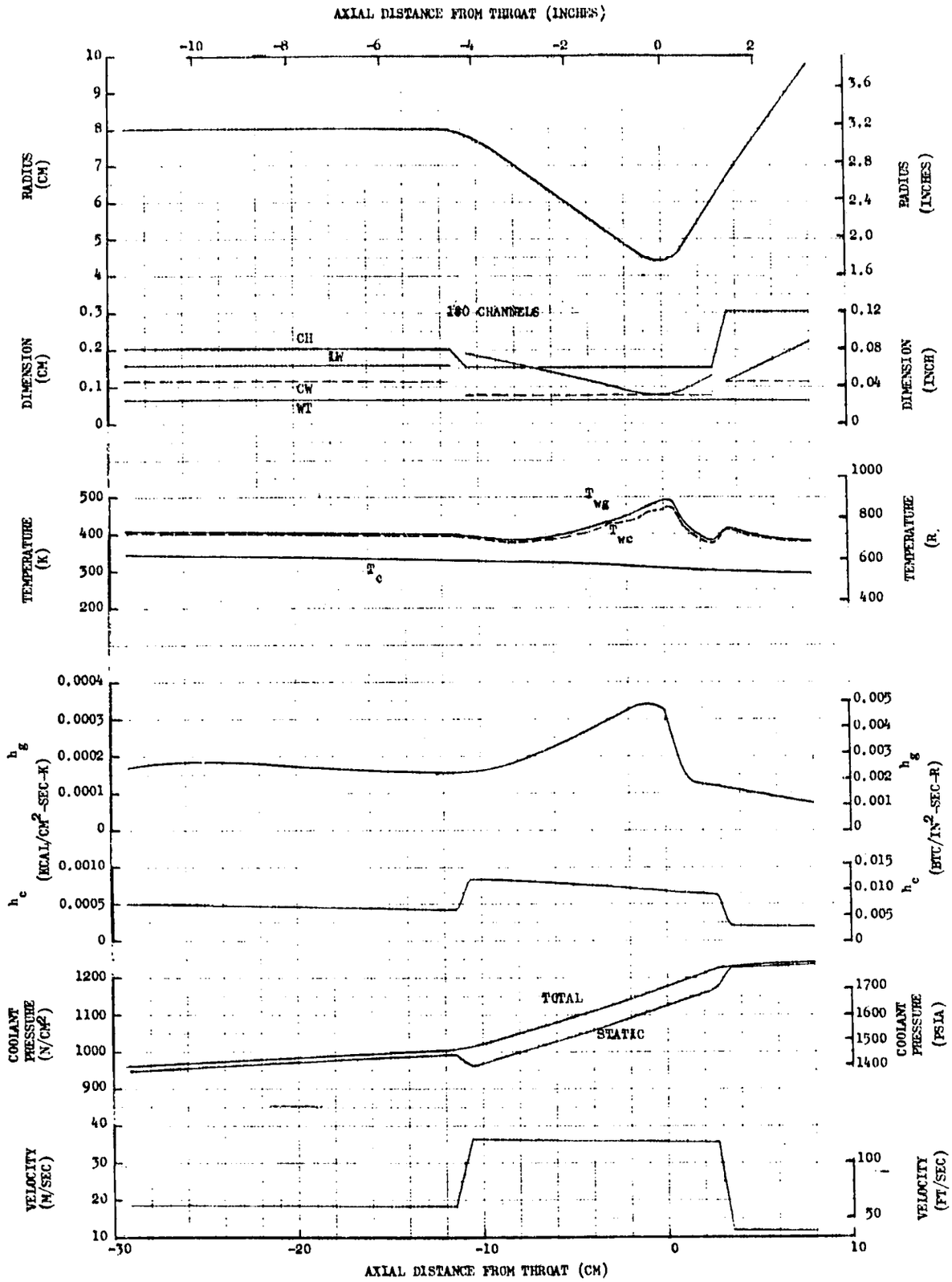

Figure 92. Parameters for the O_2/RP-1, MR = 2.8, F = 89,000 N (20,000 lbf) Coolant P_{in}/P_c = 1.8, Carbon-lined Combustion Chamber at P_c = 689 N/cm^2 (1000 psia) (Reference Case Only)

APPENDIX D

GRAPHIC PRESENTATION OF COMBUSTION CHAMBER AND NOZZLE DESIGNS FOR ENHANCED THERMAL BARRIERS AND SENSITIVITY STUDIES

The detailed combustion chamber and nozzle design analyses are presented in this appendix. Graphic presentations describe the operating parameters, coolant passage geometry, hot-gas wall geometry, and heat transfer characteristics.

The combustion chamber and nozzle designs are presented in the sequence noted in the Enhanced Designs and Sensitivity Studies section in the main body of the report.

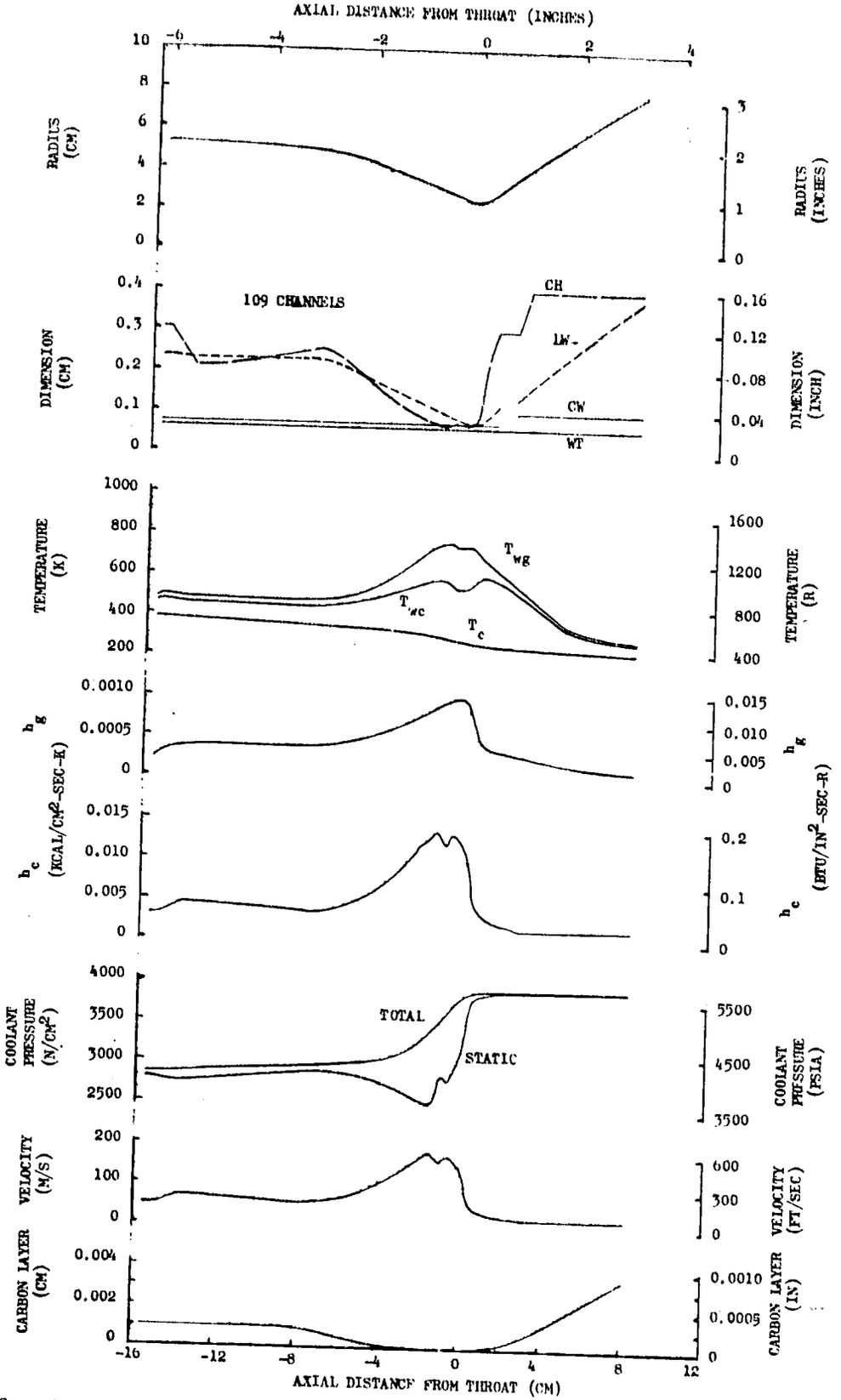

Figure 93. Parameters for the O_2/C_3H_8, MR = 3.1, F = 89,000 (20,000 lbf), Coolant P_{in}/P_c = 1.8, Combustion Chamber at P_{c-} = 2172 N/cm^2 (3150 psia) (Carbon Layer Cooling Enhancement on Combustion Chamber)

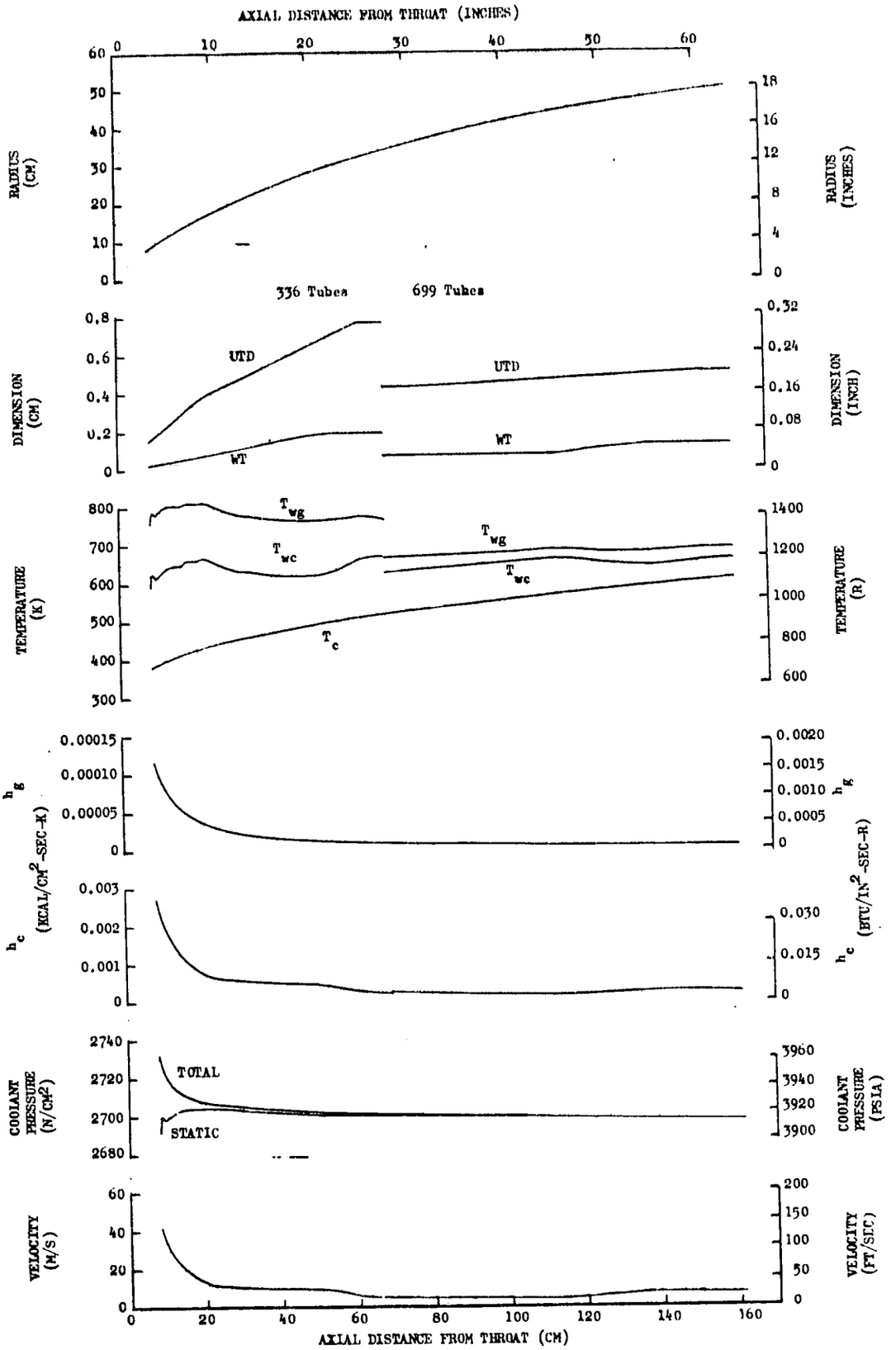

Figure 94. Parameters for the O_2/C_3H_8, MR = 3.1, F = 89,000 (20,000 lbf), Coolant P_{in}/P_c = 1.8, Combustion Nozzle at P_c = 2172 N/cm^2 (3150 psia) (For Carbon Layer Enhanced Combustion Chamber)

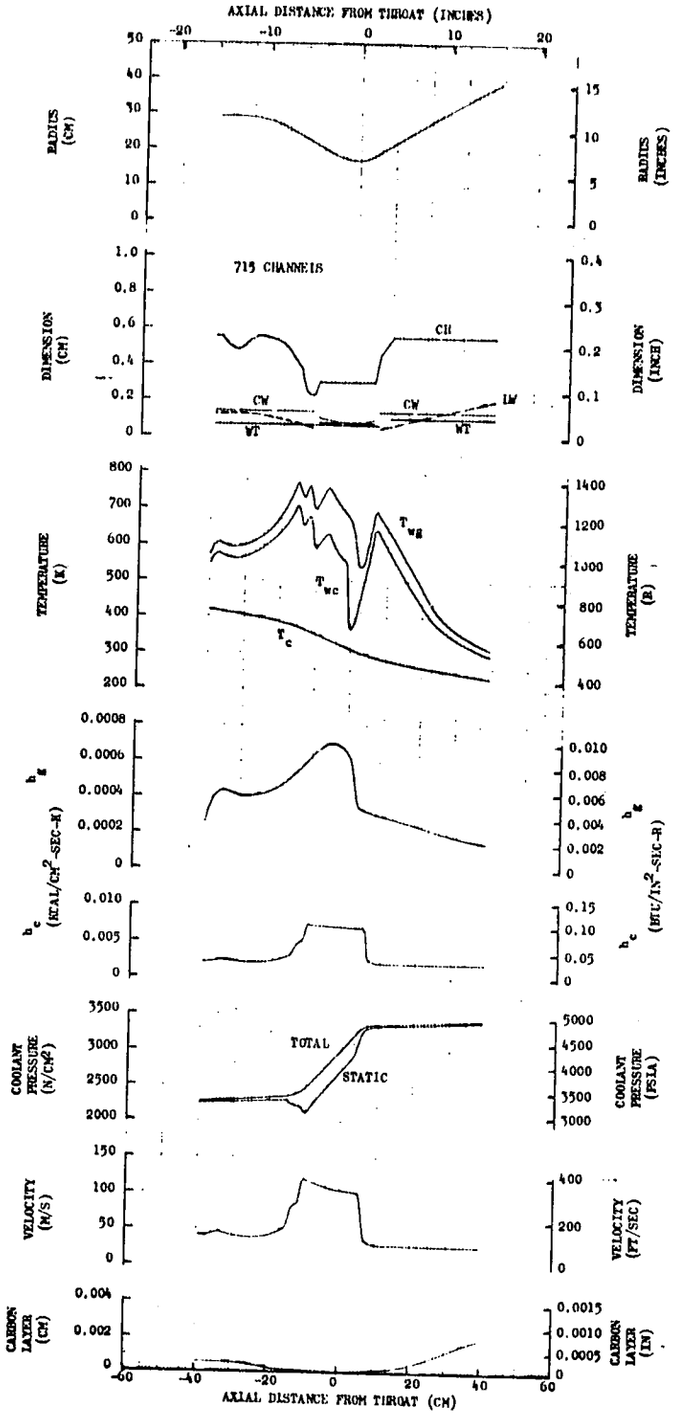

Figure 95. Parameters for the O_2/C_3H_8, MR = 3.1, F = 2,669,000 N (600,000 lbf), Coolant P_{in}/P_c = 1.8, Combustion Chamber at P_c = 1896 N/cm^2 (2750 psia) (Carbon Layer Cooling Enhancement on Combustion Chamber)

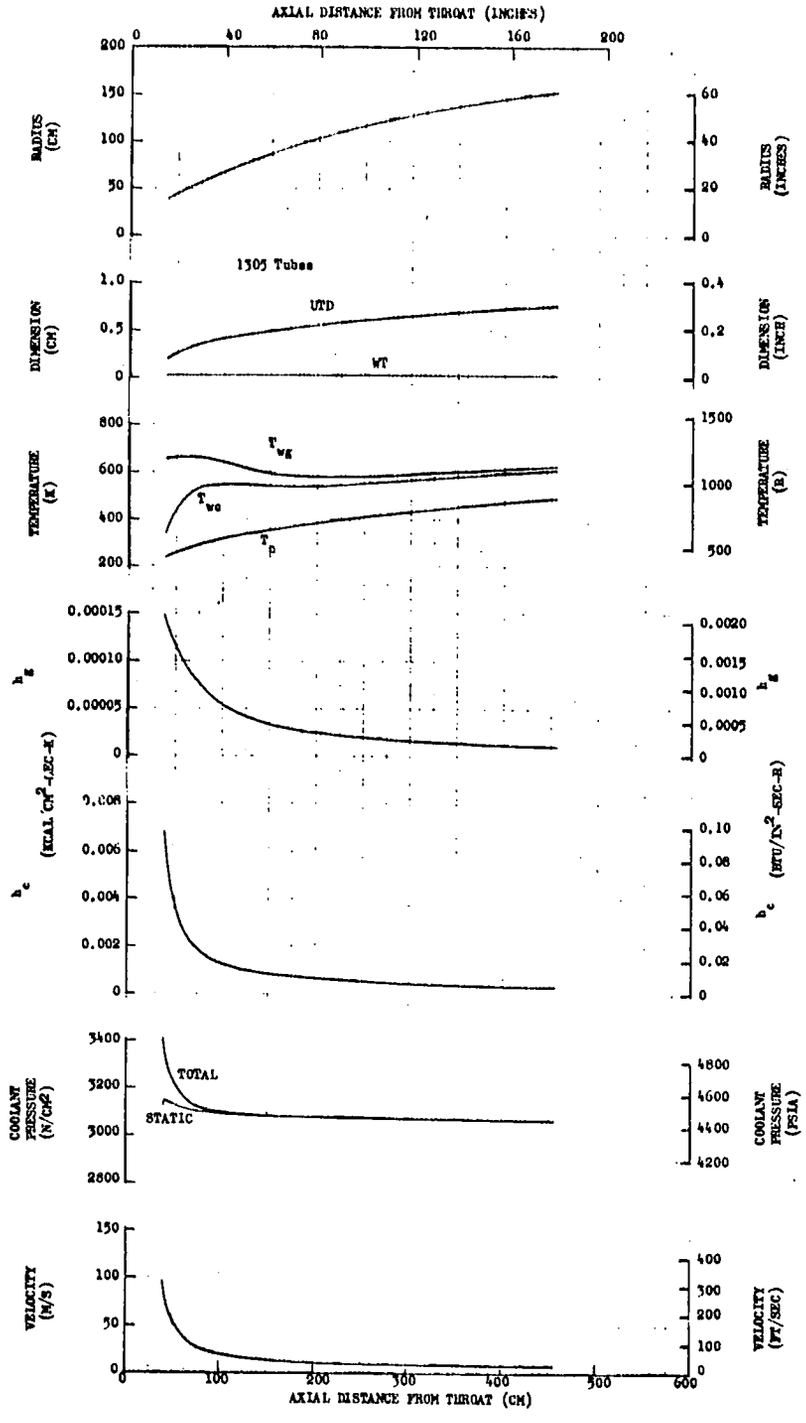

Figure 96. Parameters for the O_2/C_3H_8, MR = 3.1, F = 2,669,000 N (600,000 lbf), Coolant P_{in}/P_c = 1.8, Combustion Nozzle at P_c = 1896 N/cm^2 (2750 psia) (For Carbon Layer Enhanced Combustion Chamber)

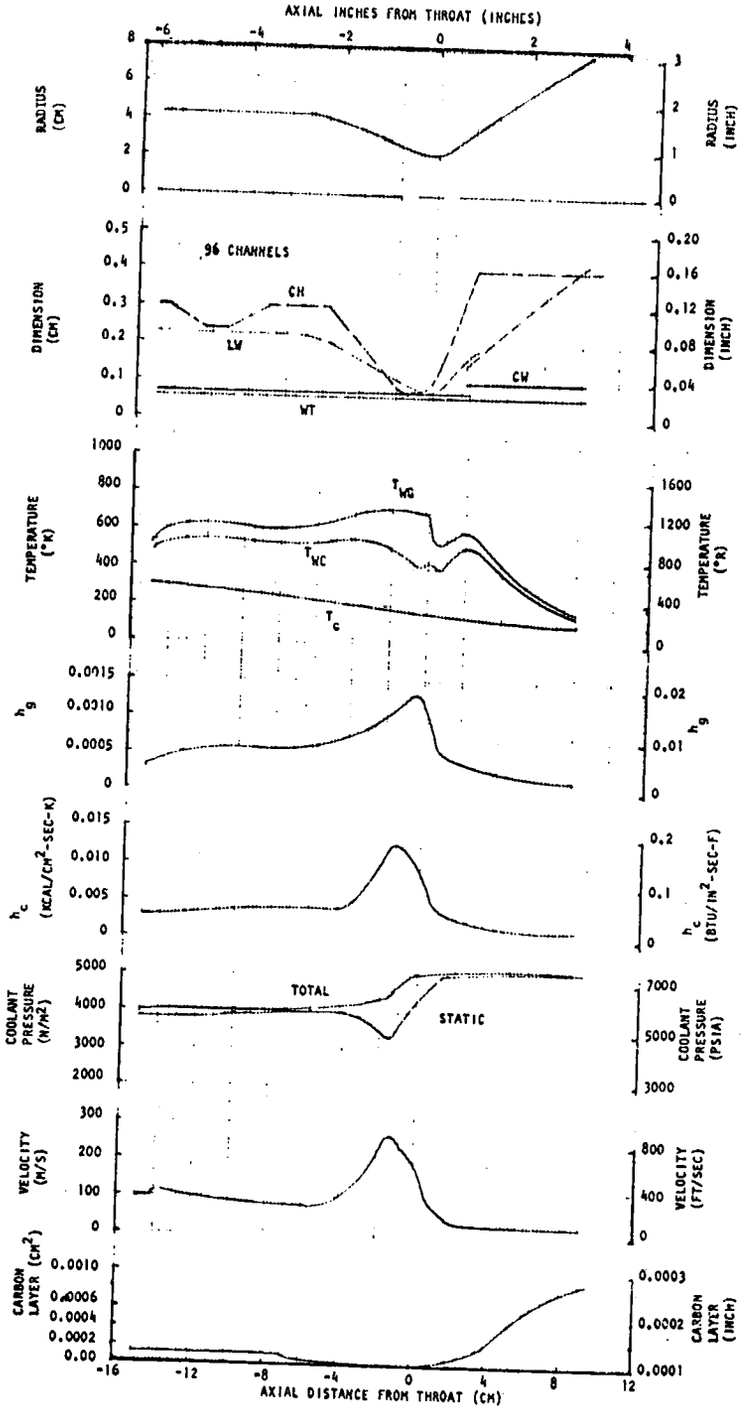

Figure 97. Parameters for the O_2/CH_4, MR = 3.5, F = 89,000 N (20,000 lbf), Coolant P_{in}/P_c = 1.8, Combustion Chamber at P_c = 2861 N/cm^2 (4150 psia) (Carbon Layer Cooling Enhancement on Combustion Chamber)

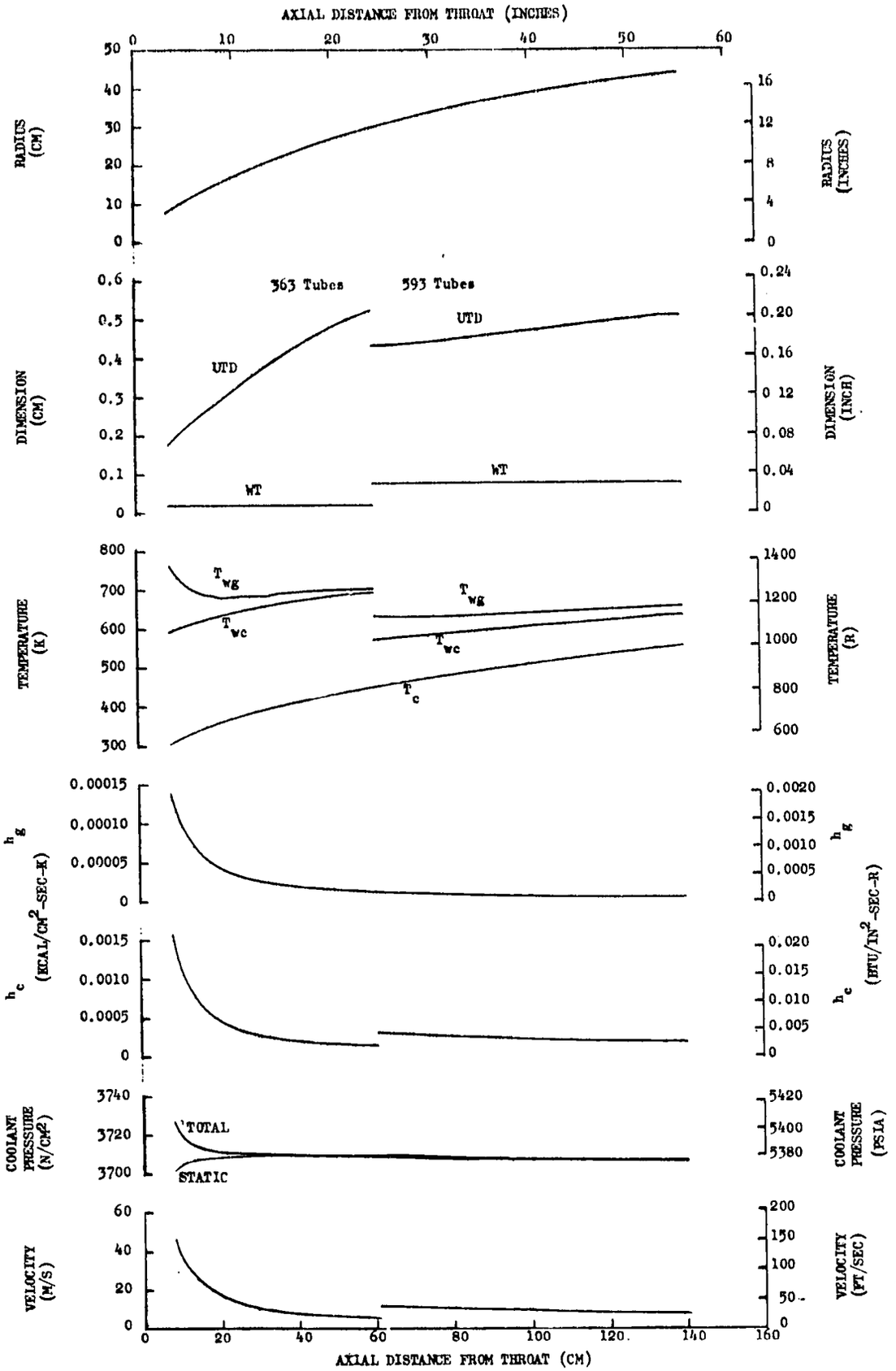

Figure 98. Parameters for the O_2/CH_4, MR = 3.5, F = 89,000 N (20,000 lbf), Coolant P_{in}/P_c = 1.8, Nozzle at 2861 N/cm^2 (4150 psia) (For Carbon Layer Enhanced Combustion Chamber)

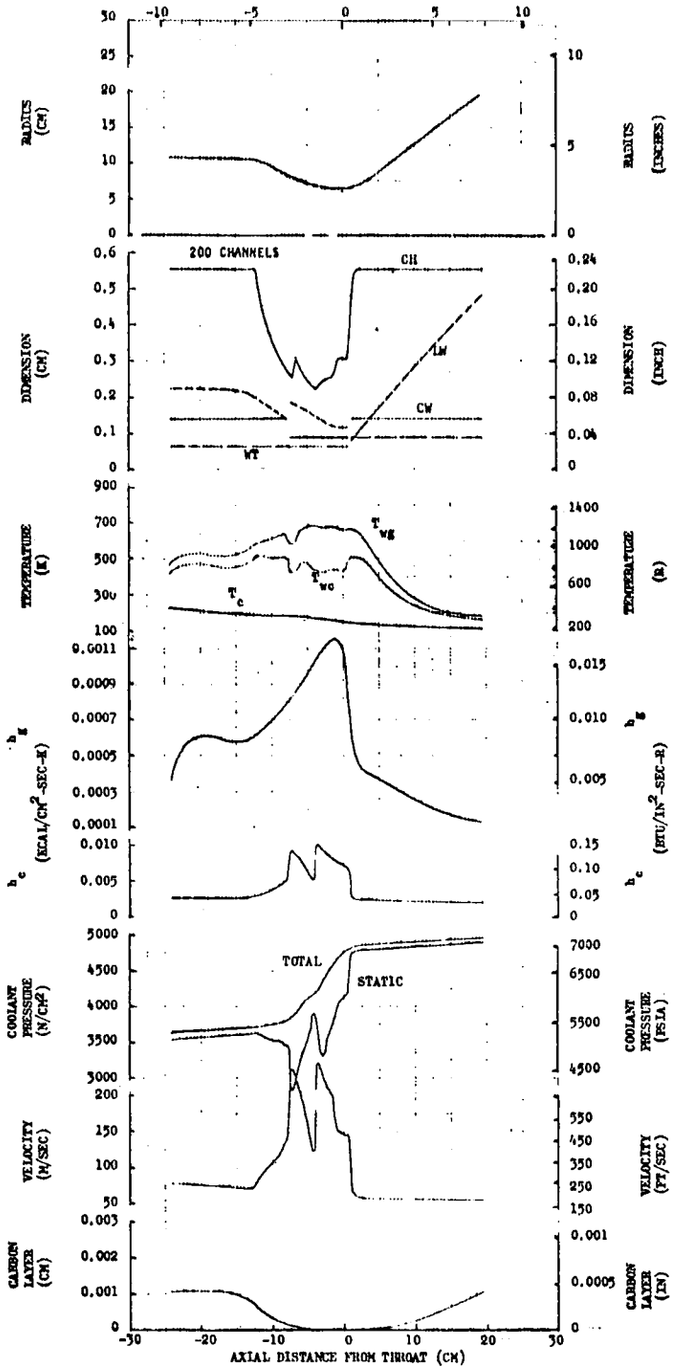

Figure 99. Parameters for the O_2/CH_4, MR = 3.5, F = 667,000 N (150,000 lbf), Coolant P_{in}/P_c = 1.8, Combustion Chamber at 2758 N/cm^2 (4000 psia) (Carbon Layer Cooling Enhancement on Combustion Chamber)

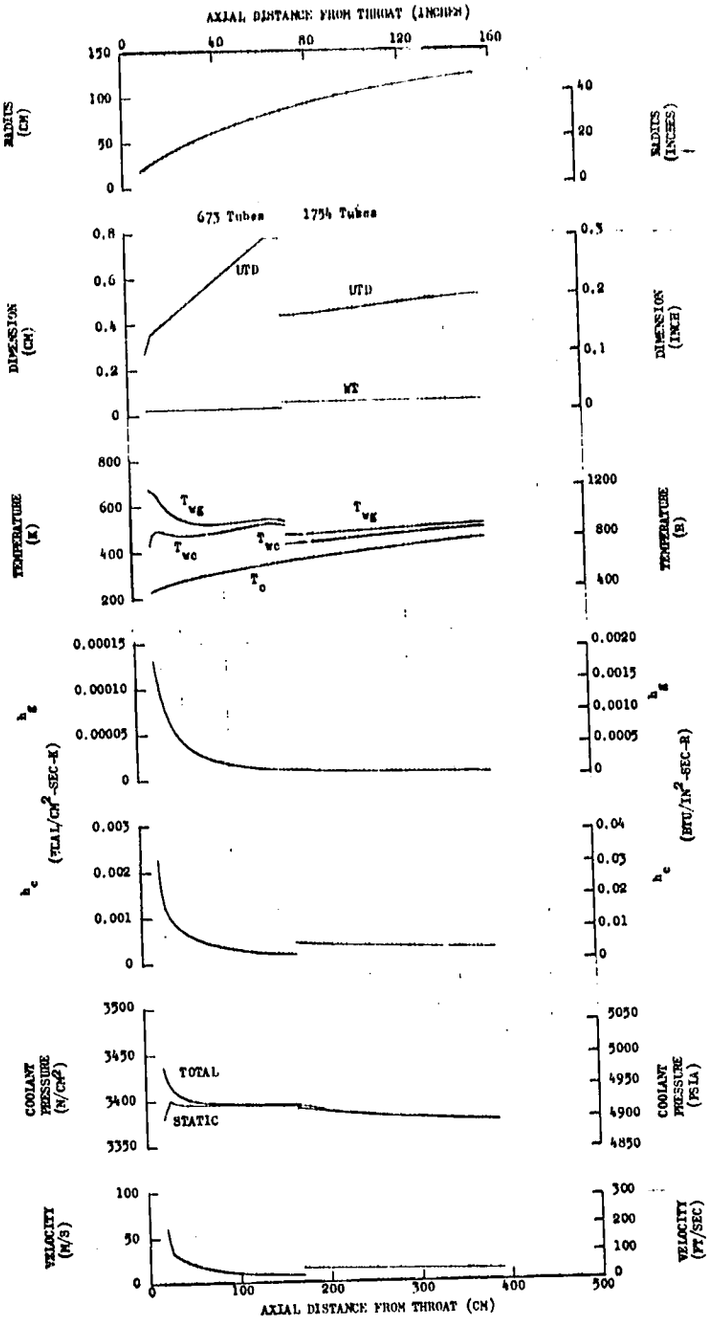

Figure 100. Parameters for the O_2/CH_4, MR = 3.5, F = 667,000 N (150,000 lbf), Coolant P_{in}/P_c = 1.8, Nozzle at 2758 N/cm^2 (4000 psia) (For Carbon Layer Enhanced Combustion Chamber)

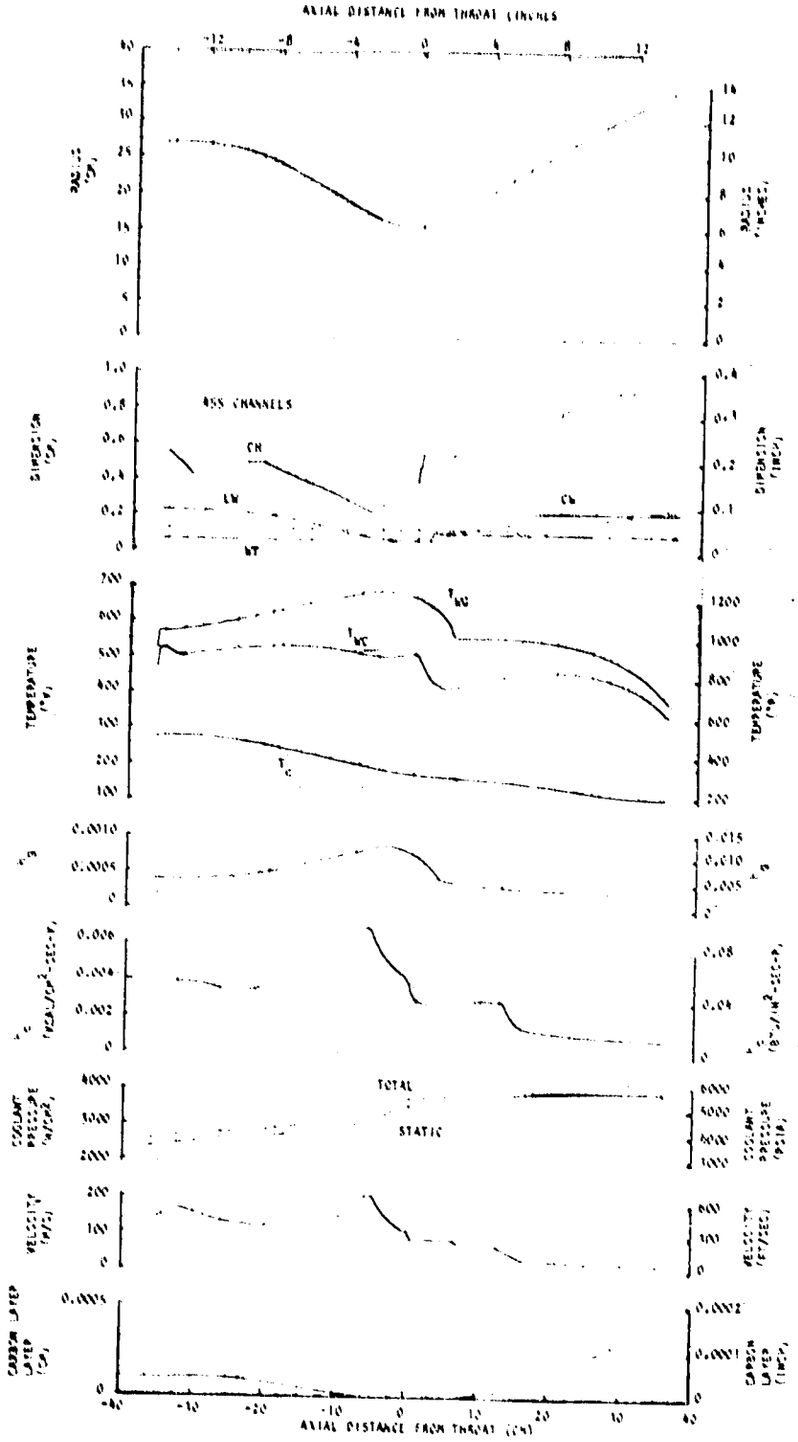

Figure 101. Parameters for the O_2/CH_4, MR = 3.5, F = 2,669,000 N (600,000 lbf), Coolant P_{in}/P_c = 1.8, Combustion Chamber at P_c = 1896 N/cm^2 (3175 psia) (Carbon Layer Cooling Enhancement on Combustion Chamber)

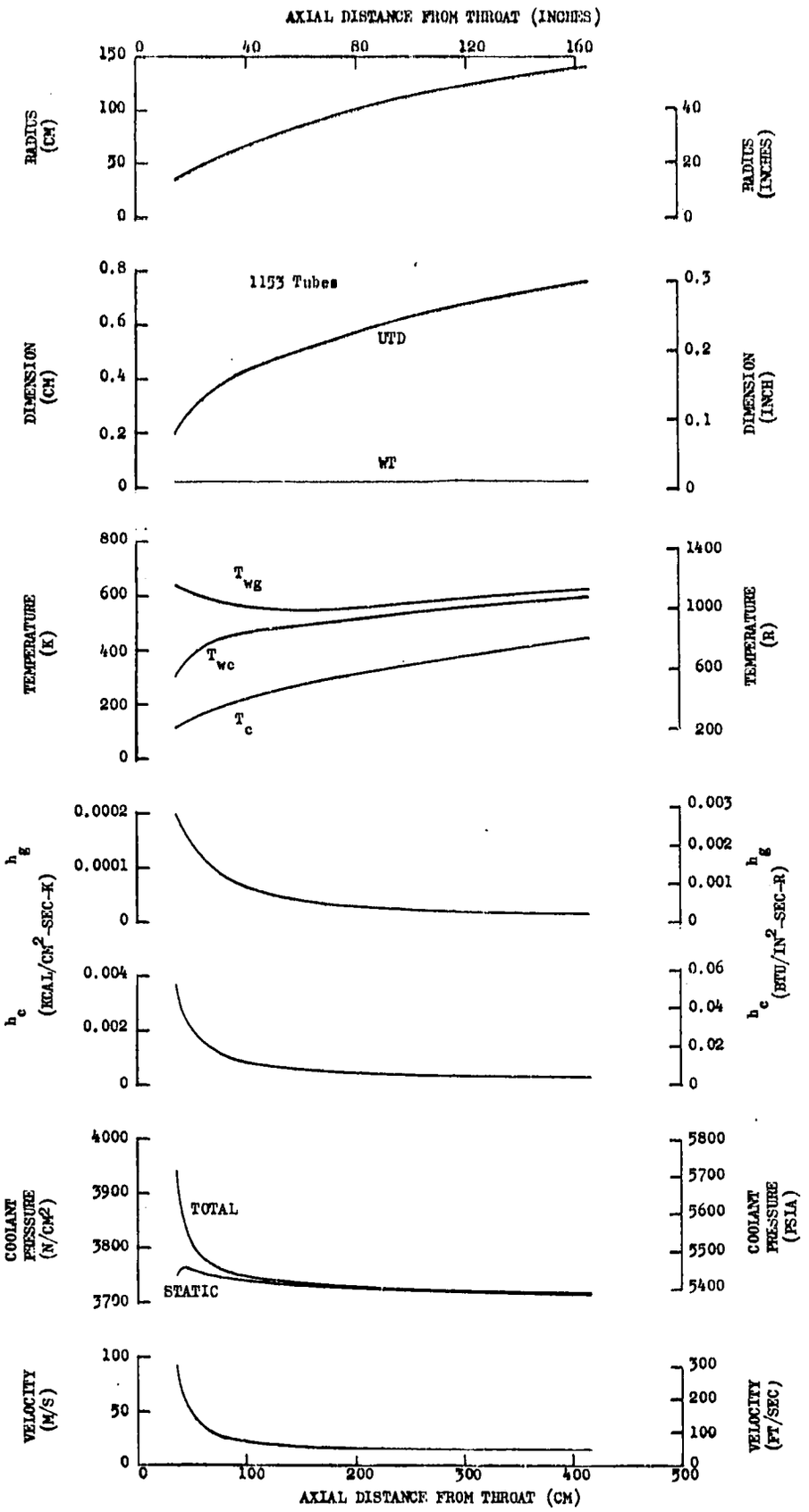

Figure 102. Parameters for the O_2/CH_4, MR = 3.5, F = 2,669,000 N (600,000 lbf), Coolant P_{in}/P_c = 1.64, Nozzle at P_c = 2189 N/cm^2 (3175 psia) (For Carbon Layer Enhanced Combustion Chamber)

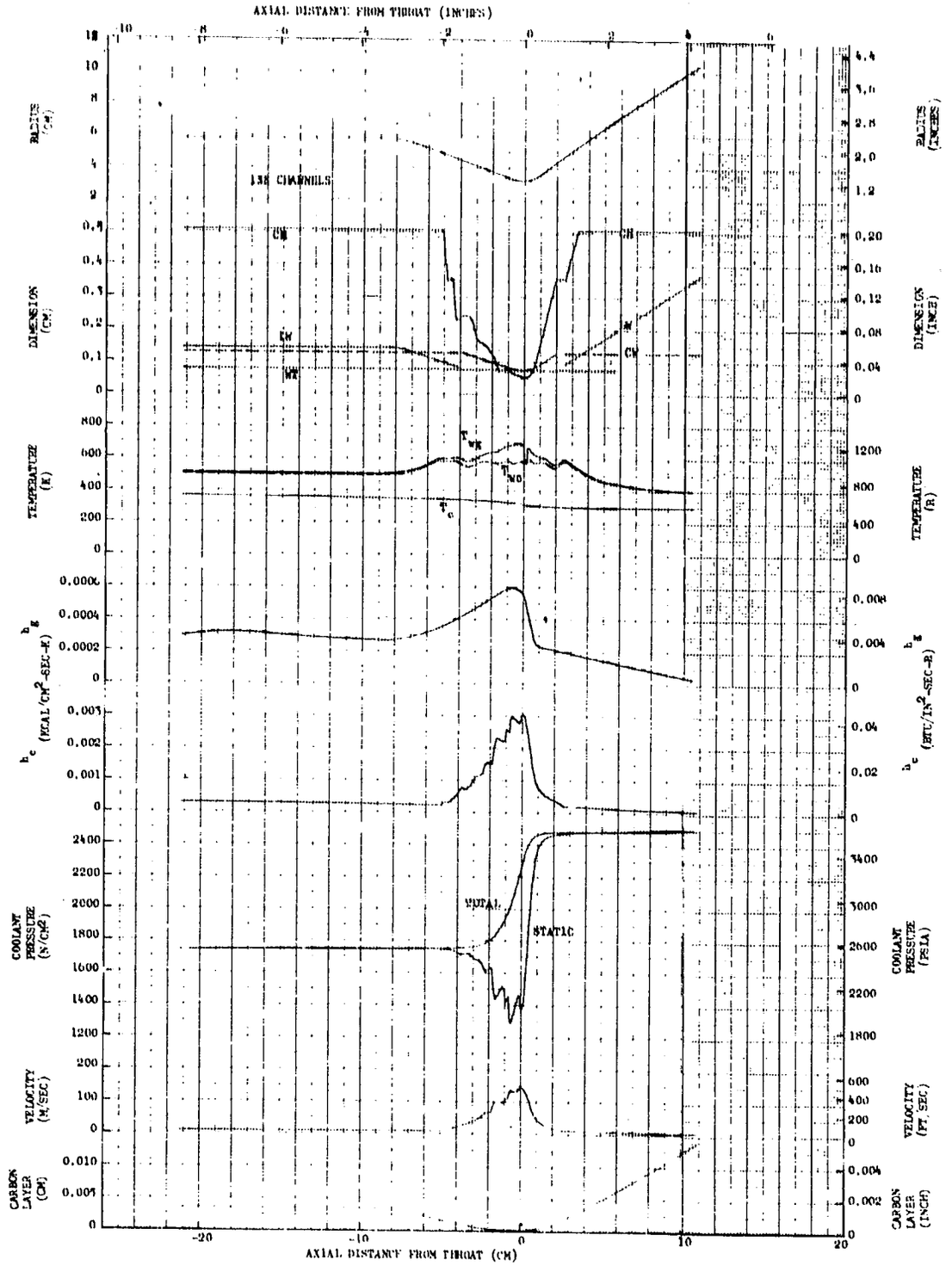

Figure 103. Parameters for the O_2/RP-1, MR = 2.8, F = 89,000 N (20,000 lbf), Coolant P_{in}/P_c = 1.8, Carbon Layer Enhanced Combustion Chamber at P_c = 1379 N/cm^2 (2000 psia) (Long Chamber)

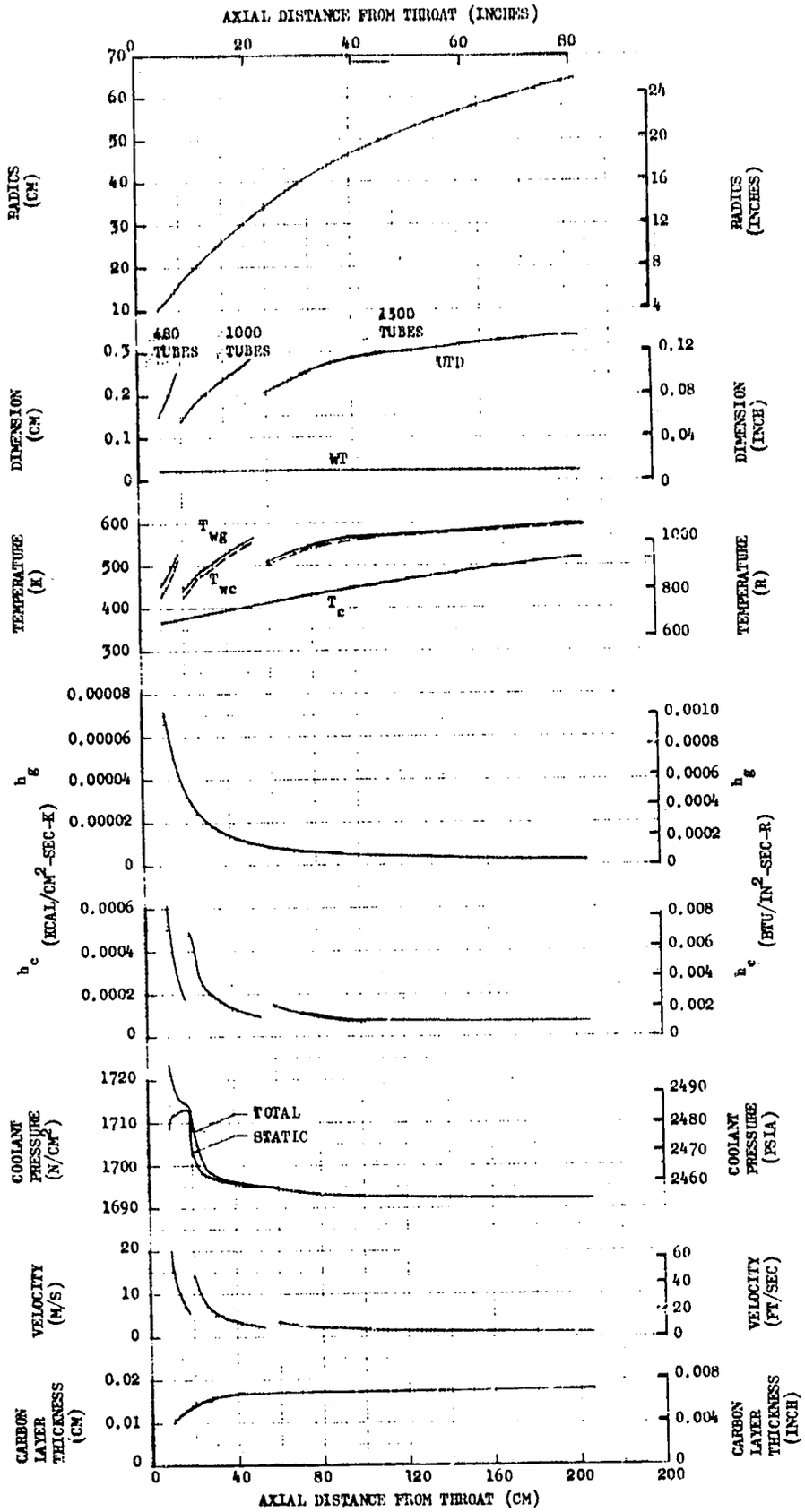

Figure 104. Parameters for the O_2/RP-1, MR = 2.8, F = 89,000 N (20,000 lbf), - Coolant P_{in}/P_c = 1.8, Nozzle at 1379 N/cm^2 (2000 psia) (For Carbon Layer Enhanced Combustion Chamber and Nozzle)

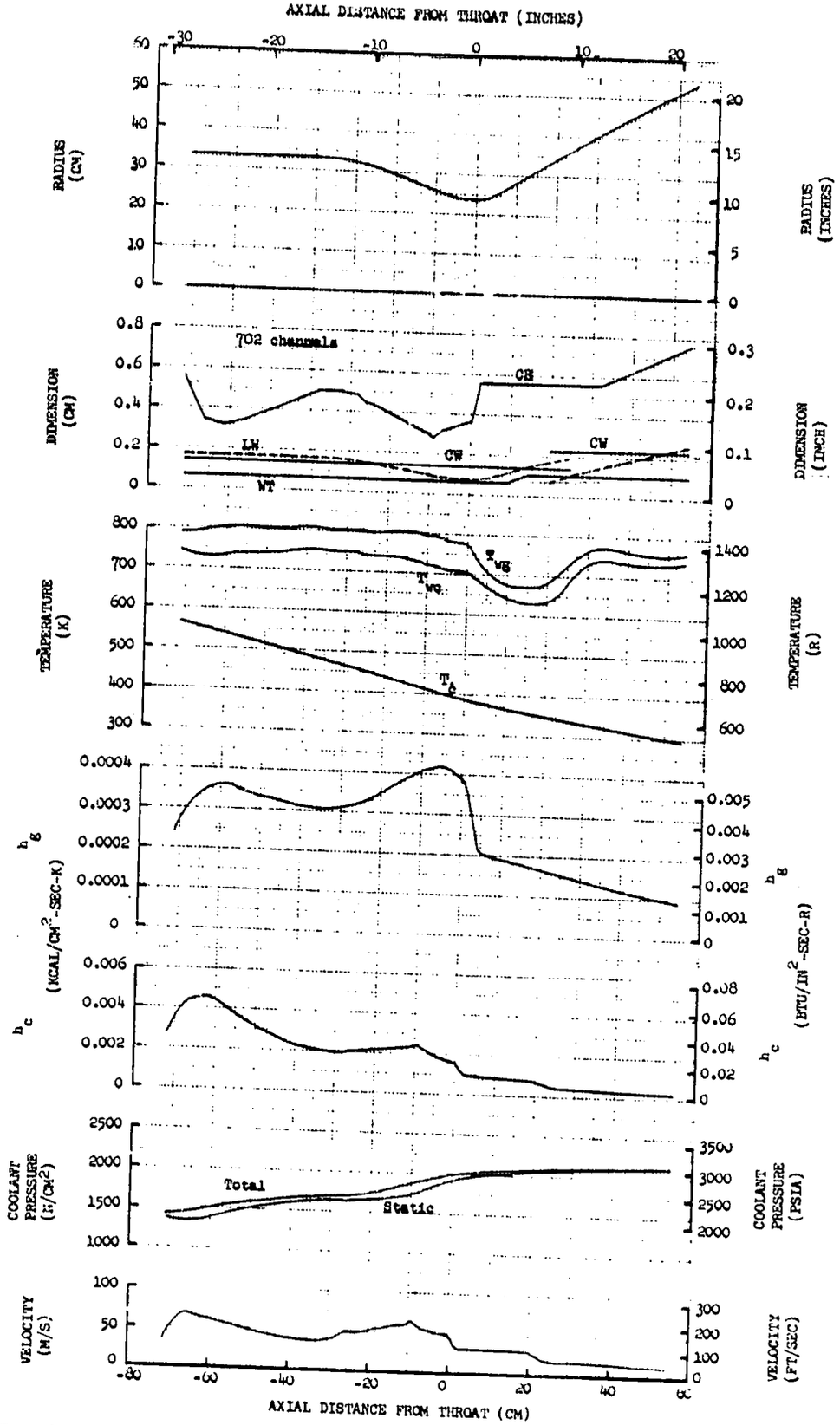

Figure 105. Parameters for the O_2/RP-1, MR = 2.8, F = 2,669,000 N (600,000 lbf), Coolant P_{in}/P_c = 1.8, Combustion Chamber at 1179 N/cm^2 (1710 psia) (For Carbon Layer Enhanced Combustion Chamber and Nozzle) (Long Chamber)

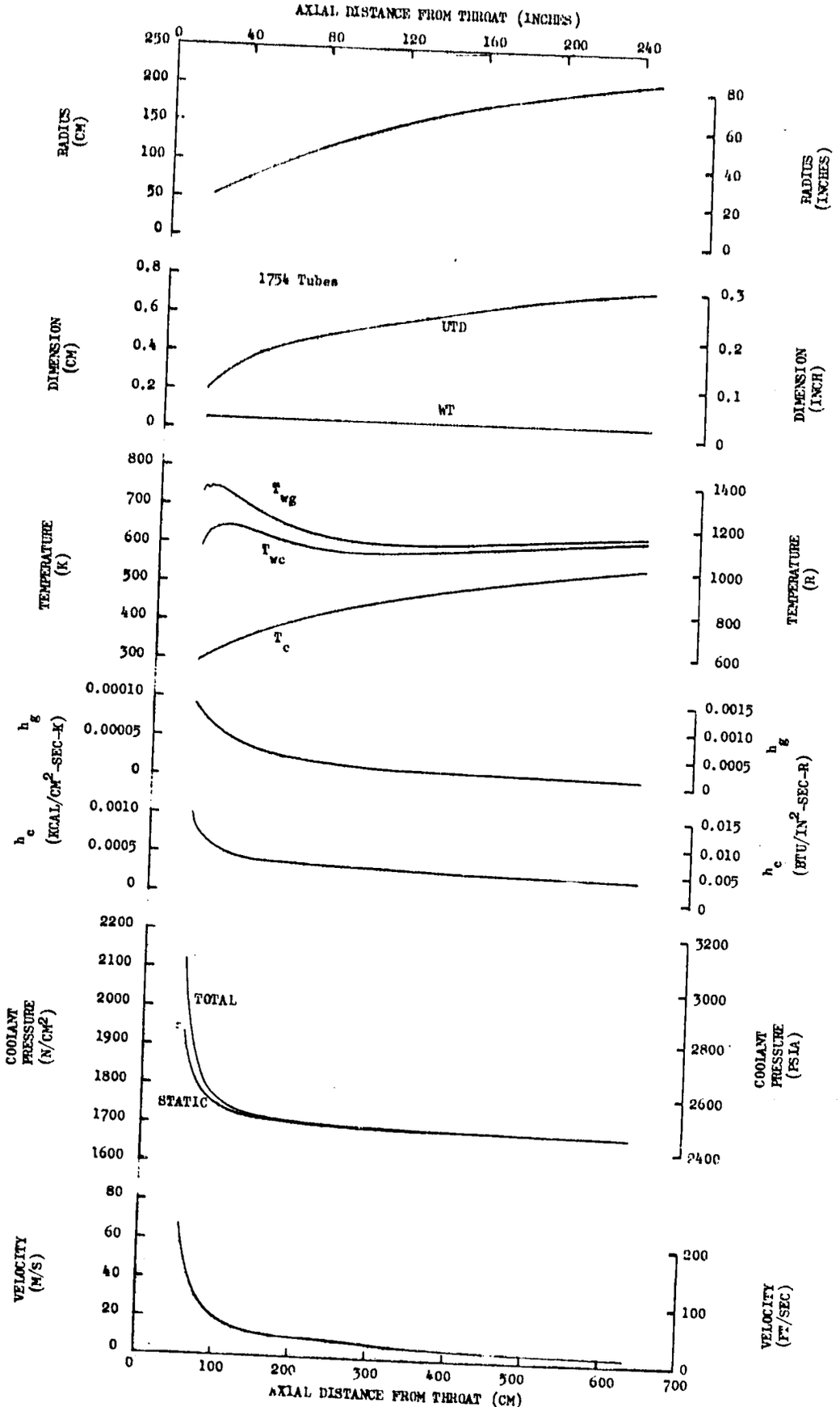

Figure 106. Parameters for the O_2/RP-1, MR = 2.8, F = 2,669,000 N (600,000 lbf), Coolant P_{in}/P_c = 1.8, Nozzle at P_c = 1179 N/cm^2 (1710 psia) (For Carbon Layer Enhanced Combustion Chamber)

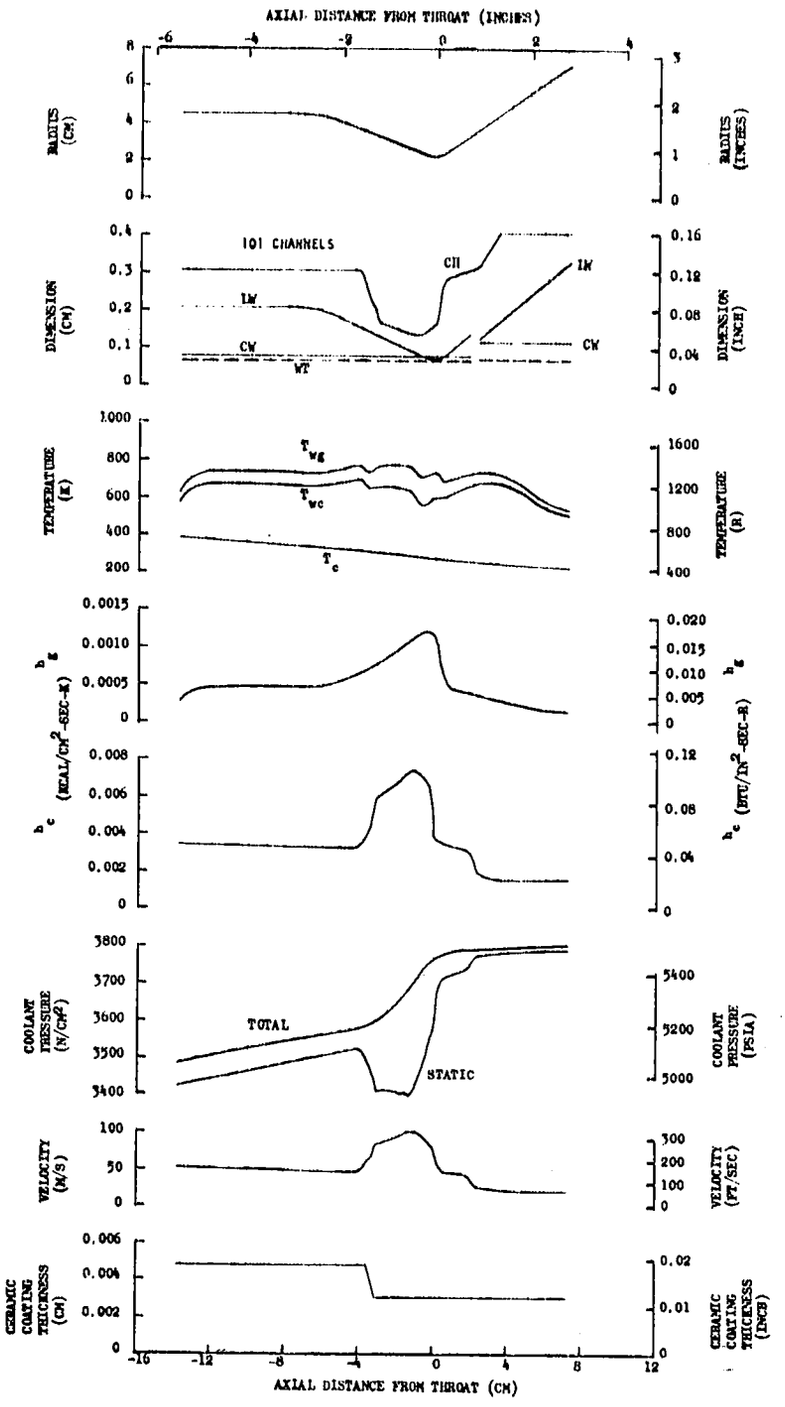

Figure 107. Parameters for the O_2/C_3H_8, MR = 3.1, F = 89,000 N (20,000 lbf), Coolant P_{in}/P_c = 1.64, Combustion Chamber at P_c = 2758 N/cm^2 (4000 psia) (Ceramic Coating Enhancement on Combustion Chamber)

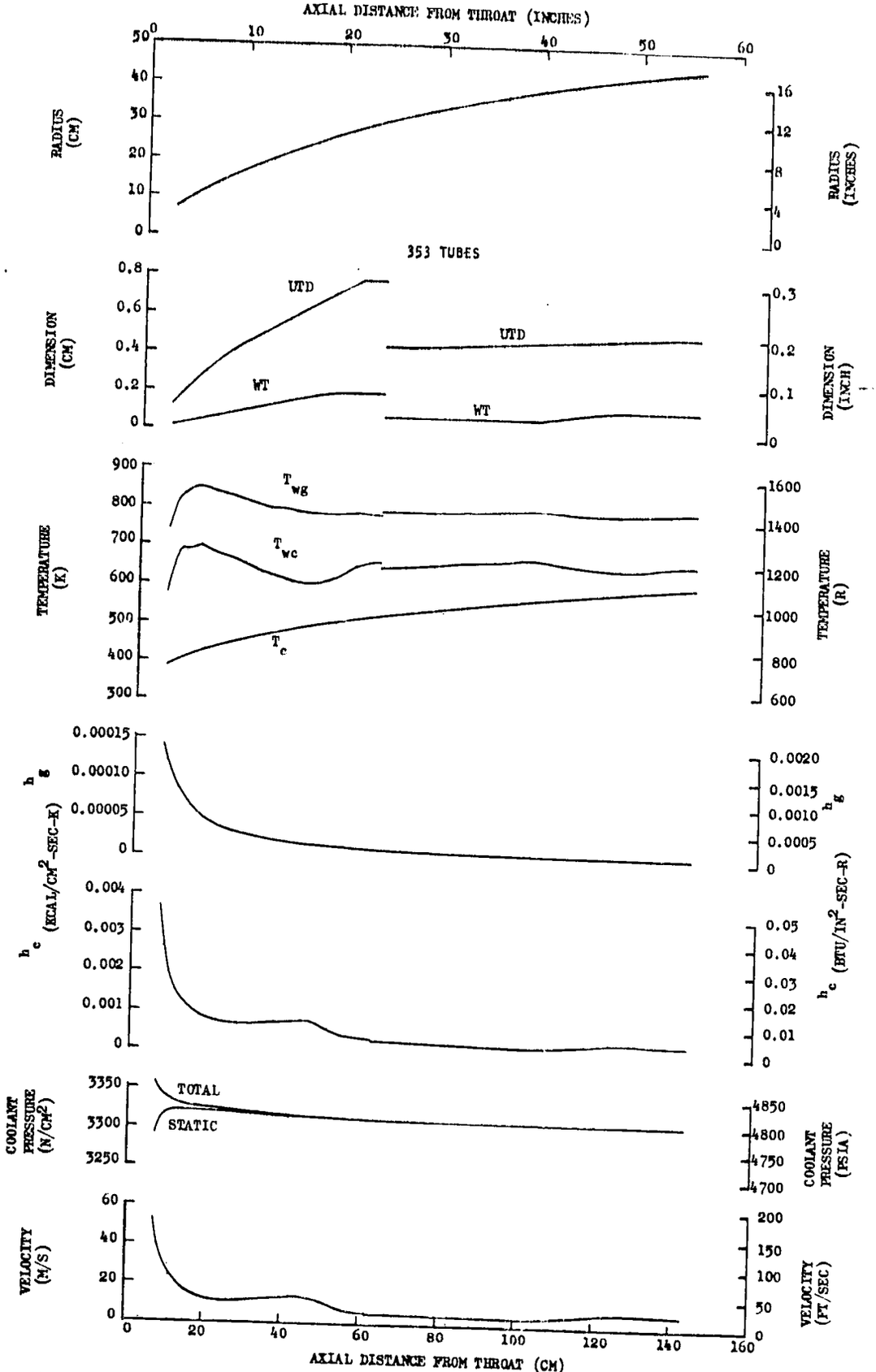

Figure 108. Parameters for the O_2/C_3H_8, MR = 3.1, F = 89,000 N (20,000 lbf), Coolant P_{in}/P_c = 1.64, Nozzle at P_c = 2758 N/cm^2 (4000 psia) (Ceramic Coating Enhancement on Combustion Chamber)

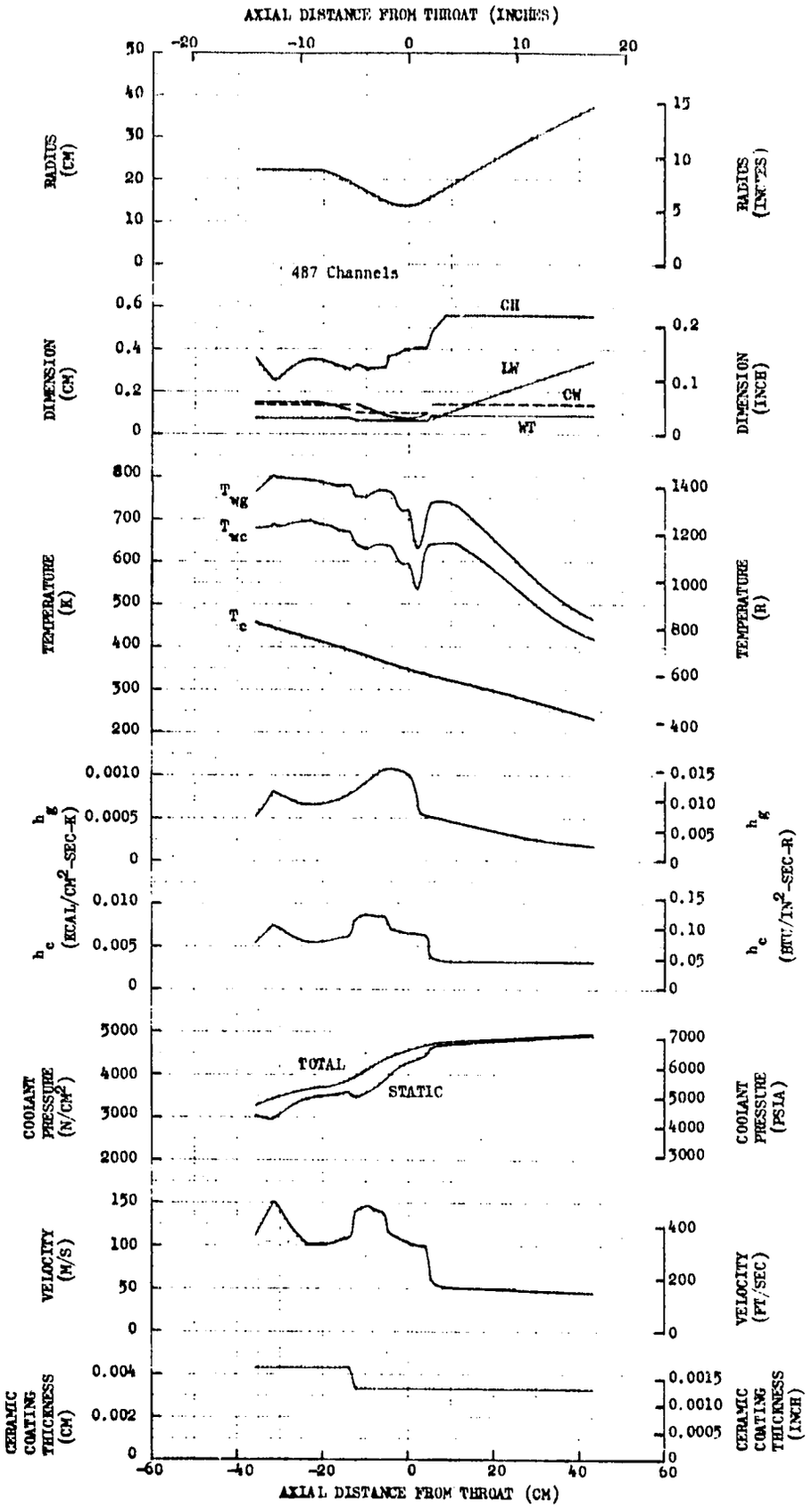

Figure 109. Parameters for the O_2/C_3H_8, MR = 3.1, F = 2,669,000 N (600,000 lbf), Coolant P_{in}/P_c = 1.8, Combustion Chamber at P_c = 2758 N/cm^2 (4000 psia) (Ceramic Coating Enhancement on Combustion Chamber)

f)

psia)

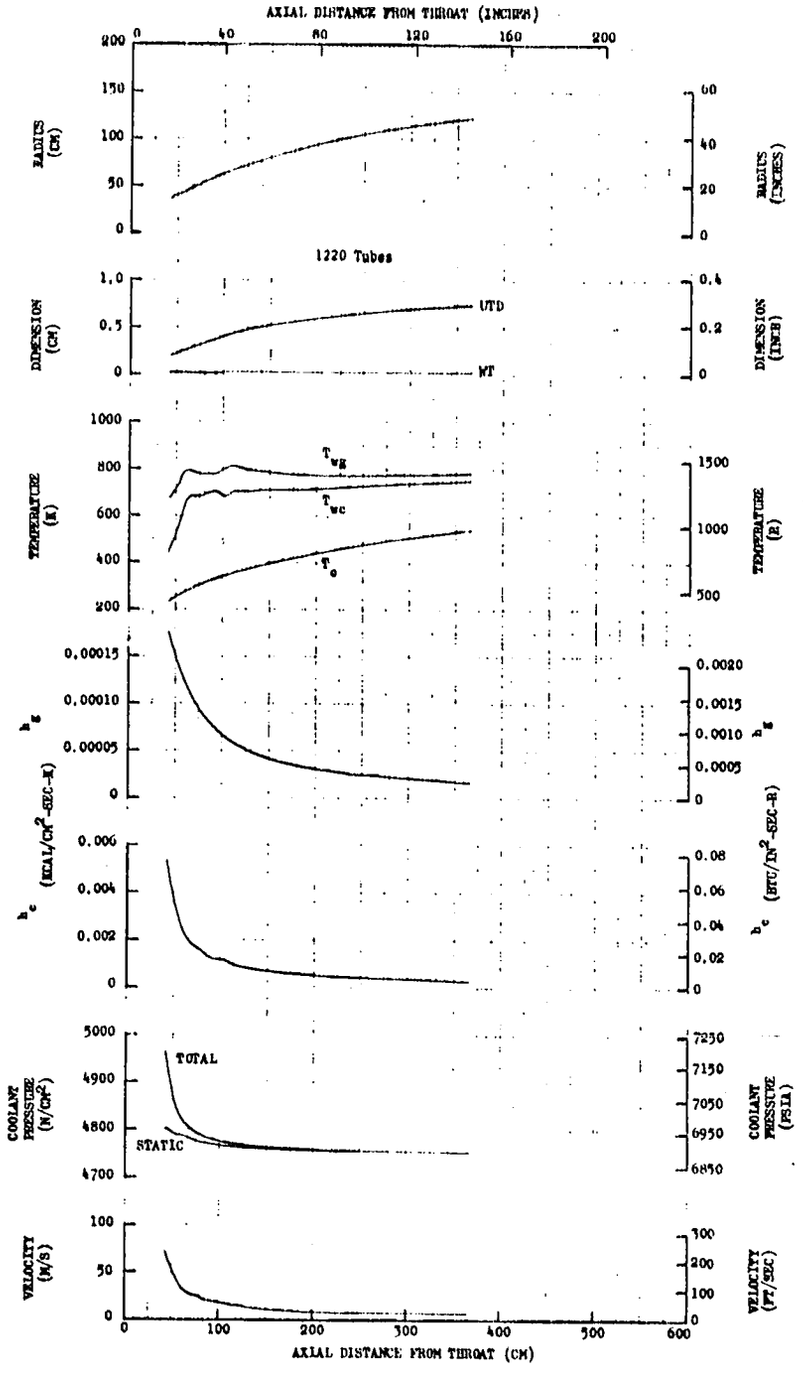

Figure 110. Parameters for the O_2/C_3H_8, MR = 3.1, F = 2,669,000 N (600,000 lbf), Coolant P_{in}/P_c = 1.8, Nozzle at P_c = 2758 N/cm^2 (4000 psia) (Ceramic Coating Enhancement on Combustion Chamber)

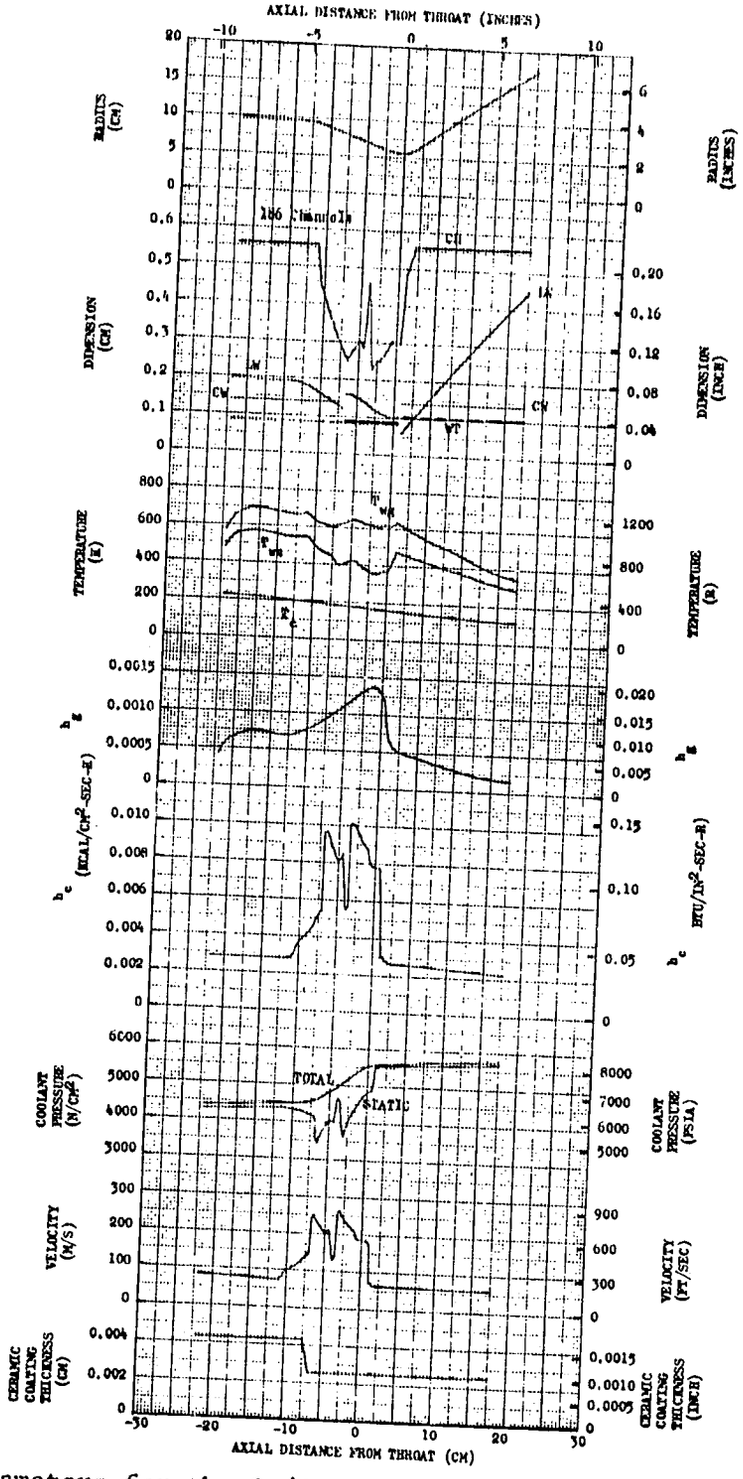

Figure 111. Parameters for the O_2/CH_4, MR = 3.5, F = 667,000 N (150,000 lbf), Coolant P_{in}/P_c = 1.67, Combustion Chamber at P_c = 3447 N/cm^2 (5000 psia) (Ceramic Coating Enhancement on Combustion Chamber)

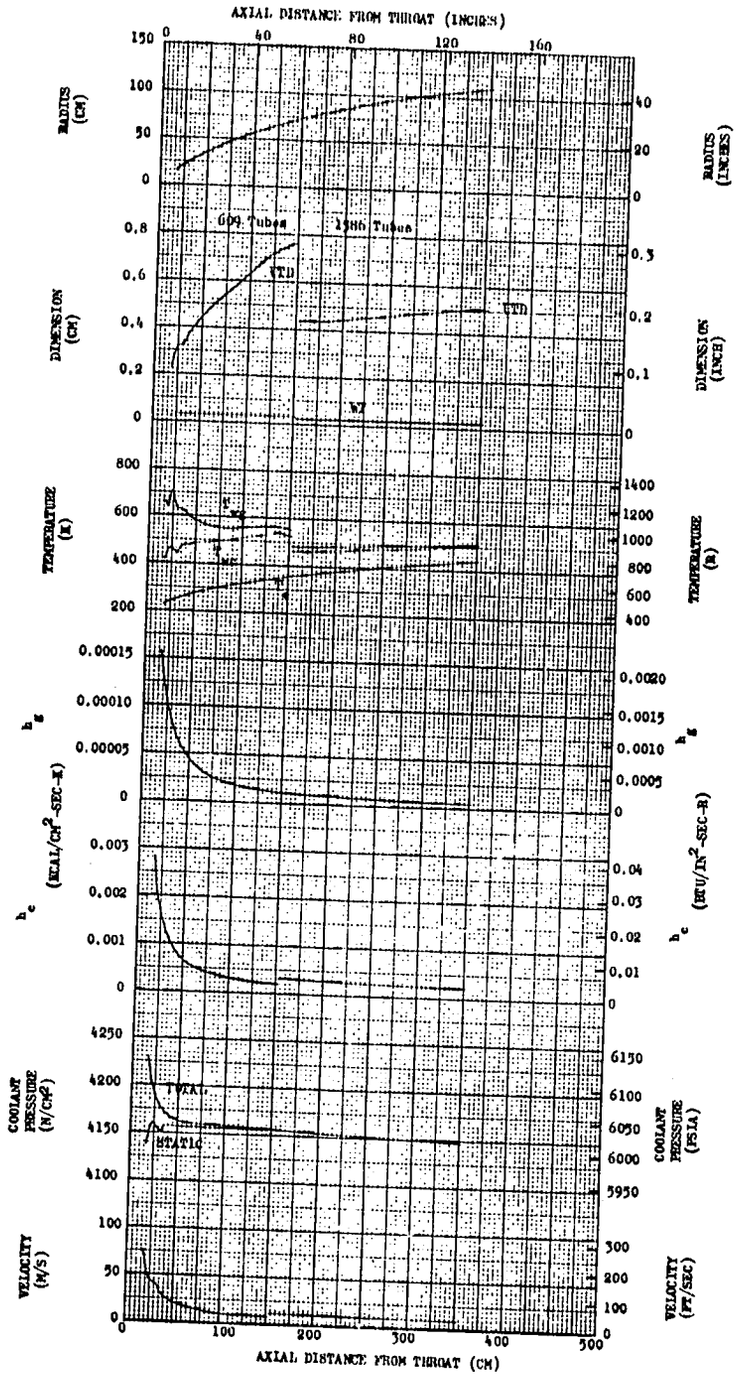

Figure 112. Parameters for the O_2/CH_4, MR = 3.5, F = 667,000 N (150,000 lbf), Coolant P_{in}/P_c = 1.67, Nozzle at P_c = 3447 N/cm^2 (5000 psia) (Ceramic Coating Enhancement on Combustion Chamber)

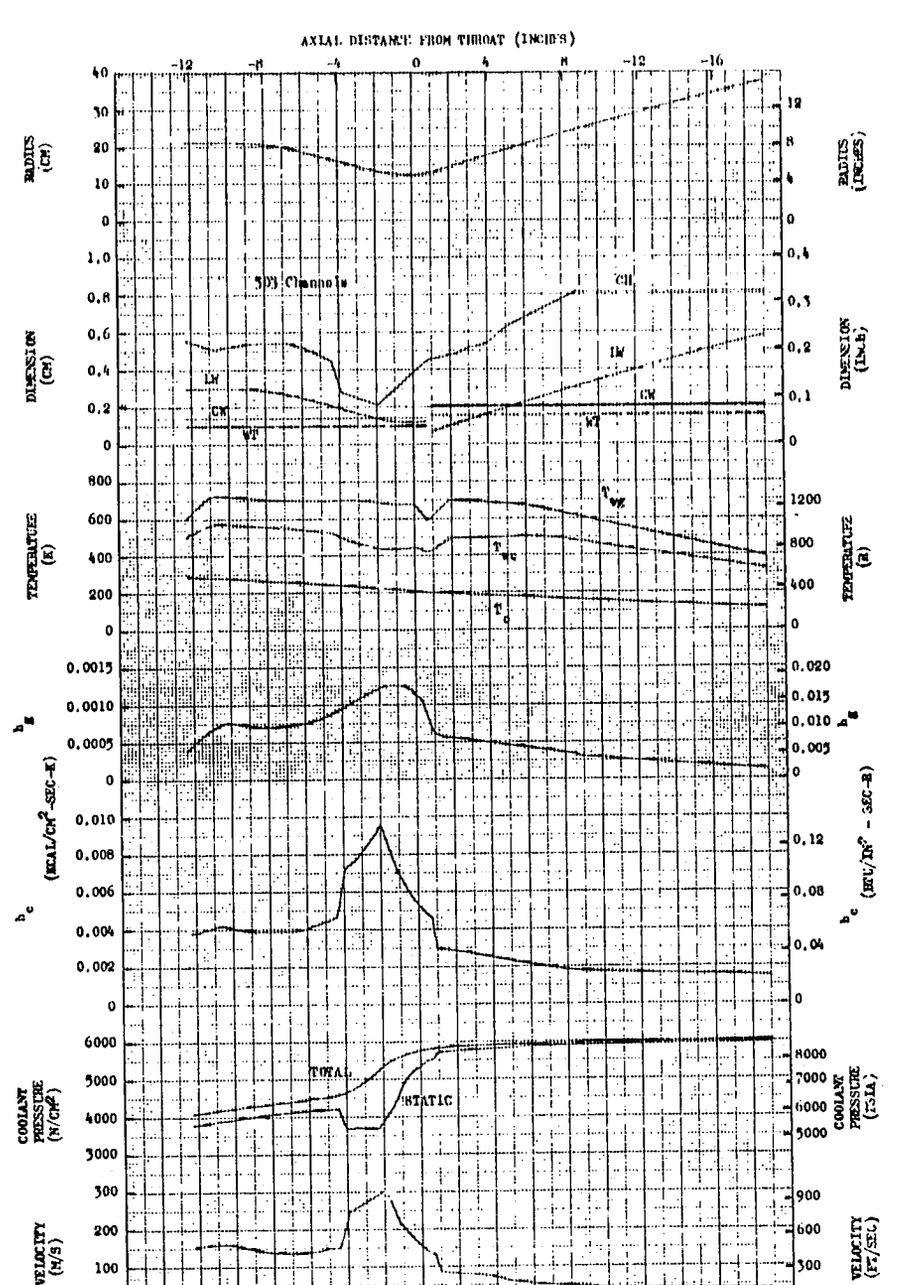

Figure 113. Parameters for the O_2/CH_4, MR = 3.5, F = 2,669,000 N (600,000 lbf), Coolant P_{in}/P_c = 1.8, Combustion Chamber at P_c = 3447 N/cm^2 (4850 psia) (Ceramic Coating Enhancement on Combustion Chamber)

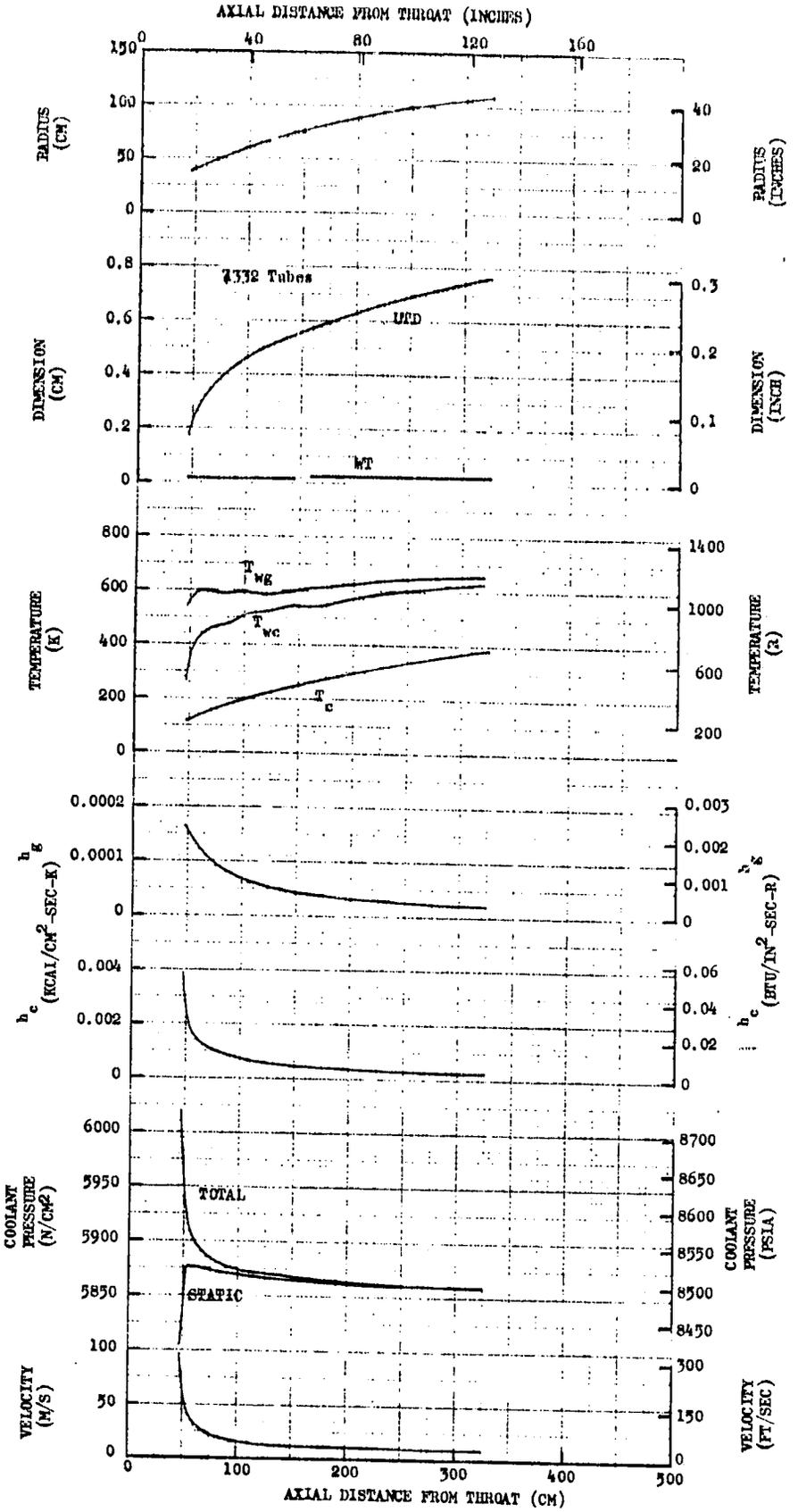

Figure 114. Parameters for the O_2/CH_4, MR = 3.5, F = 2,669,000 N (600,000 lbf), Coolant P_{in}/P_c = 1.8, Nozzle at P_c = 3447 N/cm^2 (4850 psia) (Ceramic Coating Enhancement on Combustion Chamber)

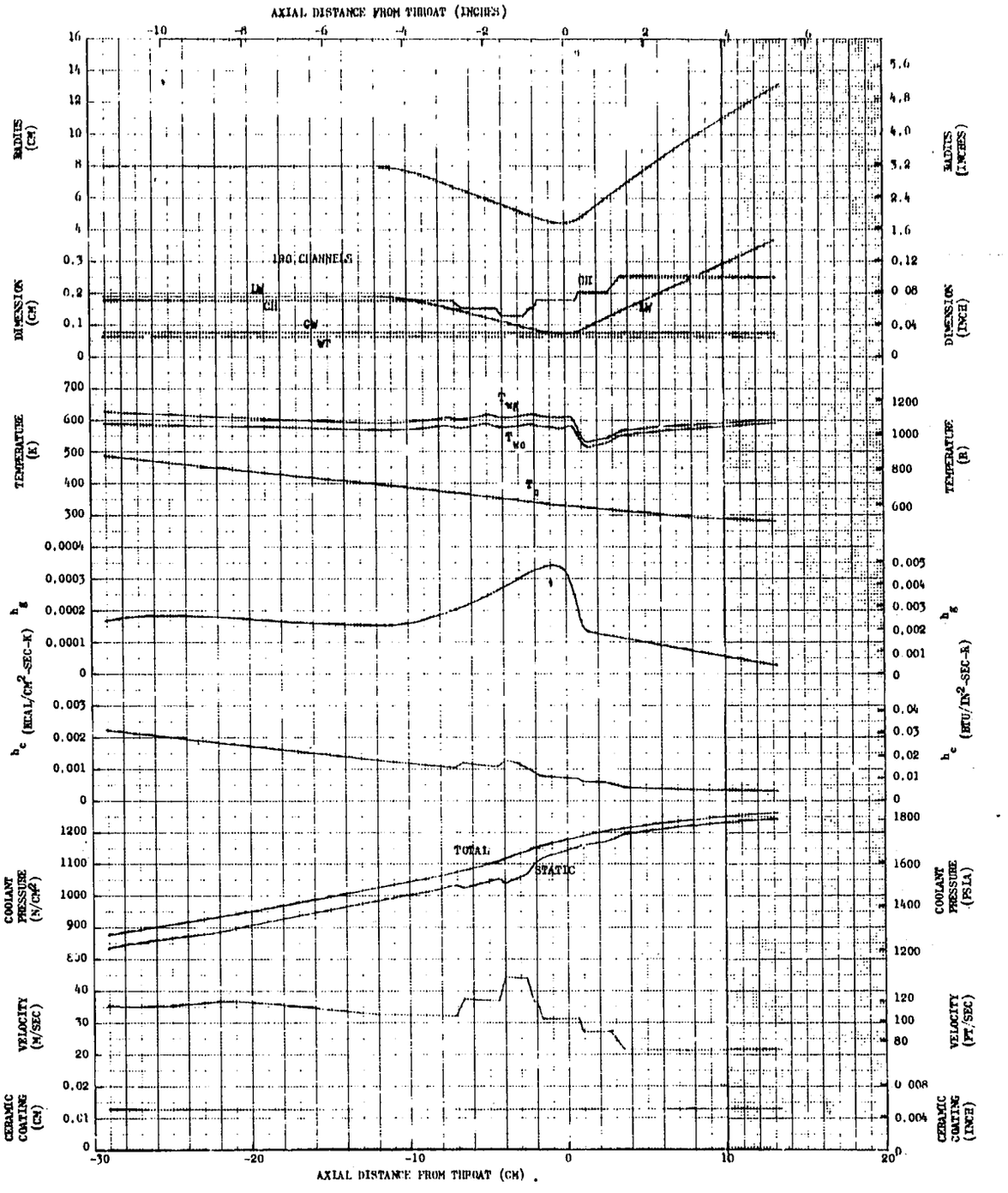

Figure 115. Parameters for the O_2/RP-1, MR = 2.8, F = 89,000 N (20,000 lbf), Coolant P_{in}/P_c = 1.8, Ceramic Coated (ZrO_2) Enhanced Combustion Chamber at P_c = 690 N/cm^2 (1000 psia) (Long Chamber)

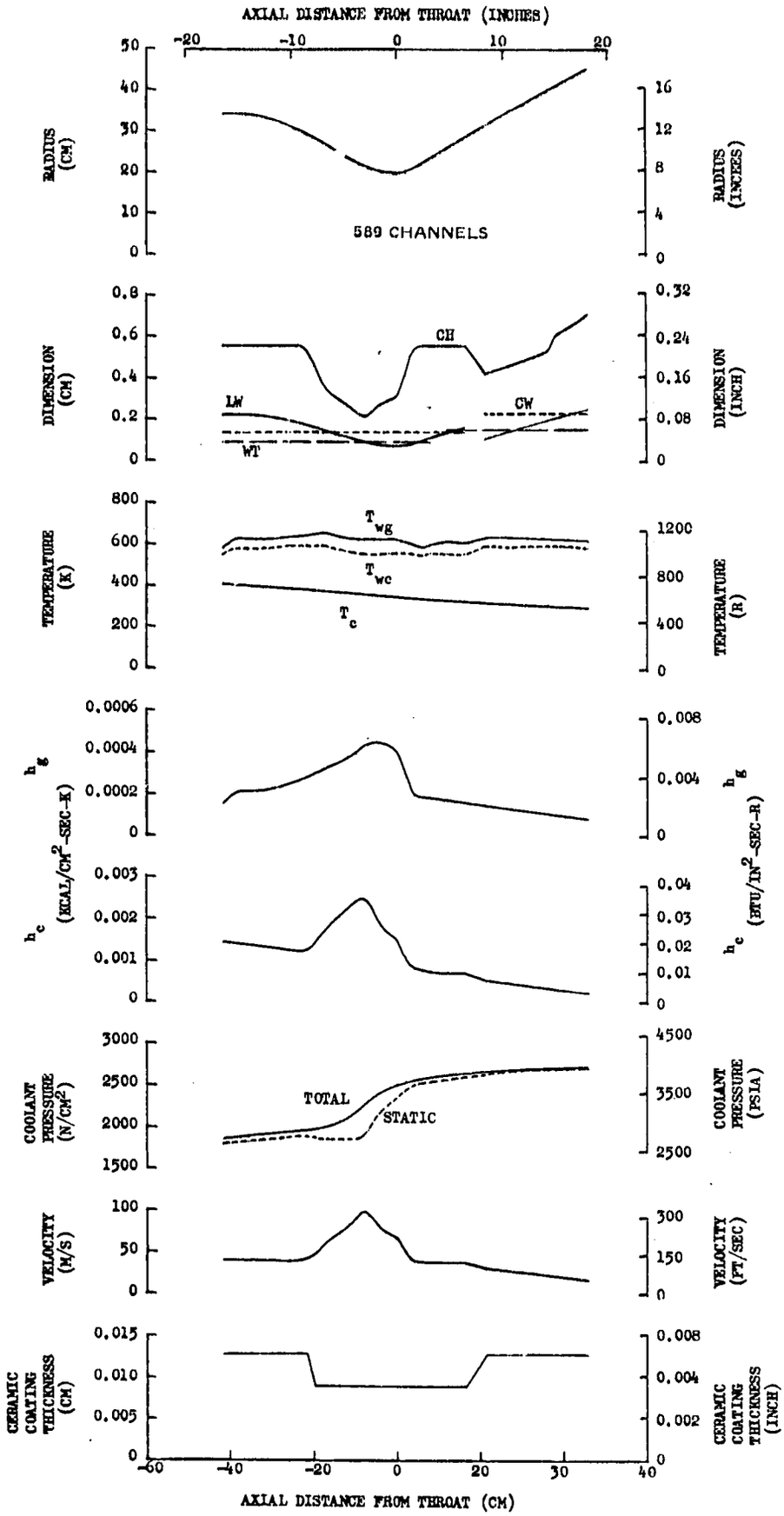

Figure 116. Parameters for the O_2/RP-1, MR = 2.8, F = 2,669,000 N (600,000 lbf), Coolant P_{in}/P_c = 1.8, Ceramic Coated (ZrO_2) Enhanced "Short" Combustion Chamber at P_c = 1516 N/cm^2 (2200 psia)

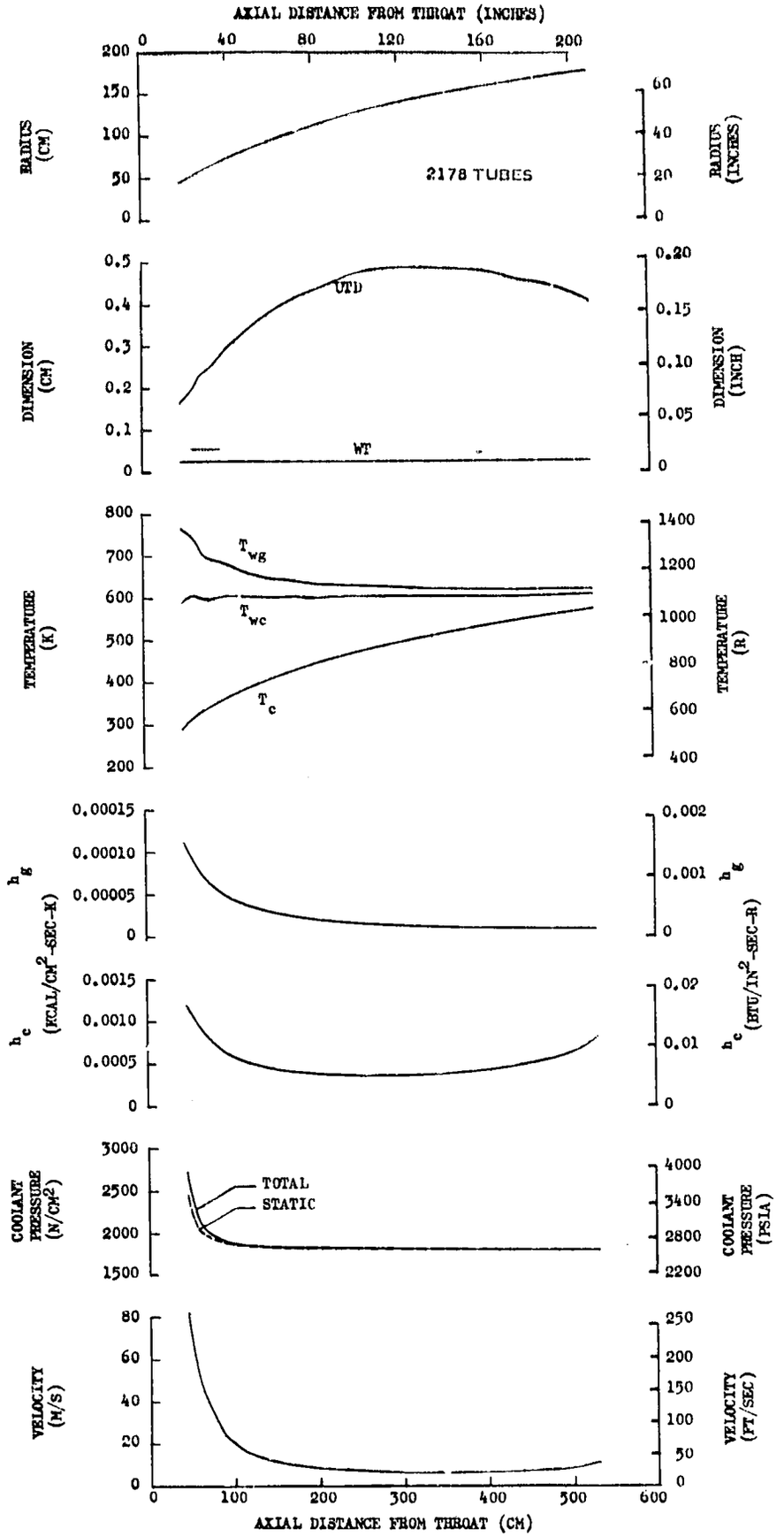

Figure 117. Parameters for the O_2/RP-1, MR = 2.8, F = 2,669,000 N (600,000 lbf), Coolant P_{in}/P_c = 1.8, Nozzle at P_c = 1516 N/cm^2 (2200 psia) (Ceramic Coating Enhancement on Combustion Chamber)

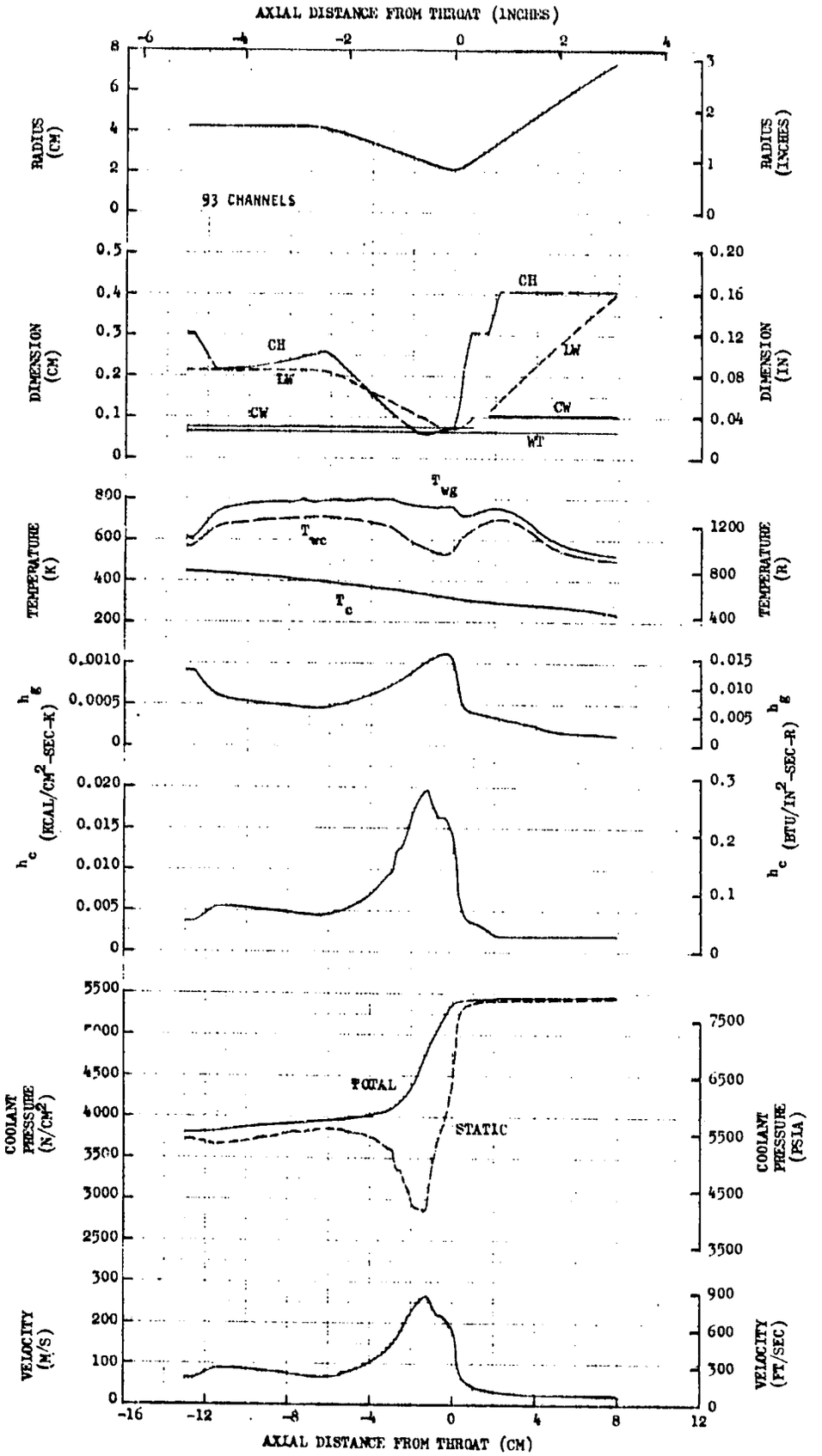

Figure 118. Parameters for the O_2/C_3H_8, MR = 3.1, F = 89,000 N (20,000 lbf), Coolant P_{in}/P_c = 1.8, Combustion Chamber at P_c = 3034 N/cm^2 (4400 psia) (Film Cooling Enhancement on Combustion Chamber)

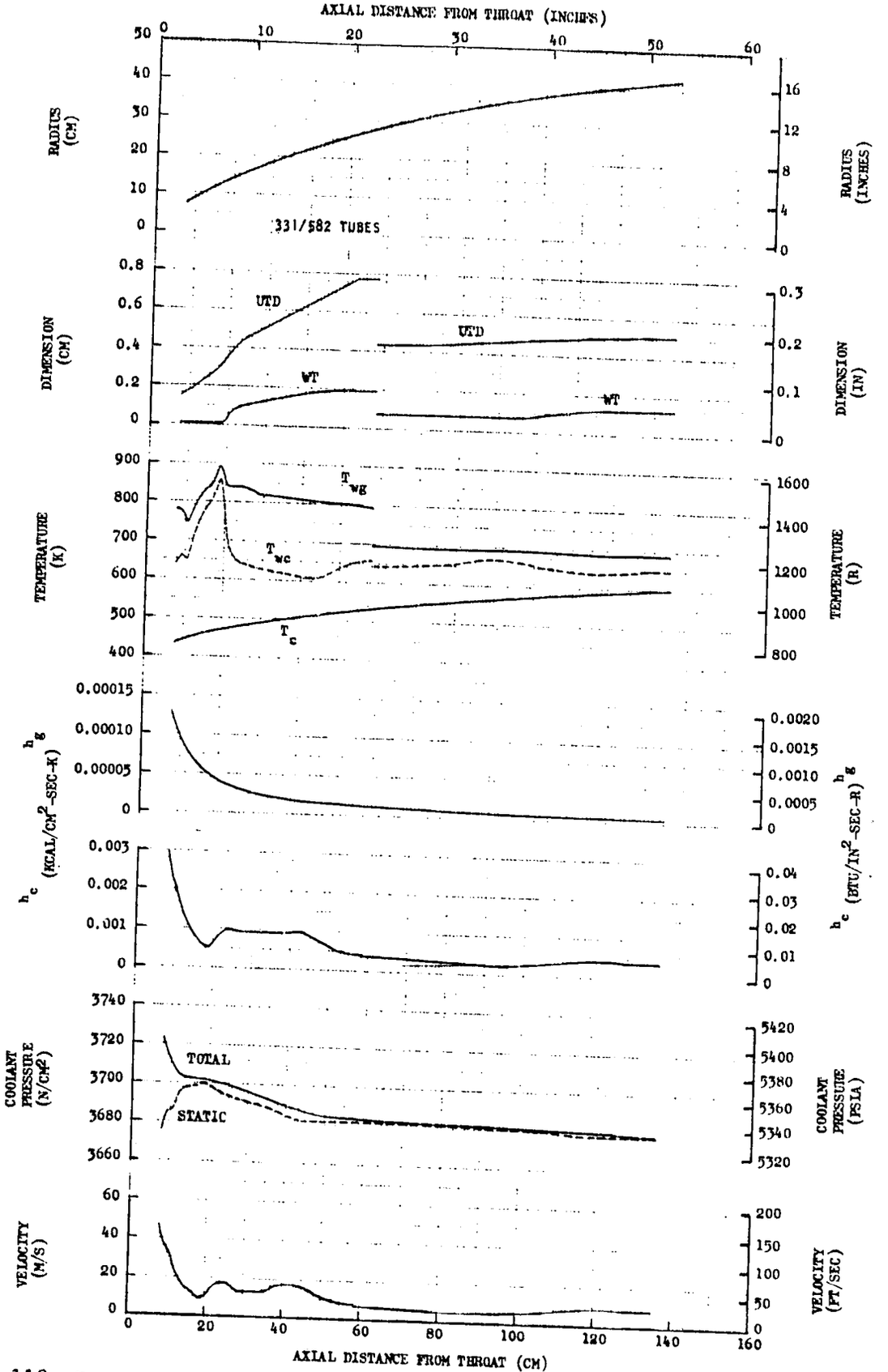

Figure 119. Parameters for the O_2/C_3H_8, MR = 3.1, F = 89,000 N (20,000 lbf), Coolant P_{in}/P_c = 1.8, Nozzle at P_c = 3034 N/cm^2 (4400 psia) (Film Cooling Enhancement on Combustion Chamber)

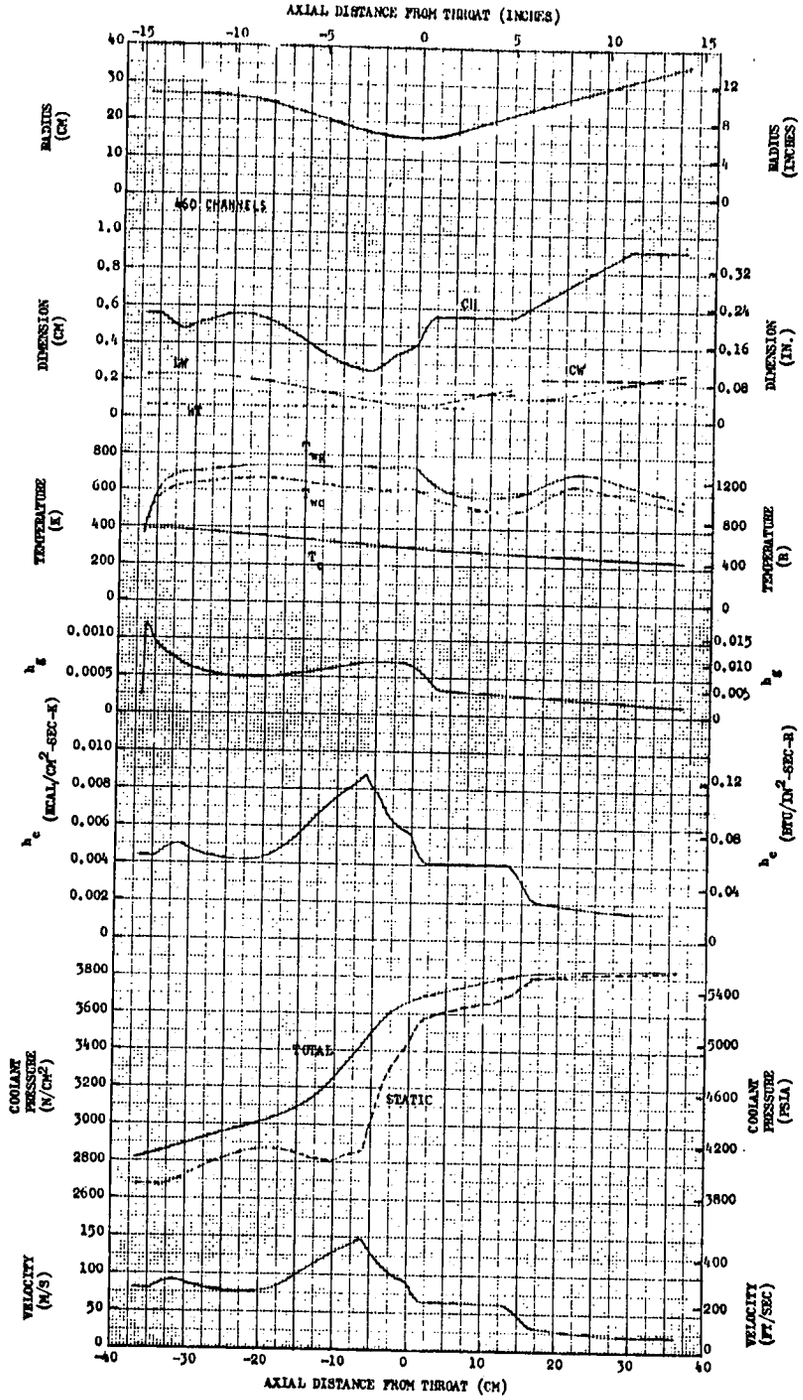

Figure 120. Parameters for the O_2/C_3H_8, MR = 3.1, F = 2,669,000 N (600,000 lbf), Coolant P_{in}/P_c = 1.8, Nozzle at P_c = 2137 N/cm^2 (3100 psia) (Film Cooling Enhancement on Combustion Chamber)

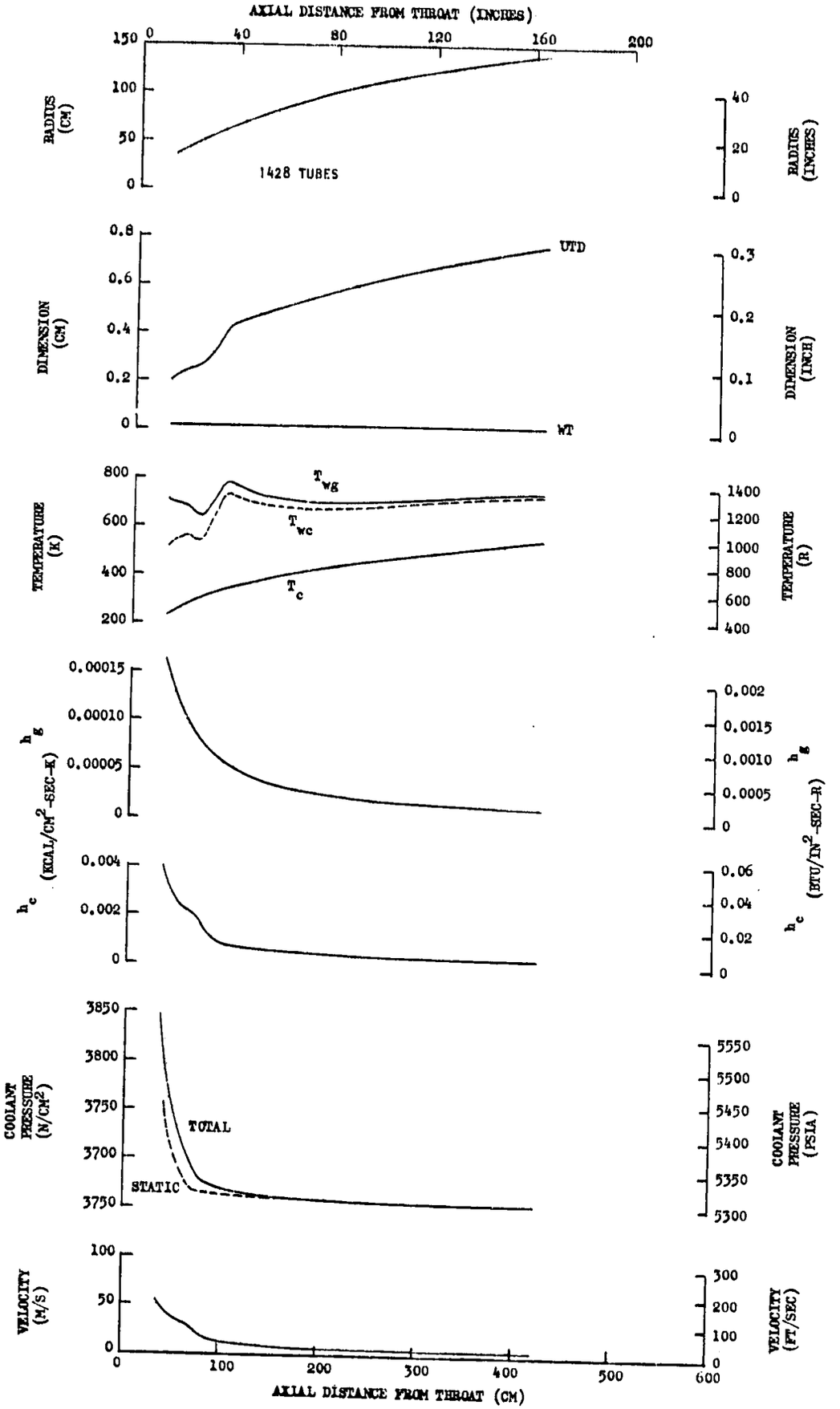

Figure 121. Parameters for the O_2/C_3H_8, MR = 3.1, F = 2,669,000 N (600,000 lbf), Coolant P_{in}/P_c = 1.8, Nozzle at P_c = 2137 N/cm^2 (3100 psia) (Film Cooling Enhancement on Combustion Chamber)

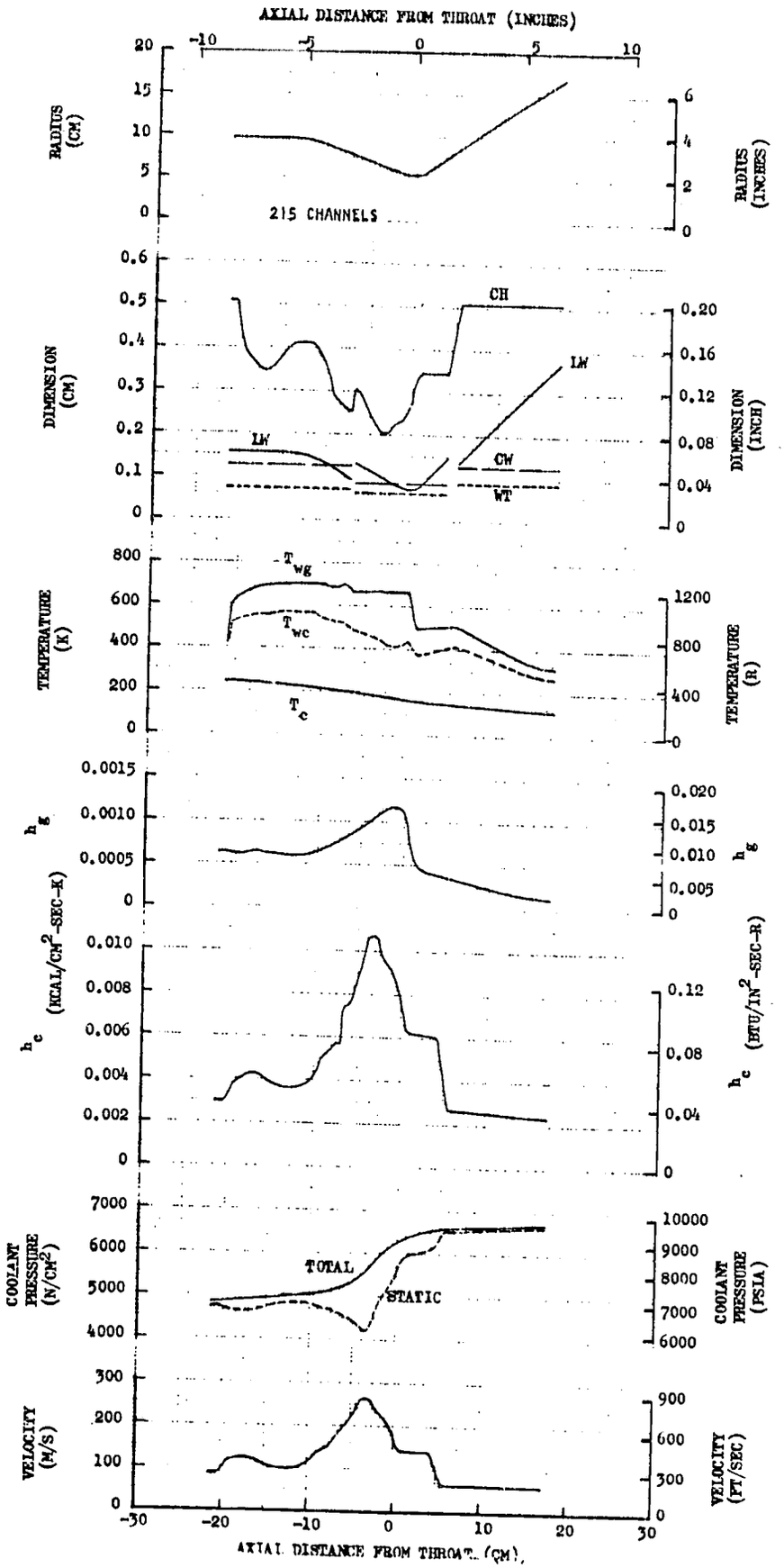

Figure 122. Parameters for the O_2/CH_4, MR = 3.5, F = 667,000 N (150,000 lbf), Coolant P_{in}/P_c = 1.8, Combustion Chamber at P_c = 3723 N/cm^2 (5400 psia) (Film Cooling Enhancement on Combustion Chamber)

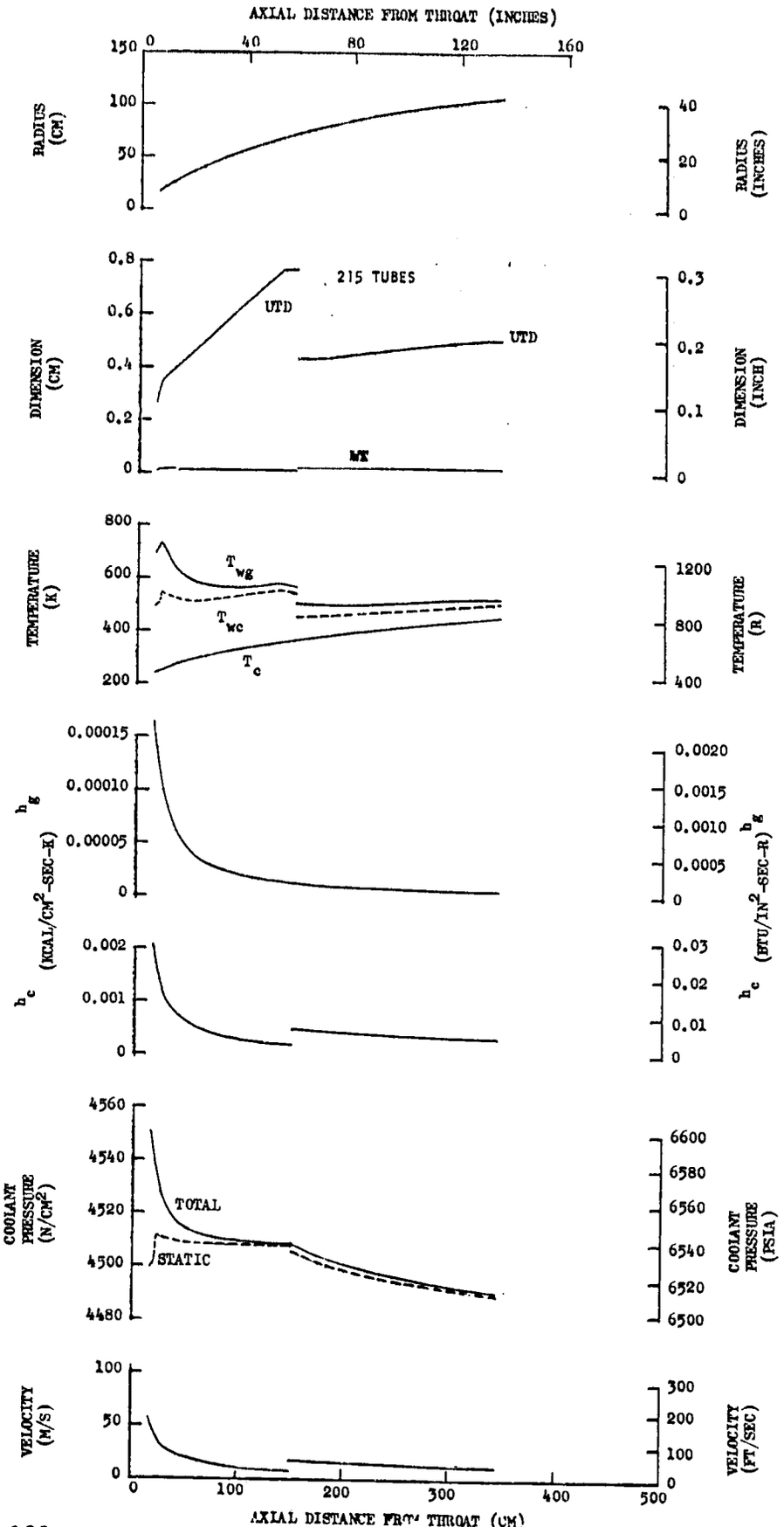

Figure 123. Parameters for the O_2/CH_4, MR = 3.5, F = 667,000 N (150,000 lbf), Coolant P_{in}/P_c = 1.8, Nozzle at P_c = 3723 N/cm^2 (5400 psia) (Film Cooling Enhancement on Combustion Chamber)

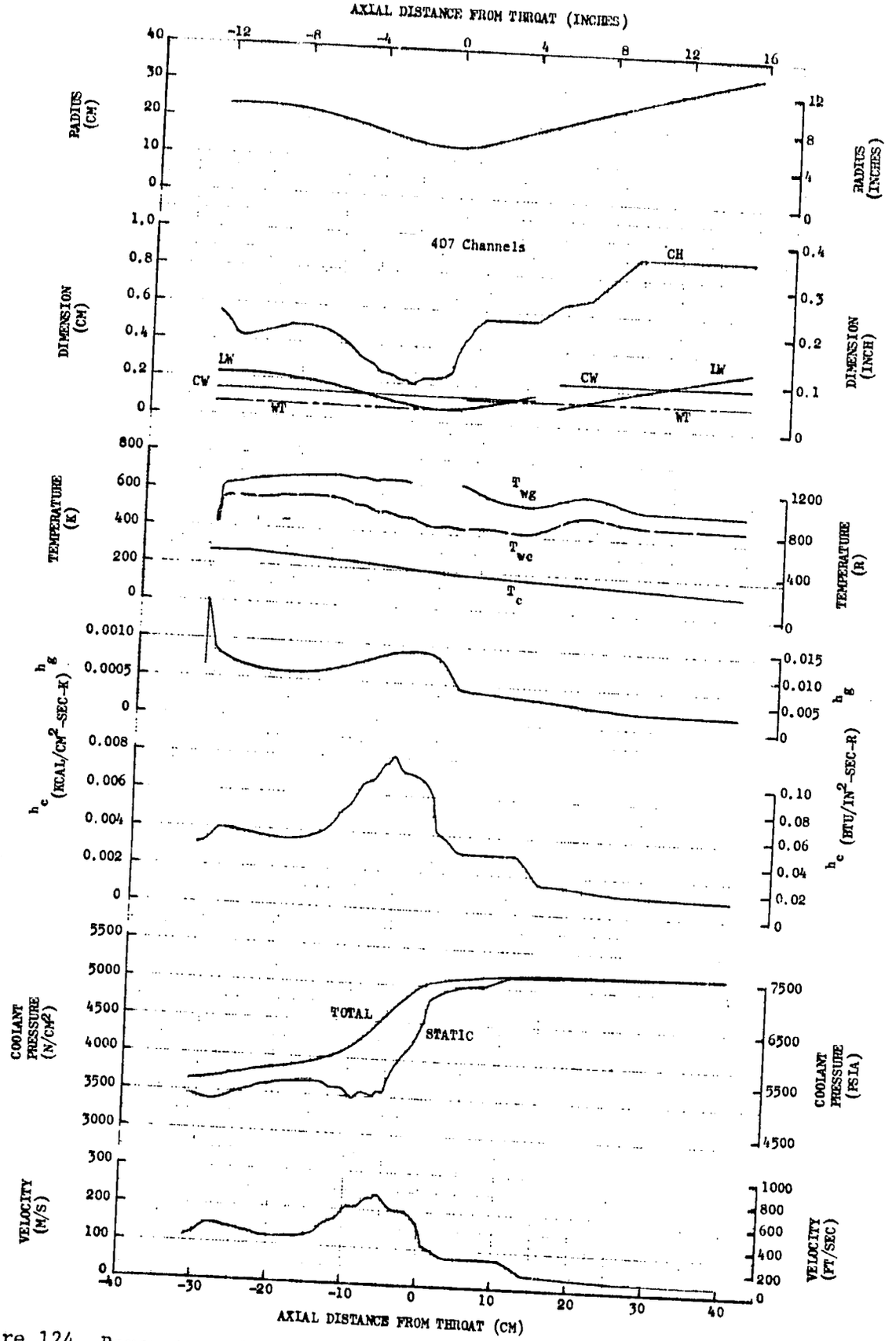

Figure 124. Parameters for the O_2/CH_4, MR = 3.5, F = 2,669,000 N (600,000 lbf), Coolant P_{in}/P_c = 1.8, Combustion Chamber at P_c = 2896 N/cm^2 (4200 psia) (Film Cooling Enhancement on Combustion Chamber)

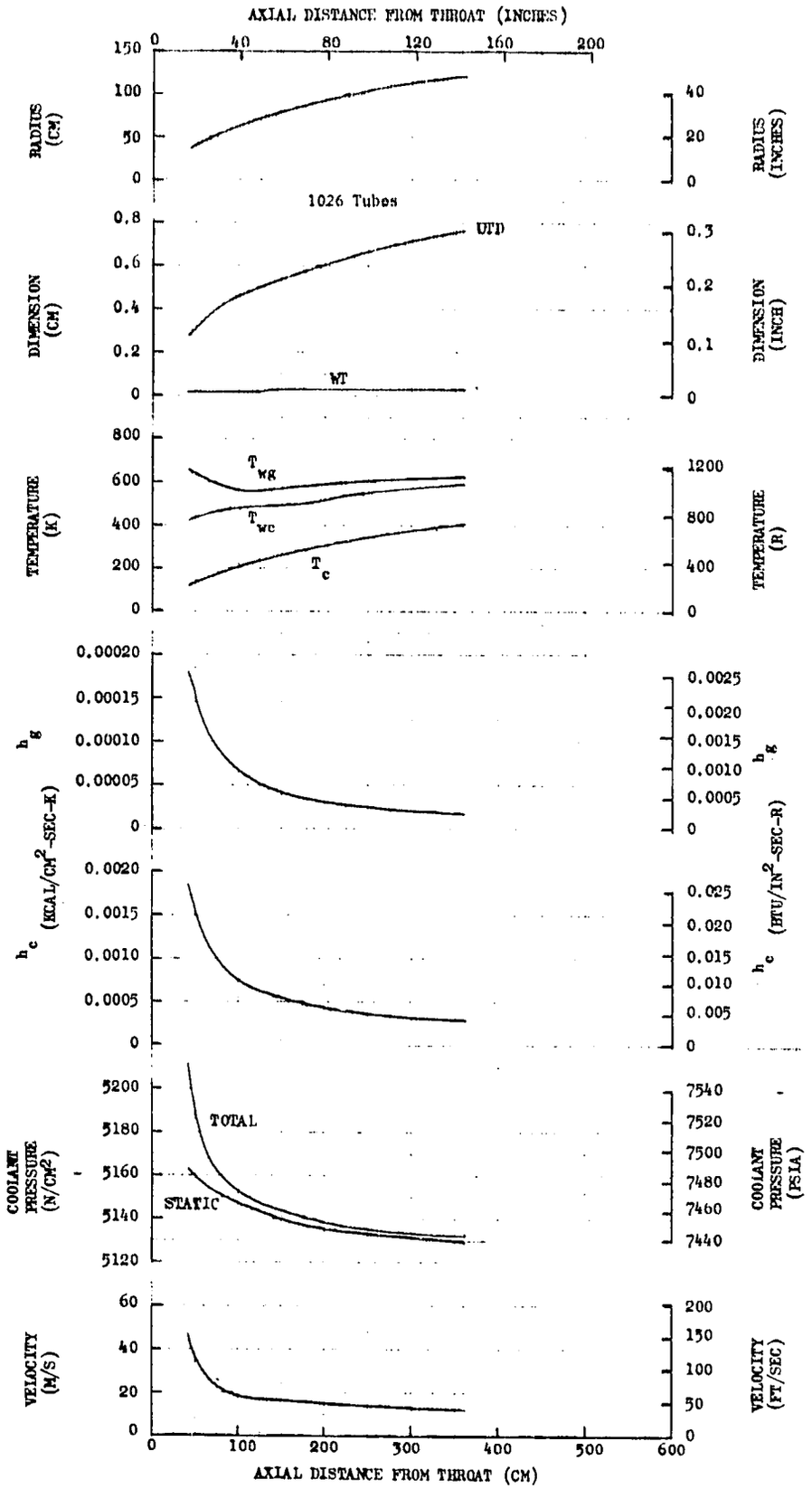

Figure 125. Parameters for the O_2/CH_4, MR = 3.5, F = 2,669,000 N (600,000 lbf), Coolant P_{in}/P_c = 1.8, Nozzle at P_c = 2896 N/cm^2 (4200 psia) (Film Cooling Enhancement on Combustion Chamber)

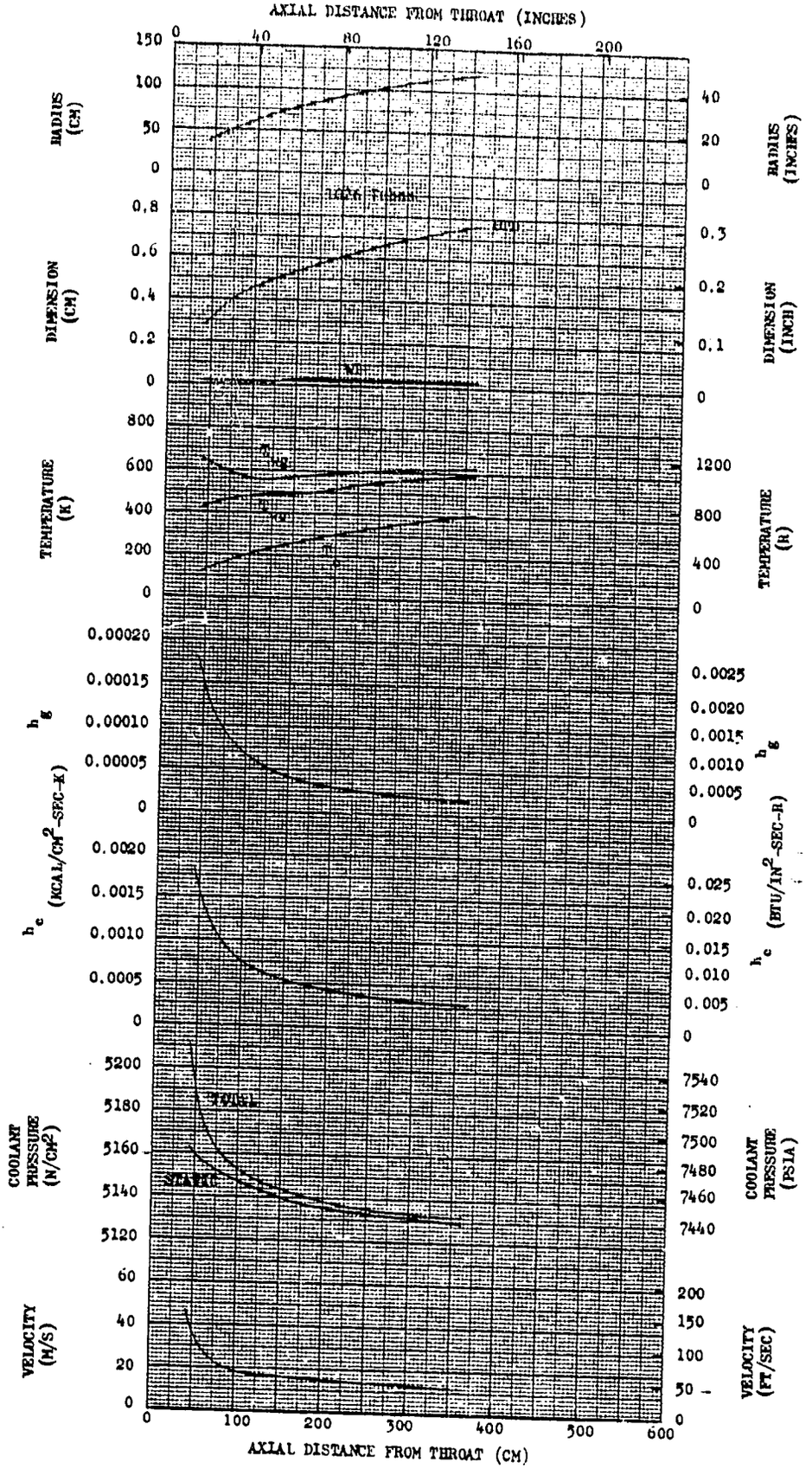

Figure 126. Parameters for the O_2/CH_4, MR = 3.5, F = 2,669,000 N (600,000 lbf), Coolant P_{in}/P_c = 1.8, Nozzle at P_c = 2896 N/cm^2 (4200 psia) (Film Cooling Enhancement on Combustion Chamber)

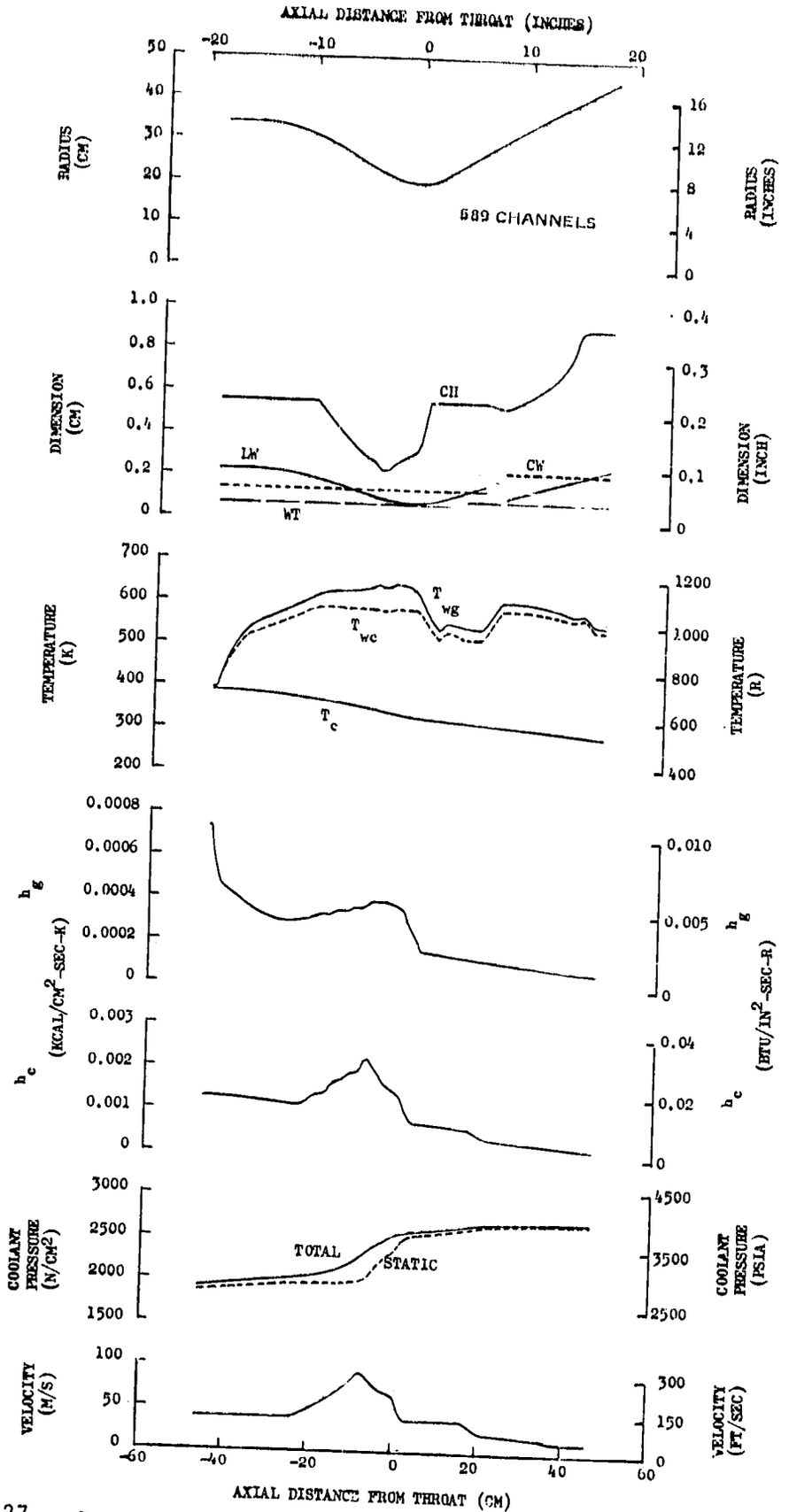

Figure 127. Parameters for the O_2/RP-1, MR = 2.8, F = 2,669,000 N (600,000 lbf), Coolant P_{in}/P_c = 1.8, Film-Cooled Enhanced "Short" Combustion Chamber at P_c = 1516 N/cm^2 (2200 psia)

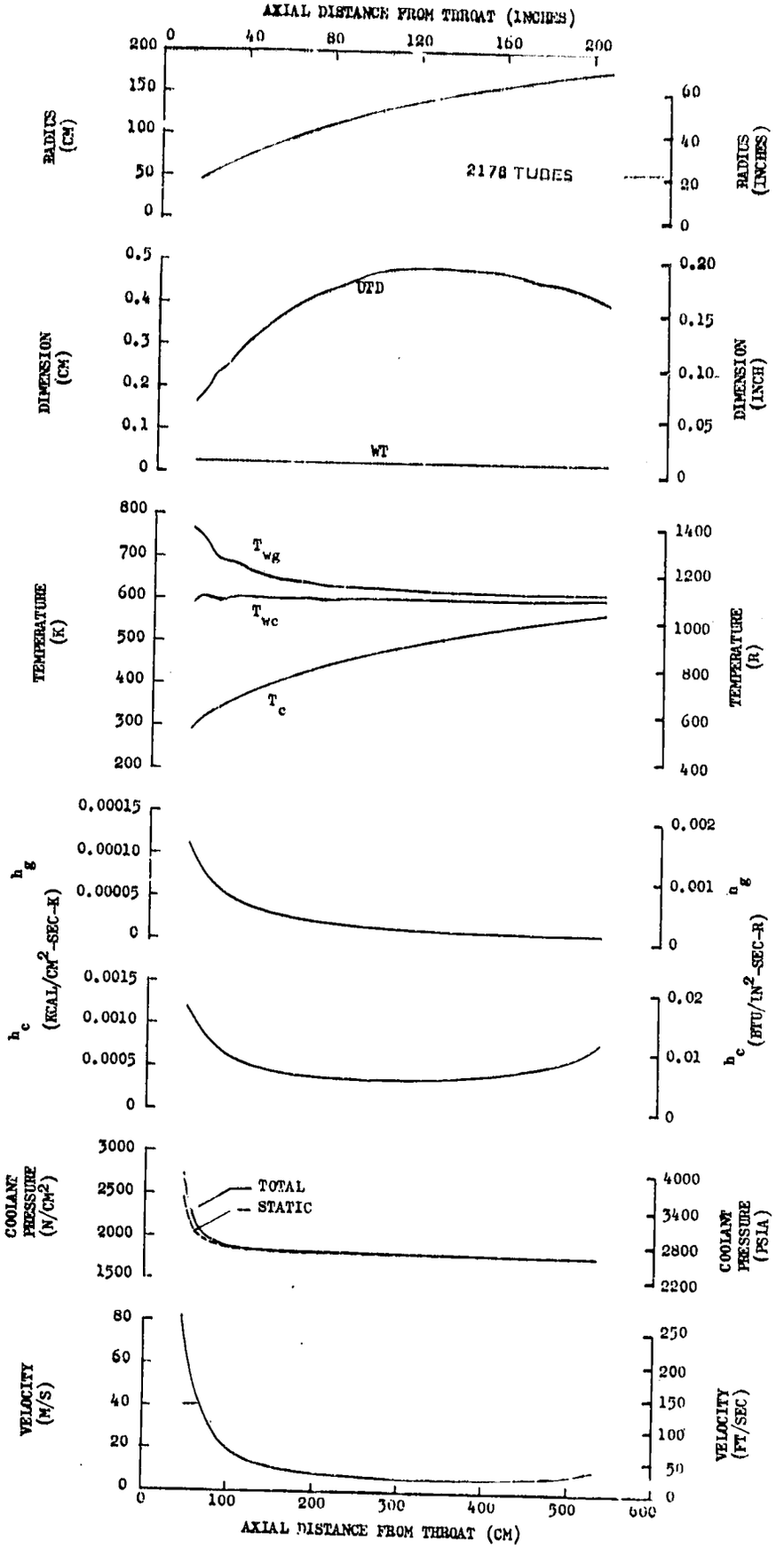

Figure 128. Parameters for the O_2/RP-1, MR = 2.8, F = 2,669,000 N (600,000 lbf), Coolant P_{in}/P_c = 1.8, Nozzle at P_c = 1516 N/cm^2 (2200 psia) (Film Cooled Enhancement on Combustion Chamber)

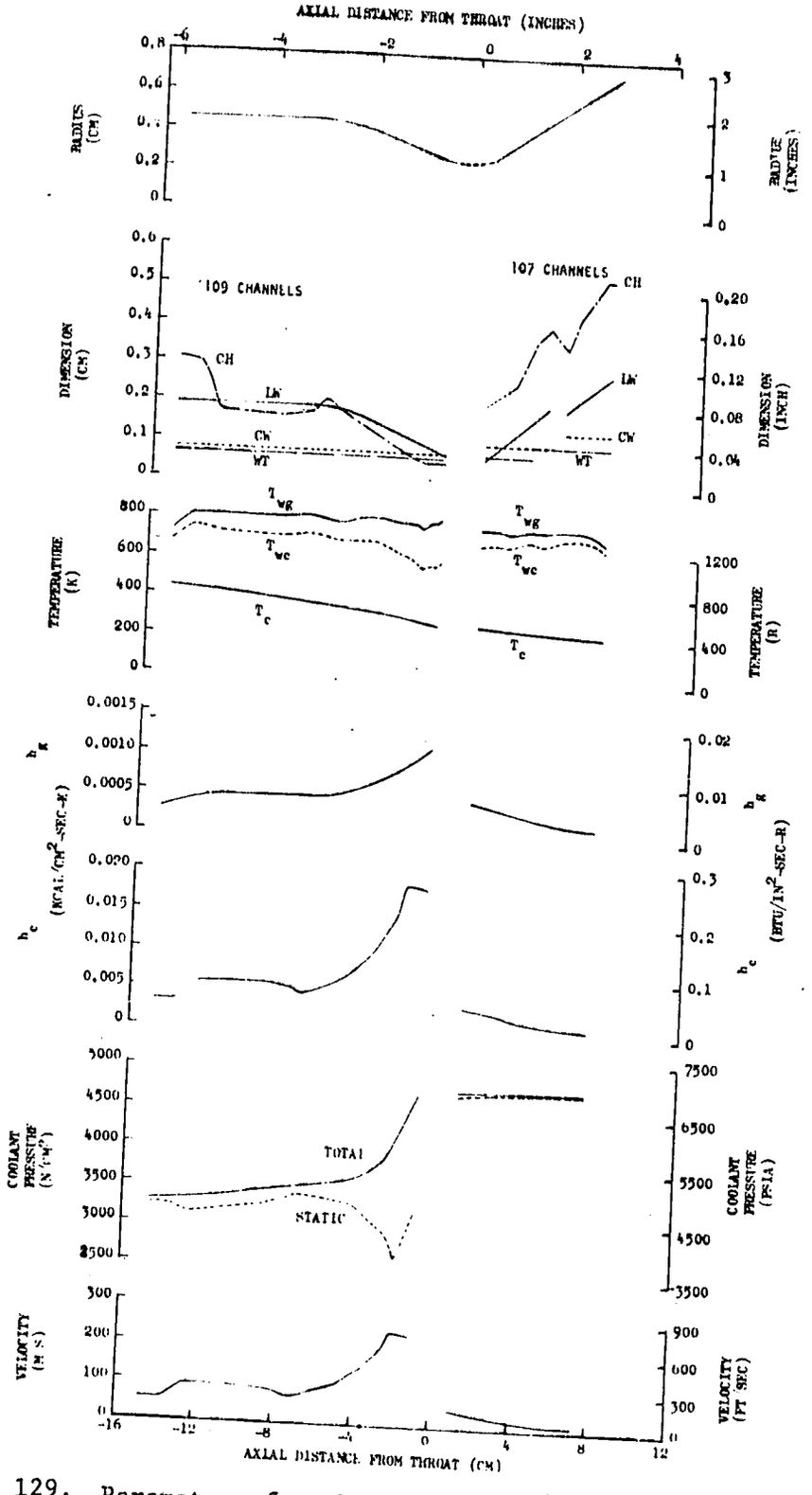

Figure 129. Parameters for the O_2/C_3H_8, MR = 3.1, F = 89,000 N (20,000 lbf), Coolant P_{in}/P_c = 1.8, Combustion Chamber at P_c = 2654 N/cm² (3850 psia) Transpiration Cooling on Throat Region)

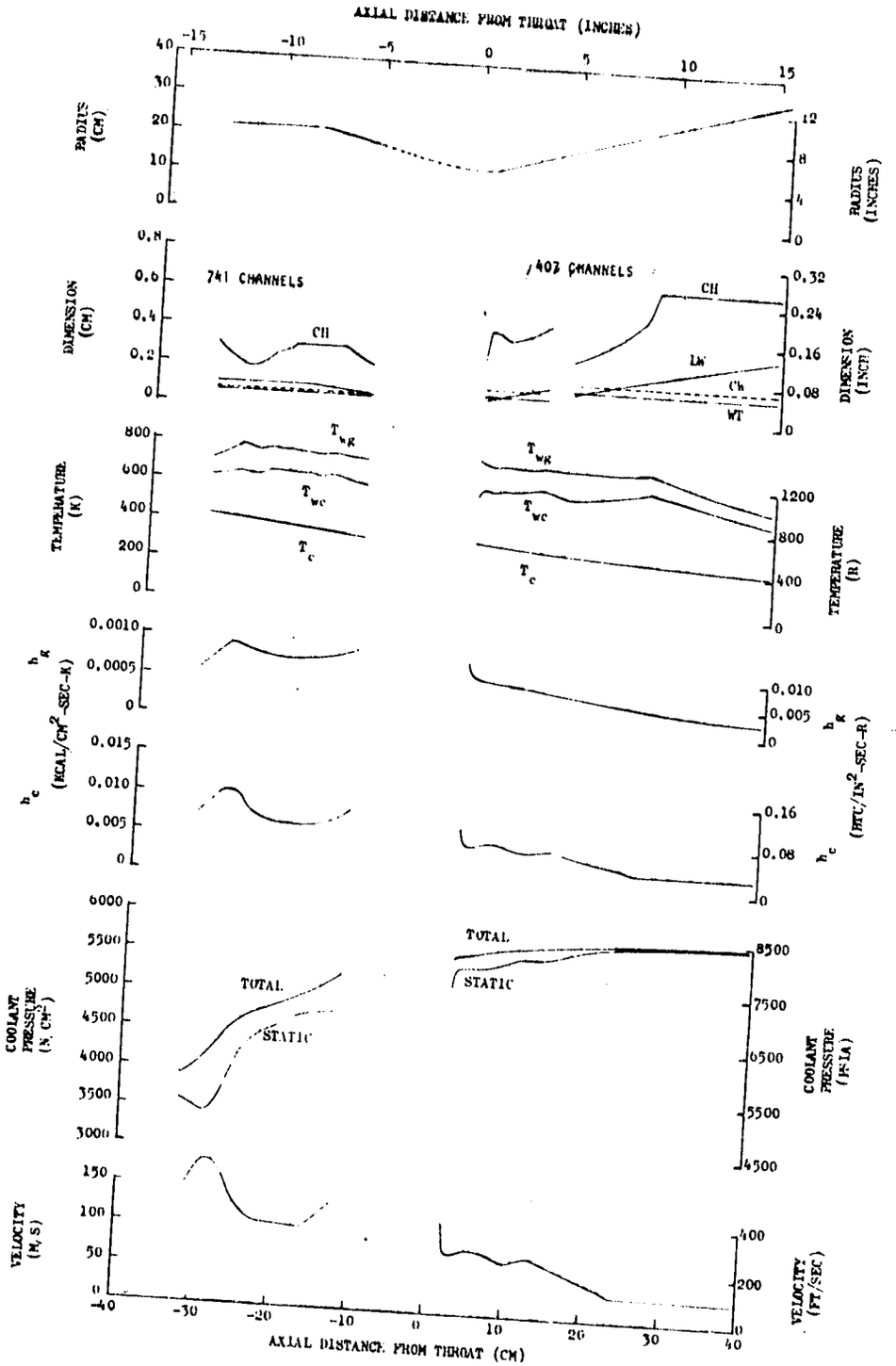

Figure 130. Parameters for the O_2/C_3H_8, MR = 3.1, F = 2,669,000 N (600,000 lbf), Coolant P_{in}/P_c = 1.8, Combustion Chamber at P_c = 3241 N/cm^2 (4700 psia) (Transpiration Cooling on Throat Region)

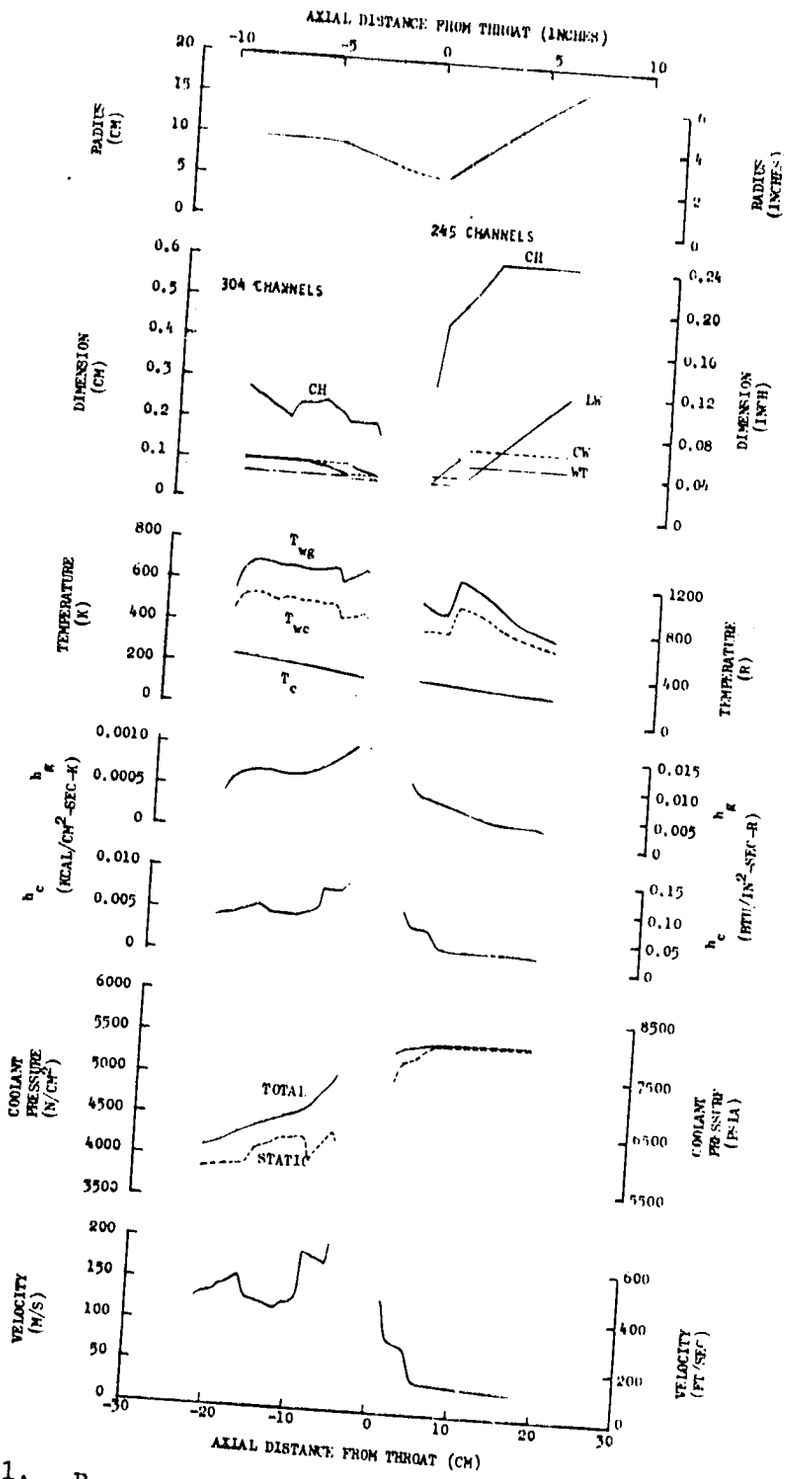

Figure 131. Parameters for the O_2/C_3H_8, MR = 3.5, F = 667,000 N (150,000 lbf), Coolant P_{in}/P_c = 1.6, Combustion Chamber at P_c = 3447 N/cm^2 (5000 psia) (Transpiration Cooling on Throat Region)

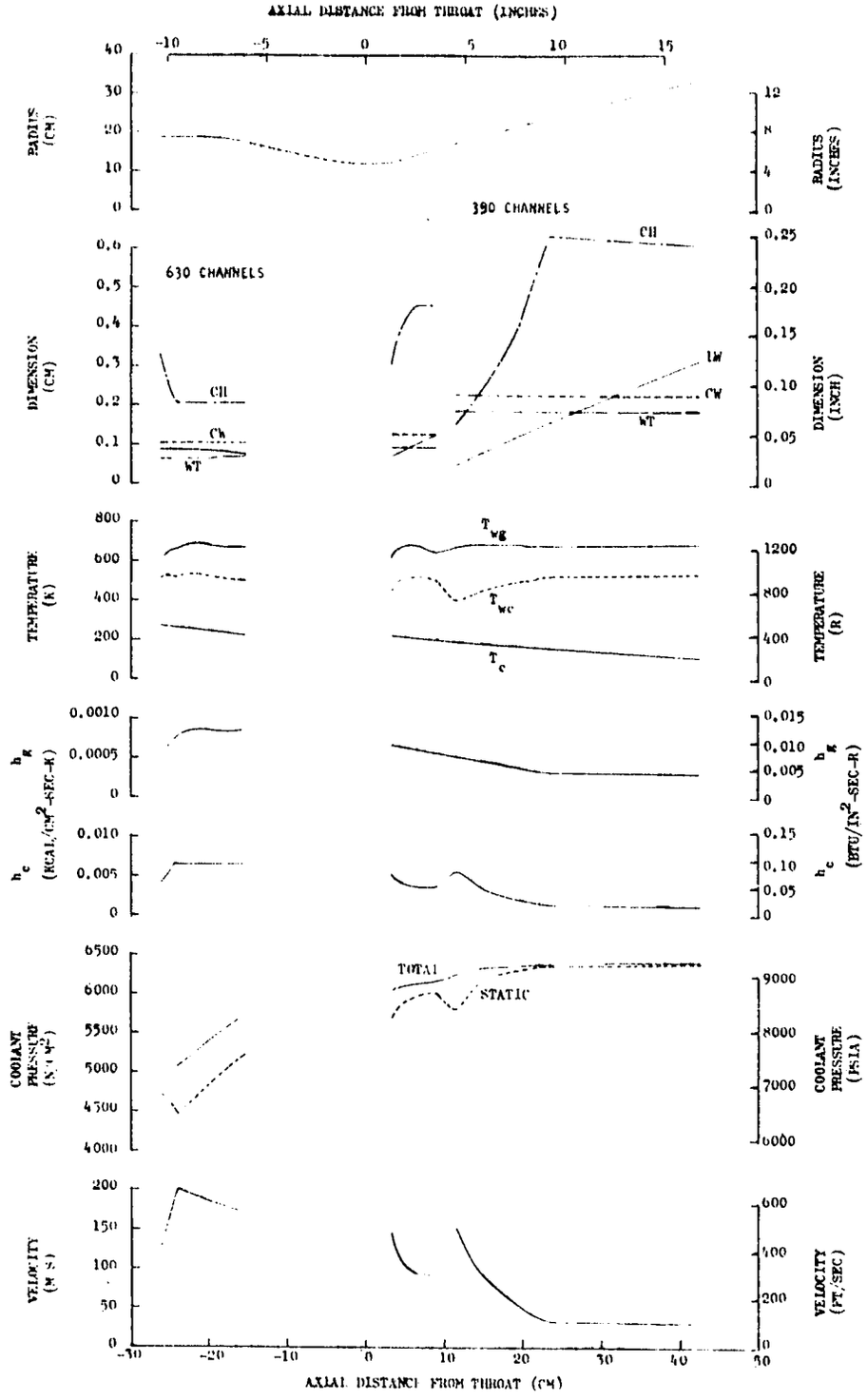

Figure 132. Parameters for the O_2/CH_4, MR = 3.5, F = 2,669,000 N (600,000 lbf), Coolant P_{in}/P_c = 1.55, Combustion Chamber at P_c = 4137 N/cm^2 (6000 psia) (Transpiration Cooling on Throat Region)

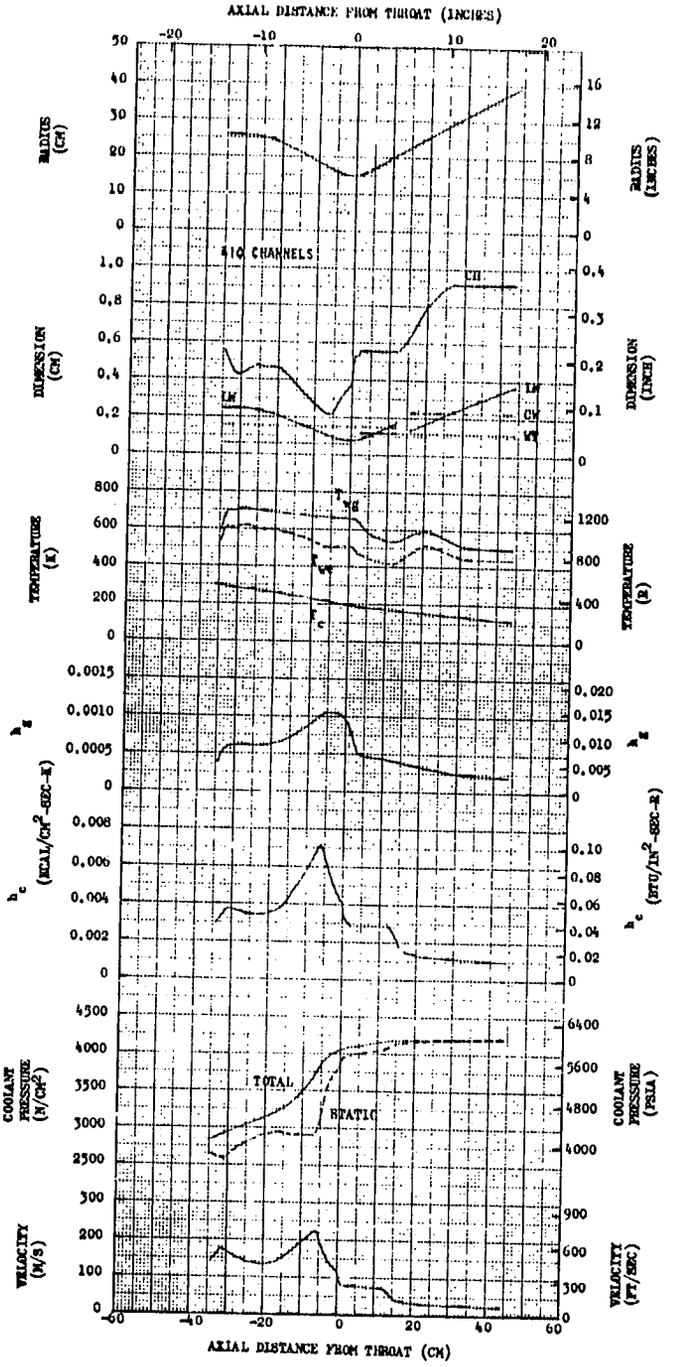

Figure 133. Parameters for the O_2/CH_4, MR = 3.5, F = 2,669,000 N (600,000 lbf), Coolant P_{in}/P_c = 1.8, Combustion Chamber at P_c = 2344 N/cm^2 (3400 psia) (Zoned Combustion Cooling Enhancement)

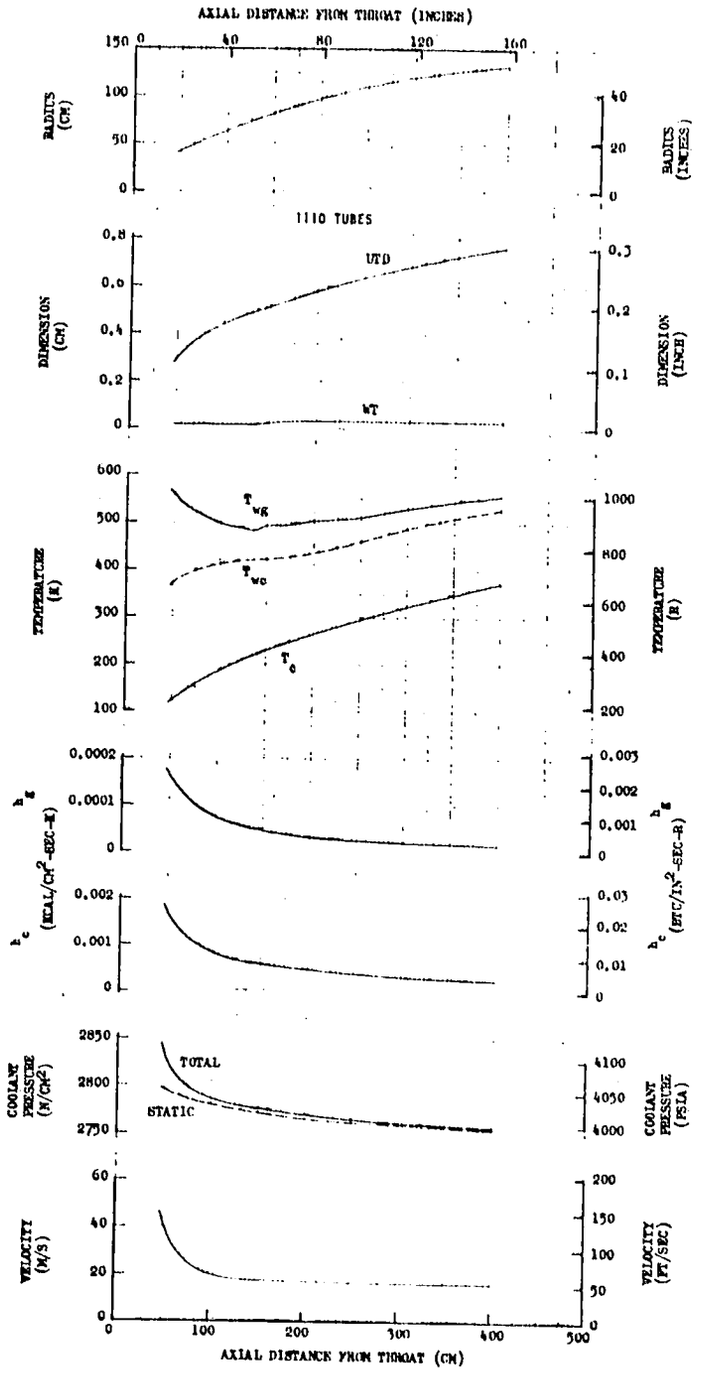

Figure 134. Parameters for the O_2/CH_4, MR = 3.5, F = 2,669,000 N (600,000 lbf), Coolant P_{in}/P_c = 1.8, Nozzle at P_c = 2344 N/cm^2 (3400 psia) (Zoned Combustion Cooling Enhancement)

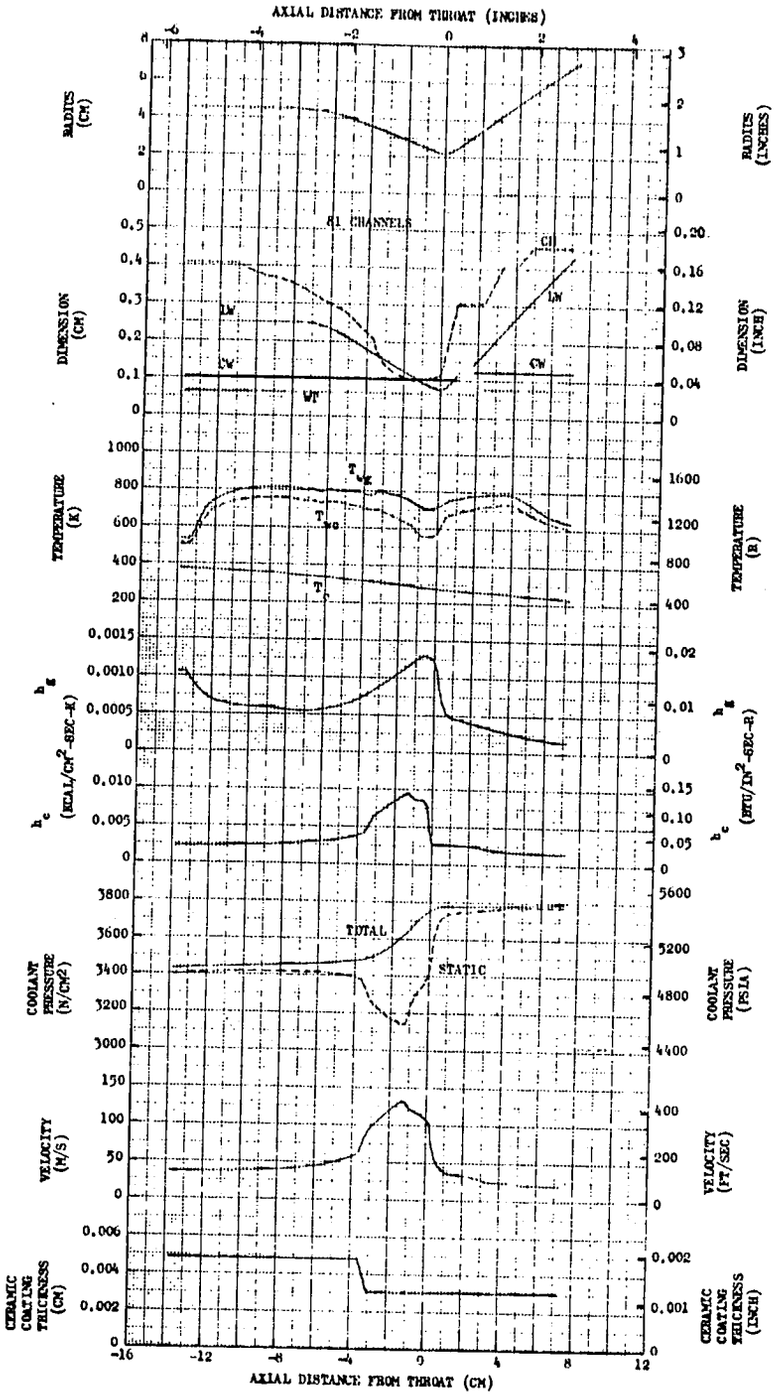

Figure 135. Parameters for the O_2/C_3H_8, MR = 3.1, F = 89,000 N (20,000 lbf), Coolant P_{in}/P_c = 1.38, Combustion Chamber at P_c = 2758 N/cm^2 (4000 psia)

(Combined Film Coolant and Ceramic Coating Enhancement on Combustion Chamber)

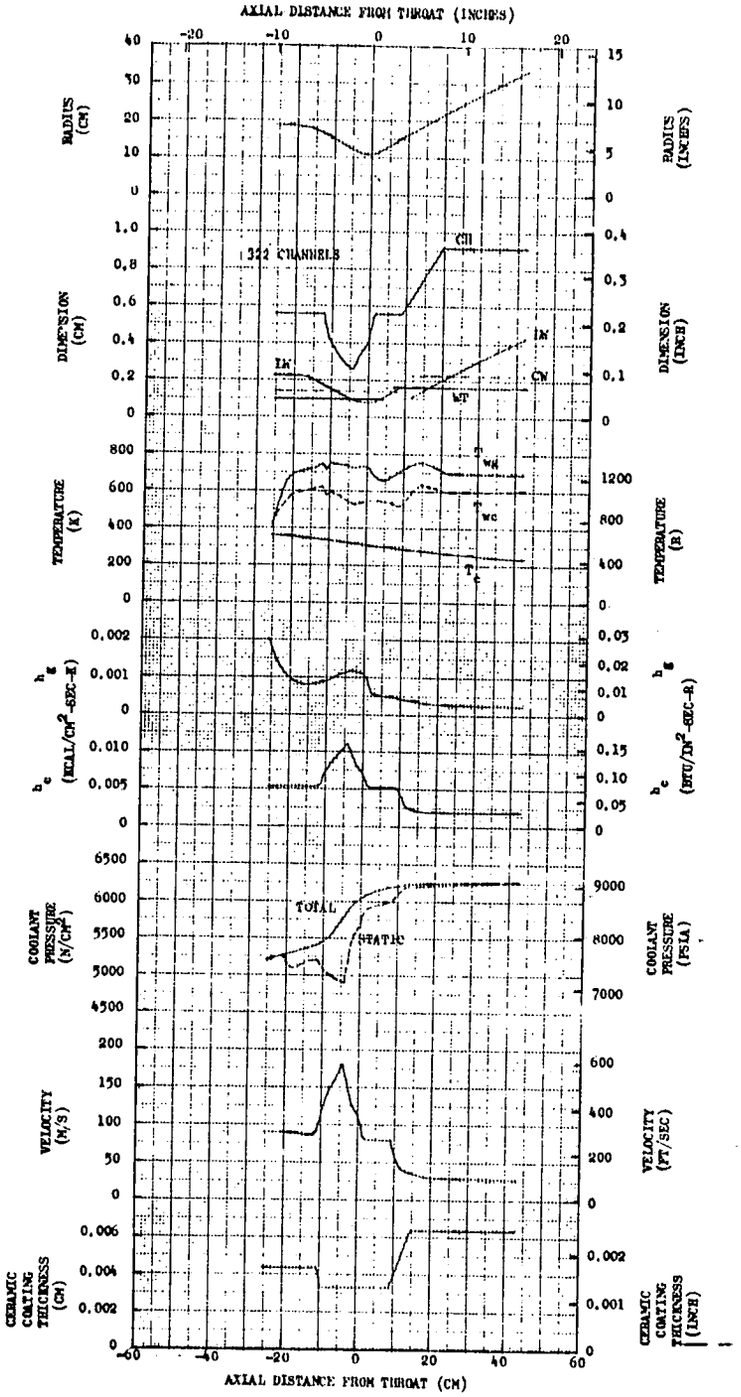

Figure 136. Parameters for the O_2/C_3H_8, MR = 3.1, F = 2,669,000 N (600,000 lbf), Coolant P_{in}/P_c = 1.5, Combustion Chamber at P_c = 4137 N/cm^2 (6000 psia) (Combined Film Coolant and Ceramic Coating Enhancement on Combustion Chamber)

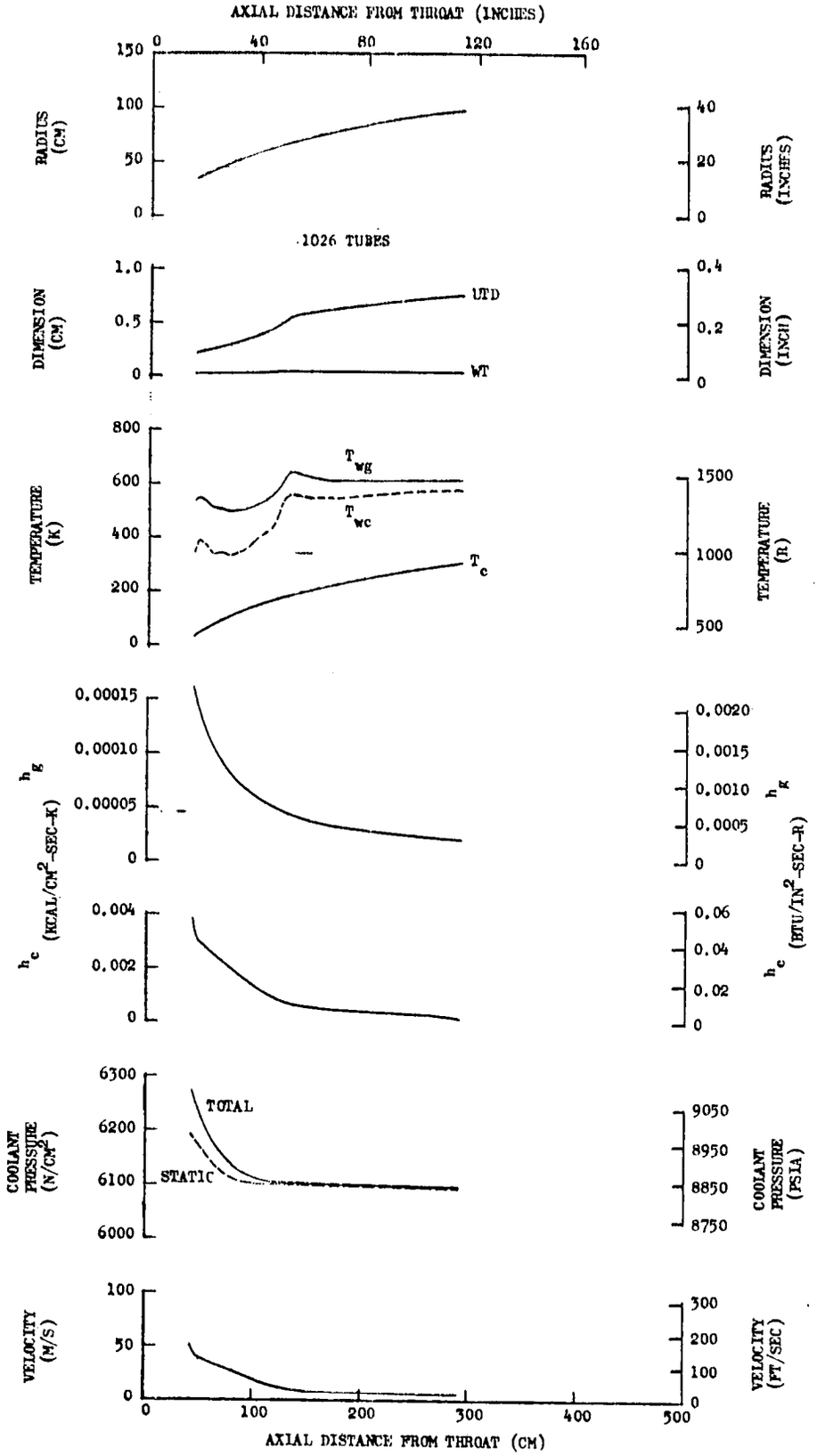

Figure 137. Parameters for the O_2/C_3H_8, MR = 3.1, F = 2,669,000 N (600,000 lbf), Coolant P_{in}/P_c = 1.52, Nozzle at P_c = 4137 N/cm^2 (6000 psia) (Combined Film Coolant and Ceramic Coating Enhancement on Combustion Chamber)

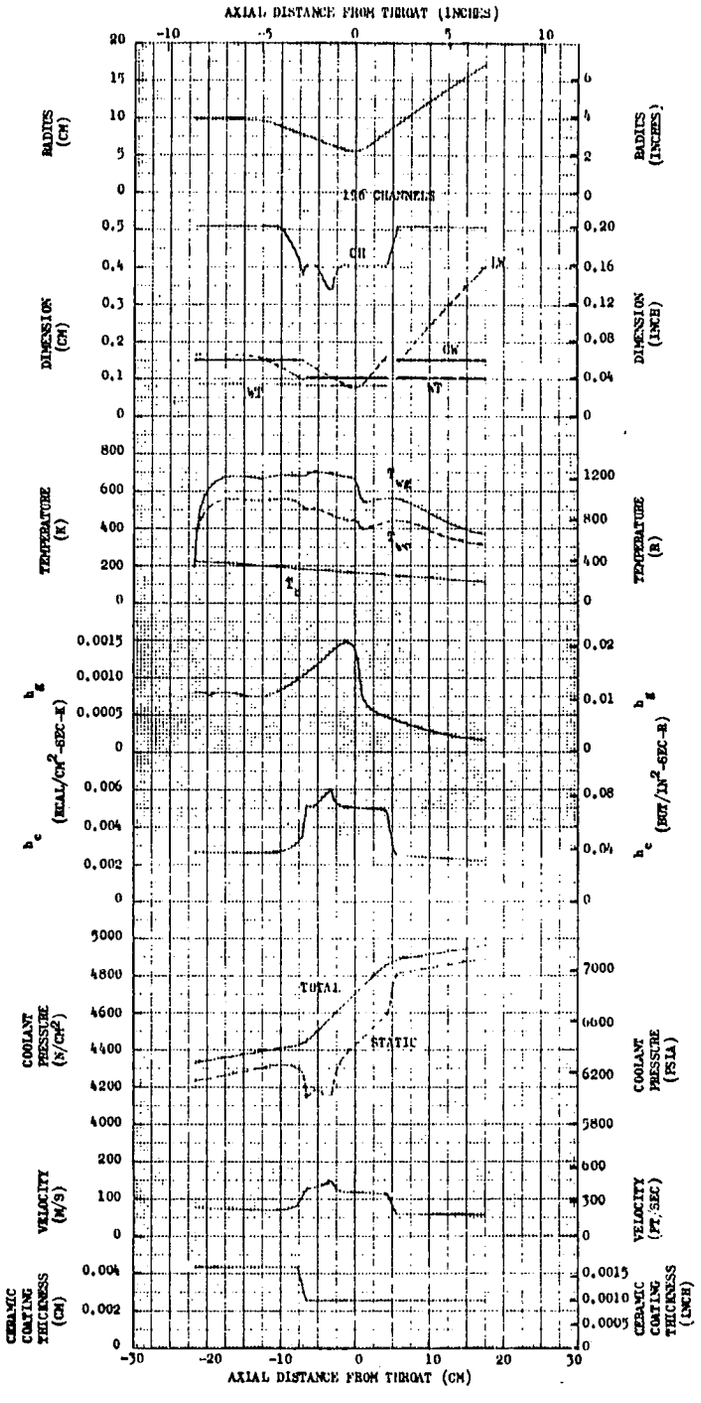

Figure 138. Parameters for the O_2/CH_4, MR = 3.5, F = 667,000 N (150,000 lbf), Coolant P_{in}/P_c = 1.44, Combustion Chamber at P_c = 3448 N/cm^2 (5000 psia) (Combined Film Coolant and Ceramic Coating Enhancement on Combustion Chamber)

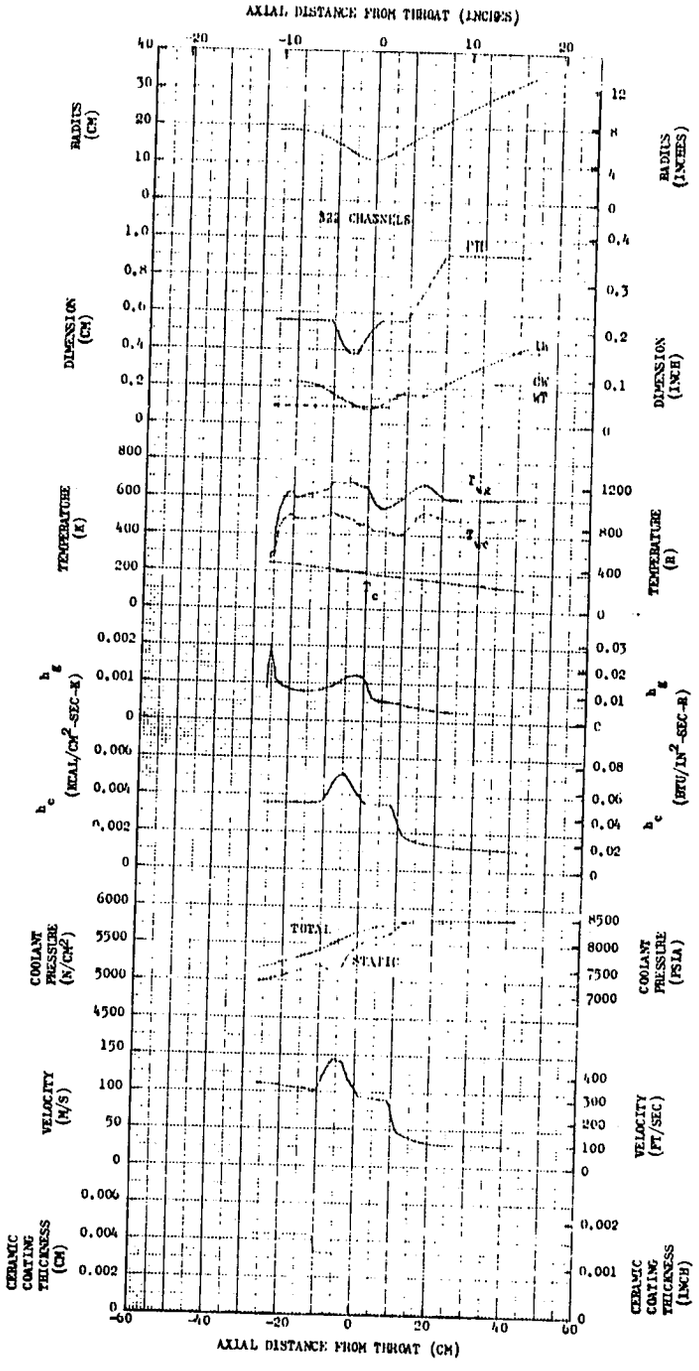

Figure 139. Parameters for the O_2/CH_4, MR = 3.5, F = 2,669,000 N 600,000 lbf), Coolant P_{in}/P_c = 1.42, Combustion Chamber at P_c = 4137 N/cm^2 (5000 psia) (Combined Film Coolant and Ceramic Coating Enhancement on Combustion Chamber)

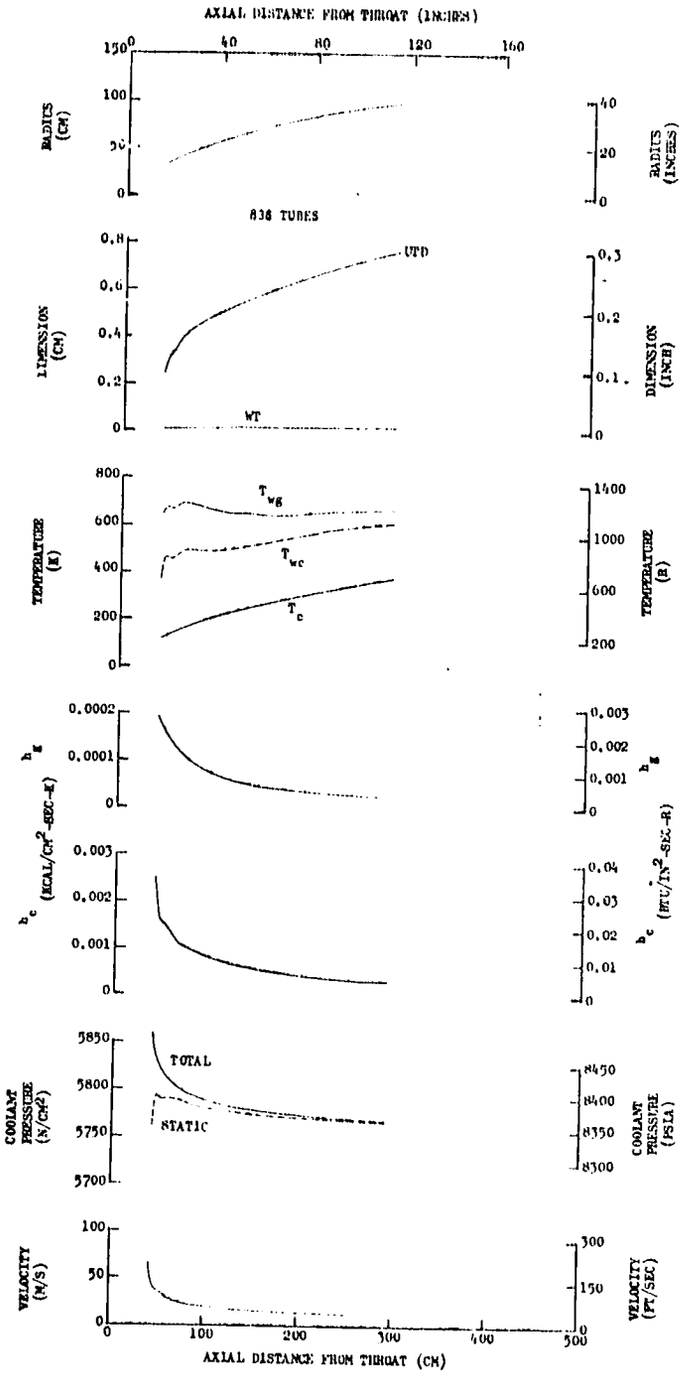

Figure 140. Parameters for the O_2/CH_4, MR = 3.5, F = 2,669,000 N (600,000 lbf), Coolant P_{in}/P_c = 1.42, Nozzle at P_c = 4137 N/cm^2 (6000 psia) (Combined Film Coolant and Ceramic Coating Enhancement on Combustion Chamber)

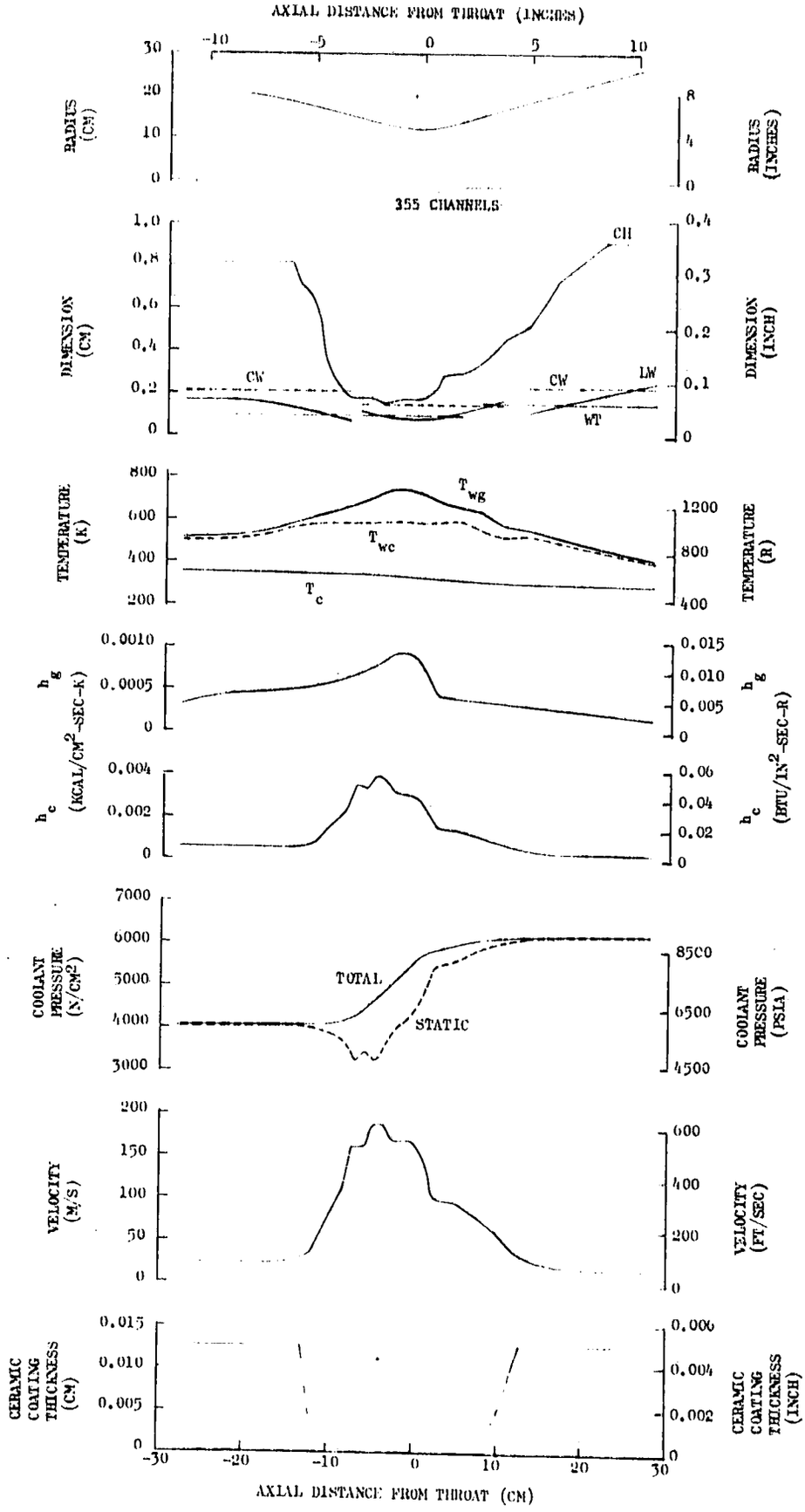

Figure 141. Parameters for the O_2/RP-1, MR = 2.8, F = 2,669,000 N (600,000 lbf), Coolant P_{in}/P_c = 1.8, Combustion Chamber at P_c = 3448 N/cm^2 (5000 psia) (Combined Carbon Layer and Zirconium Oxide Enhancement)

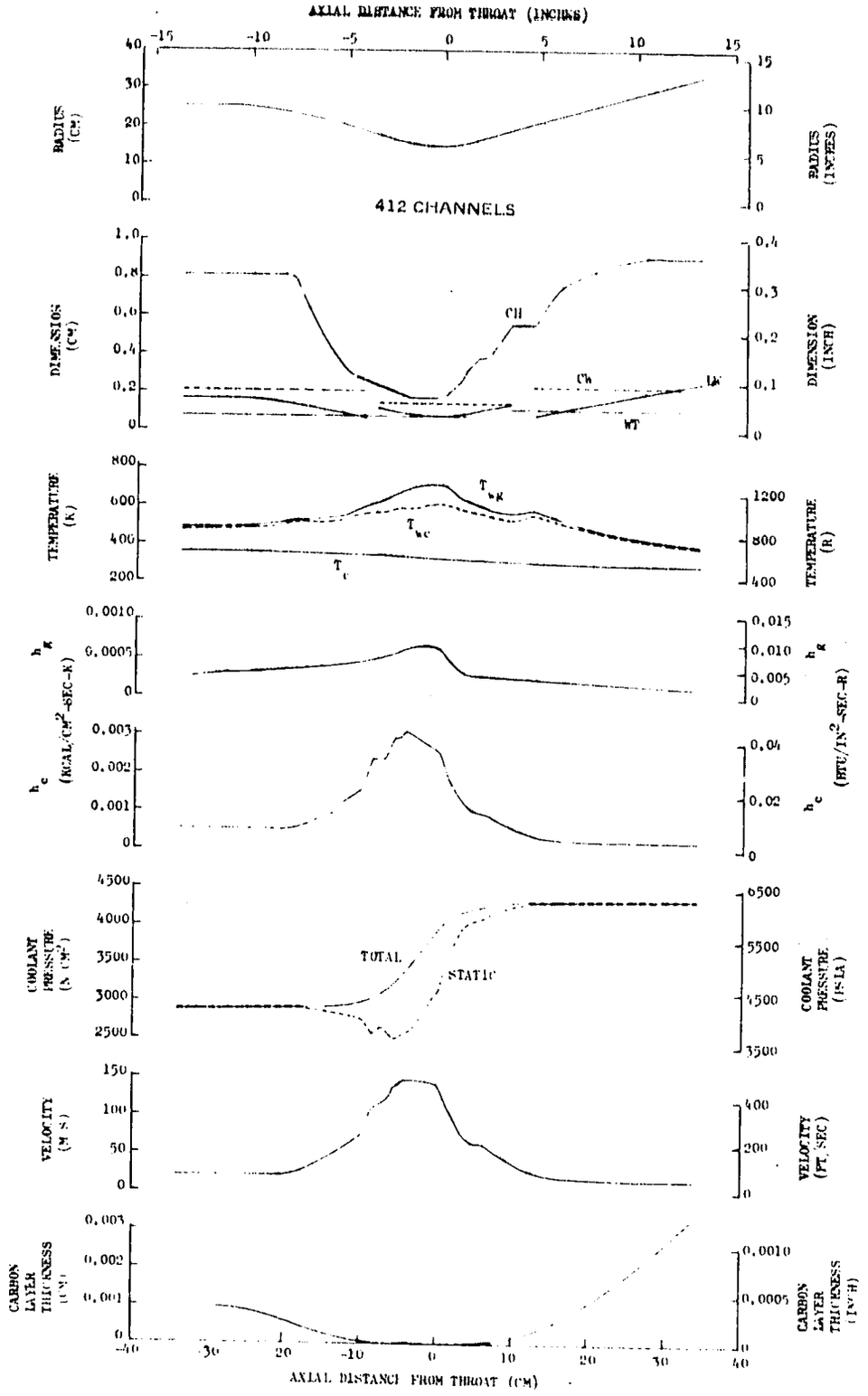

Figure 142. Parameters for the O_2/RP-1, MR = 2.8, F = 2,669,000 N (600,000 lbf), Coolant P_{in}/P_c = 1.8, Combustion Chamber at P_c = 2413 N/cm^2 (3500 psia) Carbon Layer Enhancement on Combustion Chamber (Short Chamber) (RP-1 T_{wc} Sensitivity Design)

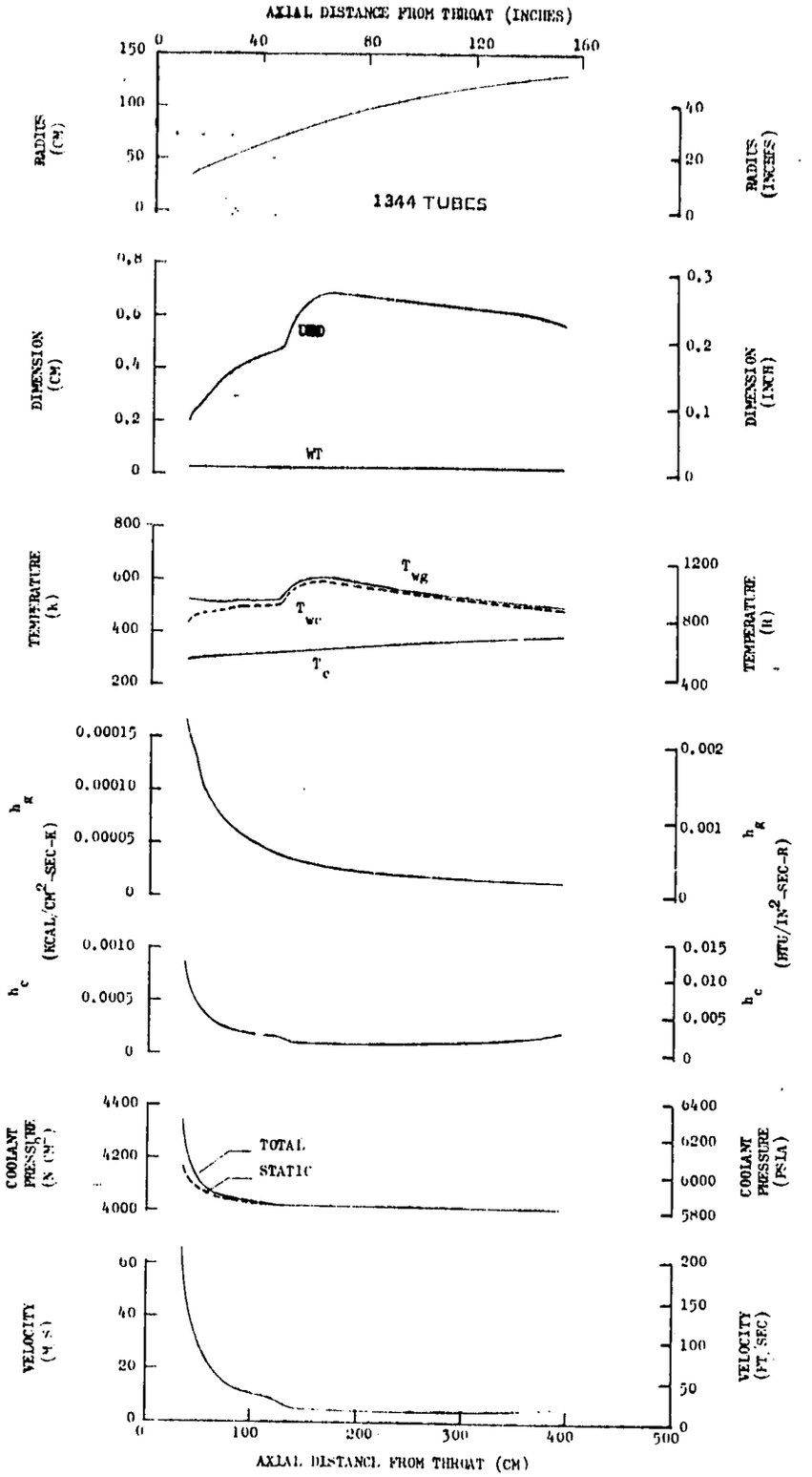

Figure 143. Parameters for the O_2/RP-1, MR = 2.8, F = 2,669,000 N (600,000 lbf), Coolant P_{in}/P_c = 1.8, Nozzle at P_c = 2413 N/cm^2 (3500 psia) Carbon Layer Enhancement on Combustion Chamber (Short Chamber) (RP-1 T_{wc} Sensitivity Design)

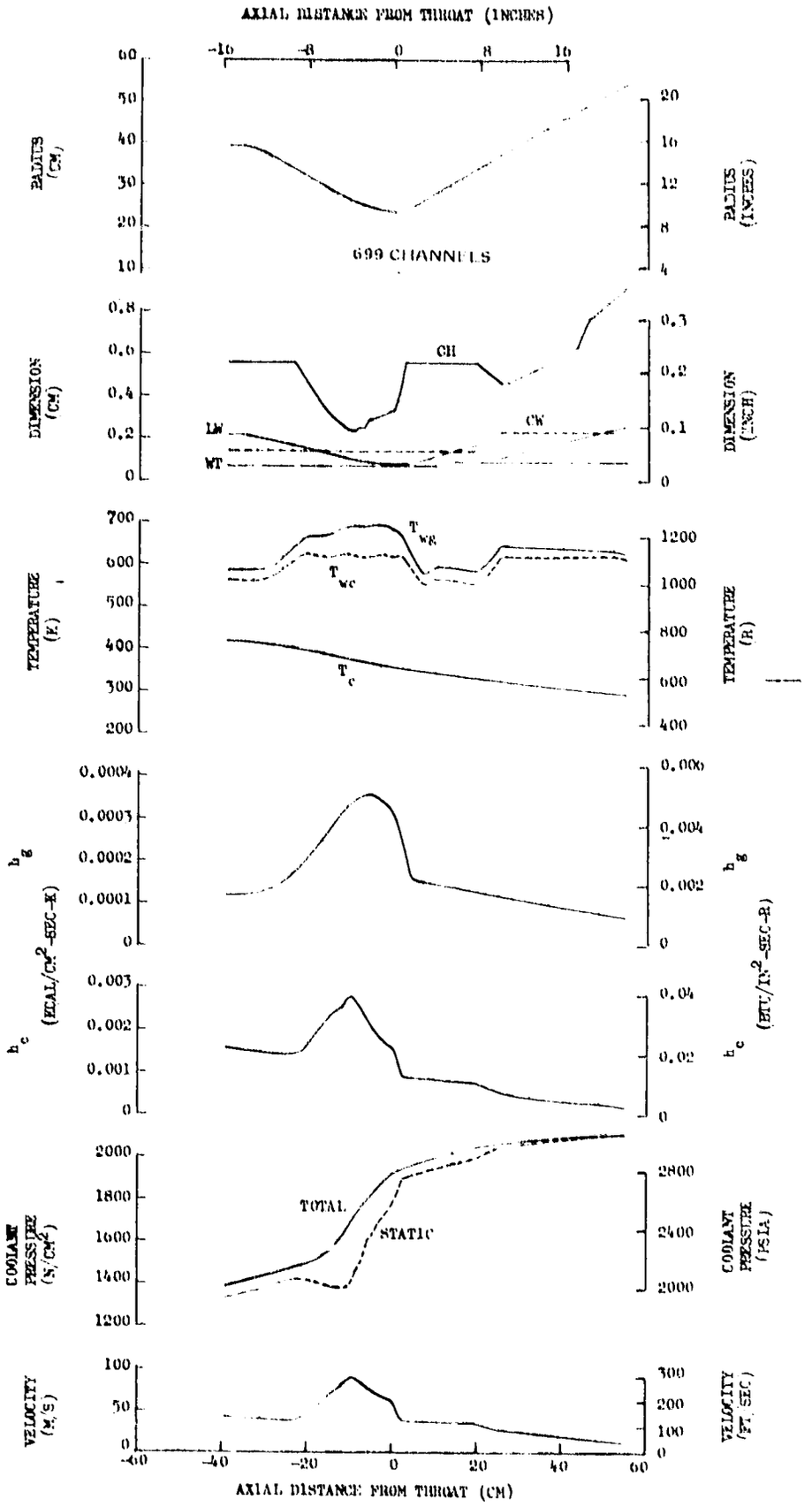

Figure 144. Parameters for the O_2/RP-1, MR = 2.8, F = 2,669,000 N 600,000 lbf), Coolant P_{in}/P_c = 1.8, Combustion Chamber at P_c = 1172 N/cm^2 (1700 psia) (Short) Chamber) (RP-1 T_{wc} Sensitivity)

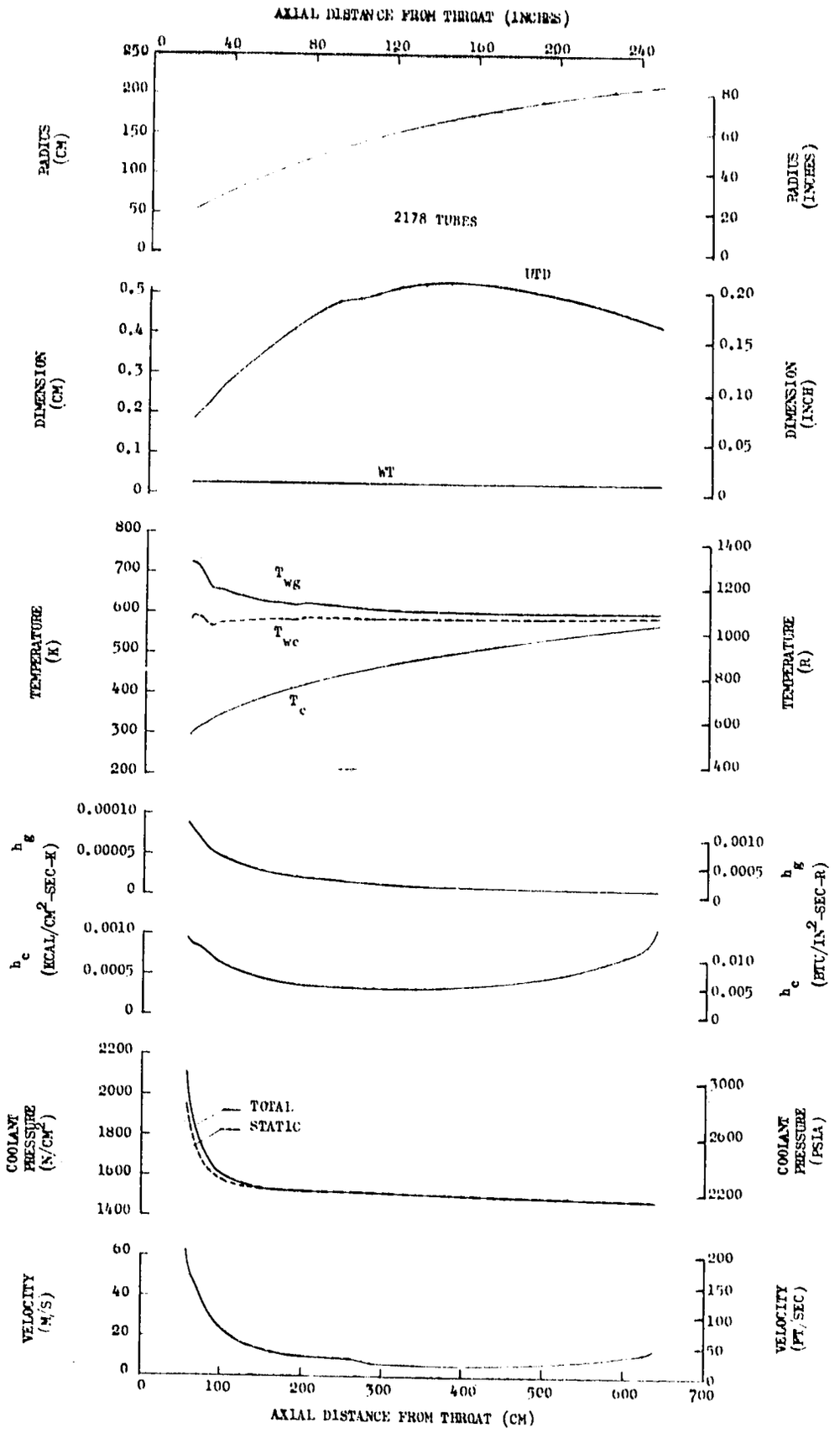

Figure 145. Parameters for the O_2/RP-1, MR = 2.8, F = 2,669,000 N (600,000 lbf), Coolant P_{in}/P_c = 1.8, Nozzle at P_c = 1172 N/cm^2 (1700 psia) (Short Chamber) (RP-1 T_{wc} Sensitivity)

NOMENCLATURE

A	area
Btu	British thermal units
C_d	discharge coefficient
CH_4	methane, fuel propellant
C_p	specific heat
C_3H_8	propane, fuel propellant
D_h	hydraulic diameter
D_t	throat diameter
F	thrust, N (lbf)
F_{tu}	ultimate strength safety factor
F_{ty}	yield strength safety factor
G	mass flux ($\dot{w}/A = \rho V$)
h_c	coolant convective heat transfer coefficient
h_g	hot-gas convective heat transfer coefficient
I_s	specific impulse
K	degrees Kelvin
k	thermal conductivity
L	length
MR	mixture ratio (o/f)
N_f	number of load cycles to failure
N_{st}	Stanton number
O_2	oxygen, oxidizer propellant
P	pressure
P_c	combustion gas chamber pressure
P_{in}	coolant inlet pressure
Pr	Prandtl number
Q	heat load
Q/A	heat flux
R	radius or degrees Rankine
Re	Reynolds number
r_i	inside tube radius
r_o	outside tube radius

RP-1	rocket fuel propellant
R_t	throat radius
T	time
T_{aw}	adiabatic wall temperature
T_b	coolant bulk temperature
T_{bw}	backwall structure temperature
T_c	combustion or coolant temperature
T_{wc}	coolant side wall temperature
T_{wg}	gas side wall temperature
w_c	coolant flowrate
w_g	hot-gas flowrate
X	thickness

SUBSCRIPTS

b	bulk
c	coolant or combustion
f	film
g	gas
s.l.	sea level
vac	vacuum

GREEK

ΔP	coolant pressure drop
ϵ	area ratio or strain
ϕ	angular displacement
ϕ_c	creep damage fraction or curvature enhancement
d_f	fatigue damage fraction
ϕ_R	surface roughness enhancement
γ	specific heat ratio
η_{c^*}	energy release efficiency or combustion efficiency
ρ	density
σ	bending stress
τ	shear stress
μ	viscosity

FILM COOLING

B^*	dimensionless parameter
C_p	specific heat at constant pressure
G	mass flow per unit area
K	constant in correlation
h	heat transfer coefficient
Le	Lewis number
M	molecular weight
Pr	Prandtl number
p	wetted perimeter
Re_x	Reynolds number based on distance
m	ratio of injection to free stream mass flux
s	injection slot height
T	temperature
w	flowrate
X	distance from injection point along surface
X_1	correction length for wall jet region

Subscripts

nw	adiabatic wall conditions
c	coolant or chamber conditions
f	film
g	free stream gas
o	zero film cooling conditions
Δ	coolant gas interface
s	coolant injection slot
fc	film coolant

Greek

η	effectiveness and efficiency
β	constant in correlation
γ	specific heat ratio
ρ	density
Δ	film thickness
μ	viscosity

REFERENCES

1. Cook, R. T. and G. A. Coffey, Space Shuttle Main Engine Combustion Chamber Cooling and Life, AIAA Paper 73-1310, November 1973.

2. Thrust Chamber Assembly, SSME 40K Subscale Chamber and Injector Cyclic Life, RSS-303-28, Contract NAS8-27980, DPD 341, Data Requirement SE-236-19, 23 September 1976.

3. Seader, J. D. et al., Investigation of Cooling Problems at High Chamber Pressures, Final Report, R-3999, Rocketdyne Division, Rockwell International, May 1963.

4. R-6199, Investigation of Cooling Problems at High Chamber Pressures, Final Report, Rocketdyne Division, Rockwell International, July 1965.

5. R-6259, Investigation of Cooling Problems at High Chamber Pressures, Final Report, Rocketdyne Division, Rockwell International, September 1966.

6. Cook, R. T. and L. H. Pidcoke, SSME Main Combustion Chamber Coolant Circuit Curvature Enhancement, Contract NAS8-27980, Rocketdyne Division, Rockwell International, November 1972.

7. Sellers, J. P., Jr., "Effect of Carbon Deposition on Heat Transfer in a LOX/RP-1 Thrust Chamber," ARS Journal, Vol. 31, 1961, pp. 662-663.

8. NASA CR-72137, Investigation of Light Hydrocarbon Fuels With Fluorine-Oxygen Mixtures as Liquid Rocket Propellants, Contract NAS3-6296, 15 September 1967.

9. Hatch, J. E. and S. S. Papell, Use of a Theoretical Flow Model to Correlate Data for Film Cooling of Heating and Adiabatic Wall by Tangential Injection of Gases of Different Fluid Properties, NASA TN-D-130, November 1959.

10. Tribus, M. and J. Klein, "Forced Convection From Non-Isothermal Surfaces," Heat-Transfer Symposium, University of Michigan Press, Ann Arbor, Michigan, Chapter 8, 1953.

11. McFarland, B. L. "Heat Transfer Considerations in Internal Regeneratively Cooled (INTEREGEN) Thrust Chamber," ASME Paper 70-HT/SPT-41, June 1970.

12. Papell, S. S. and A. M. Trout, Experimental Investigation of Air Film Cooling Applied to an Adiabatic Wall by Means of an Axially Discharging Slot, NASA TN-D-9, August 1959.

13. Chin, J. H. et al., "Film Cooling With Multiple Slots and Louvers," ASME Paper GO-HT-35, 1960.

14. Hartnett, J. P. et al., "Velocity Distributions, Temperature Distributions, Effectiveness and Heat Transfer for Air Injected Through a Tangential Slot into a Turbulent Boundary Layer," presented at ASME Heat Transfer Conference (Paper 60-HT-31), Buffalo, New York, 1960.

15. Lucas, J. G. and R. L. Golladay, Gaseous Film Cooling of a Rocket Motor With Injection Near the Throat, NASA TN-D-3836, February 1967.

16. Rannie, W. D., A Simplified Theory of Porous Wall Cooling, JPL, California Institute of Technology, Progress Report No. 4-50, November 1957.

17. Rubesin, M. W. and C. C. Pappas, An Analysis of the Turbulent Boundary Layer Characteristics on a Flat Plate Distributed Light-Gas Injection, NACA TN-4149, February 1958.